PLEASE NOTE:

In all cases this material has been filmed in the best possible way from the available copy. Problems encountered with this document have been identified here with a check mark ✓.

1. Glossy photographs _____
2. Colored illustrations _____
3. Photographs with dark background _____
4. Illustrations are poor copy _____
5. Print shows through as there is text on both sides of page _____
6. Indistinct, broken or small print on several pages ✓ throughout _____
7. Tightly bound copy with print lost in spine _____
8. Computer printout pages with indistinct print _____
9. Page(s) _____ lacking when material received, and not available from school or author _____
10. Page(s) _____ seem to be missing in numbering only as text follows _____
11. Poor carbon copy _____
12. Not original copy, several pages with blurred type _____
13. Appendix pages are poor copy _____
14. Original copy with light type _____
15. Curling and wrinkled pages _____
16. Other _____

University Microfilms International

300 N. ZEEB RD., ANN ARBOR, MI 48106 (313) 761-4700

THE UNIVERSITY OF OKLAHOMA

GRADUATE COLLEGE

MINERAL DISPERSAL PATTERNS IN THE PIERRE SHALE

A DISSERTATION

SUBMITTED TO THE GRADUATE FACULTY

in partial fulfillment of the requirements for the

degree of

DOCTOR OF PHILOSOPHY

BY

RICHARD LEWIS JONES

Norman, Oklahoma

1979

MINERAL DISPERSAL PATTERNS IN THE PIERRE SHALE

APPROVED BY

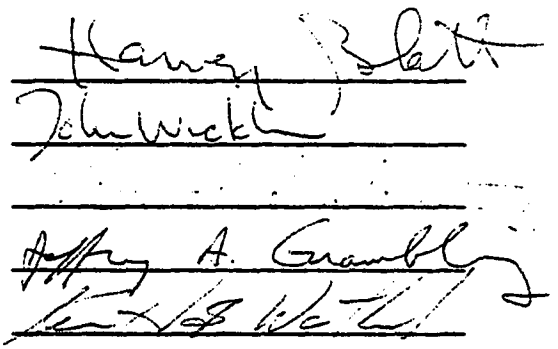

DISSERTATION COMMITTEE

ACKNOWLEDGEMENTS

I would like to acknowledge and thank Dr. Harvey Blatt for his help in directing this dissertation, for reviewing the manuscript, and the six weeks he spent in the field with me collecting samples of the Pierre Shale. Thanks are also extended to Dr. John Wickham, Dr. Frank Wantland, Dr. Jeffrey Grambling, and Dr. Leonard Schultz for their time spent in reviewing this manuscript, and for sitting on my dissertation committee.

Throughout the years spent on this project, I have received much help from the staff of the Oklahoma Geological Survey and the School of Geology and Geophysics. Among the many staff members who deserve my thanks are: Dr. L. R. Wilson for identification of the microfossils; Dr. Howard Day for his help and discussion on the methods used; and particularly, David Foster for his help with the atomic absorption analyses. Numerous graduate students also deserve my thanks for their useful suggestions and criticisms. Amoung these students are Duncan Sibley and Raymond Charles who deserve special thanks.

The suggestions and aid provided by Dr. W. G. E. Caldwell, with the University of Saskatchewan; Barry Bannatyne with the Manitoba Department of Mines; and James E. Christopher and John E. Brindle with the Saskatchewan Department of Natural Resources is also appreciated.

Thanks is also extended to John Fryberger, John Marsh, Alan Haws and all the staff of Engineering Enterprises for their moral support as well as their help in preparing the manuscript.

Most importantly, I would like to express my sincere appreciation

to my wife, Kathleen and my three sons, Mark, Eric and Stephen for their sacrifices and patience while I have been completing this degree.

ABSTRACT

Detailed mineralogic, petrologic and chemical analyses were run on a suite of Pierre Shale samples to determine whether the non-clay petrology could be used to interpret the petrogenic history of the Pierre Shales.

Mineralogic analyses indicated quartz is the major non-clay component, generally comprising 22% of the sample. The majority of quartz was derived from older sedimentary rocks. The amount of quartz found in individual samples was controlled by the influx of volcanic sediments and the distance between the sample and the nearest shoreline.

The feldspar content averages 8.5% of the whole rock and 39% of the quartz and feldspar fraction. Sixty percent of the feldspar fraction is normative plagioclase with an average normative anorthite composition of 8.2 mole percent. Petrographic and other evidence indicate that the majority of feldspar was derived from volcanic source rocks.

Size analyses of the quartz and feldspar fraction indicated that the quartz and feldspars are significantly finer than the quartz and feldspars found in other shale units. These analyses also indicated that wind and water transport of sediments into the Pierre Seaway was important, but the wind transport was dominant over water transport.

In this study the only major diagenetic change in the quartz and feldspar fraction was the authigenic production (or diagenetic conversion) of quartz and cristobalite from biogenic silica. Only one sample indicated the presence of authigenic feldspar.

A petrogenetic model for the deposition of the Pierre sediments is proposed. The model proposed is one of pelagic sedimentation into the Pierre Seaway coupled with a volcanic point source for as much as 40% of Pierre sediments.

TABLE OF CONTENTS

LIST OF TABLES

LIST OF ILLUSTRATIONS

FIGURE PAGE

FIGURE PAGE

MINERAL DISPERSAL PATTERNS IN THE PIERRE SHALE[1]

INTRODUCTION

The non-clay mineral composition of sandstones has been extensively studied in an effort to determine the petrogenetic history of sand bodies. Studies of this type have not been attempted for mudrocks, however, although mudrocks represent 65% of the sedimentary record and about one-third of the average mudrock is thought to be composed of quartz, feldspar, and rock fragments. Only Keller and Ting (1950) and Blatt and Schultz (1976) have tried to examine in detail the non-clay petrology of specific mudrock units. Keller and Ting disaggregated and studied one sample of the Perry Farm Shale. Blatt and Schultz studied quartz grains in a variety of mudrocks. Other studies have been bulk mineral analyses using X-ray diffraction; for example, Shaw and Weaver (1965), Schultz (1964), and Tourtelot (1962). One objection to using only X-ray analysis to study mudrocks is that distinctive petrographic or mineralogic characteristics of the non-clay portion cannot be determined. The significance of this objection is seen by a petrographic point count of the coarse silt size fraction of some Pierre Shale samples. The

[1] In this paper the term Pierre Shale is meant to include the Pierre Shale and adjacent marine, time-equivalent mudrock units.

point count revealed that more than 25% of the grains were chert, rock fragments (other than undisaggregated mudrock fragments) and a variety of other minerals which occurred in appreciable amounts.

The objectives of this study are to determine, in an areally extensive shale unit, if the non-clay mineral dispersal pattern can be identified and related to the following:

1. Provenance
2. Transporting mechanism
3. Paleoclimate
4. Diagenetic alterations

The general question to be studied is: can the non-clay portion of a shale be used to interpret its petrogenetic history.

GEOLOGIC SETTING

Study Area

The Pierre Shale was deposited during the Upper Cretaceous period, in a large inland seaway (Fig. 1). This seaway had an east-west width exceeding 1,200 km., a north-south length of 3,200 km., and an area of more than 3.8×10^6 km^2 (Gill and Cobban, 1966). The seaway existed for nearly 10 million years and was bounded on either side by topographically low areas of non-marine sedimentation approximately 400 km. wide.

Stratigraphy

This study includes all marine shales in the western interior of North America which are time equivalents of the Pierre Shale. The reference section of the Pierre Shale at Red Bird, Wyoming (Gill and Cobban, 1966) is considered to be the type section for the Pierre Shale in this study. However, due to the areal extent, duration of sedimentation, and regressive-transgressive character of Pierre sediments, a complex stratigraphic terminology has evolved.

The Red Bird section as well as other areas have been zoned on the basis of ammonites. The ammonite zones shown in Figure 2 allow the lithostratigraphic units of the Pierre Shale to be accurately correlated. Correlations of the equivalent marine shales and sandstones in the United States are shown in Figure 3. Although most of

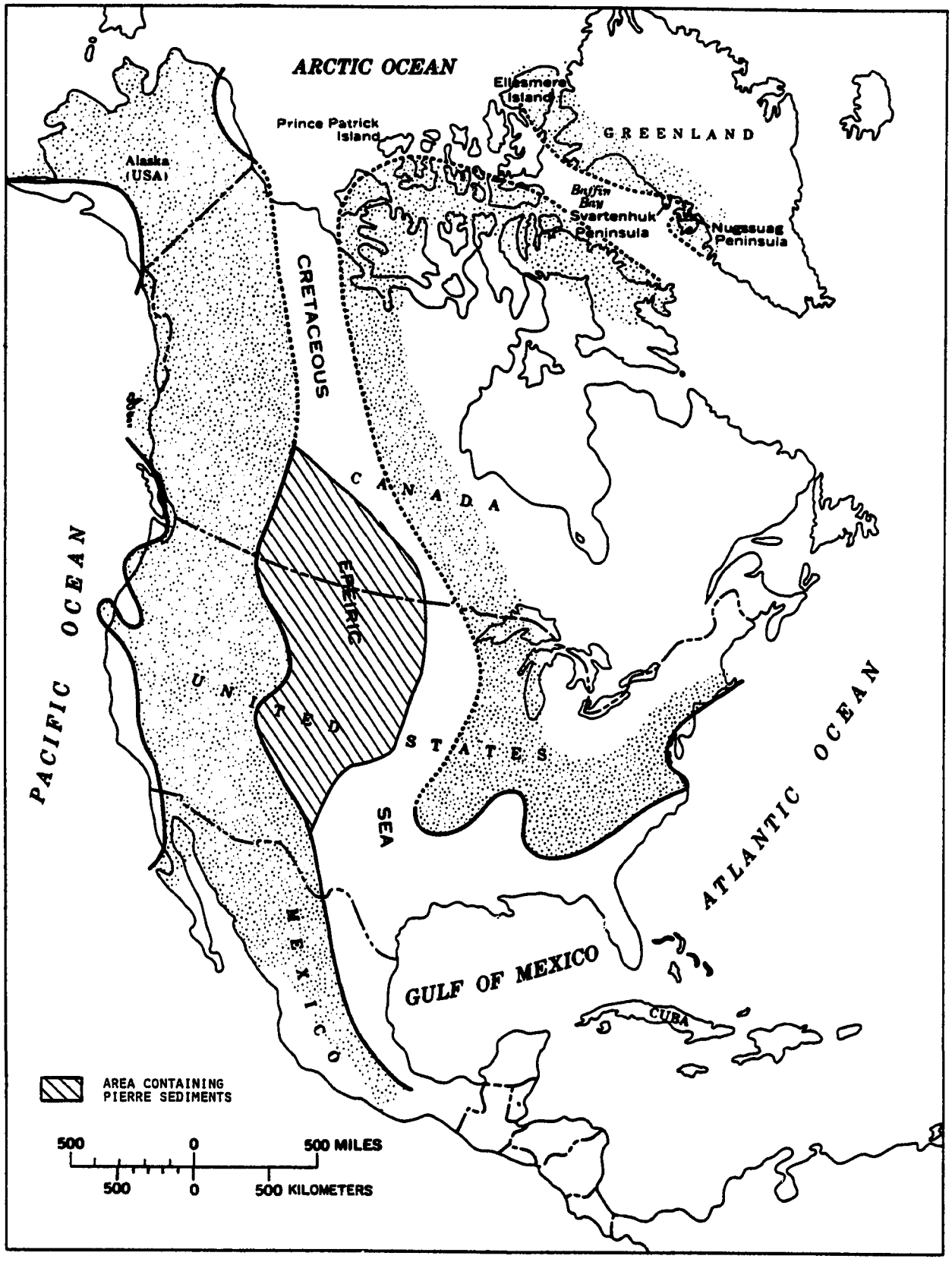

Fig. 1. Probable distribution of land and sea in North America during late Campanian time showing the geographic position of the seaway that divided the continent into eastern and western parts. Modified from Gill and Cobban (1966, fig. 15).

Upper Cretaceous stages and substages		Potassium-argon dates	Estimated dates	Western interior ammonite sequence [1]
		Millions of years		
Maestrichtian	Upper	63	63	
		64±2	64	
			65	
		66±2	66	
			67	
	Lower		68	*Discoscaphites nebrascensis*
				Discoscaphites roanensis
			69	*Sphenodiscus (Coahuilites)*
				Baculites clinolobatus 24
?		70	70	*Baculites grandis* 23
				Baculites baculus 22
Campanian	Upper		71	*Baculites eliasi* 21
				Baculites jenseni 20
			72	*Baculites reesidei* 19
				Baculites cuneatus 18
		75±2	73	*Baculites compressus* 17
				Didymoceras cheyennense 16
			74	*Exiteloceras jenneyi* 15
				Didymoceras stevensoni 14
		75.5±2	75	*Didymoceras nebrascense* 13
				Baculites scotti 12
			76	*Baculites gregoryensis* 11
				Baculites perplexus (late form)
			77	*Baculites gilberti* 10
				Baculites perplexus (early form)
			78	*Baculites* sp. (smooth)
				Baculites asperiformis 9
		79.5	79	*Baculites mclearni* 8
				Baculites obtusus 7
	Lower		80	*Baculites* sp. (weak flank ribs) 6
				Baculites sp. (smooth) 5
		81±2	81	*Scaphites hippocrepis* III
				Scaphites hippocrepis II 4
			82	*Scaphites hippocrepis* I 3
Santonian (part)	Upper			*Desmoscaphites bassleri* 2
			83	*Desmoscaphites erdmanni* 1

Type Montana Group

[1] Arabic numbers refer to strandlines shown in Gill and Cobban (1973, Figures 13-14 and 16-20).

Fig. 2 Time relation of the type Montana Group, central Montana, to the standard stages of the Upper Cretaceous, to potassium-argon dates, and to the western interior ammonite sequence (Modified from Gill and Cobban, 1973, Table 2).

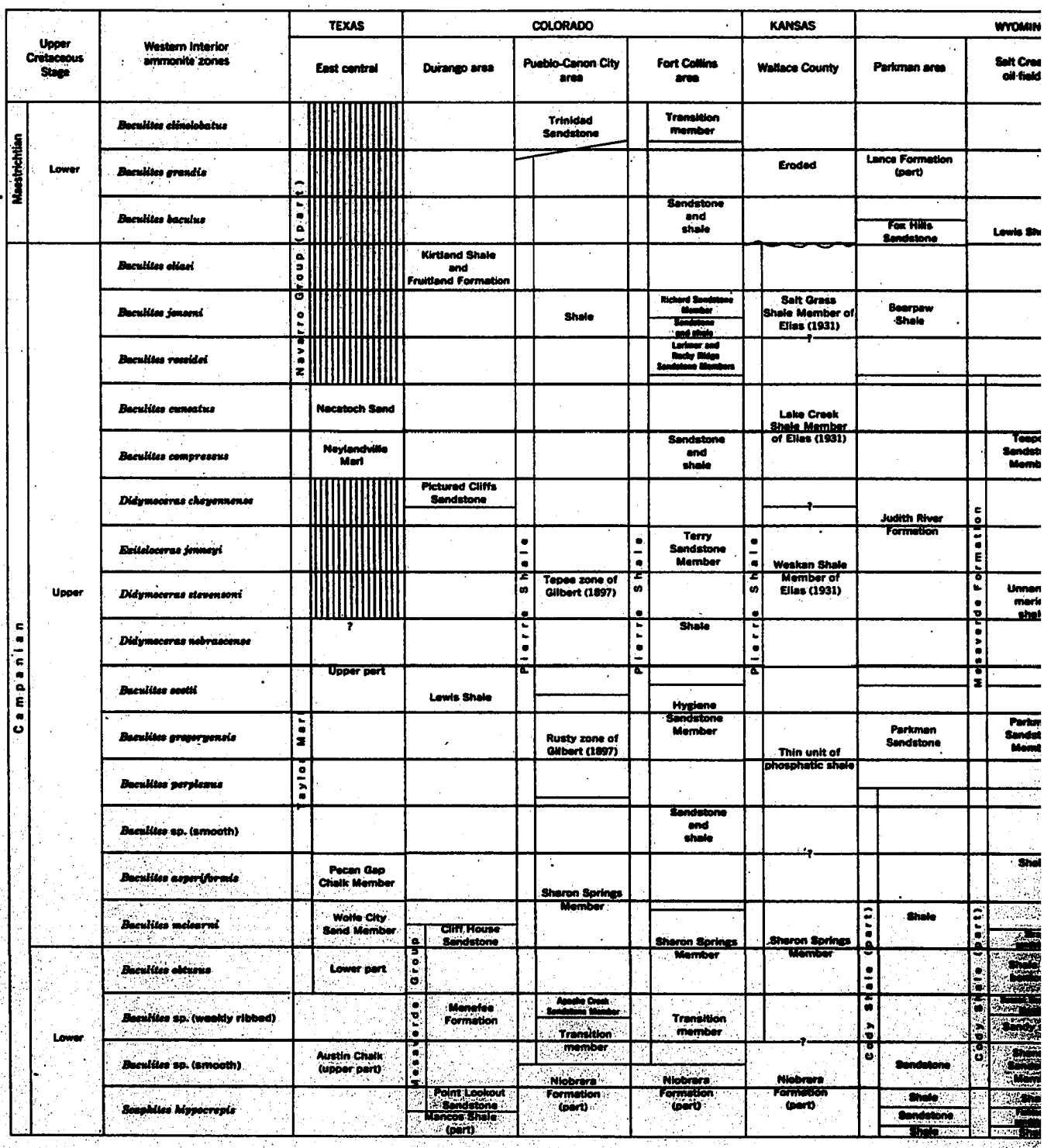

Fig. 3. Chart showing the correl
county, Wyoming, with equivalent
Alberta, and East-central Texas.

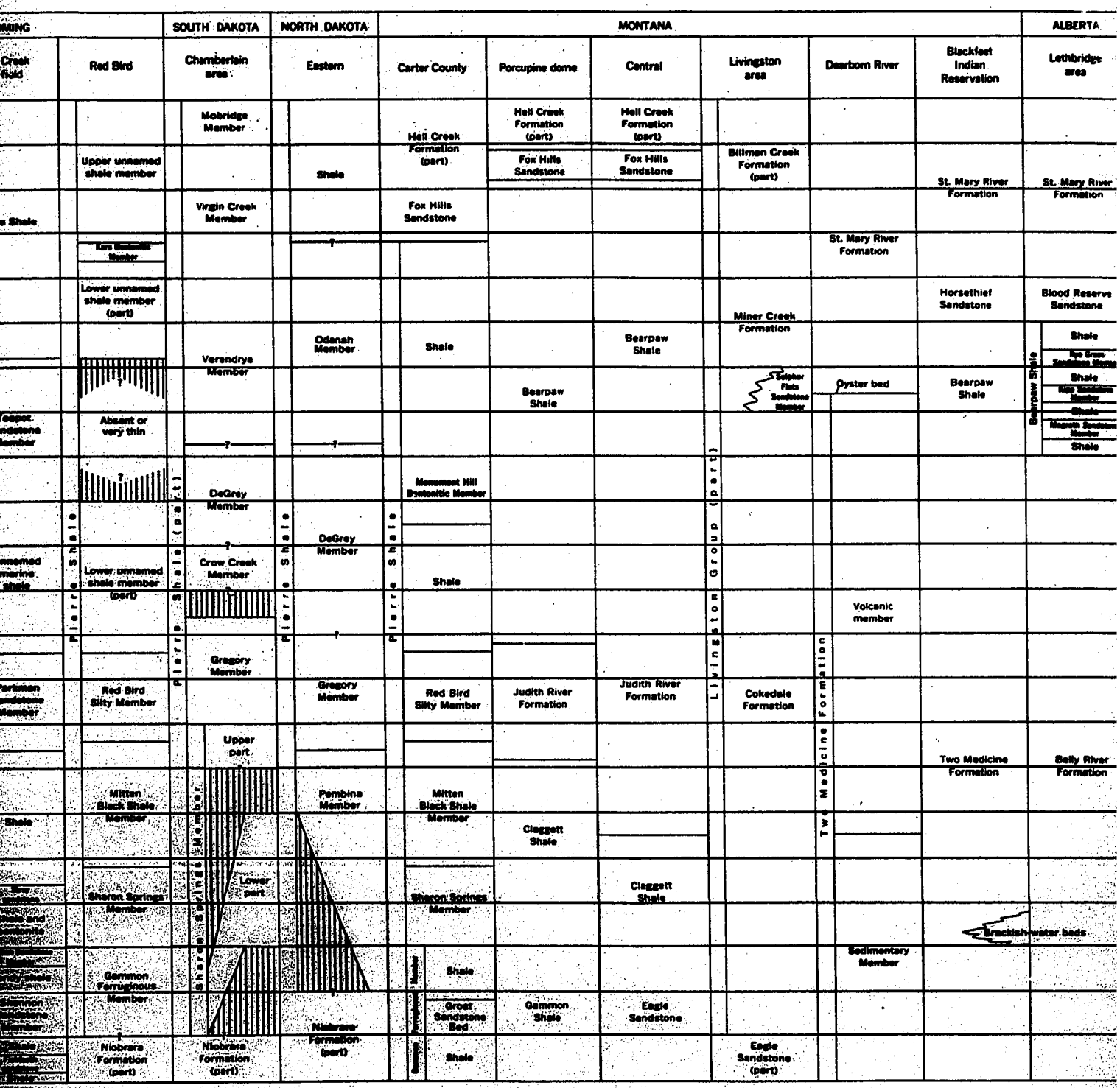

lation of the Red Bird section, Niobrara
rocks in the Western Interior, Southern
Modified from Gill and Cobban (1966, plate 1).

the lithostratigraphic units have been correlated with ammonite zones in the United States, only a few have been correlated in Canada. Therefore, the correlation of lithostratigraphic units in Canada shown in Figure 4 is based principally on lithostratigraphic correlations. The use of ammonite zones allows time-stratigraphic relationships to be determined with unusual precision. Although the lithostratigraphic correlations do not show as much detail, they still may be used to identify most of the time-stratigraphic relationships.

The stratigraphic nomenclature for the Pierre Shale and its time equivalent units are summarized by Gill and Cobban (1966) and Williams and Burk (1964).

Variations in the Extent of the Pierre Seaway

Eastern Shoreline. The position of the eastern shoreline is not known. Sediments along the eastern edge of Pierre outcrops are extremely fine grained. Deposits which are time-equivalent to the Pierre in the Gulf Coast states are also fine-grained mudstones and marls.

Previous studies have placed the eastern shoreline near the edge of Cretaceous deposits (see fig. 1). However, there is little evidence to support this location as the shoreline position and the eastern shoreline may have been as far east as the Appalachian Mountains.

Western Shoreline. Stratigraphic studies of the western shoreline of the Pierre seaway by Weimer (1960) showed two regional transgressive cycles which affected sedimentation throughout the seaway. The

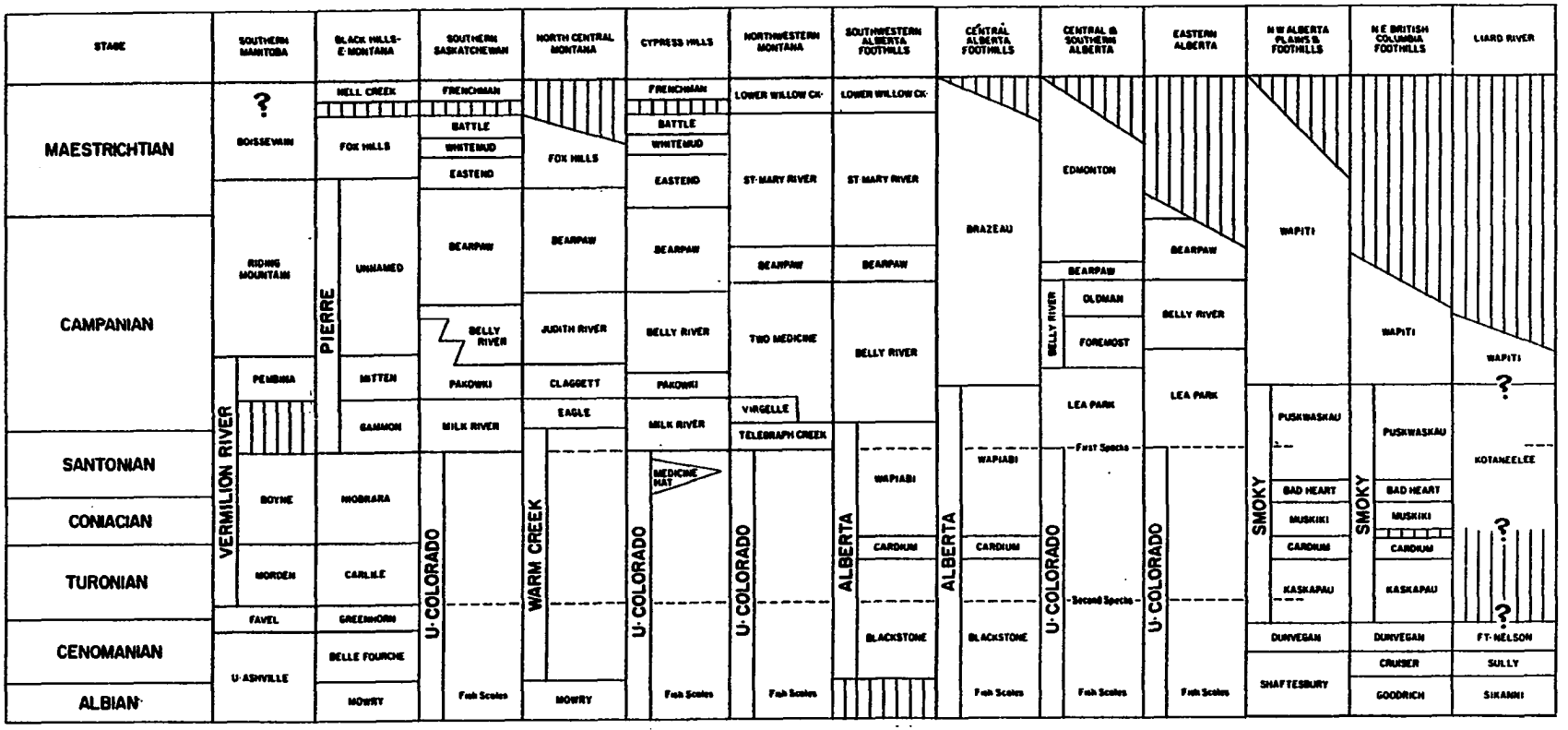

Fig. 4. Upper Cretaceous correlation chart, western Canadian plains and foothills. Modified from Williams and Burk (1964, fig. 12-1).

shorelines during the first transgressive-regressive cycle varied by approximately 150 km.; during the second cycle, shoreline position migrated over a distance of up to 600 km. Weimer (1960) states that movements of strandlines were controlled largely by basin tectonics, rather than by the supply of sediments; also that gaps in the stratigraphic record are the result of periods of non-deposition rather than unconformities.

Gill and Cobban (1973, 1966) also interpreted the cycles of sedimentation in the Pierre Shale. They, too, interpret the Pierre seaway to have had two transgressive and regressive cycles. The positions of strandlines during the periods of near-maximum transgression and regression are shown in Figure 5. The cycles of Gill and Cobban are compatible with those of Weimer (1960). Gill and Cobban (1973), however, stated that the regression and transgression were controlled largely by local crustal instabilities and sediment supply, rather than eustatic or epeirogenic movements as Weimer believed.

As shown by Gill and Cobban, not all of the movements of strandline can be explained in terms of eustatic movements. But to have had as much movement of the strandline as occurred over the entire depositional basin of the Pierre during the Judith River regression, some eustatic movements must have occurred.

In general the depositional history of the Pierre Shale can be summarized as resulting from a slowly narrowing seaway with two major transgressive pulses. Regional movements of the strandlines were controlled largely by rapid epeirogenic movements of the crust, while local crustal movements and sedimentation rates controlled the rate

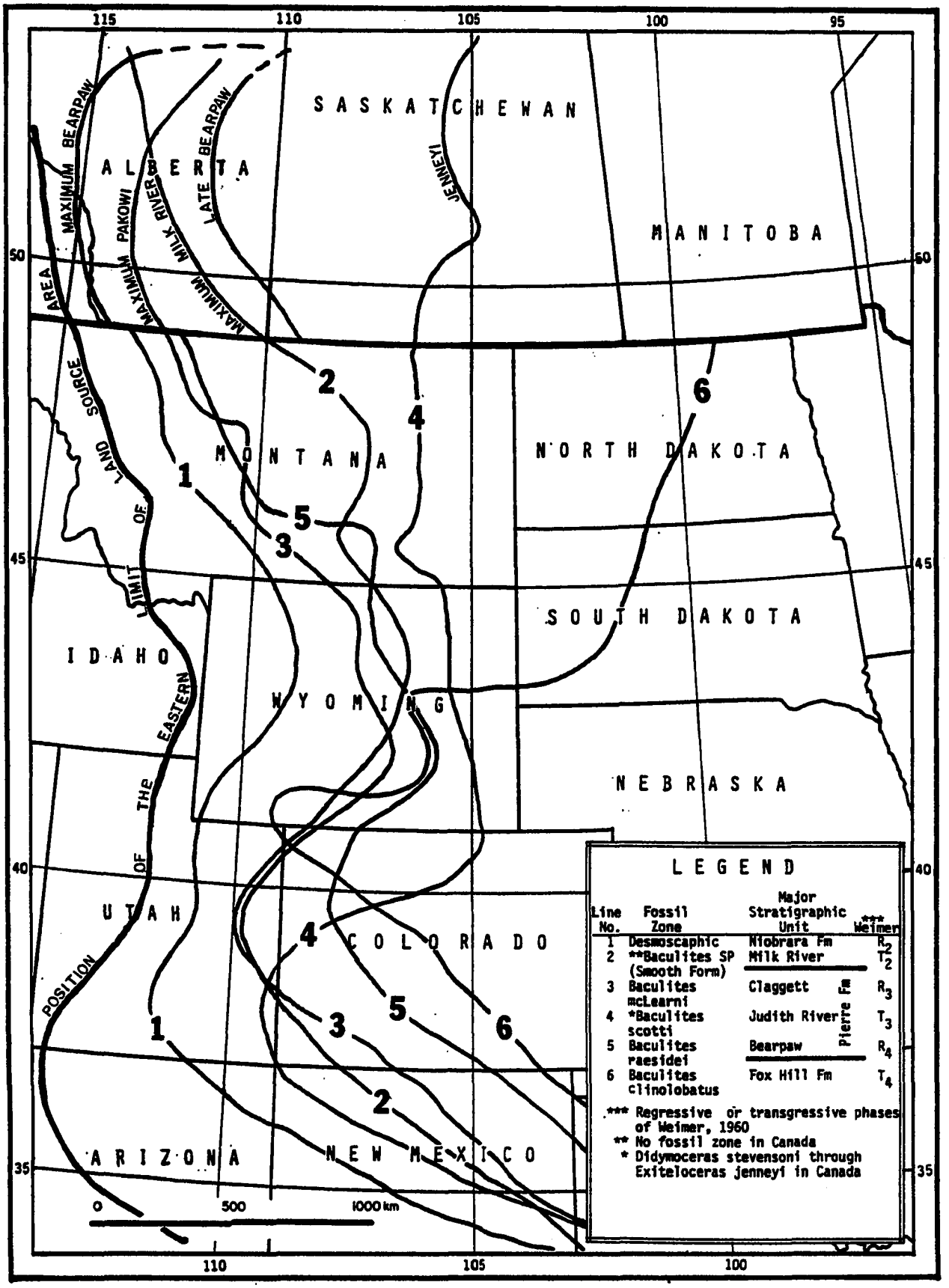

Fig. 5. Positions of the Pierre Seaway during near-maximum regressions and transgressions of the Pierre Seaway. Modified from the data of Gill and Cobban (1969), Caldwell (1968), and Russell (1939).

and direction of strandline movement locally.

Possible Source Areas

The possible source areas of sediment for the Pierre Shale can be grouped on the basis of their predominant rock type. For this study the areas have been broken down as shown in Figure 6 and Table 1.

Eastern U.S. Source Areas. The source areas in the eastern United States must have been almost entirely sedimentary as this area is presently covered by sedimentary rocks older than Upper Cretaceous. Most of the rocks which are still present in this area are Paleozoic limestones and shales. Although it is possible that some Mesozoic rocks were present and being eroded during Pierre time, it is unlikely that they were extensive units. Published data indicate that this area was positive during most of the Mesozoic. There may have been a number of small areas of exposed igneous and metamorphic rocks, but the amount furnished would have been insignificant as a source for Pierre sediments.

Eastern Canadian Source Areas. Rocks presently exposed in areas of eastern Canada (including northern portions of Minnesota and Wisconsin) are predominantly Precambrian igneous and metamorphic rocks. This source area could have had a much larger percentage of sedimentary rock cover during the deposition of Pierre sediments.

Western Canadian and Northern U.S. Source Areas. Due to the intrusion of many igneous rocks, and the post-Cretaceous deformations which have occurred in this area, not much is known about the source rocks which

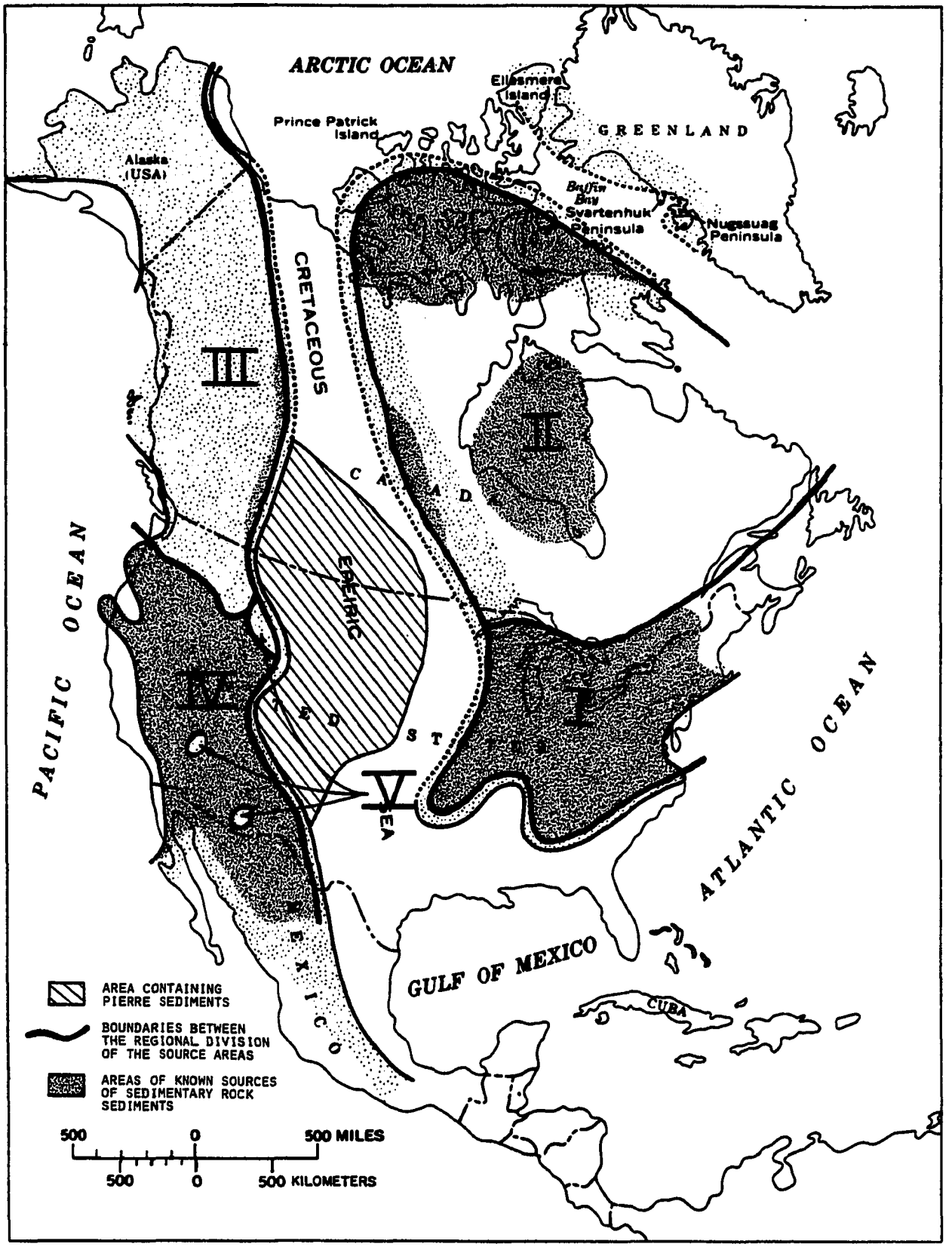

Fig. 6. Generalized map showing the regional breakdown of the sediment source areas as discussed in the text. The map also shows the areas which are known to have provided sedimentary rock detritus to the Pierre Seaway. Base map modified from Gill and Cobban (1966, fig. 15).

Table 1. Composition of the possible source areas for the Pierre sediments.

		Major Rock Types	Minor Rock Types
I	Eastern U. S.	Sedimentary (Mostly Carbonates)	
II	Eastern Canada	Igneous and Metamorphic	Sedimentary
III	Western Canada and Northern U. S.	Sedimentary	Igneous, Metamorphic, and Volcanic
IV	West-Central and Southwestern U. S.	Sedimentary (Mostly Carbonates)*	
V	Areas with Active Volcanism During Pierre Time	Volcanic Ash	

Data summarized from the Geological Map of North America (Goddard, 1965).

* Gilluly (1963)

were present during the deposition of Pierre sediments. As shown in Figure 7, sedimentary and possibly metamorphosed sedimentary rocks were an important source of sediments. Possible volcanic source rocks will be discussed in a later section.

West-Central and Southwestern U.S. Source Areas. Source areas in this region have also been affected by post-Cretaceous deformation. The type and nature of this deformation allow the reconstruction of the area before the tectonic events, and shows that nearly all of the source rocks were sedimentary (McGookey, 1972). The volcanic source rocks in this area will be discussed in the next section.

Areas with Active Volcanism During Pierre Time. Five areas in the western United States and Canada are known to have had volcanic activity during Pierre time. Other areas are known to have had either igneous intrusions or active volcanism just before or after Pierre time. Figure 8 gives the position of known igneous activity during the time of deposition of the Pierre Shale.

Three of the active volcanic areas were located in central and southwestern Montana, the Elkhorn, Adell Mountain, and Livingston Volcanics. These areas are important in considering possible source rocks as they were located at the edge of the seaway.

The Elkhorn Mountain Volcanics were associated with the intrusion of the Boulder Batholith. Their remnants form one of the three largest ash-flow fields known (Smith, 1960). These volcanics once covered an area of 25,000 km^2, were more than 3 km. thick, and had an estimated volume of 2000 to 4000 km^3. Their composition varies from rhyolites to basalts with andesites being most common.

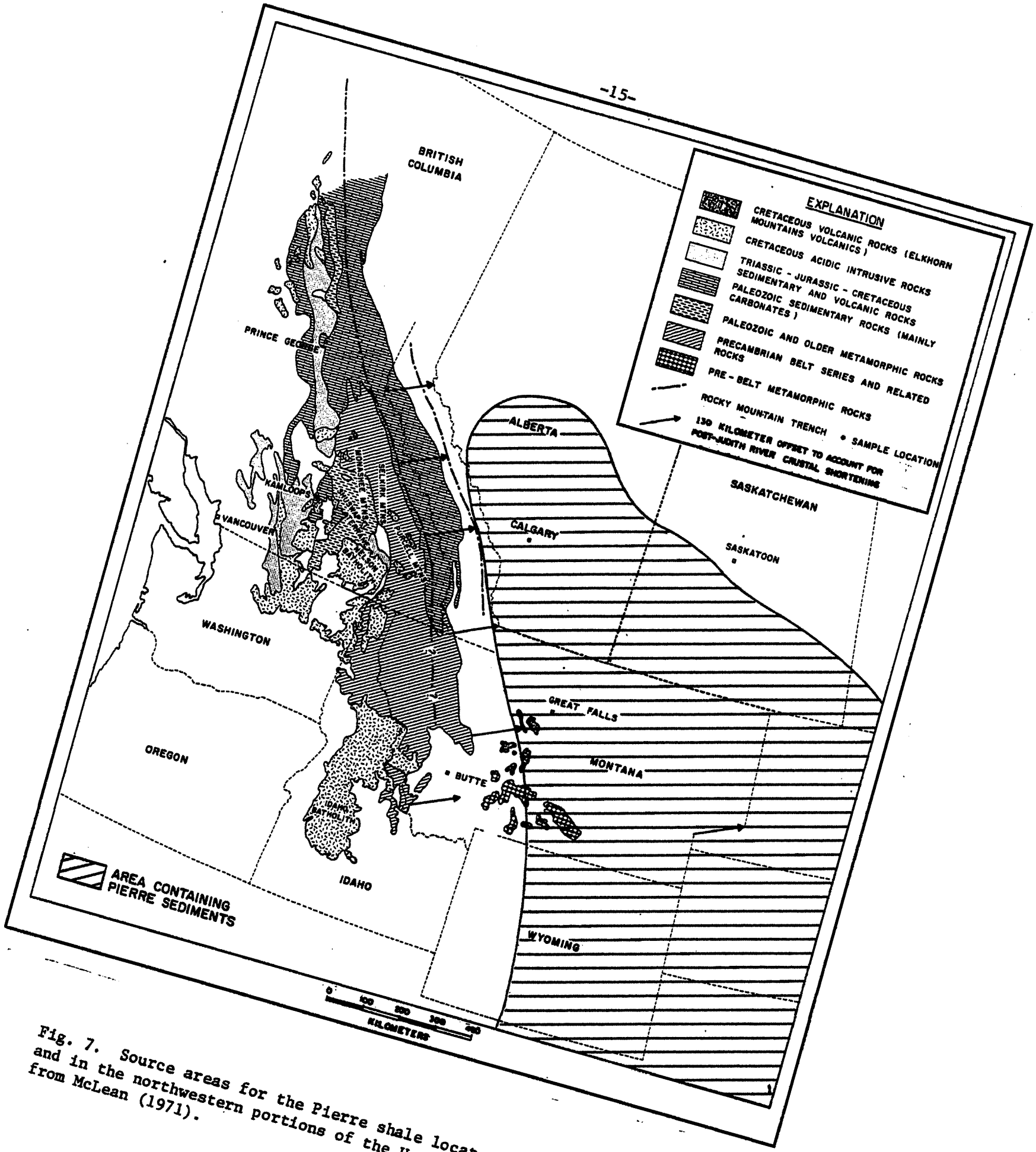

Fig. 7. Source areas for the Pierre shale located in western Canada and in the northwestern portions of the United States. Modified from McLean (1971).

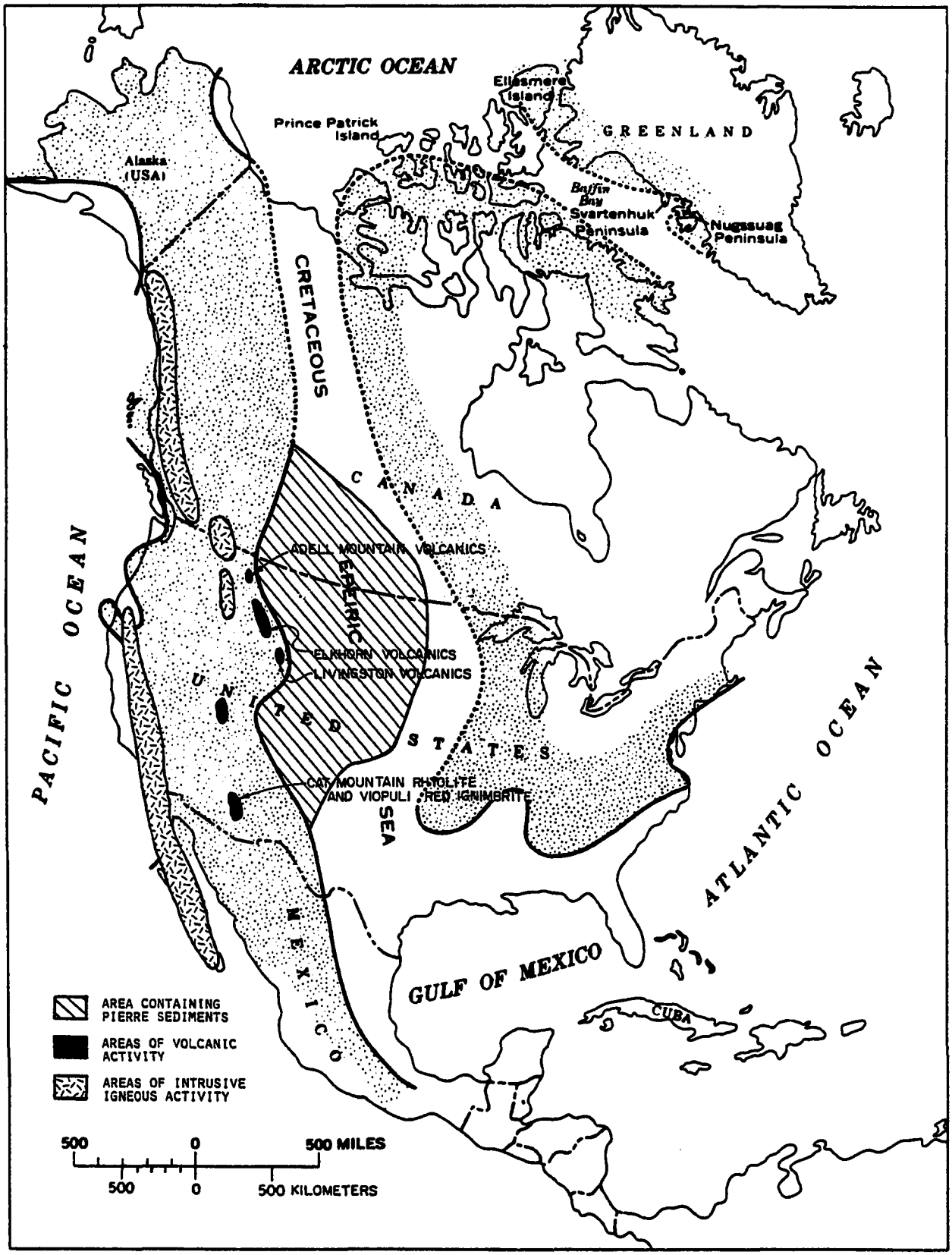

Fig. 8. Generalized map showing areas of igneous activity known to be active during the time of the deposition of the Pierre sediments. Base map modified from Gill and Cobban (1966, fig. 15).

The Adell Mountain Volcanics are located east of the Elkhorn Volcanics. Remnants of these volcanics are considerably smaller in size and are generally of trachybasalts and basalt agglomerates.

The Livingston Volcanics are the same composition as the Elkhorn Volcanics, but only a few small volcanic vents have been found. The existence of extensive volcanism in the area can be inferred only from the volcanogenic sediments of this area.

The Elkhorn and Livingston volcanics are known to have been active throughout the deposition of Pierre sediments. The Adell Mountain Volcanics were active only during latest Pierre time.

The Cat Mountain Rhyolite and the Viopuli Red Ignimbrite in southeastern Arizona are equivalent in age to late Pierre deposits. These deposits are now thin and not laterally extensive, and formed only during latest Pierre time.

Rhyolitic and andesitic volcanic rocks equivalent in age to Pierre sediments are also found in eastern Utah and western Nevada.

There could have been volcanic source rocks in other parts of the western source area during Pierre time which have been removed by erosion. In many areas of the western source area there are intrusive igneous rocks which were emplaced during Pierre time. The possibility that these igneous bodies had associated volcanic deposits is suggested by Hamilton and Myers (1967):

> A survey of features of batholiths in the United States is interpretated to indicate that batholiths are thin, having spread out laterally at shallow depth, and that many of them reach the surface and crystallize beneath a cover of their own volcanic ejecta.

This also raises the possibility that areas which now have exposed igneous rock which were emplaced before and during Pierre time were covered

with volcanic rocks during Pierre time.

Relative Importance of These Source Areas

The thickness of the Pierre Shale and the inferred directions of sediment transport can be used to evaluate the relative importance of these source areas. Figure 9 is an isopach map of the Pierre Shale. From this map it seems likely that nearly all of the sediments were derived from the western shore. Based on rates of sedimentation into the Pierre seaway Gill and Cobban (1973) concluded that the source area was mainly from eastern Idaho, the Elkhorn Volcanics and sources to the north. Gilluly (1963), in trying to reconcile the volume (4×10^6 cubic km^3) of Upper Cretaceous sediments with the source area, concluded that all of these sediments could not have been derived from this source and that the majority of Upper Cretaceous sediments were transported in from Mexico or Canada.

In conclusion, then, it appears that the eastern shoreline did not furnish a significant amount of sediment into the Pierre seaway and that the most important sources were along the western shore.

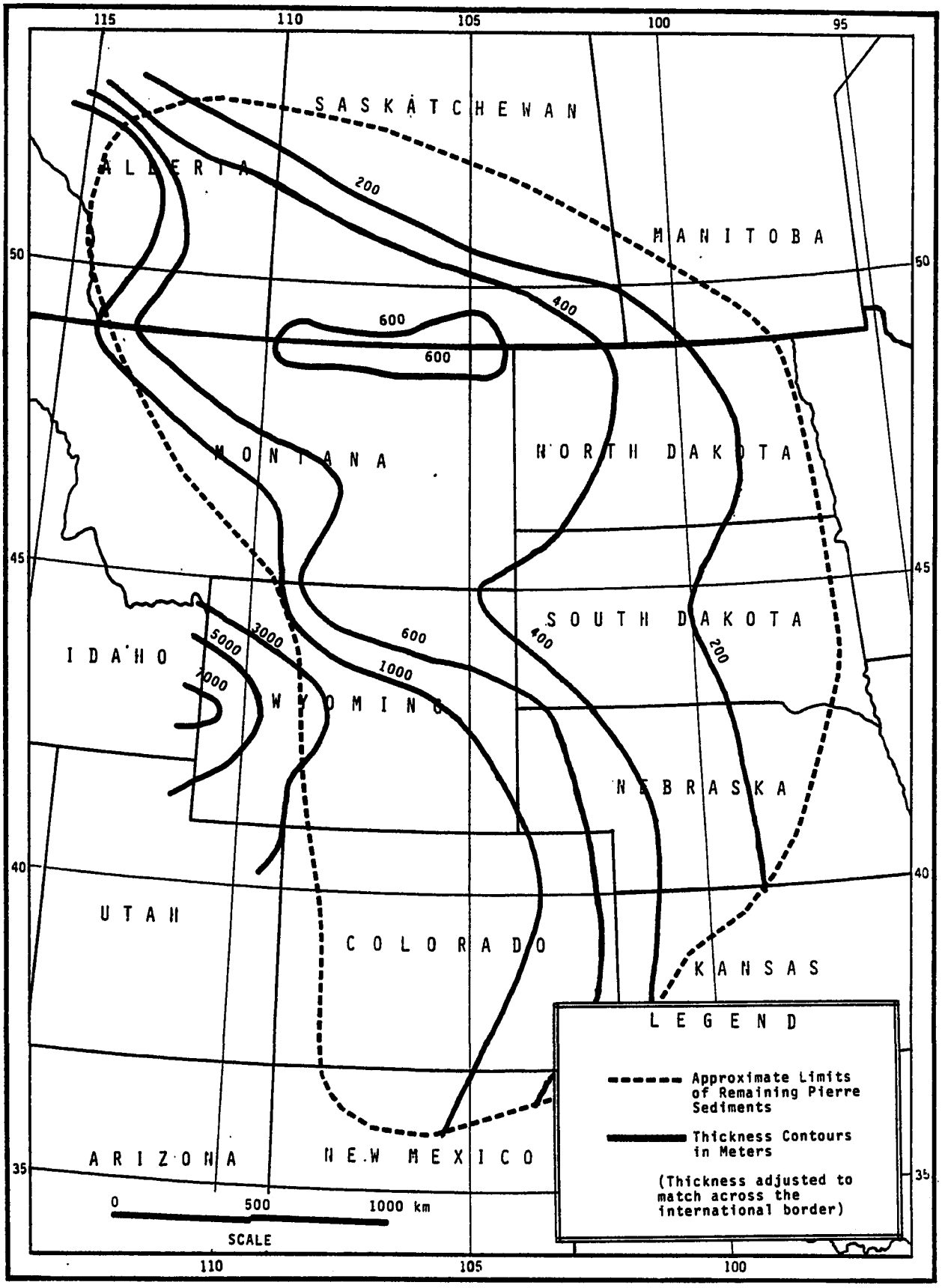

Fig. 9. Generalized Isopach Map of Pierre Sediments.
Modified from maps by Reeside (1944) and Williams and Burk (1964).

SAMPLING AND METHOD OF STUDY

The Pierre Shale was sampled throughout most of its extent. After sampling, three basic groups of data were collected.

1. General characterization of the physical and mineralogic characteristics of the samples.
2. Detailed mineralogic and petrographic analysis of the non-clay portion of the sample.
3. Size analysis of the non-clay portion of the sample.

Sampling

Surface samples were obtained by digging a hole in the outcrop about 0.5 m deep, then picking out approximately 500 grams of shale chips from the bottom of the hole. Samples were taken only if the shale chips were solid and did not appear to be weathered. The location of each sample is given in Appendix 1.

The stratigraphic position in the Pierre Shale from which each sample was taken was identified using geologic reports that discuss the stratigraphy of the area. The stratigraphic intervals were then related to the ammonite range zones found within them. The approximate distances of the samples from the western shoreline were determined using the paleogeographic maps of Gill and Cobban (1969, 1973) which show the approximate position of the shoreline during the intervals of time occupied by specific ammonite zones. Also used were the paleogeographic maps by Russell (1939) and Caldwell

(1968) for samples located in Canada. Details of how the ammonite zones and the distance to the shore were determined are given in Appendix III. The ammonite zones and the distance to the nearest western shoreline of each sample are given in Appendix III. The paleogeographic maps of Gill and Cobban (1969, 1973) also were used to estimate the distance to the volcanic source areas in southwestern Montana.

A few areas which were mapped as shale contained only muddy siltstones and sandstones. If these units could be identified as Pierre Shale equivalents, they were sampled. All of the subsurface samples used were from cores supplied by the Saskatchewan Provincial Core Library.

Sites were chosen for intensive sampling to evaluate stratigraphic variations in mineral composition, one at Red Bird, Wyoming, the other from a core from an oil well in southeastern Manitoba. The samples from Red Bird were surface samples from an area in which the ammonite zones had been mapped in detail by Gill and Cobban (1966). The oil well samples are from the Bobjo Alameda Well #1 located in southeastern Manitoba. The stratigraphic intervals sampled by each of the cores are shown in Appendix I.

General Characteristics of Samples

Characteristics which were described for each sample were rock type, rock color, and the presence of secondary minerals or mineral coatings. These descriptions are given in Appendix I.

Qualitative X-ray analyses were made to identify the minerals present in each sample. By measuring the height of the major X-ray peak for each mineral it is possible to make comparisons of the relative amounts of minerals present. The results of these analyses are given in Appendix II, and a more detailed discussion of this method is given in Appendix IV.

Detailed Mineralogic, Petrographic and Chemical Analyses

The chemical, mineralogic, and petrographic data used in this study were collected using the methods listed below:

1. Bulk chemical analyses
2. Quantitative X-ray diffraction analyses
3. Selective mineral destruction analyses (bisulfate fusions)
4. Petrographic analyses

These data then were combined to give a systematic mineralogic characterization of the shale samples.

Bulk Chemical Analyses

Bulk chemical analyses were made for the oxides SiO_2, Al_2O_3, K_2O and SO_3, These analyses were made using standard X-ray fluorescence techniques which are described in Appendix V. The standards used for these analyses were Pierre Shale samples which had been previously analyzed by wet chemical methods. The reproducibility of this method was determined to be ±5 percent of the amount present and the accuracy to be ±10 percent of the amount present. The techniques used are described more completely in Appendix V and the results also are given in Appendix II.

The percentage of carbonate was determined from the percentage of sample soluble in 1.0 N HCl. The accuracy of this method was evaluated using blank samples (samples containing no carbonate as determined by X-ray diffraction), and samples in which the percentage of CO_3^{-2} had been previously determined using wet chemical techniques. From this evaluation the accuracy was determined to be ±0.5 percent of the sample. The percentage of water loss after drying for 24 hours at 110°C also was determined when the carbonate analyses were done. A more detailed discussion of the water

loss and carbonate analyses is given in Appendix VI and the results are given in Appendix II.

Quantitative X-ray Diffraction

The concentrations of quartz and cristobalite were determined using quantitative X-ray diffraction methods. The samples and standards used for the X-ray diffraction analyses were ground to less than 80 mesh and compressed into spectrographic pellets 2.5 cm in diameter and approximately 4 mm thick. X-ray diffractograms were made of these pellets while the pellet was being rotated in the focusing plane of a powder diffractometer. Through the use of this procedure the reproducibility of the measurements of the diffraction peaks (height times width at 1/2 height) was better than ±5 percent of the amount present. The standards for the quartz concentrations were obtained from Pierre samples which were analyzed using the procedures described in the next section. The accuracy of the X-ray quartz determinations are considered to be ±5 percent of the amount present.

Cristobalite standards used for the X-ray analyses were Pierre Shale samples in which the cristobalite concentrations were very high and the percentage of cristobalite could be accurately calculated based on a chemical and mineralogic mass balance. The accuracy of this method was estimated to be ±10% of the amount present. A detailed description of how the accuracy of this method was evaluated is given in Appendix IV.

Selective Mineral Destruction Analyses (bisulfate fusions)

The selective mineral destruction techniques are based on the differential chemical solubilities of minerals in sodium bisulfate. This technique was used primarily to isolate the quartz and feldspars in the shale samples.

The technique used is a variation of the technique described by Kiely

and Jackson (1965). The technique selectively removes the clay mineral fraction by fusing it with sodium bisulfate and then dissolving the fused product in sodium hydroxide. This procedure also removes the iron oxides, carbonates, gypsum, zeolites, cristobalite, and most of the heavy minerals. Quartz and feldspars are affected only slightly by this technique.

The effect of the bisulfate fusion on the quartz and feldspar fraction (Q + F fraction) is a function of both size and feldspar composition. The effect of grain size and composition can be seen in Table 2 and Table 3.

After the Q + F fraction (the residue remaining after the bisulfate and sodium hydroxide treatments) was obtained, chemical analyses for K, Na and Ca were made of the Q + F fraction by means of atomic absorption spectrophotometry. The results of these chemical analyses were used to calculate the amounts of normative potassium, sodium, and calcium feldspars present. From these calculations the percentage of quartz in the quartz plus feldspar fraction and in the whole rock was determined.

The bisulfate and sodium hydroxide treatments cause a small change in the chemical composition of the feldspar. These effects are controlled by the composition and size of the feldspar grains (Table 2). The effect is to reduce the amounts of quartz and feldspar present and to increase the amounts of sodium feldspar relative to potassium and calcium feldspar. Unless the samples have radically different grain size distributions or plagioclase compositions, the relative differences between samples are not affected by these techniques.

The amounts of feldspar and quartz determined are corrected for the effects of these techniques using the data given in Table 2 and Table 3. However, the correction of the amounts of quartz and feldspar assumes the

Table 2. Affects of the bisulfate fusion on the chemistry of various feldspars.

Mineral	Size Range in Microns	% Retained in Fusion	Concentration Before Fusion Ca	K	Na	Concentration After Fusion * Ca	K	Na
Microcline	61-43	97.5	.07	10.37	2.19	.07	10.23	2.29
	43-30	95.4	.13	9.89	2.14	.12	9.92	2.27
	30-20	95.1	.09	9.98	2.16	.07	9.53	2.42
	20-10	95.4	.14	9.82	2.16	.08	8.42	2.31
	10- 4	94.9	.06	9.77	2.16	.07	9.26	2.49
	4- 1	82.1	.06	9.65	2.20	.04	7.24	3.13
Albite (Ab 91.3%, An 8.7%)	61-43	94.5	1.03	.75	7.01	1.12	.56	7.36
	43-30	94.3	1.07	.74	6.83	1.12	.56	7.26
	30-20	94.4	1.06	.75	6.75	1.19	.54	7.26
	20-10	96.3	1.06	.84	6.71	1.10	.57	7.25
	10- 4	89.0	1.06	.88	6.83	1.13	.53	7.26
	4- 1	82.7	1.03	.99	6.78	1.11	.52	7.43
Oligoclase (Ab 77.2%, An 22.3%)	61-43	95.4 96.0 94.6	2.85	.77	5.74	2.97	.68	6.01
	43-30	97.2	2.68	.68	5.63	2.68	.58	5.84
	30-20	94.6	2.59	.83	5.61	2.70	.67	5.75
	20-10	89.5	2.59	.73	5.54	2.62	.60	5.76
	10- 4	91.5	2.78	.83	5.86	2.90	.60	6.09
	4- 1	83.3	2.76	1.34	5.73	2.93	.31	6.35
Andesine (Ab 52.2%, An 47.8%)	61-43	88.3	5.98	.68	3.88	5.93	.68	3.88
	43-30	85.8	5.63	.74	3.68	5.81	.76	3.92
	30-20	83.8	5.40	.81	3.54	5.70	.85	3.84
	20-10	77.1	5.28	.87	3.46	5.47	.96	3.71
	10- 4	74.8	5.16	.65	3.52	5.72	.55	3.99
	4- 1	66.0	5.00	.69	3.39	5.77	.45	4.09
Bytownite (Ab 26.0%, An 74.0%)	61-43	76.4	8.99	.07	1.96	8.11	.06	1.73
	43-30	66.8	9.34	.07	1.95	8.54	.06	2.03
	30-20	62.9	9.01	.05	1.89	8.61	.06	1.98
	20- 4	22.4	8.96	.05	1.91	2.48	.04	4.44
	4-.2	18.6	9.03	.08	2.06	2.99	.05	3.51

* Concentration given as weight % element.

Size μm	% Loss in Fusion
61 - 43	.8
43 - 32	.6
32 - 16	.7
16 - 8	.9
8 - 4	3.0
4 - 2	2.0
2 - 1	10.8

Table 3. Effect of pyrosulfate fusion on quartz.

following:

1. The size distribution of the feldspar is similar to that of the quartz in the sample.
2. The plagioclase feldspars have an anorthite composition of less than 30%, as plagioclase with higher anorthite compositions are more soluble in the bisulfate fusion.

Details of this technique and its error are given in Appendix VII, and the data collected using this technique are given in Appendix II.

Petrographic Analyses

Petrographic analyses were made of the >43 μm size fraction of samples which had been disaggregated. The objective of the petrographic analyses was to determine the mineralogic compositions and petrographic characteristics of this fraction of the samples. Petrographic analyses were also made of this fraction after the quartz and feldspar had been isolated by bisulfate fusions.

Normative Calculations of the Clay Fraction and Sulfur-bearing Minerals

Due to variations in the mineralogic structures, chemistry, and particle sizes, the concentrations of the clay and sulfur-bearing minerals could not be directly determined, and therefore their concentrations had to be estimated using normative calculations.

Sulfur-bearing minerals. Only three sulfur-bearing mineral phases are found commonly in the Pierre Shale. These are gypsum, pyrite, and jarosite. The concentrations of these constituents were determined by normative calculations based on the amount of SO_3 present in the sample and the mineralogy of the sulfur-bearing minerals as determined by the qualitative X-ray analysis. For example, if the X-ray data indicated that gypsum was the

sulfur-bearing mineral present, the concentration of SO_3 was multiplied by the ratio of the weight of SO_3 in gypsum to weight of SO_3. Since sulfur also is found in the organic matter present in these shales, the results of the normative calculations are considered to be the maximum amount of sulfur-bearing mineral phases that could be present in these samples. The results of these calculations are given in Appendix II.

Clay Fraction. The concentration of clays in the samples was calculated by subtracting the concentration of all of the non-clay phases from 100 percent. The phases considered not to be clay were quartz, cristobalite, feldspar, carbonates, gypsum, pyrite, jarosite, and uncombined water. The only phases commonly found in the Pierre Shale which are not listed above are generally considered to be clay phases or are clay in terms of size. These include zeolites, iron oxides, amorphous material and the phyllosilicates. The only zeolite identified in these samples was clinoptilolite and it was found in only one sample. The amounts of zeolites, iron oxides and amorphous material present in these samples could not be estimated accurately, but are considered to be less than a few percent of the whole sample. Therefore, the clay fraction is assumed to be composed of predominantly phyllosilicate minerals.

The error caused by evaluating the amount of clay in this manner is estimated to be ±5 percent of the amount present because this is the error in the determination of the concentration of quartz, the most abundant of all of the phases subtracted to determine the clay concentration.

Phyllosilicate Minerals. Previous studies of the clay mineralogy of the Pierre Shale (Schultz,

1964, 1965, 1978; Tourtlelot, 1962) have shown that illites, montmorillonites and mixed layered illite and montmorillonite are the dominant clay minerals; only minor amounts of kaolinite and chlorites are present. Qualitative analyses of the amounts of illite, chlorite, and kaolinite were made using X-ray diffraction techniques. The procedures used are given in Appendix IV. A complete mineralogic analysis of the phyllosilicate fraction was beyond the scope of this study. However, in order to characterize the general nature of the phyllosilicates, an estimate of the concentration of illite was made. In making this estimate no attempt was made to separate the illite present in mixed layered phases from illite present as a separate phase.

The amount of illite in the sample is estimated from the concentration of potassium in the whole sample. This is done by assuming that illite contains 6.0% potassium and multiplying the concentration of potassium found in the whole rock by 16.6 (100/6.0). The value of 6.0% potassium in illite is the value given by Grim (1968) for the average illite. Other minerals commonly found in the Pierre Shale which contain potassium are potassium feldspars, biotite and jarosite. Biotite has been identified petrographically in the >43 μm fraction of the sample but only in trace amounts. Small amounts of fine-grained biotite cannot be distinguished from illite and therefore no attempt was made to distinguish biotite from illite. The qualitative X-ray diffraction analysis indicates that jarosite is present in only two of the samples, and the calculations indicate that the concentration of jarosite in these two samples is less than 2.6 percent of the whole rock. Since jarosite contains 6.5% potassium and illite contains 6.0% of potassium, the error

caused by neglecting the concentration of potassium in jarosite will be less than 2.6% of the sample. The potassium feldspar concentrations for the 32 samples in which the feldspars were known were analyzed using the bisulfate fusion. For these samples the potassium concentrations were adjusted by subtracting the amount of potassium found in the potassium feldspars, and therefore in these samples the potassium feldspar did not affect the illite concentrations. The potassium concentrations of the remaining samples were adjusted by subtracting the average amount of feldspar potassium (0.36% K_2O) found in the 32 samples in which the potassium feldspar concentrations were known. Based on the standard deviations calculated for these 32 samples (0.23), the error caused by evaluating feldspar potassium in this manner will cause an error in the illite concentrations of less than 7.7 percent 95% of the time.

Size Analyses

Grain size analyses were made of the quartz plus feldspar portion of the sample. The fraction of the sample coarser than 43 μm was obtained by disaggregating approximately 50 grams of sample. The material coarser than 43 μm was then fused to obtain the quartz plus feldspar fraction. This fraction was sieved and the size distribution of the coarser than 43 μm fraction was determined. The size distributions of the less than 43 μm fraction of the fused samples were determined using a photo-electric settling tube and a computer to interpret the data. The data from these two analyses were then combined. For details on the theory and operation of the photo-electric settling tube see Appendix VIII and Appendix IX.

It has been shown in this and previous studies (Dauphine, 1974) that the size distributions of the quartz plus feldspar fraction are not

appreciably affected by the fusion technique. For a more detailed discussion of this method and the data obtained see Appendix VII.

PROVENANCE STUDIES

The primary goal of this study was to determine whether these samples could be used to determine the petrogenetic history of the Pierre Shale. Specifically, how well can the mineralogy of these samples be used to interpret the provenance, mechanism of transport, and paleoclimate?

Stratigraphic Controls

A random sampling of the Pierre Shale was not possible as a large portion of the Pierre Shale is not available to be sampled. Therefore, the samples are biased with respect to their geographic locations, stratigraphic position and other parameters. Even had the sampling not been biased with respect to one variable (say the stratigraphic position of the sample), the fact that it was not biased in this respect means that it would probably be biased with respect to other potentially important variables (perhaps geographic or petrologic variables). Also during the sampling phase of this study, little was known about which sampling variables would be the most important.

Stratigraphic Variables

Stratigraphic variables may bias the study in many ways, some of which are:

1. Changes in the sediment source area compositions with respect to time.
2. Changes in the distance to the source area with respect to time.

3. Changes in the depositional environment with time.
4. Changes in the mechanics of the sediment deposition with time, through biologic and/or tectonic controls.

The effect of these variables was reduced, however, by the methods used to interpret the data.

To reduce the effects of the biologic controls, the data were normalized to exclude the carbonates and cristobalite, constituents which are largely biogenic. However, most specimens contain no carbonate.

Table 4 shows a significant change in the mean percentage of quartz found in the Q + F + C fractions of the samples between the lower Pierre samples (36% quartz) and the middle and upper Pierre samples (27% quartz). As can also been seen in the table there is a significant difference in the mean distance to the nearest shoreline between these sets of samples (lower 187 km, middle 264 km, upper 317 km). As shown in Figure 10, and also in later discussion, the percentage of quartz in the Q + F + C fraction of each sample is related to the distance between the sample location and the nearest shoreline at the time of deposition. Therefore, all data were treated by considering distance to the nearest shoreline as a significant variable.

Using similar lines of reasoning, all of the apparent significant stratigraphic variations seen between the upper, middle, and lower Pierre data subsets can be shown to be related to variables other than general stratigraphic variations. Also, in Tables 5 and 6, the data collected for the stratigraphic cross section samples collected at Red Bird, Wyoming, and from the Bobjo oil well are shown. A comparison of the data from these samples and the stratigraphic

Table 4. Statistical comparison of the data as a function of the samples geographic and stratigraphic locations and type.*

Set or Subset	No. of Elements in Data	COMPONENT ** Distance to nearest Shoreline		% Quartz in Q + F + C		% SiO_2 in Q + F + C		% SiO_2 in F + C		% Al_2O_3 in F + C		% K_2O in F + C		% K_2O in Q + F + C	
Region 1	26	172	122	27.7	5.97	35.9	4.29	49.5	2.40	22.3	1.47	3.58	0.77	2.57	0.51
Region 2	24	634	109	25.6	7.62	36.4	4.79	48.5	4.35	21.9	1.63	3.55	0.62	2.62	0.49
Region 3	24	138	67.6	29.2	7.41	35.4	4.22	50.12	3.79	22.5	1.52	3.89		2.71	0.36
Region 4	9	530	142	15.6	3.87	42.4	4.38	50.26	4.70	20.4	2.13	3.23		2.70	0.37
Region 5	23	134	67.4	32.0	4.45	33.4	5.87	49.0	6.63	23.7	1.58	4.54	0.44	3.07	0.22
Region 6	6	434	146	21.6	6.39	41.47	6.38	52.65	4.00	21.6	1.24	4.30	0.49	3.35	0.24
Lower Pierre	8	187	138	36.0	8.04	34.09	7.99	53.2	9.05	23.8	1.64	5.00	0.56	3.17	0.27
Middle Pierre	24	264	205	26.5	6.30	35.83	5.54	48.6	4.27	23.1	1.34	3.93	0.53	2.87	0.29
Upper Pierre	77	317	249	26.7	7.33	36.2	4.91	49.4	3.71	22.03	1.79	3.70	0.74	2.68	0.48
Bentonites	5	320	235	3.23	5.68	59.4	1.80	61.7	5.15	21.3	2.26	0.69	0.23	0.66	0.17
Red Bird	11	157	62	26.7	4.55	35.6	3.61	48.5	2.49	22.51	1.45	3.87	0.68	2.81	0.34
Well Section	15	582	102	29.2	6.30	35.3	3.33	49.9	2.53	22.2	1.70	3.62	0.33	2.57	0.35
All Except Unusual	107	293	231	27.0	7.36	36.07	5.31	49.35	4.44	22.5	1.75	3.89	0.74	2.80	0.42
Unfused Except Bentonites	79	291	229	27.7	6.73	35.1	4.72	48.54	4.26	22.5	1.76	3.85	0.72	2.76	0.43
Fused Except Bentonites	32	306	240	26.3	8.90	38.2	5.80	51.79	4.13	22.05	1.86	3.92	0.76	2.85	0.42
Fused Feldspar-rich	20	346	234	21.7	5.62	40.50	5.08	51.60	3.70	21.44	1.26	3.64	0.49	2.84	0.34
Fused Feldspar-poor	12	241	247	34.0	8.08	34.3	4.88	52.11	4.93	23.1	2.19	4.38	0.93	2.86	0.55
All Samples	117	300	233	26.12	8.91	37.14	7.10	50.1	5.13	22.32	1.90	3.71	0.99	2.68	0.62

* For the definition of the samples stratigraphic or geographic location see Appendix I.

** The abbreviation Q + F + C stands for the fraction of the sample composed only of quartz, feldspar and clay. The abbreviation F + C represents the fraction of the sample composed of only feldspar and clay.

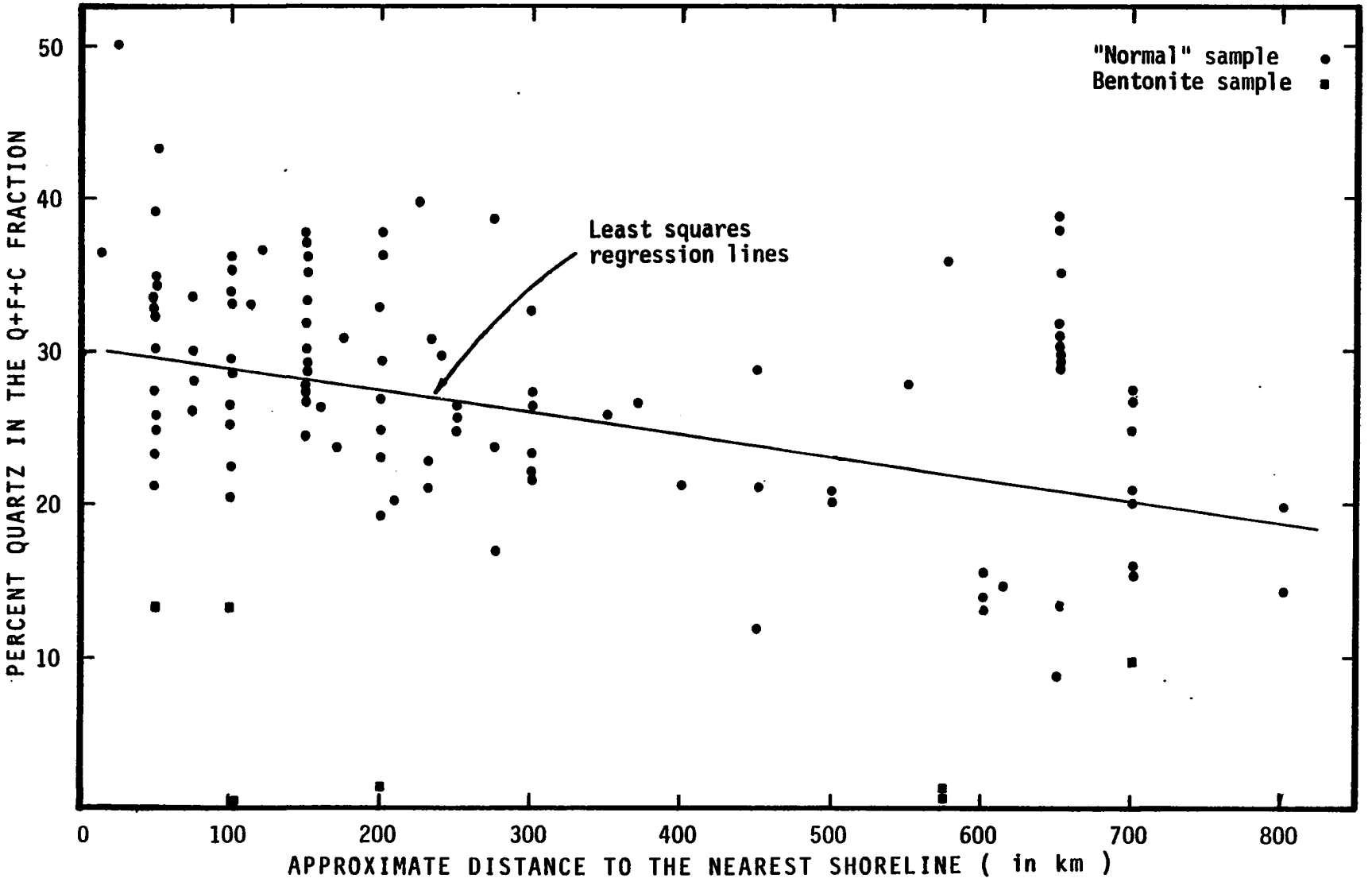

Fig. 10 Relationship between the quartz concentration of the Q + F + C (quartz, feldspar, and clay) fraction of the sample and the distance to the nearest shoreline. Correlation coefficient for the 117 samples shown is -0.364. The correlation coefficient for all samples except the bentonites is -0.483 (p=0.73).

Table 5. Stratigraphic variations seen at the Red Bird Section.

Sample Number	% Quartz in Q + F + C Fraction	% Feldspar in Q + F + C Fraction	% Al_2O_3 in F + C Fraction	% Potassim in F + C Fraction	Mean Size of Q + F Fraction	% Feldspar in Q + F Fraction	Distance to nearest Shoreline
RB-1	29.4		25.13	3.99			240
RB-2	22.7		21.74	3.49			230
RB-3	20.9	11.23	22.10	3.05	1.70	35.44	230
RB-4	26.3	11.65	22.41	3.38	1.88	31.60	100
RB-5	28.4	15.71	23.72	3.70	1.85	36.17	100
RB-6	23.6		22.53	3.61			170
RB-7	20.2		20.11	3.18			210
RB-8	26.3	13.77	21.25	4.21	2.12	35.28	160
RB-9	33.2		22.82	5.34			115
RB-10	29.5	22.55	21.45	3.98	1.85	43.69	75
RB-23	33.38		24.34	4.68			100
Mean	26.7	14.98	22.51	3.87	1.88	36.44	157
Standard Deviation	4.6	4.58	1.45	0.68			62

Table 6. Stratigraphic variations seen in Bobjo Well Samples *

Sample Number	% Quartz in Q + F + C Fraction	% Al_2O_3 in F + C Fraction	% K_2O in F + C Fraction	% SiO_2 in F + C Fraction	Distance to nearest Shoreline
W-0	29.64	22.84	3.55	49.48	650
W-1	35.13	23.07	3.78	49.31	650
W-2	31.62	21.82	3.16	51.61	650
W-3	30.91	22.21	3.78	51.90	650
W-4	30.35	21.97	3.68	50.24	650
W-5	29.11	21.76	3.66	50.83	650
W-6	29.14	20.87	3.38	52.07	650
W-7	37.92	20.57	3.41	50.81	650
W-8	38.54	18.44	3.17	54.28	650
W-9	27.07	24.33	3.19	47.57	300
W-10	21.07	22.56	3.82	50.14	500
W-11	20.50	22.81	3.86	50.29	500
W-12	20.61	22.76	3.83	47.15	500
W-13	20.11	21.03	3.69	49.91	500
W-15	35.88	25.89	4.41	43.34	575
$\bar{x}$	29.17	22.20	3.62	49.93	581
Standard Deviation	6.30	1.70	0.33	2.53	103

* Samples WA-14 and WB-14 were not included as they were bentonites.

subsets of all samples shown in Table 4 shows that few, if any, trends seen in the stratigraphic subsets can be seen in the stratigraphic cross sections.

The occurrence of cristobalite in the Pierre does, however, seem to be stratigraphically controlled. Cristobalite is found in many of the samples which were Upper Pierre age, but only in a few samples which were Middle Pierre age, and in none of the samples which were of Lower Pierre age. This reflects the biogenic control of the cristobalite, that is, the cristobalite is a non-detrital component of the shale. Comparisons of Upper and Middle Pierre samples show no significant differences when only the detrital components are considered. Furthermore, cristobalite is only found in the most easterly areas of the Pierre.

The nature of the Pierre sediment source area and the seaway in which Pierre sediment was deposited places many controls on the changes which could have resulted from stratigraphic variations. Due to the vast extent of the seaway, the effect of stratigraphic variation would be seen primarily in the near-shore areas, with only a small change seen well away from the shoreline areas. This occurs because the regressions and transgressions of the shorelines apparently were the result of rather uniform epeirogenic forces and/or local basin teconic movements rather than general orogenic tectonic forces throughout the depositional basin. Due to the size of the sediment source area, the distance of sediment transport, and the necessary mixing of sediments during transport, changes which could have occurred in the composition of the source area during the time span of the Pierre Shale disposition would have been minor and insignificant. There is, however, one major exception to this and that is changes which would be caused by volcanic events. As

volcanic events are nearly instantaneous with respect to geologic time, changes which would have occurred as a result of volcanic events are so rapid that even the smallest stratigraphic divisions of the Pierre Shale could not be used to obtain stratigraphically unbiased samples of the Pierre Shale.

Changes in meteorologic variables could have caused significant change in areas from which Pierre sediments were derived and in the intensity of the transporting mechanisms. However, each Pierre sample represents more than a thousand years of Pierre time. Therefore, most temporal changes should average out.

Because most of the important stratigraphic variables are treated independently and because the data generally show no significant stratigraphic trends in detrital mineralogy which cannot be interpreted in terms of these variables, it is assumed that the remaining stratigraphic variables are subordinate.

Size Analyses of the Quartz and Feldspar Fraction

The results of the particle size analyses of the Q + F fraction of the samples are given in table 7. In general the size distributions can be characterized as being polymodal, poorly sorted, nearly symmetrical and platykurtic to mesokurtic. A frequency plot of the positions of the modes (Fig. 11) occurring in all of the samples indicated that the distribution of the modes also is polymodal.

The average of the mean size of the Q + F fraction is 6.1 microns or 7.36ϕ. A comparison of the mean size of the Q + F fraction of the Pierre samples with

Table 7. SUMMARY OF SIZE DISTRIBUTIONS

Sample Number	Mean Size in μ	Phi Standard Deviation	Skewness	Kurtosis	MODES IN ϕ														
					> 3.5	3.5 to 4.0	4.0 to 4.5	4.5 to 5.0	5.0 to 5.5	5.5 to 6.0	6.0 to 6.5	6.5 to 7.0	7.0 to 7.5	7.5 to 8.0	8.0 to 8.5	8.5 to 9.0	9.0 to 9.5	9.5 to 10.0	< 10ϕ
P-2	6.69	1.56	.05	1.03				x			x			x					
P-24	5.10	1.32	.01	.93								x				x		x	
P-51	3.92	1.65	-.40	.99				x									x		x
P-66	3.99	1.50	.05	.75						x			x				x		x
P-70	2.82	1.42	-.14	1.04													x		x
P-75	3.02	1.65	-.21	1.04				x								x			x
P-101	3.87	1.47	-.09	.87								x				x			x
P-139	4.76	1.64	.01	.84							x					x			x
P-186	2.68	1.50	-.05	.96													x		x
P-187	2.36	1.02	-.10	1.09												x			x
P-193	7.15	1.82	.12	.79				x		x						x			x
P-203	6.68	1.94	-.03	.77												x			x
P-252	7.01	1.58	.20	.81							x			x			x		x
P-261	8.74	1.88	.27	.66				x				x						x	
P-270	3.55	1.24	-.08	.83													x		x
P-273	3.45	1.73	-.06	.90				x						x					x
P-279	2.64	1.45	-.39	1.12				x									x		
P-313	5.32	1.44	.21	.73							x					x			
P-318	5.17	1.48	.12	.75							x		x			x			

Sample Number	Mean Size in μ	Phi Standard Deviation	Skewness	Kurtosis	MODES IN ϕ													
					> 3.5	3.5 to 4.0	4.0 to 4.5	4.5 to 5.0	5.0 to 5.5	5.5 to 6.0	6.0 to 6.5	6.5 to 7.0	7.0 to 7.5	7.5 to 8.0	8.0 to 8.5	8.5 to 9.0	9.0 to 9.5	9.5 to 10.0	< 10ϕ
P-325	5.13	1.47	.11	.84								x			x			x	
P-327	3.33	1.53	-.16	1.12			x								x		x		x
P-331	5.04	1.68	.05	.79							x						x		x
P-334	12.10	1.67	.38	.98				x						x		x			x
P-343	4.13	1.72	-.09	.73														x	
P-350	4.90	2.09	-.31	.59			x						x						x
P-351	14.63	2.40	-.02	.73		x					x						x		x
P-353	16.32	1.96	.29	.89			x			x						x			x
RB-3	4.84	1.70	-.07	.86												x			
RB-4	11.59	1.88	.38	.78					x							x			x
RB-5	10.26	1.85	.42	.73				x									x		
RB-8	9.06	2.12	.00	.86			x			x				x				x	
RB-10	17.09	1.85	.54	.75			x										x		x
W-8	2.06	1.33	-.29	.85													x		x
$\bar{x}$	6.09																		

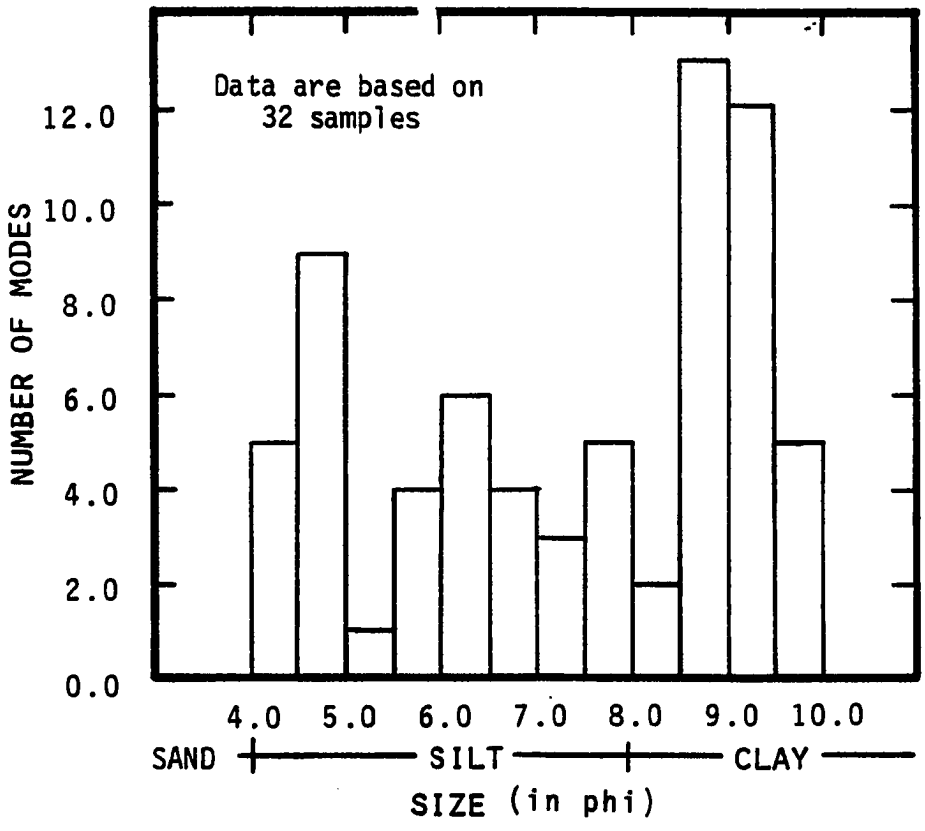

Fig. 11 Relationship between the number of modes and the particle size of the modes.

the mean quartz size reported in other studies is shown in table 8. The mean size of quartz and feldspar in the Pierre samples is significantly finer than found in most other shales and is similar to the size distributions found in pelagic sediments and atmospheric dust. The relationship between the mean size and the distance to the nearest shoreline is shown in figure 12. This figure shows that the mean size of the Q + F fraction generally decreases with increasing distance from the nearest shoreline.*

The methods of size analyses used in this study determined only the size distribution of the quartz and feldspar fraction. Due to potential differences in the provenance, mechanisms of transport, and diagenetic alterations between the quartz and feldspar, it is possible that the size distributions of the quartz differ greatly from the size distributions of the feldspar. In order to evaluate this potential difference, normative feldspar analyses were done on individual size fractions of the Q + F fractions of six samples. The results, shown in table 9, indicated that for the three samples which contained sediment coarser than 43 microns, the percentage of quartz was lower than that of the whole Q + F fraction. In five of the six samples, the quartz concentrations of the less than 4 micron portion of the Q + F fraction were larger than those found in whole Q + F fractions.

On the basis of these data, it seems apparent that the size of the feldspar fraction generally is somewhat coarser than the quartz fraction. However, because the differences in the feldspar concentrations between these size

---

*In this and all subsequent discussion the phrase "distance to nearest shoreline is defined to mean the distance between the sample location and the inferred location of the shoreline at the time the sample was deposited (see Appendix I).

Table 8. Quartz Size Distribution

Sediment Type	Name	Mean Size	Reference
Aerosolic Dust	Barbados #1	8.1 PHI	DeLaney, et al, 1967
Aerosolic Dust	Barbados #2	8.4 PHI	DeLaney, et al, 1967
Pelagic	Mid-Latitude[a]	8.0 PHI	Bedtagy, et al, 1972
Pelagic	Equatorial[b]	9.3 PHI	Bedtagy, et al, 1972
Pelagic	Chubasco	8.2 PHI	Jackson, et al, 1971
Pelagic	Chinook	7.5 PHI	Jackson, et al, 1971
Pelagic	Pas 19121	7.2 PHI	Rex and Goldberg, 1958
Soil[c]	Hawaiian Low[d]	8.4 PHI	Jackson, et al, 1971
Soil[c]	Hawaiian High[e]	7.7 PHI	Jackson, et al, 1971
Shale	Average Shale[f]	6.2 PHI	Schultz, 1975
Shale	Average Shale[g]	5.2 PHI	Fleury, 1971
Pierre	Coarsest (RB-10)	5.87 PHI	This Study
Pierre	Finest (P-187)	8.67 PHI	This Study
Pierre	Weighted Average	8.1 PHI	This Study
Pierre	Simple Average	7.4 PHI	This Study

a- Average of twelve (12) samples

b- Average of eighteen (18) samples

c- The quartz in the samples is infered to be Aerosolic Dust

d- The coarsest of eleven (11) samples

e- The finest of eleven (11) samples

f- Average of sixteen (16) samples

g- Average of seventeen (17) samples

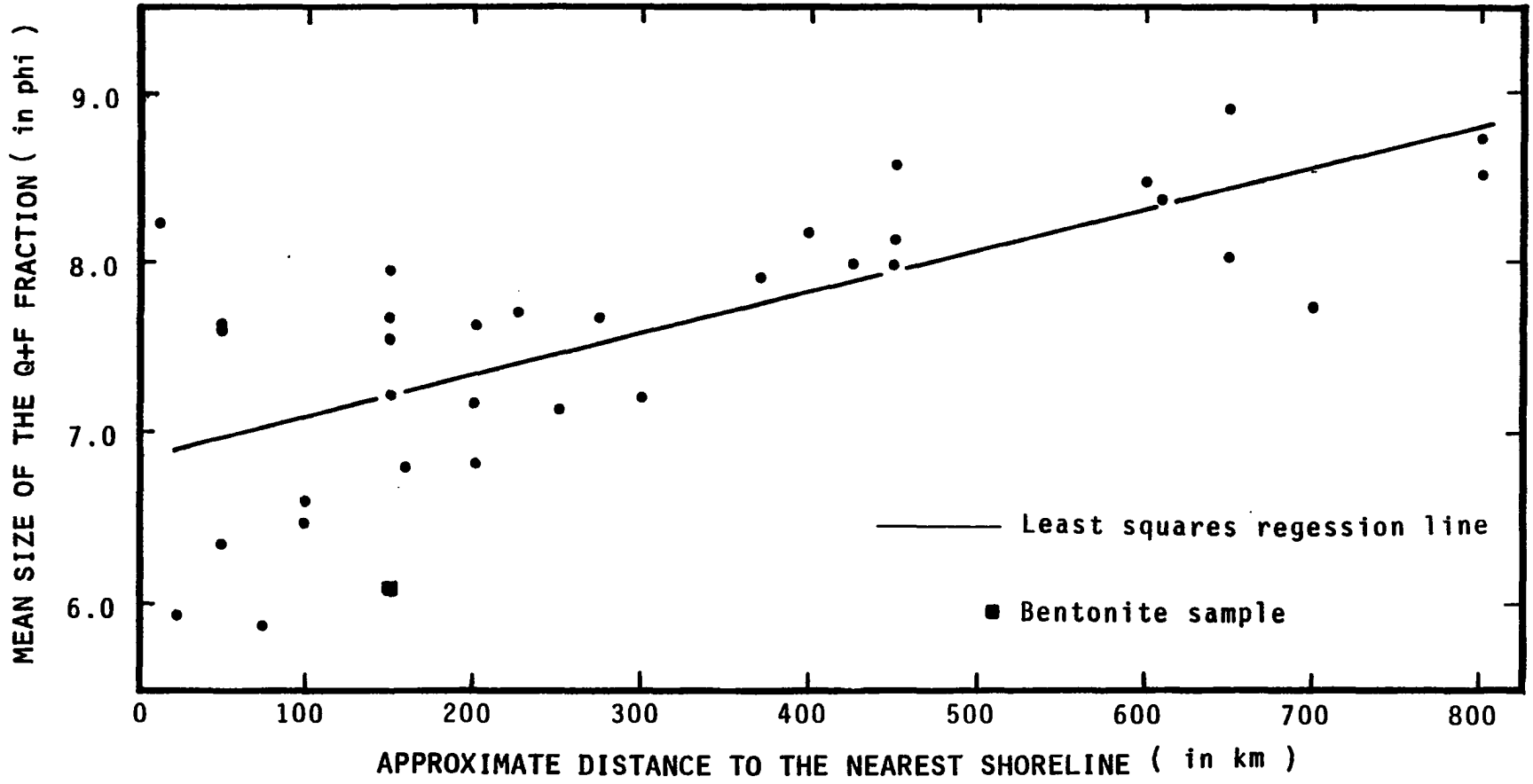

Fig. 12 Relationship between the mean size of the Q + F (quartz and feldspar) fraction and the approximate distance to the nearest shoreline. The correlation coefficient for the 32 non-bentonite samples is 0.71.

Table 9. Normative feldspar analyses of size fractions of the Q + F fraction.

Sample Number	% Quartz in Whole Sample	% Feldspar in Whole Sample	% Q + F >43 μm	% Q + F <4 μm	% Quartz of Q + F Fraction		
					Whole Q + F	Q + F >43μm	Q + F <4μm
RB-4	25.7	10.2	13.7	25	70.0	64.9	64.4
RB-10	29.4	18.3	35	20	59.3	59.3	89.8
P-343	29.4	7.5	<1	42	79.7	62.9	85.7
P-325	34.2	5.6	<1	40	85.3	--	92.2
P-186	18.7	5.2	<1	61	77.6	--	82.4
P-318	22.5	2.9	<1	40	88.4	--	91.6

fractions generally are small and because the feldspars generally comprise less than one-third of the Q + F fraction, it is believed that the size distributions of the quartz fraction are not significantly different than those of the Q + F fraction as a whole.

Mineral Dispersal Patterns - Amounts and Areal Distributions

Cristobalite*

The concentration of cristobalite ranges from 0% to 70% of the whole sample. As shown in figure 13 the occurrence of cristobalite is generally limited to the northeastern outcrops of the Pierre Shale; also, most of the cristobalite occurs in the Odahna Member of the Pierre Shale. The samples containing the cristobalite are commonly referred to as siliceous shales and have the following features:

1. Low density
2. Light color (generally N6 or N7 on the GSA Rock Color Chart)
3. Low quartz and feldspar content
4. Little or no carbonate
5. Slate-like cleavage
6. Iron and manganese stains

Petrographic data indicate that the cristobalite is generally very fine grained, although in a few samples the large grains can be found. The petrographic identification of these grains is based on their extremely low interference colors and their very low relief. X-ray data show that the very fine grained cristobalite may be classified, according to the nomenclature of Jones and Signet (1971), as opal-CT, while some of the coarse grains are opal-C.

---

*In this paper the term cristobalite is used to identify all of the crystalline varieties of the opal-cristobalite-tridymite mineral series. When a specific reference is made to the mineralogic structure, the nomenclature of Jones and Signet (1971) will be used. The use of this nomenclature, however, requires identification using X-ray diffraction techniques.

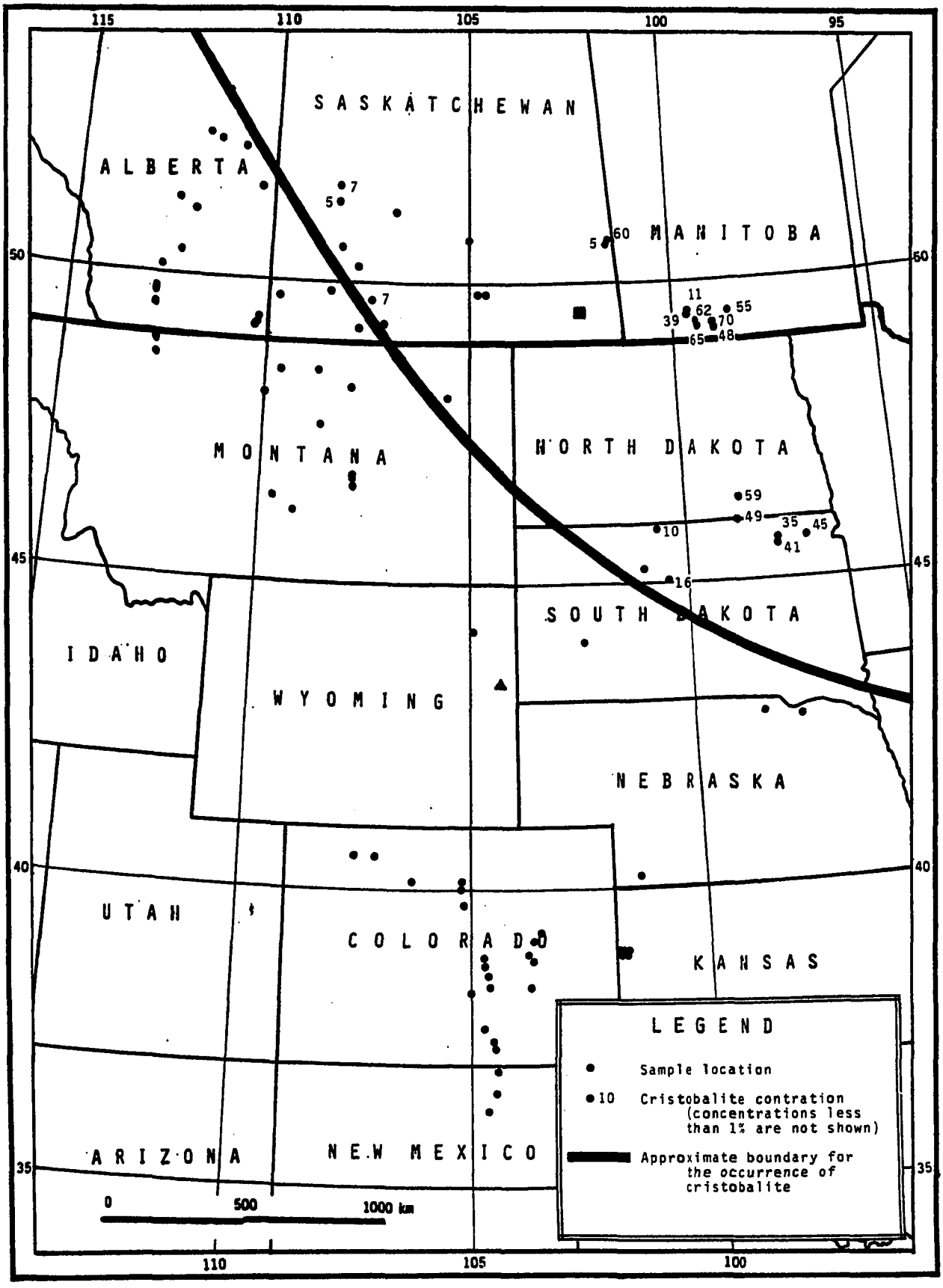

Fig. 13. Areal distribution of Cristobalite

Quartz

The whole rock concentrations of quartz in the Pierre range from 1.0 (from a bentonitic sample, P-251) to 37.9% (W-8) with a mean of 22.9% and a standard deviation of 9.34%. As shown in figure 14 there is a general trend toward decreasing percentages of quartz towards the eastern edge of the Pierre outcrops. This appears to be related to the increasing distance from the western detrital source area. In figure 10 (p. 36) the relationship between the distance to the closest western shoreline and the amount of quartz in the Q + F + C (quartz plus feldspar plus clay) fraction of the sample is shown. The relationship is considered to be linear. A linear regression of these data gives a corrrelation coefficient of -.36 ($P > .99$). This trend indicates that quartz concentrations are being reduced as a function of increasing distance from the western source area, and that eastern sediment source areas are not supplying noticeable quantities of quartz.

Polycrystalline quartz is present in all of the samples. The crystal size of the quartz in these polycrystalline grains is extremely variable, ranging in size from less than 1 μm to greater than 100 μm. Most of the crystals, however, are less than 10 μm in size.

Feldspar

The feldspar compositions determined using sodium bisulfate fusion and atomic absorption spectrophotometry are given in table 10. The average Pierre sample contains 8.5 percent feldspar of which 60 percent is plagioclase. The areal distribution of the feldspars in the Pierre sediments is shown in figure 15. As can be seen in this figure, there seems to be little correlation between sample locations and the concentration of feldspars found in the Q + F + C fraction of the samples. The ratio of plagioclase

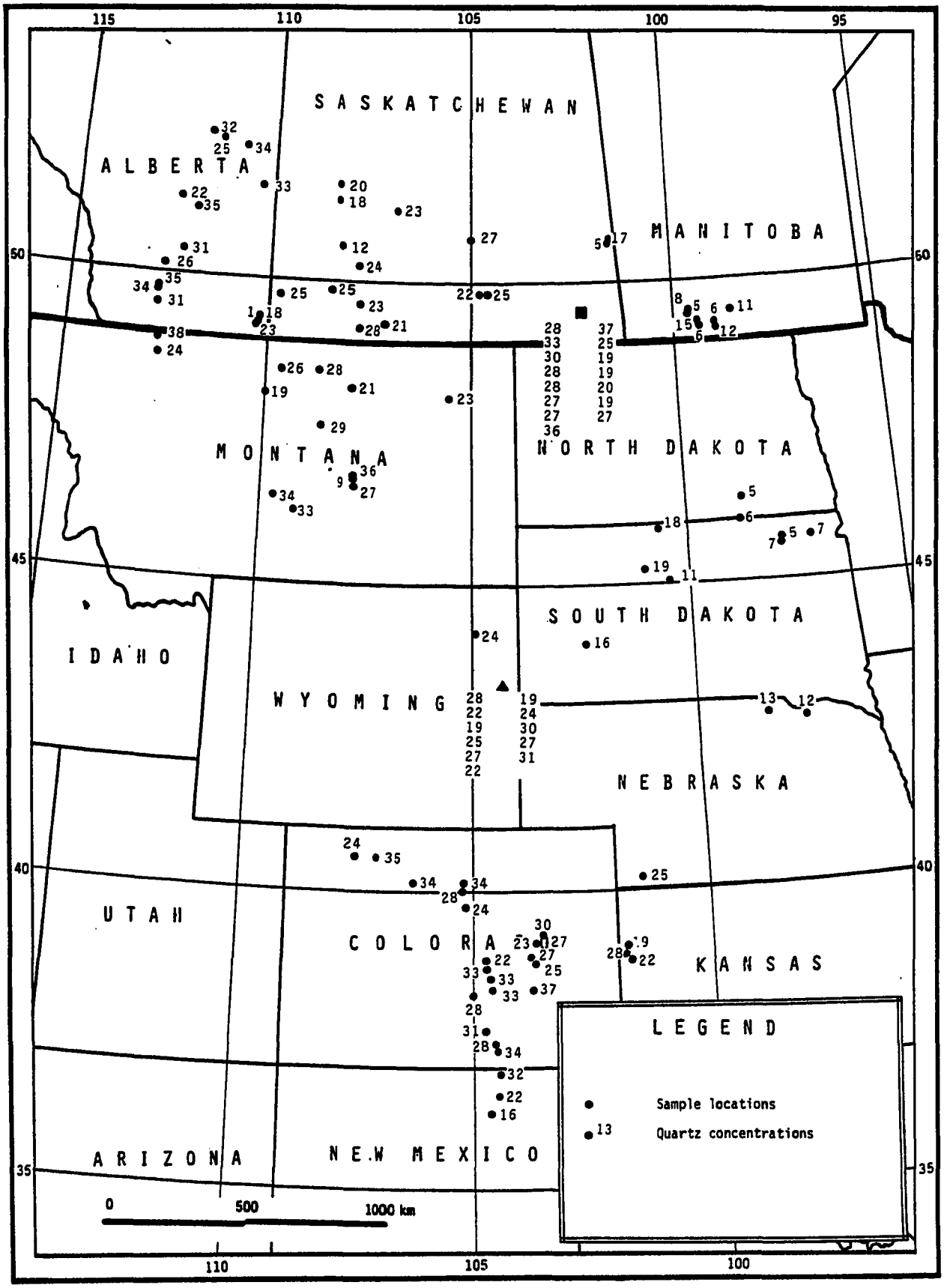

Fig. 14. Map showing the areal distribution of quartz concentrations in the Pierre Shale. Quartz concentrations are given in terms of the concentration found in the whole rock.

Table 10. Chemical and normative analyses for feldspar compositions and concentrations.

Sample Number	Percent of Whole Rock Fused	Norminative Feldspar Concentration (as percentage of Whole Rock)					Mole Percent Anorthite
		Quartz	Orthoclase	Albite	Anorthite	Total Feldspar	
P-2	61.23	24.26	4.38	9.62	0.52	14.52	5.1
P-24	76.26	16.41	2.78	4.32	0.23	7.33	5.1
P-51	66.19	28.46	1.83	3.36	0.16	5.35	4.5
P-66	62.84	25.68	2.74	8.31	0.42	11.48	4.8
P-70	74.48	12.62	7.14	5.32	0.45	12.91	7.1
P-75	80.12	13.78	2.52	3.42	0.16	6.10	4.4
P-101	90.22	7.10	1.04	1.43	0.21	2.68	12.7
P-139	87.62	10.64	.56	1.08	0.10	1.74	8.6
P-186	75.70	17.80	1.75	4.36	0.39	6.50	8.3
P-187	92.84	5.25	0.67	1.05	0.19	1.91	15.2
P-193	64.31	23.03	2.58	9.03	1.04	12.66	10.4
P-203	64.27	22.02	2.62	9.97	1.13	13.71	10.1
P-252	69.74	18.15	2.37	8.52	1.22	12.11	12.5
P-261	65.06	23,23	2.46	8.21	1.04	11.71	11.2
P-270	73.19	18.27	2.66	5.30	0.58	8.54	9.9
P-273	75.89	19.15	1.39	3.54	0.04	4.97	1.0
P-279	86.09	10.63	0.92	2.17	0.18	3.28	7.7
P-313	63.60	27.90	0.87	7.24	0.39	8.50	5.0
P-318	74.55	22.34	0.09	2.97	0.05	3.11	1.6
P-325	59.91	33.90	0.94	5.07	0.18	6.19	3.4
P-327	57.75	35.83	2.87	3.48	0.08	6.42	2.2
P-331	71.30	24.46	1.00	3.13	0.10	4.23	3.2
P-334	60.22	33.98	1.94	3.77	0.08	5.80	2.2
P-343	62.72	29.10	1.80	5.95	0.44	8.18	6.9
P-350	55.42	36.23	1.95	5.48	0.92	8.35	14.4
P-351	82.45	9.54	0.91	4.78	2.31	8.00	32.6
P-353	59.40	33.70	2.63	4.12	0.16	6.90	3.6
RB-3	69.90	19.43	2.62	7.65	0.40	10.67	4.9
RB-4	63.40	25.03	2.51	8.04	1.01	11.56	11.2
RB-5	57.43	27.17	4.72	10.03	0.64	15.40	6.0
RB-8	61.98	24.60	3.33	8.60	1.47	13.41	14.6
RB-10	50.85	27.67	7.09	12.35	2.03	21.47	14.1
W-8	56.48	37.49	0.69	3.98	0.15	4.82	3.6
		$\bar{x}$ =22.3	$\bar{x}$ =2.43	$\bar{x}$ =5.53	$\bar{x}$ =0.54	$\bar{x}$ =8.5	$\bar{x}$ =8.2

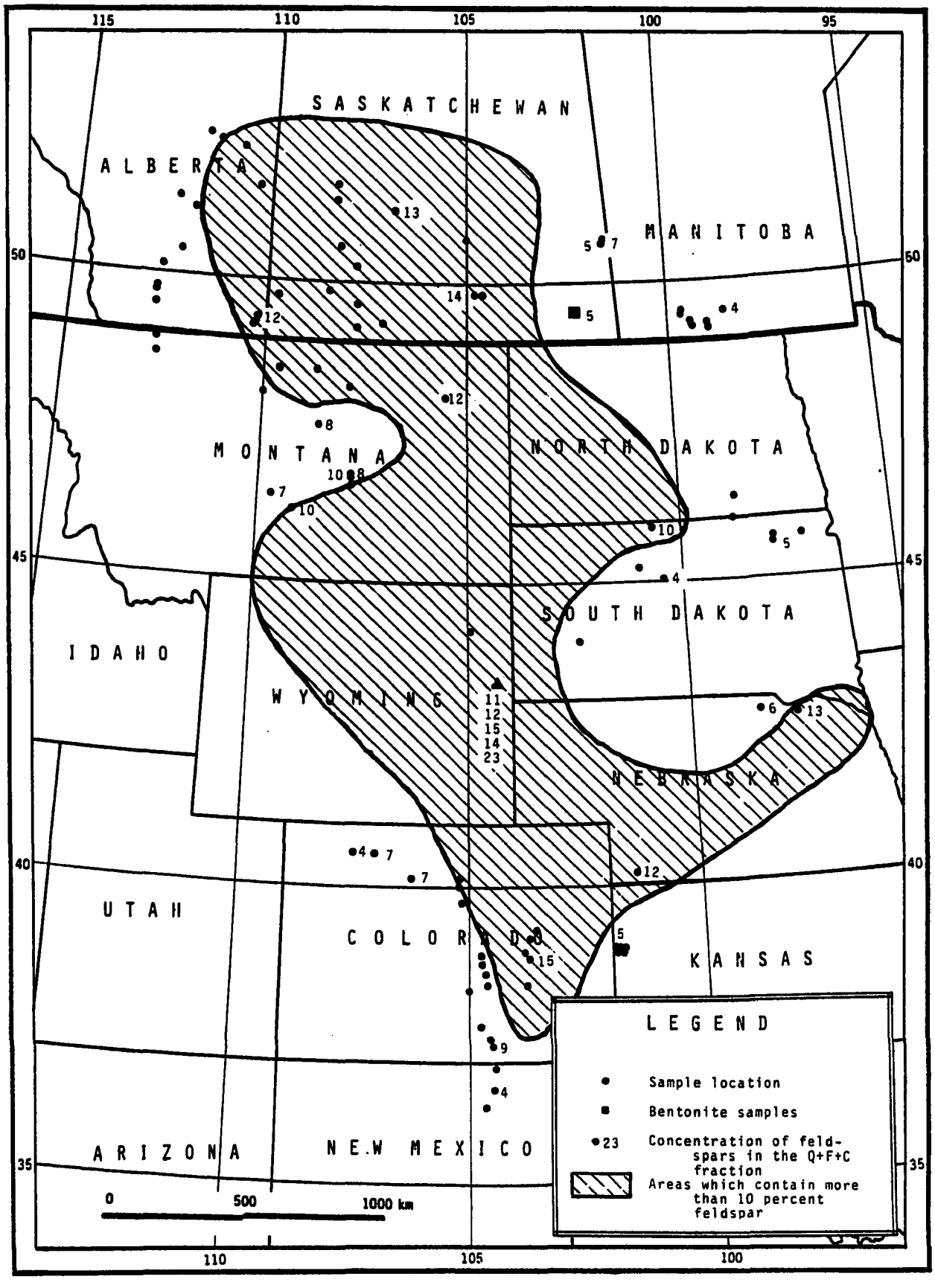

Fig. 15. Map showing the normative concentration of feldspar in the Q + F + C (quartz, feldspar, and clay) fraction of the samples.

feldspars to the potassium feldspars of 2.5:1 is near constant for all of the samples. A comparison of the potassium feldspars to the plagioclase feldspars is shown in figure 16.

The normative composition of the plagioclase*, of ranges for the non-bentonite samples, from 1 to 15 mole percent anorthite, with an average plagioclase composition of 8.2 mole percent anorthite. In general, the anorthite content of the Q + F fraction of these samples increases as a function of the total amount of feldspar in the Q + F fraction as shown in figure 17. As can also be seen in figure 17 the majority of the feldspars have normative plagioclase compositions of albite with the rest falling in the sodic oligoclase compositional range.

Several attempts were made to determine the structural state of the feldspars by isolating the potassium and plagioclase feldspars and then using the X-ray techniques of Wright (1968) and Bambauer et al. (1967). The results of these procedures were inconclusive, and because the feldspars in these samples were mixed phases rather than one phase the use of these techniques is of questionable validity.

In table 9 (Page 46) the relative proportions of quartz and feldspar from 6 samples are compared to the relative proportions of quartz and feldspar less than 4 μm and the greater than 43 μm portions of each sample. The results show a definite decrease in the feldspar concentration with decrease in size. Figure 18 shows the relationship between the percentage of feldspar in the Q + F fraction and the distance to the closest western shoreline.

---

*The plagioclase feldspars are assumed to be homogeneous plagioclase feldspars rather than mixtures of the plagioclase end members. Optical data indicate that the most calcic plagioclase grains present have anorthite compositions of less than 50 mole percent anorthite.

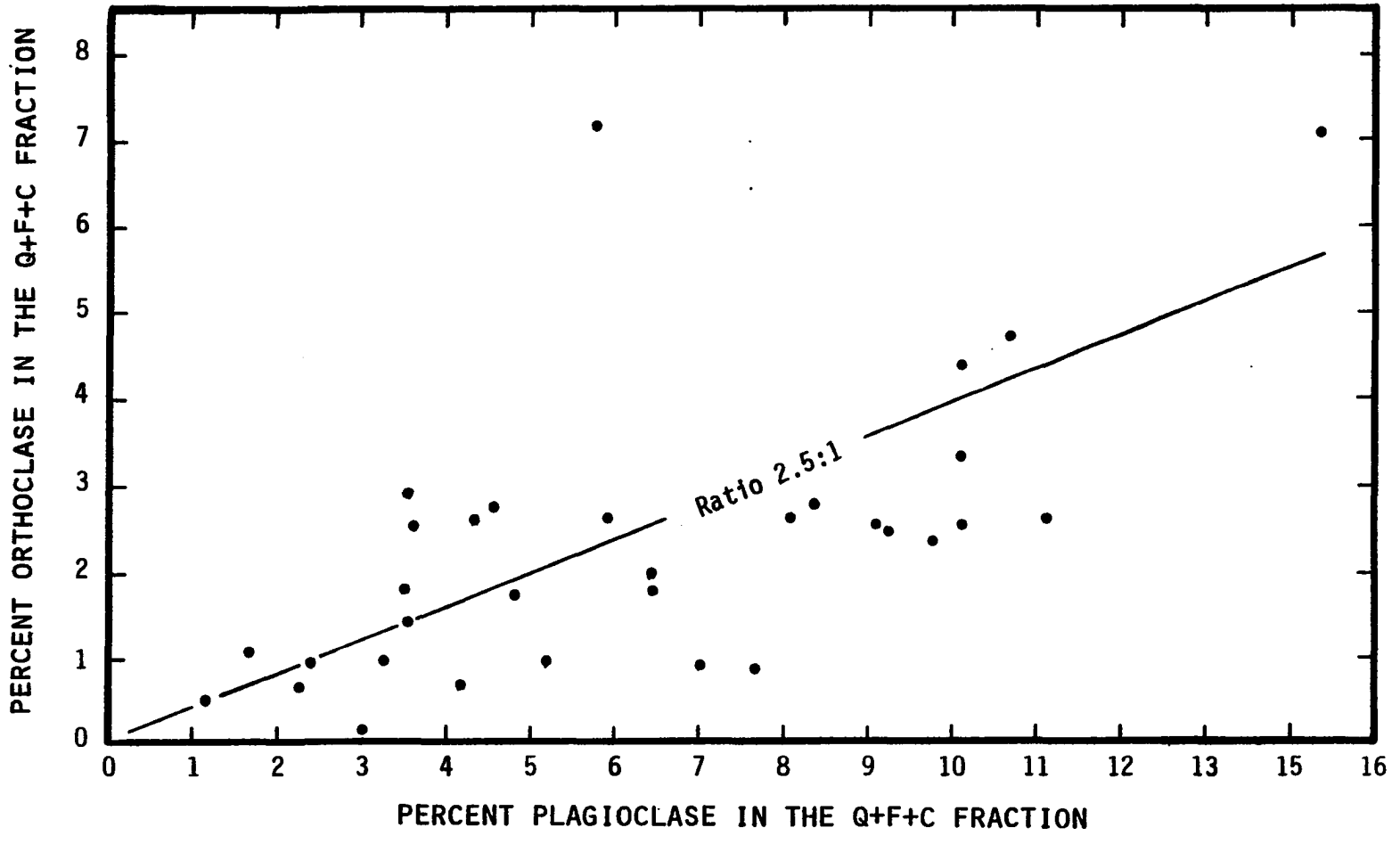

Fig. 16 Relationship between the orthoclase and plagioclase concentrations in the Q + F + C (quartz, feldspar, and clay) fraction.

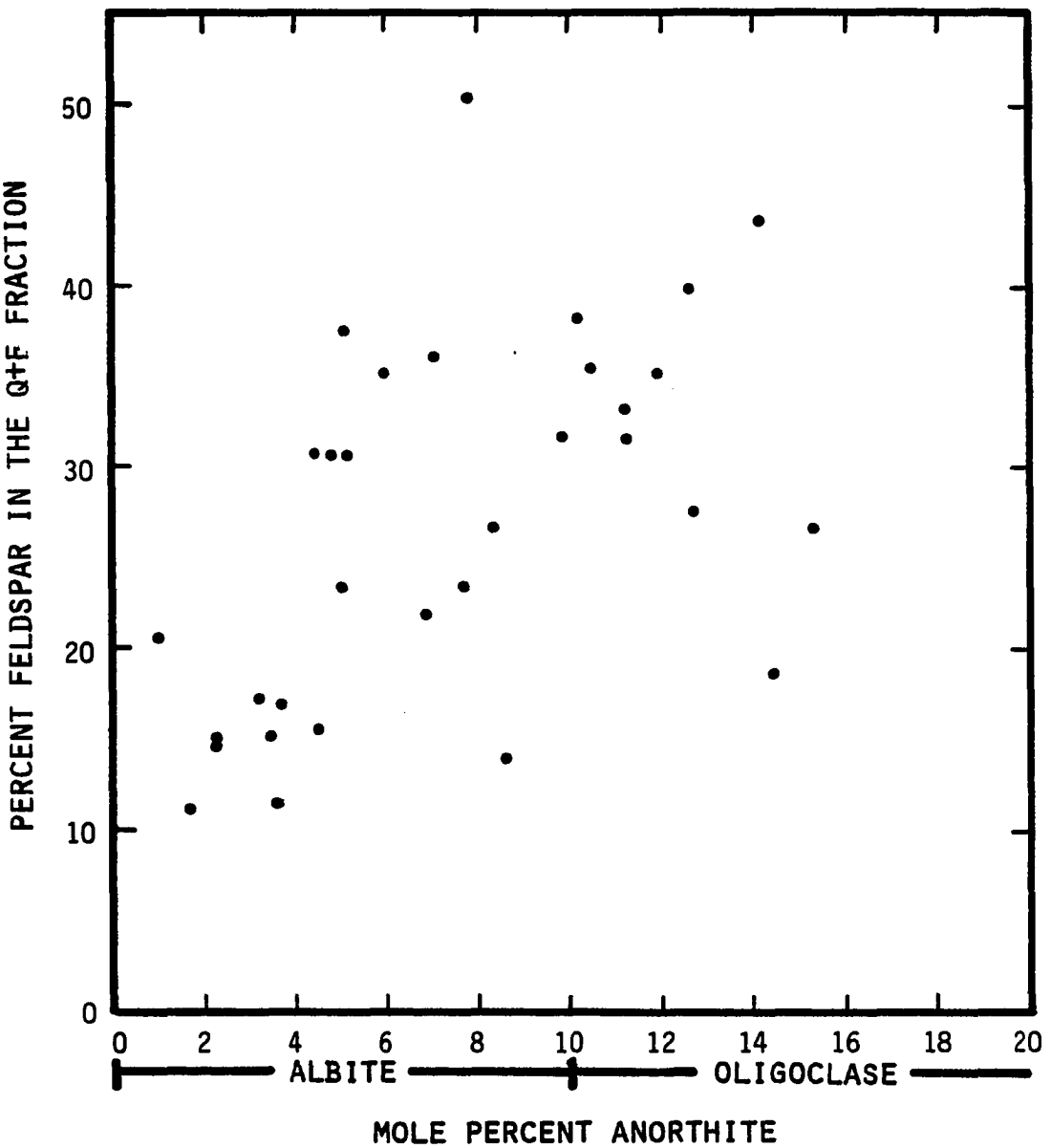

Fig. 17 Relationship between the percentage feldspar in the Q+F (quartz and feldspar) fraction and the normative plagioclase composition of the feldspar.

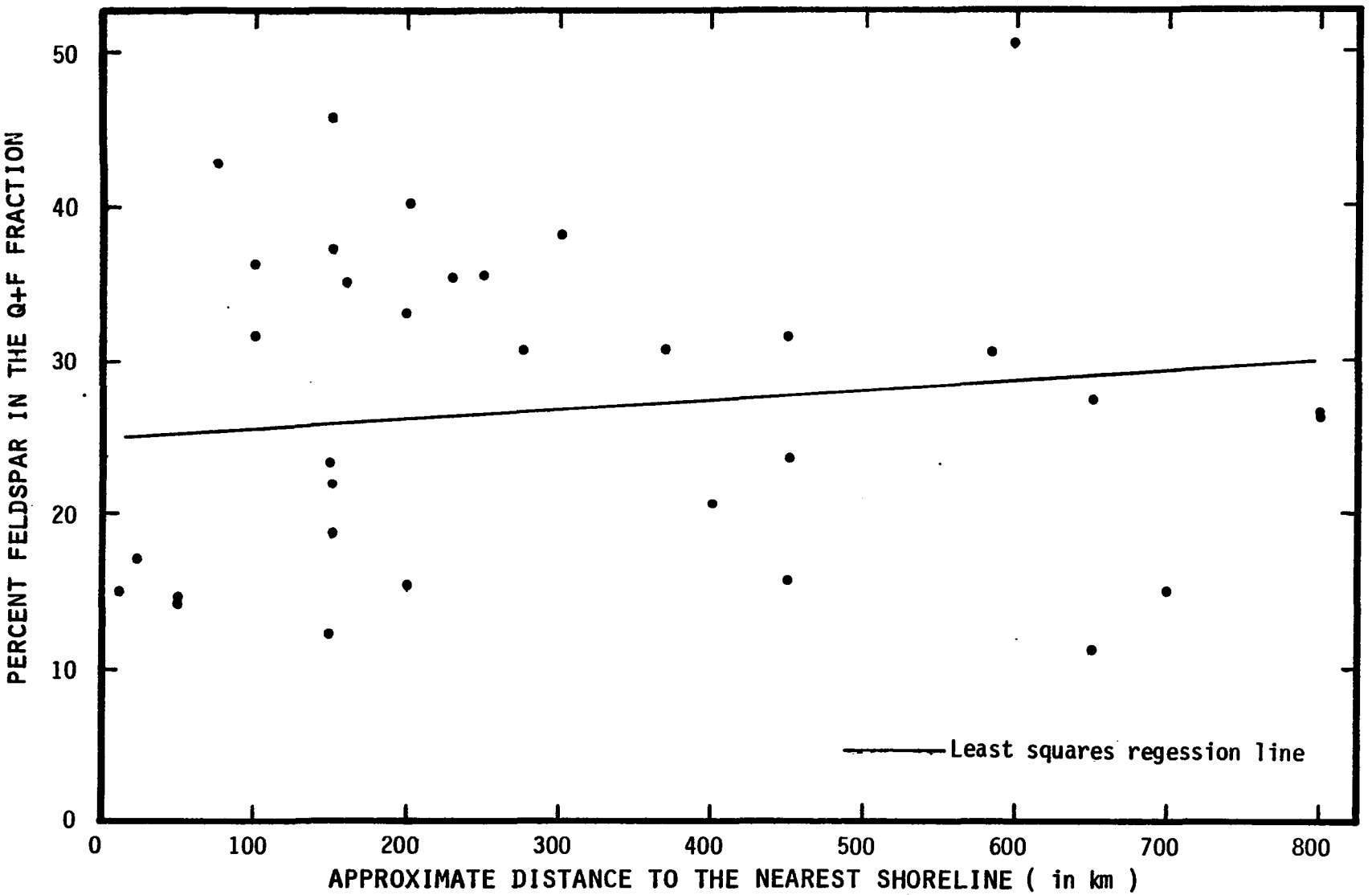

Fig. 18 Relationship between the percentage of feldspar in the Q+F (quartz and feldspar) fraction of the sample and the distance to the nearest shoreline. The least squares regression was calculated using all 33 data points. The correlation coefficient for these data is 0.16.

All of the samples contain feldspar in the fraction coarser than 43 μm. Nevertheless, determination of the exact composition and mineralogic structure of the feldspars can be made only on a few grains, as the majority of grains are too small to provide good optical data.

Listed below are some of the petrographic characteristics of the feldspars, coarser than 43 μm, which are common to most of the samples.

1. Euhedral and subhedral crystals are common.
2. Microcline twinning is only rarely present.
3. Alkali feldspar is less common than twinned plagioclase.
4. Alkali feldspar is generally more altered or weathered than plagioclase.
5. Plagioclase is polysynthetically twinned.
6. Some of the plagioclase is compositionally zoned.
7. The composition of twinned plagioclase grains is typically oligoclase or andesine.

Because exact compositions of the feldspars could not be obtained optically, normative compositions of the feldspars were obtained using the methods given in Appendix VII. The results of the normative determinations for the > 43 μm fraction are given in table 11. These analyses show that the feldspar comprises an average of 36% of the Q + F fraction coarser than 43 μm and that the ratio of plagioclase to alkali feldspars is 2.9"1. These results are consistent with the optical data. If the percentage of polycrystalline quartz is not included in this fraction, the relative percentage of feldspar increases to approximately 50%.

Table 11. Chemical and petrographic data on Q + F fraction between 61-43 μm.

Sample Number	% of Sample	% of Q + F Fraction 61-43 μm					Composition Plagioclase in mole % An
		Quartz	Orthoclase	Albite	Anorthite	Polycrystalline Quartz	
RB-4	4.6	66.3	11.0	18.6	4.0		17.6
RB-10	16.9	61.4	12.6	21.1	4.8	27	18.5
P-343	.8	64.7	7.5	21.5	6.2		22.7
P-350	4.5	65.6	5.5	22.0	7.2	26	24.6
P-351*	4.3	28.1	6.3	40.2	25.4	5	38.8

* Bentonite

Phyllosilicates and Clays

Pierre Shale samples generally contain 70 to 80 percent clay size material. The vast majority of these particles is phyllosilicates. Amorphous material, iron oxides, zeolites, and other clay-sized minerals form only a small percentage of the total sample. Five phyllosilicate phases are found commonly; these are illite, mixed layer illite-smectites, smectites, kaolinite and chlorite. Other studies of the Pierre Shale (particularly Schultz, 1964) have determined that the dominant phases present are illite and mixed layer illite-smectites and smectites, with kaolinite and chlorite present only in minor amounts. No attempt was made in this study to determine quantitatively the various concentrations of these mineral phases. Instead, the qualitative analyses were made for kaolinite and chlorite based on the size (height x width at 1/2 height) of the 7Å X-ray diffraction peak, which is common to both phases, and normative analyses for illite and smectite.

The results of the qualitative X-ray analyses for the 7Å peak are shown in figure 19. As can be seen in this figure, the amounts of kaolinite and chlorite (the 7Å X-ray peak) generally decrease with increasing distance away from the western shore. This trend is perhaps best explained in terms of selective removal of these minerals relative to illite and smectite with increasing distances of transport. Other studies such as Whitehouse et al. (1960) have shown that this can be caused by the differential flocculation and sedimentation. Also, the particle sizes of kaolinite and chlorite tend to be larger than the particle sizes of illite and smectite and this results in their earlier deposition.

In figure 20 the areal distribution of normative illite is shown. The concentration of this mineral also tends to increase towards the western edge.

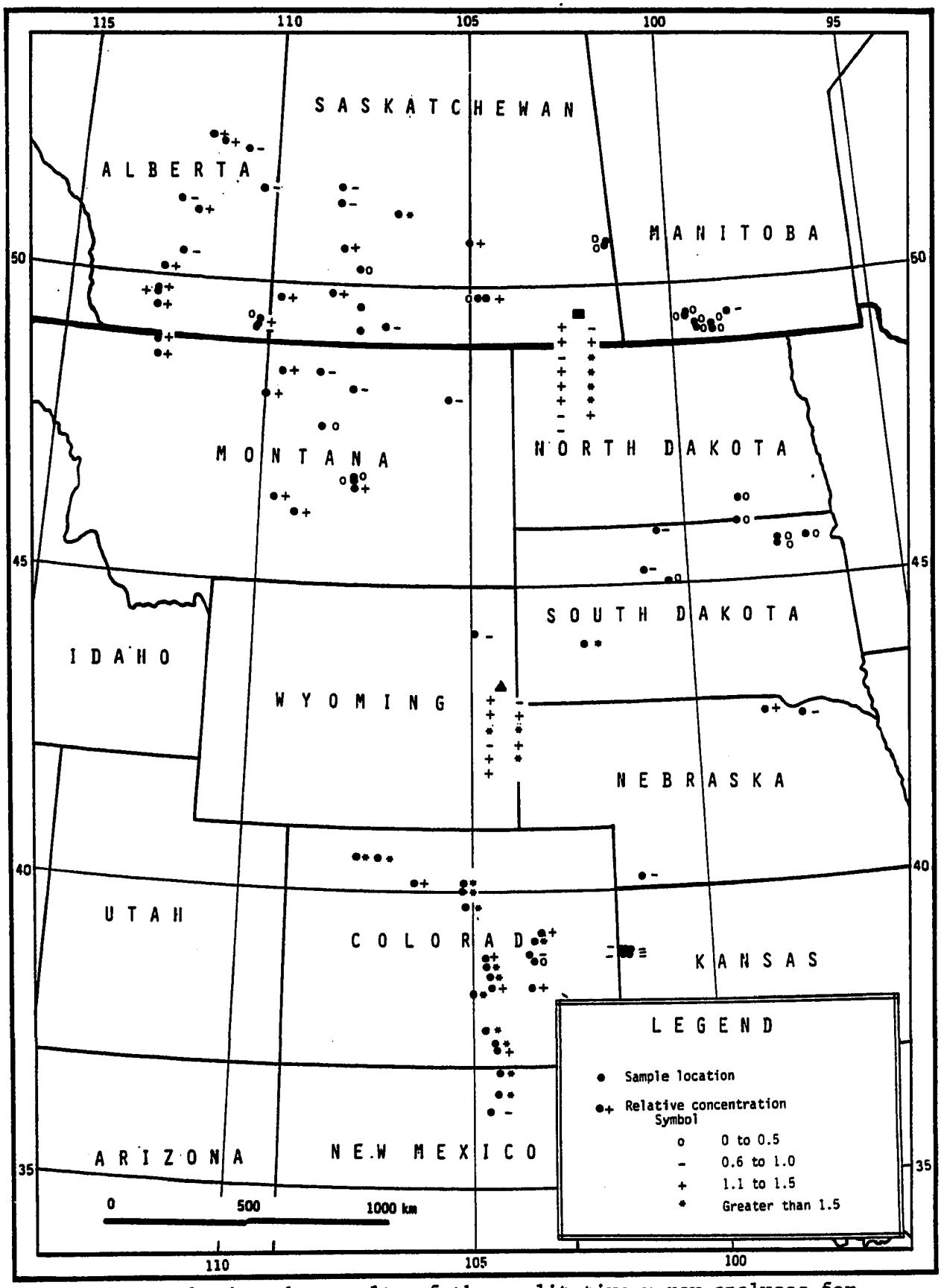

Fig. 19. Map showing the results of the qualitative x-ray analyses for the relative amount of clays containing an x-ray peak 7Å (kaolinite and chlorite). Values are compared relative to the height of their x-ray peak at 12.5° 2θ, using Cu kα radiation, using standard conditions for each sample.

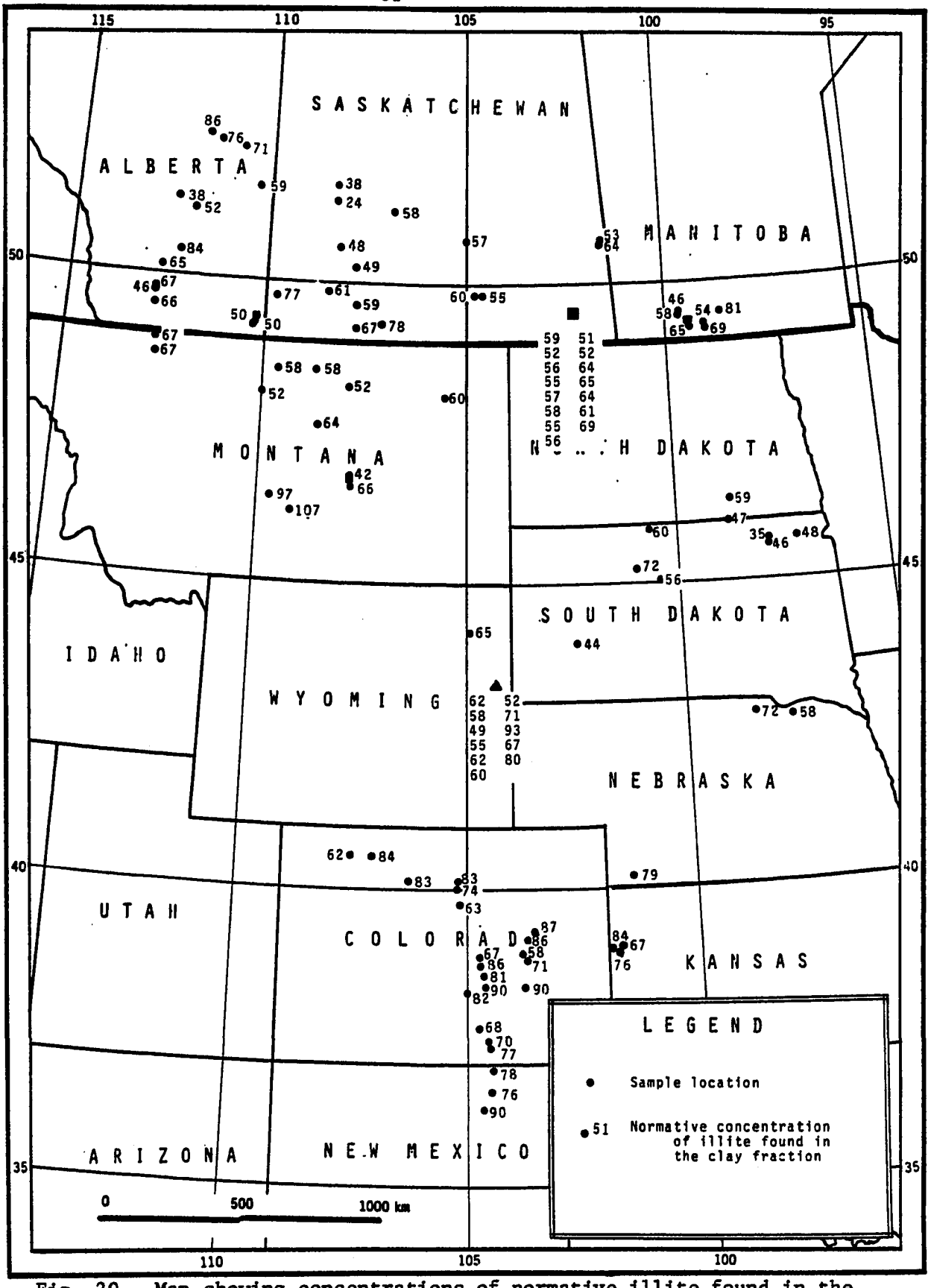

Fig. 20. Map showing concentrations of normative illite found in the Pierre Shale. All concentrations are given in terms of the concentrations found in the clay fraction. Note that the concentration of illite found in one sample (P-354) exceeds 100%. This is the result of using too low of a value for the amount of potassium contained in illite. See text for further discussion.

The explanation for this trend is also probably related to the differential flocculation and sedimentation of these minerals. A slight decrease in the illite concentration is also seen in the northwestern areas relative to the illite concentration in the southwestern area. This probably is related to the volcanic source areas located in southwestern Montana.

Provenance

In studying the possible compositions of sediments delivered to the Pierre sea, the following factors must be realized:

1. Due to the geographic extent of the Pierre sediments, variations in local source rock types cannot be used to explain major compositional variations.
2. Once these sediments have arrived in the Pierre seaway they will be sorted on the basis of size and mineralogy by the transporting agent.
3. The original mineral composition of the source rocks has been altered prior to deposition.
4. As previously discussed, since delivery to the seaway, these sediments have been diagenetically altered.

Volcanic source rocks are an exception to some of the factors listed above. This is a result of the variable nature of volcanic activity and the fact that the volume of sediments produced by volcanic source rocks need not be related to the area of volcanic rocks exposed on the surface.

Volcanic Source Rocks

Volcanic source rocks for the Pierre sediments have been recognized as significant (Gill and Cobban, 1973; Tourtelot, 1962; and Schultz, 1978)

but this recognition generally has been limited to the bentonite beds found within the Pierre sediments. Little attention has been paid to possible volcanic contributions to the rest of the formation. A recent exception to this is the paper of Schultz, 1978, where he attributes 50% of the clay fraction to altered volcanics.

Quartz and feldspars. The most direct evidence of volcanic contributions to the Pierre sediments can be found in the nature and occurrence of the feldspars in the Pierre Shale. The average feldspar content of these samples is 8.5%, while the average for all shales is 4.5% (Shaw and Weaver, 1965). If 4.5% feldspar is a valid figure for the shales in the sediment source area, then clearly these high feldspar contents cannot be the result of the reworking of older sediments.

While the total amount of feldspars in the samples varies, the ratios of the different feldspar types remain quite similar among samples. The normative ratios of sodium to potassium feldspars show few variations. The ratios of sodium to calcium feldspars change toward higher calcium content as a function of increasing feldspar concentration. The ratio of plagioclase to K-spar is approximately 2.5:1 and the average plagioclase composition is approximately $Ab_{90}An_{10}$.

Petrographic observations of the fraction of the sample coarser than 43 μm also support a volcanic source for the origin of the feldspars. These observations are:

1. Zoned plagioclase feldspars.
2. Euhedral and subhedral feldspars.
3. High concentration of feldspars relative to monocrystalline quartz (commonly 40 to 60% of the monocrystalline quartz plus feldspar fraction).

4. The association of high concentrations of feldspars and biotite.

5. The near absence of microcline as a potassium feldspar phase.

The distribution of feldspars in samples of the Pierre Shale also places controls on the rock types from which they could have been derived, and it is significant that areas of Pierre sediments which are the closest to the igneous and metamorphic source rocks of the Canadian Shield have the lowest feldspar concentrations. Other areas of possible igneous and metamorphic source rocks were not of a large enough magnitude to have furnished these feldspars.

If the feldspars were derived from the reworking of sediments, the concentration of feldspars relative to quartz should be more or less constant throughout the extent of the Pierre sediments for the following reasons:

1. The mixing of these sediments with others during transport to the shoreline. (Based on published paleogeographic maps, Gill and Cobban (1969), most of the sediments on the west side were transported more than 300 miles before deposition.)

2. The wide geographic extent of the Pierre deposits.

As can be seen in figure 21, the F/Q ratio is not constant. The feldspathic source rocks in the western source areas are the low grade metasedimentary rocks of the Precambrian Belt Series. Both the types of feldspars present in the Belt rocks and the quantity of rocks which would need to have been eroded, indicate that these low grade metasedimentary rocks were not the source of the majority of these feldspars.

In summary, the feldspars in the Q + F fraction suggests that the majority of feldspars were derived from a volcanic source rather than a metamorphic, granitic and sedimentary source rock.

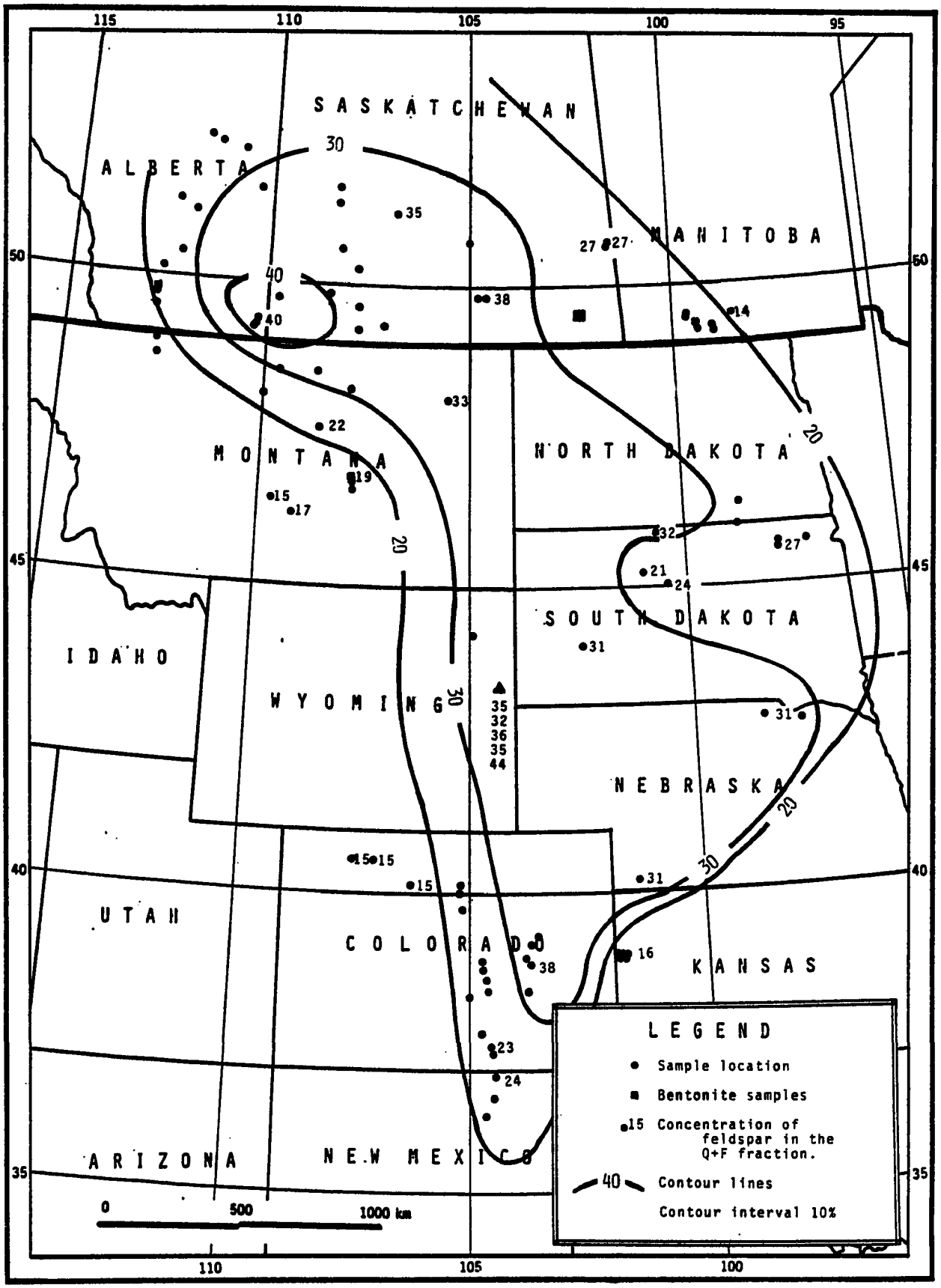

Fig. 21. Map showing the normative concentration of feldspars in the Q + F (quartz and feldspar) fraction of the samples. Concentrations for samples P-70, P-350, and W-8 are not shown as they are interpreted to contain authigenic quartz or feldspar.

Assuming that these feldspars are from a volcanic source, the model of deposition which seems most likely is the following. The nearest area of active volcanism was the Elkhorn Mountain Volcanics located in southwestern Montana. These volcanics are largely rhyolitic and andesitic in composition. Although some of the magma came out as lava and welded tuffs, the majority was deposited as volcanic ash. Some of this ash was deposited directly on the sea floor in large enough quantities to form bentonites. However, much of the ash was not deposited in sufficient quantities to form beds which could be recognized as bentonites, or the ash may have been reworked while on the sea floor. Also, much of the ash was not deposited directly in the marine seaway. Volcanic ash which was not deposited directly into the marine seaway would then be mixed with other sediments and carried into the marine basin by normal stream flow.

The mineralogic composition of the quartz plus feldspar fraction greater than 43 μm clearly indicates that the feldspars in this fraction are of volcanic origin. The results of the grain size analyses suggest that most of the fraction of the sample greater than 43 microns was transported to the site of deposition as a volcanic ash. Assuming that this fraction of the sample was transported as a volcanic ash, it is possible to make a rough estimate of the percentage of the average sample derived from direct transport of a volcanic ash.

Felsic volcanics contain from 0 to 90% phenocrysts. The average phenocryst content of the bentonites of the Mowry Formation is 2.9% (Slaughter and Earley, 1965). Using a low value of 0.5% phenocrysts in the Pierre samples (assuming that the monocrystalline quartz and feldspars greater than 43 um were original phenocrysts) and an average of 3.0% phenocrysts in the average volcanic ash,

then approximately 16% of the average Pierre sample was derived from a volcanic ash. This figure (16%) is low as the percentage of phenocrysts found in the Mowry Formation would be higher than in the Pierre Shale because most of the Mowry samples were located much closer to the volcanic source than are the Pierre samples, and the phenocryst content of volcanic ash decreases with increasing distance from the source (Mohr and Van Baren, 1954).

These calculations are related only to ash which was carried directly from the volcano to the depositional site. Normal transport could also have contributed much volcanic material into the Pierre seaway. A rough estimate of the total percentage of the average Pierre sediment derived from volcanic sources can be made using the feldspar data. In order to make an estimate of the percentage of Pierre sediments derived from volcanic rock, the feldspar concentration of the volcanic source rocks and other possible sediment source rocks must be known. Other than volcanic rocks the only other major sediment source rocks are assumed to be sedimentary rocks, which contain an average of 4.5% feldspar (Shaw and Weaver, 1965).

Assuming that the bentonites of the Mowry Shale (Lower Cretaceous) are representative of volcanic source rocks of Cretaceous age in this portion of western America, the feldspar content of the volcanic source rocks for the Pierre sediments can be determined by using the data of Slaughter and Earley (1965). In their study of the Mowry bentonites they concluded that the average bentonite contains 17% non-clay minerals, of which 70% is composed of feldspars. Based on this estimate, the average Mowry bentonite contains 12% feldspar and, therefore, the assumed volcanic source rock should contain 12% feldspar.

$$Pv = \frac{100 \times Cp - 100 \times Cs}{Cv - Cs}$$

where: Cp = Concentration of feldspar in the Pierre = 8.5
Cv = Concentration of feldspar in volcanics = 12.0
Cs = Concentration of feldspar in sediments = 4.5
Pv = Percent volcanics in the Pierre sediments

These calculations then show that a minimum of 50% of the average Pierre sediment was derived from volcanic sources. While these calculations are very speculative, the results do indicate that a substantial amount of the non-bentonitic Pierre samples are of volcanic origin.

Cristobalite and Smectites The occurrences of cristobalite and the clay mineralogy of Pierre samples also suggest that volcanic source rocks have contributed substantial volumes of sediment into the Pierre seaway.

The presence of cristobalite generally indicates one of two possible conditions: (1) the presence of large volumes of source rocks in which the majority of the silica is present in minerals or glasses which are easily weathered to produce hydrated silica ions, or (2) that the climate in the source area is sufficiently severe to cause the weathering of minerals in which the silica is tightly chemically bound. There is no evidence in the mineralogy of the Pierre Shale or in the associated nonmarine sediments to indicate that such a severe climate existed during Pierre time. In the source area of the Pierre Shale, the only major rock type present which could have been altered or weathered to produce a significant volume of hydrated silica is the volcanic rocks.

The clay fraction of the Pierre samples has large amounts of smectite and mixed layer illite/smectite. This is particularly true when the Pierre Shales are compared to Paleozoic shales which are presently found in the source areas of the Pierre Shale. The origin of these smectite-rich clays may have resulted from the weathering of the source rocks before

deposition. However, an alternative source for these smectitic clays in the Pierre Shale, as suggested by Grim (1968, p. 553) and Schultz (1978), is the alteration of volcanic ash to produce the large amounts of bentonites and smectites.

Sedimentary Source Rocks

Sedimentary rocks occupied the majority of the sediment source area for the Pierre Shale and therefore it is reasonable to assume that the majority of the Pierre sediments are recycled sedimentary rocks. The mineralogy and grain size of the Pierre Shale indicates, however, that the majority of the recycled sediments were derived from fine grained sedimentary rocks (such as shales) rather than from coarse grained sedimentary rocks such as sandstones. Although some of the Pierre sediments may have been derived from sedimentary carbonate rocks, such as limestones and marls, most of these rock types would have been weathered during transport and the sediment delivered to the seaway as dissolved salts and the insoluble residues found in original rock. Therefore, the volume of detrital sediments derived from the carbonate source rocks can be assumed to be minor.

Assuming that the majority of the recycled sediments delivered to the Pierre seaway were derived from shales and other fine grained mudrocks, the composition and grain size of the average shale should be similar to the composition and grain size of material deposited into the Pierre seaway.

Table 12 shows a comparison of the grain size and mineralogic characteristics of samples analyzed in other studies which are considered to be representative of the average shale. The mineralogic compositions determined by Clarke (1924) and Leith and Mead (1915) are not considered to be representative of the average shale as they are strictly normative analyses and

Table 12. Comparison of the grain size and mineralogic characteristics of the Pierre Shale to "average" shales.

Mineralogic Composition	Leith and Mead (1915)	Clark (1924)	Shaw and Weaver (1965)	Fleury (1971)	Blatt and Schultz (1975)	Pierre
Clay minerals	34	25.0	60.9	ND	ND	64.8
Quartz	32	22.3	30.8	30.9	27.6	22.9
Feldspars	18	30.0	4.5	ND	ND	8.5
Carbonates	8	5.7	3.6	ND	ND	2.8
Other Minerals	7	17.0	<3.5	ND	ND	<1.0
Mean size of quartz fraction in phi	ND	ND	ND	5.2	6.1	7.6

ND = Not Determined

were done before the chemical compositions of clay minerals were known. The data in table 12 clearly show that the Pierre Shale compositions and grain sizes are not well represented by the composition of the "average shale." Most of these differences may be explained in terms of weathering, transportation, diagenetic alterations, and dilution of the average shale sample.

Before attempting to explain these differences, it is instructive to compare the composition and grain size characteristics of the Pierre sediments to the characteristics of modern-day pelagic sediments. Such a comparison also is shown in table 8 and 12 and also in figure 22. These tables and the figure show that in some respects the compositions and grain size characteristics of Pierre sediments are comparable to these modern pelagic sediments. However, there are no known major pelagic deposits in the source area of the Pierre sediments. It is possible, however, that the same processes which differentiated these modern-day sediments from the "average shale" may also have differentiated the Pierre Shale sediments from the "average shale."

Sedimentary clays and clay minerals. The composition of the clay mineral fraction of the Pierre Shale samples shows that the clay mineralogy of the Pierre Shale is quite different from the "average shale." This difference is even greater when the clay composition of the Pierre Shale is compared to the clay mineral composition of shales older than the Pierre Shale. The principal difference found between the clay minerals found in the Pierre Shale and the "average shale" is the large volume of smectites found the Pierre Shale.

The occurrence of much of the smectites in the Pierre Shale was shown in earlier sections of this report to be related to the volcanic sediments deposited

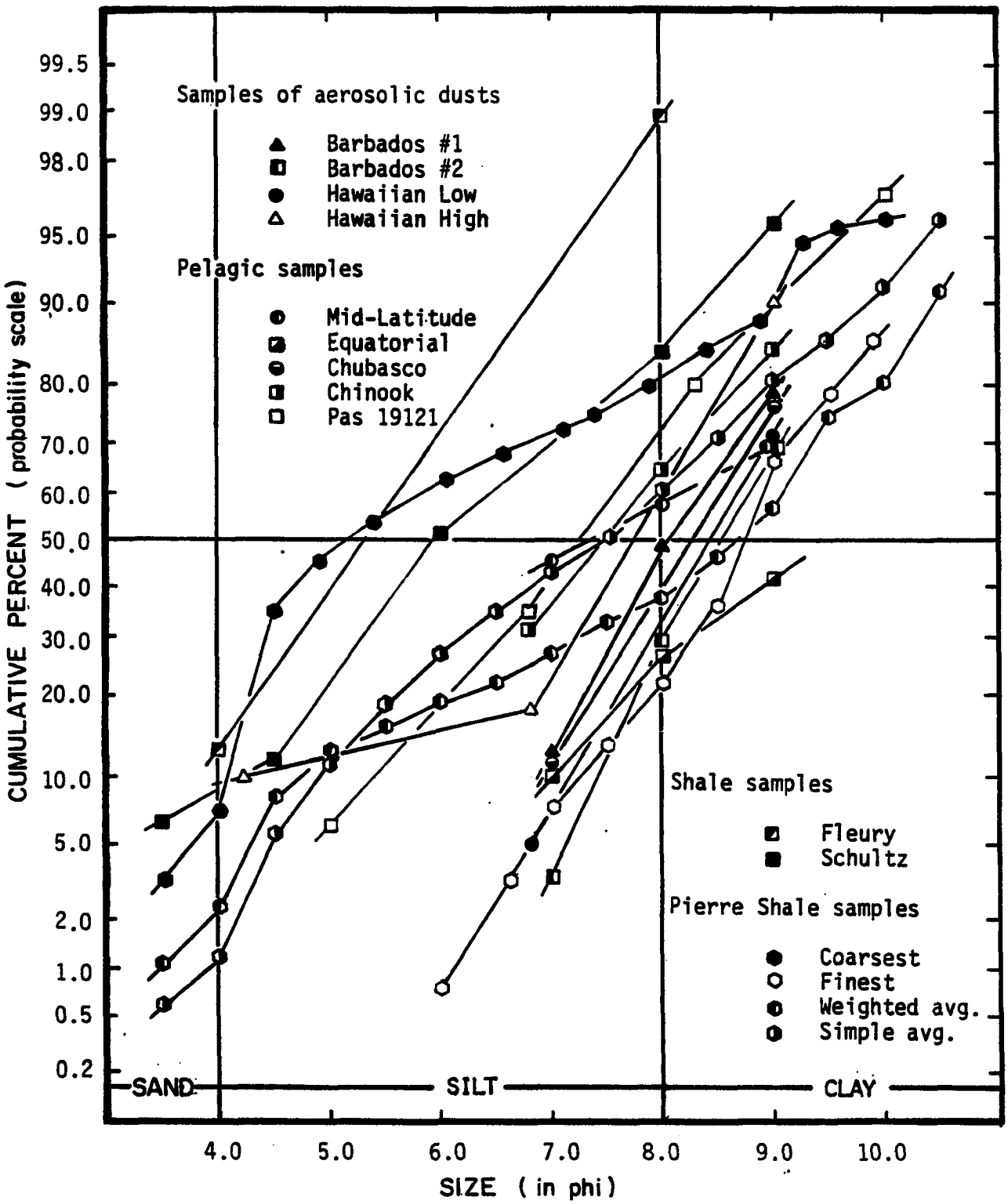

Fig. 22 Size distributions of the quartz fraction of some aersolic dusts, pelagic sediments, shales, and Pierre shale samples. More specific information concerning each of these samples can be found in table 8.

into the Pierre seaway. If the smectite composition of the clay mineral fraction of the Pierre Shale is neglected, then the remaining clay fraction would more closely resemble the clay mineral composition of the shales older than the Pierre Shale. Due to this resemblance and the previously mentioned distribution patterns of the clay minerals, it seems most likely that the origin of most of the clays, other than smectite, was from older recycled shale.

Igneous and metamorphic source rocks. Other than for volcanic sources there is no mineralogical evidence that a significant volume of sediments was derived from igneous or metamorphic source rocks. The only possible evidence of sediments derived from these sources is the concentrations of feldspars found within the Pierre Shale. However, neither the size, composition nor the areal distribution of the feldspars suggest that they were derived from either intrusive igneous or metamorphic rocks (see section on volcanic source rocks).

Transporting Mechanisms

The approach used to study the transporting agents was to examine the size distribution of the quartz plus feldspar fraction of the samples. The size distributions were used because changes in type or velocity of the transporting agent should be reflected in the grain size of the sediment. The quartz plus feldspar fraction was used because it is less susceptible than other minerals to diagenetic alteration.

The authigenic production of quartz in Pierre sediments has been shown to occur (see previous section) and this has unquestionably affected the size distribution of the quartz plus feldspar fraction of these samples. How great this effect has been cannot be accurately determined, but it is believed not

to be significant (see section on diagenetic alterations). In the present discussion, the effect of authigenic production of silica will not be considered as a significant factor in modification of the size distribution of the quartz plus feldspar (Q+F) fraction of the samples, except in those samples which are identified in the section on diagenetic alterations. It is possible that some of the quartz and/or feldspars have been removed by diagenetic changes that occurred since the sediment was deposited. However, no evidence has been found to suggest that any diagenetic changes have occurred which would have caused any significant changes in the size distribution of the Q + F fraction.

The size distributions of the Q + F fraction is polymodal (figure 11). Figure 23 is a graph of the weighted average size distribution of the Q + F fraction found in the Pierre Shale and the size distribution of the quartz in the "average shale." This figure shows that there is no correlation between the quartz available for deposition (assuming the quartz present in the "average shale" represents the available quartz) and the quartz found in the Pierre Shale. As can also be seen in figure 29, three of the four modes shown in figure 11 are present in the weighted average size distribution.

The transportation of detrital sediments into the Pierre seaway must have been the result of a combination of several transporting mechanisms. Had the Q + F fraction been transported by only one mechanism these size distributions should be unimodal or at least reflect the size distribution of the Q + F fraction available in the source area. The most important of these transporting mechanisms must be those controlled by water currents within the seaway and wind currents carrying sediments from the land areas and then

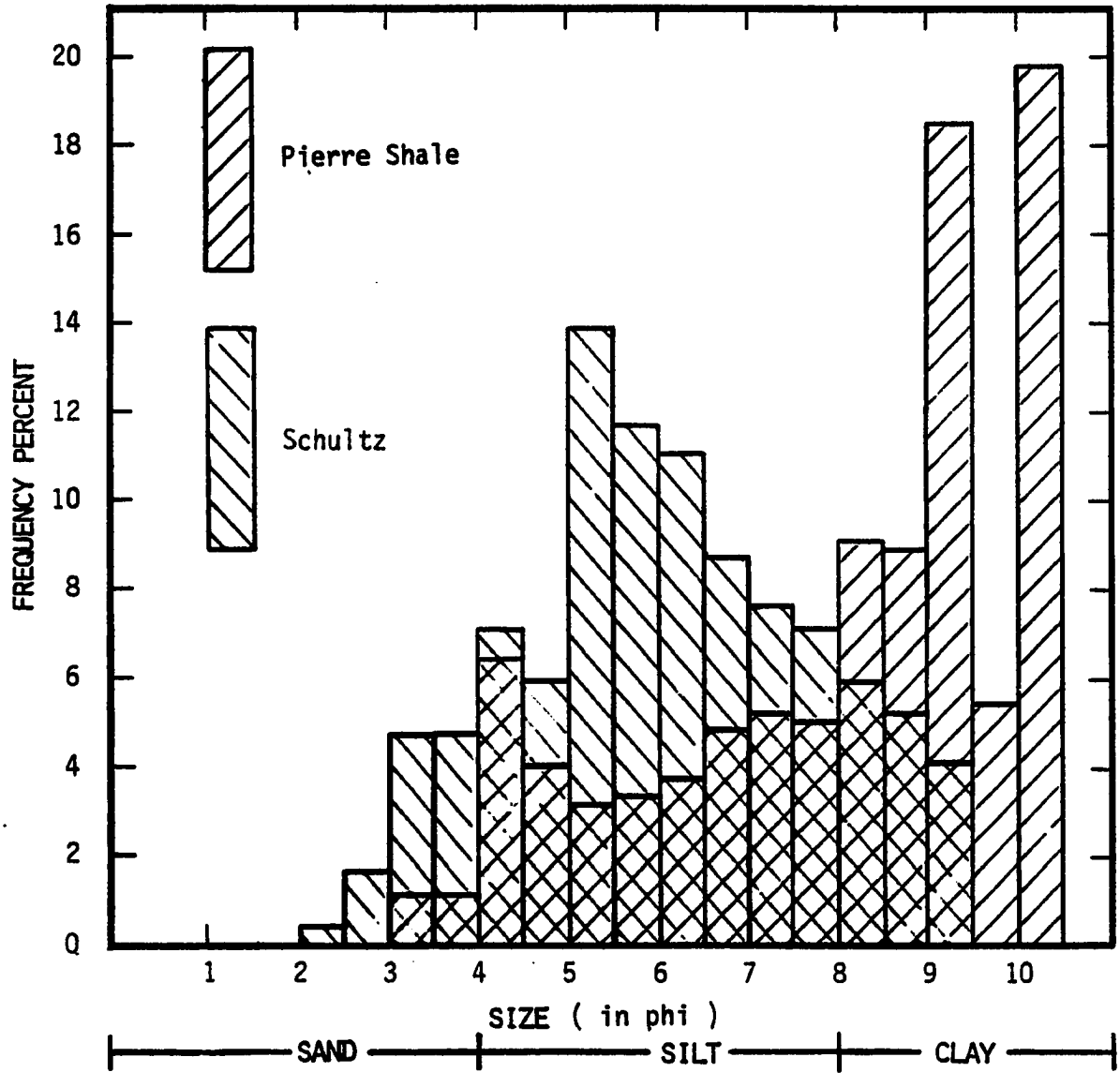

Fig. 23 Size distribution of the quartz and feldspar fraction in the weighted average Pierre Shale sample. Each sample was weighted proportionately according to the concentration of quartz found in the sample. Shown for reference is the size distribution of the average of the shale samples reported by Schultz (1975).

depositing these sediments within the seaway. Wind currents would normally carry only very fine grained sediments into the Pierre Seaway, compared to the size of the sediments which could be carried in by the water currents. Therefore, by evaluating the grain size distribution of these sediments it should be possible to evaluate the relative importance of these two transporting mechanisms. However, due to the active volcanic source areas present during the deposition of the Pierre Shale, the expected grain size distributions could be modified because of the wind transport of volcanic ash into the seaway. These size distributions would be modified because, during the volcanic event, the size of material blown into the atmosphere is significantly larger than could normally be picked up by the wind.

Direct Wind Transport of Volcanic Ash

There are several lines of evidence to suggest that the direct wind transport of volcanic ash into the Pierre seaway is a major source of Pierre sediments. Most of this evidence is related to the occurrence of feldspars. As shown in previous discussions, the most likely source for the majority of the feldspars found in the Pierre Shale is volcanic.

As shown in figure 24 there is a relationship between the mean grain size of the Q + F fraction and the concentration of feldspars in the Q + F + C fraction of the sample. The concentration of feldspars in the Q + F + C fraction of the samples increases as the mean size of the Q + F fraction increases. This trend was verified by analyzing the feldspar content of six samples as a function of the grain size of the Q + F fraction. The results of these analyses are shown in table 9. Also, the results of petrographic as well as feldspar analyses of the Q + F fraction greater than 43 microns showed that the majority of this fraction was quartz and feldspar. Much of the quartz

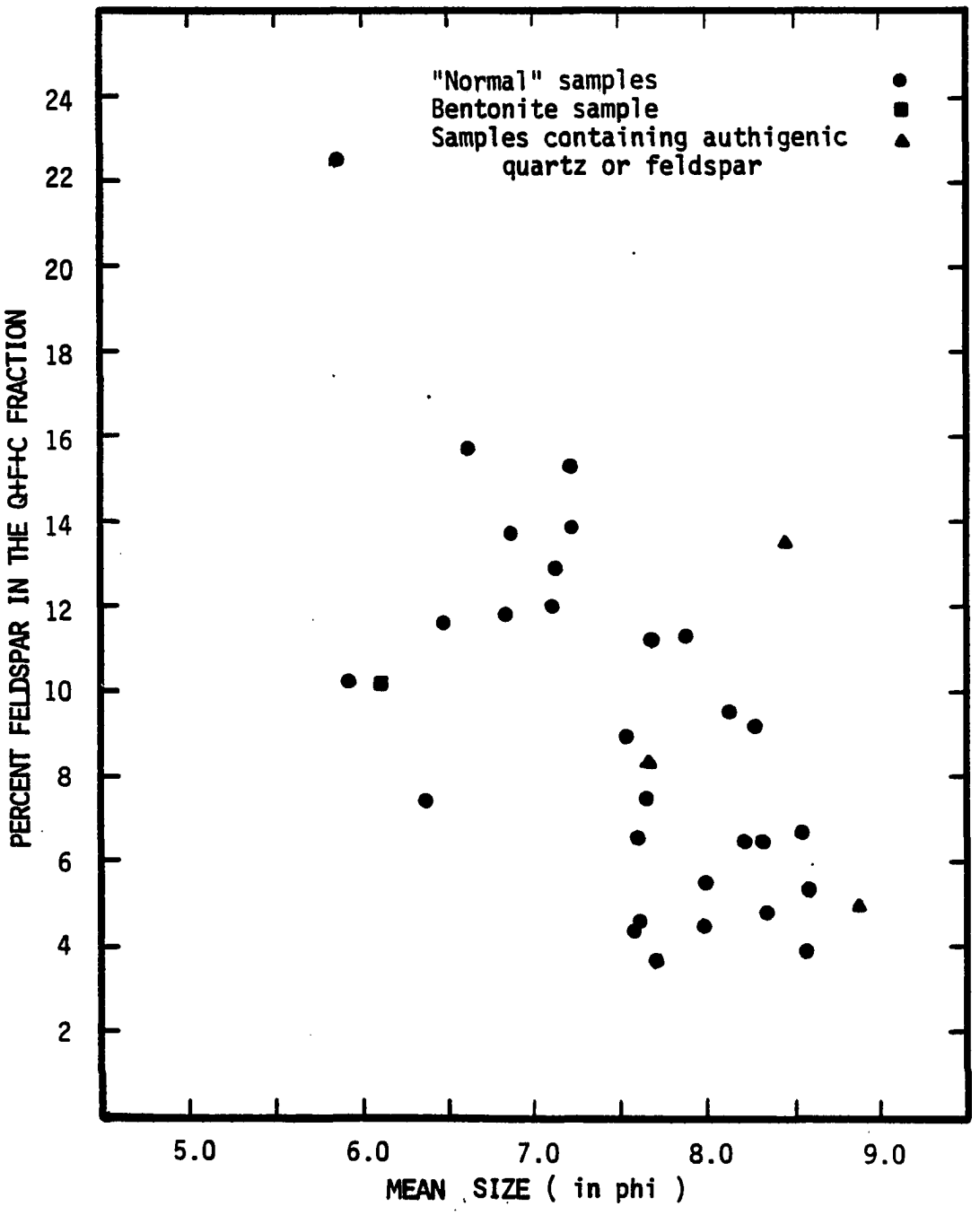

Fig. 24 Relationship between the mean size of the Q+F (quartz and feldspar) fraction and the feldspar concentration of the Q+F+C (quartz, feldspar, and clay) fraction of the whole rock.

found in this fraction is polycrystalline (see table 11) and is probably authigenic. This further emphasizes the importance of the feldspars found in this fraction.

The size fractionation of the feldspar indicates that the coarser sizes of the Q + F fraction have been transported in a different manner, and/or is derived from a different source, than the finer Q + F fractions. For the reasons listed above it is believed that coarse size distributions of the samples containing high feldspar concentrations are primarily the result of the direct transport of volcanic ash. Transport as a volcanic ash explains the concentration, composition and large particle size of feldspars present in these samples.

Wind Transport of Detrital Sediments

The fine-grained characteristics of the Q + F fraction of the Pierre samples suggest the wind transport of sediments into the Pierre seaway may have been a dominant process. Studies (Delany et al., 1968; Radezewski, 1939; Rex and Goldberg, 1958; Jackson et al., 1971; and Clayton et al., 1972) of the size distributions of wind transported quartz have shown that when transported over long distances, 25-70% of the quartz is clay sized. Furthermore, these studies and other studies of pelagic sediments have shown that the wind is an effective medium for concentrating and delivering clay-size quartz to areas of extremely slow rates of sedimentation (Rex and Goldberg, 1958). It therefore seems likely that wind transport of sediments into the Pierre seaway may explain many of the characteristics of the Pierre Shale.

Recurring particle size modes between 8.5 phi (2.7 microns) and 9.5 phi (1.4 microns) shown in figure 11 suggest that this fraction of the Q + F

fraction was wind transported. Rex and Goldberg (1958), Beltagy et al. (1972) and Delaney et al. (1967) have shown that in pelagic sediments wind blown quartz dust has a mode between 4μ and 1μ (see Fig. 22). The modes between 6.0 and 7.0 phi are explained as the result of water transport. The principal modes in samples near the western shoreline are generally between 6.0 and 7.0 phi, while the principal modes in samples taken near the eastern edge of the Pierre outcrops are all between 8.5 and 9.5 phi. This indicates a change in the transporting agent from water transport to wind transport with increasing distance from the western shore. Because the quartz and feldspars less than 6.0 phi are so small it seems unlikely that this size separation is caused by a gradual settling out of particles as a function of the length of transport time (that is distance of transport).

The relationship between the distance to the closest shore and the quartz concentration is shown in Figure 10. Although there is considerable scatter in the data, they do show a definite decrease in the quartz content as a function of increasing distance away from the western shore. This decrease is probably the result of the decreasing amounts of the sediment being supplied by water currents. As the amount of water-transported sediment decreases the relative importance of wind-transported sediment increases. With only a few exceptions of the samples deposited at distances greater than 100 km from the shoreline do not contain appreciable amounts of quartz and feldspars larger than 7.5 phi (22 microns). The exceptions are generally the highly feldspathic samples. This indicates transport of Q + F fractions away from the shoreline is generally limited to grains less than 7.5 phi (22 microns) in size, except in the highly feldspathic samples.

PROPOSED DEPOSITIONAL MODEL FOR THE PIERRE SEAWAY

Throughout the earlier sections much scatter in the data has been noted and many of the trends noted are not distinct. The scatter and the uncertain trends in the data can be explained if the interaction between the dominant processes are considered. Therefore, in this section a simplified model of the deposition of sediments into the Pierre seaway will be presented. The presentation of this model will then be followed by a discussion and review of the data in terms of this model.

Essential Features of the Model

The sediments delivered into the Pierre seaway were from two separate and distinct sources. These sources were the sedimentary rocks located on the western margin of the seaway and the volcanic source rocks located in southwestern Montana.

The volcanic source rocks are a particularly important source of sediments for the Pierre seaway as they contributed 30 to 50 percent of the detrital sediments. Much of this volcanic sediment was delivered directly into the seaway as volcanic ash. Some of the volcanic ash, however, was deposited on the land surface where it was weathered and then transported into the seaway by the same processes which were carrying in the recycled sedimentary grains.

The sediments derived from sedimentary rocks were mostly from shales and other fine grained rocks. The majority of these sediments were then transported into the seaway by eolian processes. During their transport, these sediments were size fractionated and their coarser fractions removed and deposited before arriving at the seaway. The source areas for these sediments must have been very extensive and not restricted to the close proximity of the seaway. Water transport may have carried much sediment into the seaway; however the coarse size fractions were deposited very near the shoreline with only minor amounts being carried further out into the seaway. Much of this coarse size fraction was carried north or south along the shoreline by longshore currents before being deposited.

Nearly all of the sediments were derived from the west and transported towards the east. The rates of deposition were slow near the western shoreline (see table 13) and even slower in the eastern areas of the seaway. In the eastern areas the rates of deposition, <18m/million years, were lower than those generally found in modern deep ocean environments, 30m/million years (Gill and Cobban, 1973).

The most characteristic feature of this sort of model is the variability of the mineralogic composition of sediments deposited under these conditions. This results from the eposodic nature of the volcanic events and the near instantaneous deposition of the volcanic ash. For example, compare the feldspar composition of two hypothetical sediment samples deposited at the same location during two different time periods, but one sample deposited during a period of active volcanism, the other during a period of volcanic quiescence (assuming no changes in other pertinent factors). Under these conditions we would expect the feldspar content to be very high in the sample deposited during the period of active volcanism, while

Table 13. Comparison of Average Rates of Sedimentation for the Pierre Shale and some Modern Marine Environments

Environment	Deposition Rate (In Meters Per Million Years)	Location	Formation	Reference
Non-marine Sedimentary Source	115	Wyoming	Pierre	Gill and Cobban (1973)
Non-marine Sedimentary Source	49	Montana	Pierre	Gill and Cobban (1973)
Non-marine Volcanic Source	104	Montana	Pierre	Gill and Cobban (1973)
Nearshore Marine	284	Wyoming	Pierre	Gill and Cobban (1973)
Nearshore Marine	70	Montana	Pierre	Gill and Cobban (1973)
Offshore Marine	<18	South Dakota	Pierre	Gill and Cobban (1973)
Offshore Marine	<18	North Dakota	Pierre	Gill and Cobban (1973)
Average of all Cretaceous Sediments	236	Not Given	Not Given	Kay (1955, table 2)
Deep Ocean	25	Atlantic	Modern Sediment	Erickson et al (1964, p. 731)
Deep Ocean	35	Not Given	Modern Sediment	Twenhofel (1939, p. 230)
Shoreline	900-1500	Sapelo, Ga.	Modern Sediment	Weimer (1970, p. 274)
Barrier Island	1200-1800	Gulf Coast	Modern Sediment	Weimer (1970, p. 274)
Deltaic	6000-12000	Mississippi Delta	Modern Sediment	Weimer (1970, p. 274)
Deltaic	5000-12000	Pendernales, Venezuela	Modern Sediment	Kidwell and Hunt (1958, p. 800)

the other sample should reflect the average feldspar composition of the sedimentary source rocks. As each sample represents only a short interval of geologic time (approximately 1000 years*) it is very probable that some samples would show no signs of volcanic activity while others show very prominent signs of volcanic activity. Also as the volcanic source area is relatively small and the transport of the volcanic material is towards the east, samples located near the shoreline but at a great distance north or south of the volcanic activity can be expected to show much less evidence of volcanic activity.

Fit of the Data to This Model

In this section the data collected will be reviewed and interpreted in terms of the preceding model. The main objective here is to show that the data can be explained in terms of this model.

The samples have been divided into two sets on the basis of their feldspar content. The first set contains less than 22.5 percent feldspar in the Q + F fraction, the second contains all of the remaining samples. The value of 22.5 was suggested by the distributional data points. The reason for differentiating the data on the basis of feldspar composition is that the concentration of feldspar is the best indicator of volcanic activity in these samples.

This grouping of the data into two different trends is shown in Figure 25. This figure shows a comparison of the feldspar composition of the Q + F fraction and the distance to the volcanic source. If all of the quartz and feldspar had been derived from sedimentary rocks we would

*These samples were collected from an interval approximately 2 inches (7.6 cm) thick. Assuming that the average depositional rate for the Pierre Shale was 7.31 cm/1000 years (Gill and Cobban, 1973) then each sample would represent one thousand years.

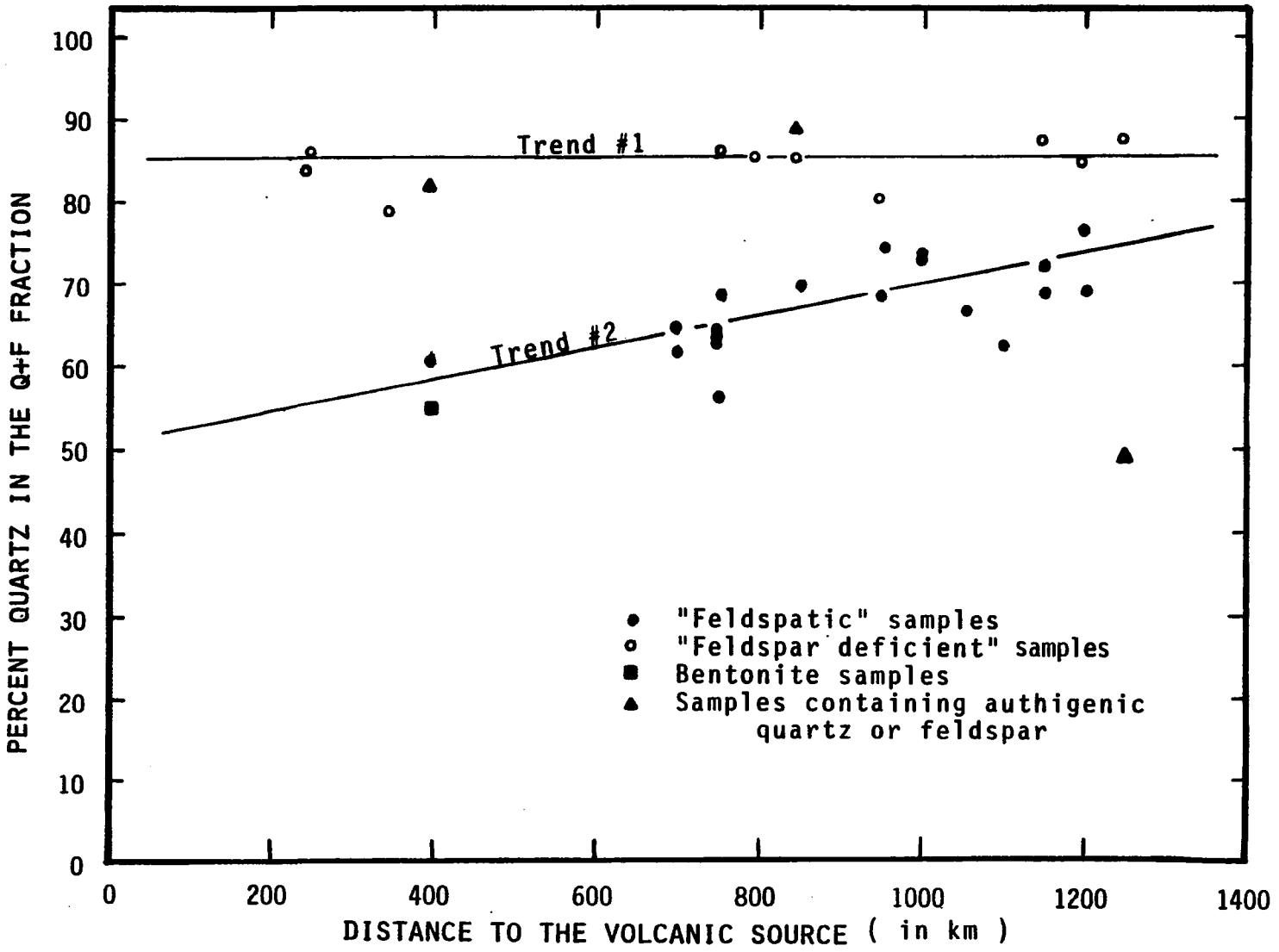

Fig. 25 Relationship between the percentage of quartz in the Q+F (quartz and feldspar) fraction of the sample and the distance to volcanic source area in west-central Montana.

would expect to find a constant percentage of quartz in the Q + F fraction due to the large and rather homogeneous characteristics of the sedimentary source rocks. Under these conditions we should expect the quartz to be approximately 87 percent of the Q + F fraction and the concentration of quartz in the Q + F fraction to show no trend with increasing distance from a possible volcanic source area. (The value of 87 percent was obtained from the data of Shaw and Weaver (1965) where they suggested that the "average shale" contained 4.5 percent feldspar and 30.8 percent quartz.) As indicated in prior discussions of the model it is reasonable to expect that many of the Pierre samples would contain few, if any, volcanogenic sediments. The feldspar deficient samples shown along the line marked "trend one" in figure 25, reflect samples in which little, if any, volcanogenic sediment is present.

In samples which contain appreciable volumes of volcanogenic sediments, the concentration of quartz in the Q + F fraction would depend on the amount, composition, and size of the volcanogenic sediments present. Even though these factors may be highly variable at a set distance from the volcanic source, the concentration of quartz in the Q + F fraction should increase with the distance from the volcanic source. This is due to the decrease in the volcanic source. Additionally, because the size of the volcanic ash decreases away from the volcanic source, so does the concentration of the phenocrysts and, therefore the concentration of feldspars is also reduced. The trend shown in figure 25 and marked "trend two" results from the mixing of quartz and feldspars from these different source areas. However, this "trend" may be largely coincidental. That is, it is possible that by mixing different proportions of the sedimentary and volcanic rock the concentration of quartz in the Q + F fraction could

range anywhere between zero and 87 percent quartz, although the most probable concentrations would be located near the line marked "trend 2" as shown in figure 25.

In figure 26 the relationship between the distance to the volcanic source and the feldspar concentration of the whole rock is shown. This figure shows no discernible trends in the feldspar concentrations of the "feldspathic samples" as a function of distance from the volcanic source. However, the "feldspar-deficient samples" do show that the amount of feldspars decreases as a function of increasing distance from the volcanic source (marked trend #1 in figure 26).

The trend shown in the "feldspar-deficient samples" is related to the amount of Q + F found in the sediments derived from the sedimentary rocks. As the volcanic sources were located near the edge of the seaway, the distance to the nearest shoreline is related to the distance to the volcanic source. Because the amount of quartz and feldspar in the "feldspar-deficient samples" is related to the distance to the nearest shoreline, the trend shown in the "feldspar-deficient samples" results. From a theoretical basis the "feldspar-deficient samples" could be found anywhere within the area shown in figure 26 depending only on their quartz concentration.

The model predicts that the amount of feldspar found in the "feldspathic samples" is partly a function of the distance from the volcanic source; therefore, the absence of a trend was unexpected. The absence of this trend is explained by variations in the amount of feldspar derived from sedimentary source rocks. These variations are related to the factors which controlled the amount of quartz and feldspar found in the sediments (derived from sedimentary rocks) delivered into the seaway. Because the percentage of Q + F fraction in the sediments derived from sedimentary

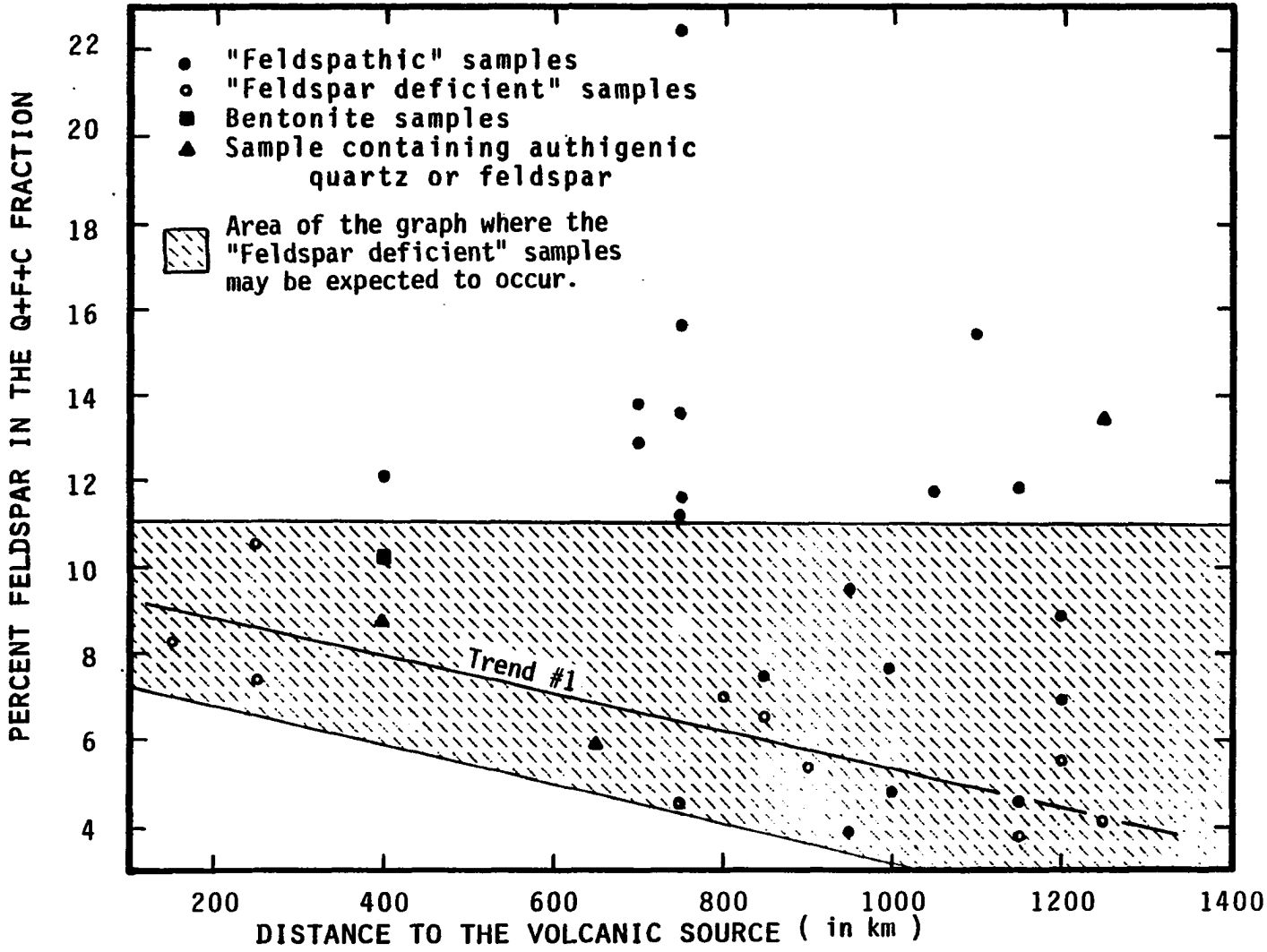

Fig.26 Relationship between the percentage of feldspar in the Q+F+C (quartz, feldspar, and clay) fraction and the distance to the volcanic source area in west-central Montana. Trend #1 represent the trend shown the "feldspar deficient" samples.

rocks varies depending on the distance of transport, the mode of transport, and many other factors, the percentage of feldspars found in the whole rock also varied as a function of these factors. For example, compare two hypothetical samples composed entirely of sediments from sedimentary rocks, one containing 50% Q + F, 50% clay and the other containing 10% Q + F, 90% clay. Assuming that 13% of the Q + F would be feldspar, one sample would contain 6.5% feldspar and the other sample would contain 1.3% feldspar. These factors cause a great deal of scatter when the feldspar data are compared to whole rock data but do not cause scatter when the feldspar is compared only to the Q + F fraction as shown in figure 25.

Figure 27 shows the relationship between the concentration of feldspar and the concentration of quartz in the whole sample. The data separate into two different trends, one for the feldspathic samples and the other for feldspar deficient samples. The feldspar deficient samples follow a trend which appears to be linear and can be extrapolated to zero, showing that the ratio between the feldspar and quartz is constant. This constant ratio would be expected if the quartz and feldspars were derived from the same source. On the basis of the average shale we would expect the ratio of quartz to feldspar to be 6.7. The ratio calculated from the best fit linear regression line using only the feldspar deficient datais 5.7.

The trend shown by the feldspathic samples may also be explained in terms of a straight line. A least squares linear regression of the feldspathic samples shows a best fit line with an intercept of 10.8 and a slope of 0.97. If we assume that the average feldspathic sample was composed of one-third sediment from sedimentary source rocks and two-thirds

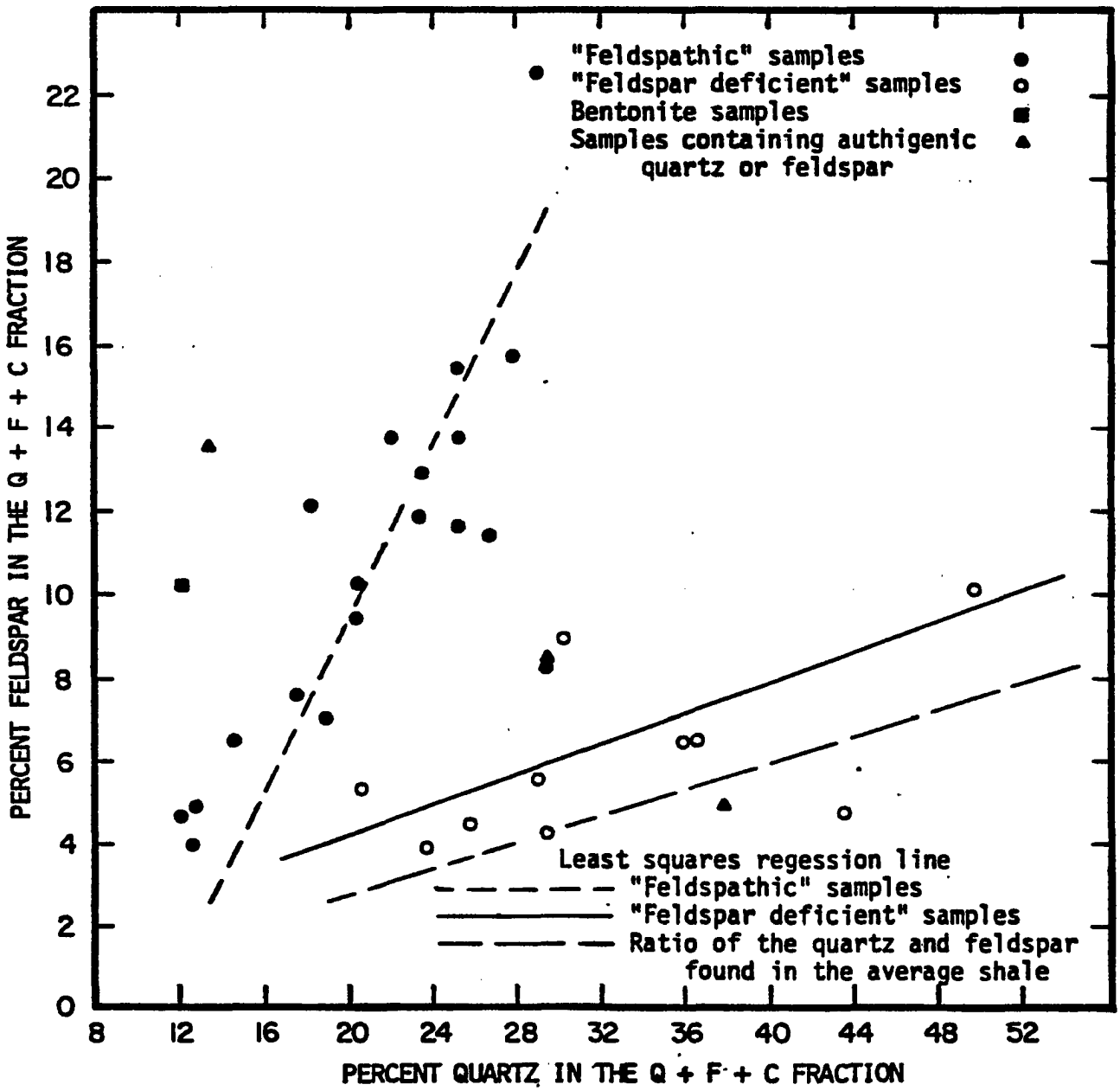

Fig. 27. Relationship between the percentage of quartz and normative feldspar in the Q + F + C (quartz, feldspar, and clay) fraction of the whole rock. The correlation coefficient for the "feldspathic" samples is 0.81 and the correlation coefficient for the "feldspar deficient" samples is 0.79. The ratio of quartz to feldspar found in the average shale was obtained from the data of Schultz (1975).

bentonite, and also assume the quartz to feldspar ratio in the volcanic ash to be 1.0, a trend similar to the trend shown by the feldspathic samples would result.

The trends seen in the comparison of quartz to feldspar composition in the whole rock (see figure 27) are also seen when only specific types of feldspars are considered as shown in figure 28 and 29.

From figure 30 it can be seen that the quartz and feldspar concentrations appear to be at least partly controlled by the particle size of the Q + F fraction. Again two different trends are shown , the "feldspar-deficient" and "feldspathic" sample subsets. The proposed model predicts that in the sample derived mainly from sedimentary rocks, the percentage of feldspars found in the Q + F fraction would be approximately 13 percent, and completely independent of the grain size. Thus, one would expect the trend shown for the "feldspar deficient sample." However, the model does predict that the concentration and size of the feldspar in the "feldspathic" sample is dependent on the nature and quantity of the volcanic ash.

The trend in the "feldspathic sample" can be explained as the mixing of varying amounts of volcanic ash having relatively coarse grained feldspar and quartz phenocrysts with sediments having relatively fine grained quartz and feldspars derived from sedimentary rocks. Alternatively, we could explain this trend in terms of constant proportion of the two different sediment types, but with the size of the quartz and feldspar phenocrysts in the various volcanic ashes varying from very fine grained sizes ($<9\phi$) to very large grained sizes ($<6\phi$).

As shown in figure 31 there is a grouping of the "feldspar deficient" and "feldspathic" samples even though the feldspar composition is not

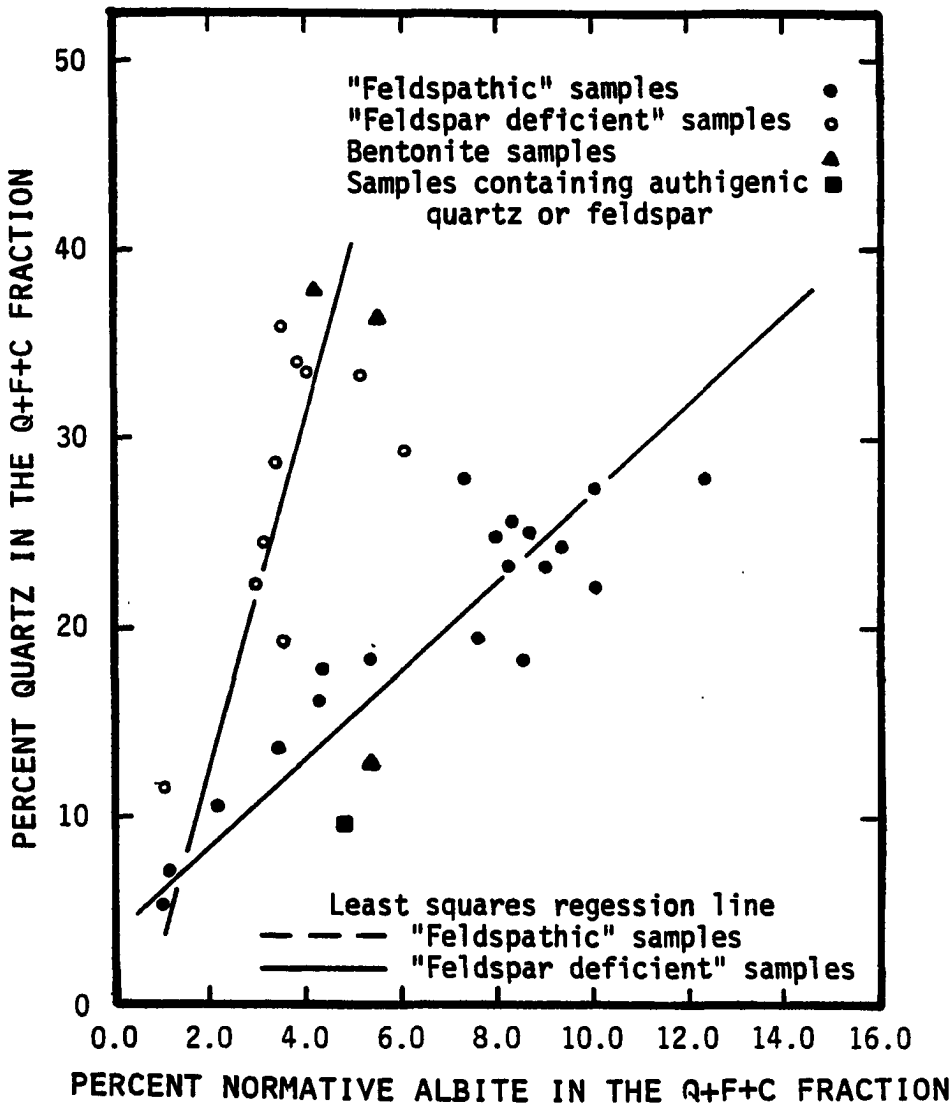

Fig. 28 Relationship between the percentage of normative albite and quartz in the Q+F+C (quartz, feldspar, and clay) fraction of the whole rock. The correlation coefficient for the "feldspathic" samples is 0.90 and the correlation coefficient for the "feldspar deficient" samples is 0.69 .

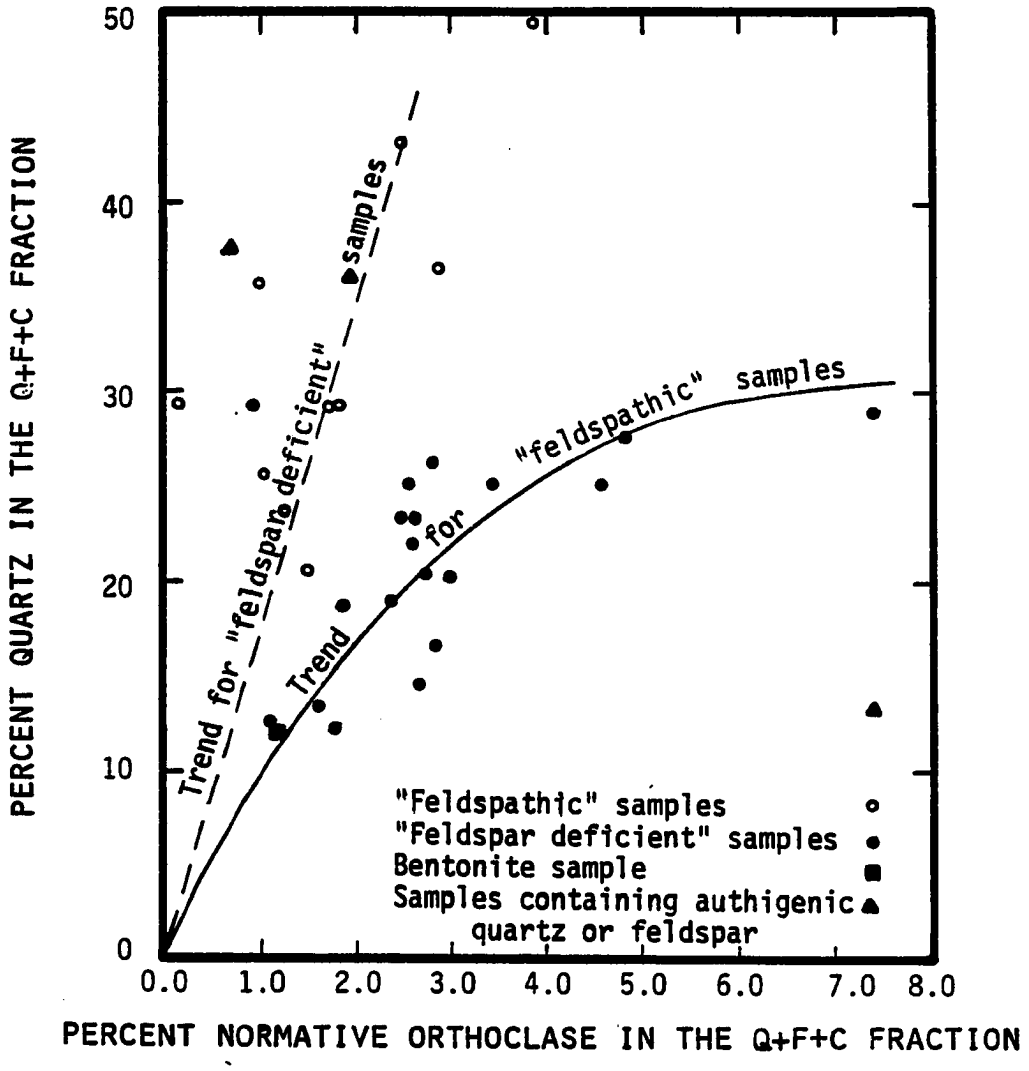

Fig. 29 Relationship between the percentage of normative orthoclase and quartz in the Q+F+C (quartz, feldspar, and clay) fraction of the whole rock. Trend lines have no mathmatical significance.

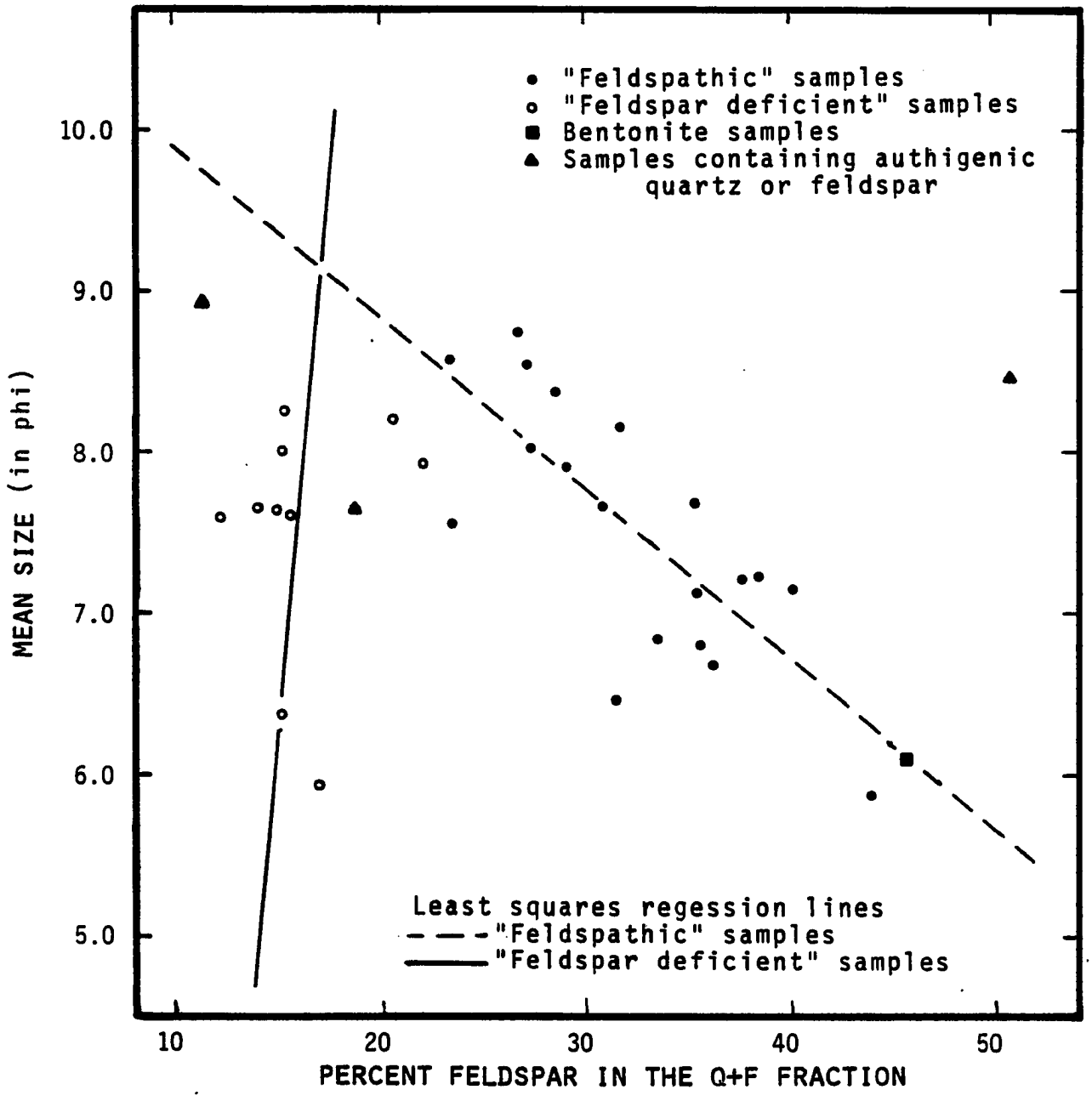

Fig. 30 Relationship between the percentage of feldspar in the Q+F (quartz and feldspar) fraction and the mean grain size of the Q+F fraction. The correlation coefficient for the "feldspathic" samples is -0.75 and the correlation coefficient for the "feldspar deficient" samples is 0.19.

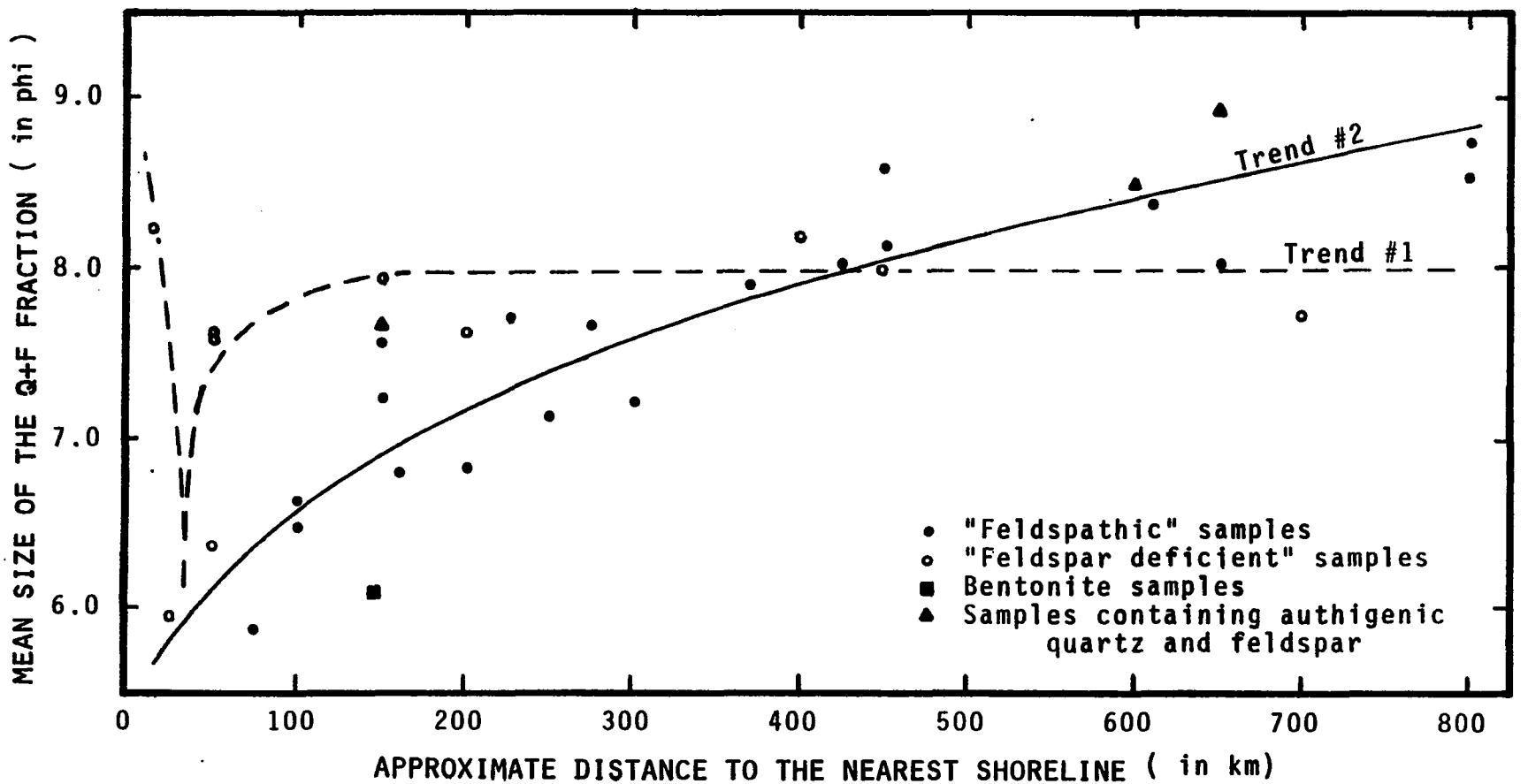

Fig. 31 Realationship between the mean size of the Q+F (quartz and feldspar) fraction and the approx-distance to the nearest shoreline. The lines shown for trends 1 and 2 are drawn only to help visulize the trends and have no mathmatical significance.

included as one of the sample variables. This figure indicates that for the "feldspar deficient" samples the mean size of the Q + F fraction is controlled by the distance of the sample to the nearest shoreline. That is, the size of the Q + F fraction may vary between 6 and 8 phi when the sample is located within 50 km of the shoreline but that at greater distances the mean size of the Q + F fraction is relatively constant and averages approximately 7.8 phi. This is interpreted to mean that the various effects of shoreline processes do not extend beyond 50 km from the shoreline and that the conditions and mechanics of non-volcanic sedimentation are stable and constant beyond 50 km from the shoreline.

The size of the Q + F fraction in the feldspathic samples, however, depends on the volcanic content of the sample as well as on the size of the Q + F fraction in sediments derived from sedimentary rocks. Because of the volcanic input, the size of the Q + F fraction in these samples will be controlled by the size of the quartz and feldspar phenocrysts found in the volcanic fraction of these samples. As the volcanic sources are located near the shoreline, we can expect the distance to the volcanic source to also increase as does the distance to the nearest shoreline. Studies of volcanic ash have shown that the size of volcanic ash decreases as the distance of transport increases. As the size of the volcanic ash decreases we would also expect the size of the quartz and feldspar phenocrysts to decrease. Therefore the trend shown by the feldspathic samples in figure 31 should be expected.

The data of Slaughter and Earley (1965) as well as the data of Baak (1949) (referenced in Mohr and Van Baren , 1954) indicate that the phenocryst content of volcanic ash and amount of the quartz and feldspars decrease with decreasing size of the volcanic ash and with increasing distance away

from the volcanic source. The decrease in phenocryst content with distance of transport would explain the trend of the feldspathic samples shown in figure 32. This figure relates the percentage of feldspars in the Q + F fraction to the distance to the nearest shoreline. The trend shown by the "feldspathic samples" is one of decreasing feldspar content as a function of increasing distance away from the shoreline and as mentioned earlier, the distance is related to the distance of volcanic transport. Had more samples been taken we might expect to see the entire area between the "feldspathic" and "feldspar-deficient" samples filled with samples depending on the amount of volcanic material contained in each sample. Again the trend seen in the "feldspar-deficient" samples reflect the unchanging feldspar composition of their source area.

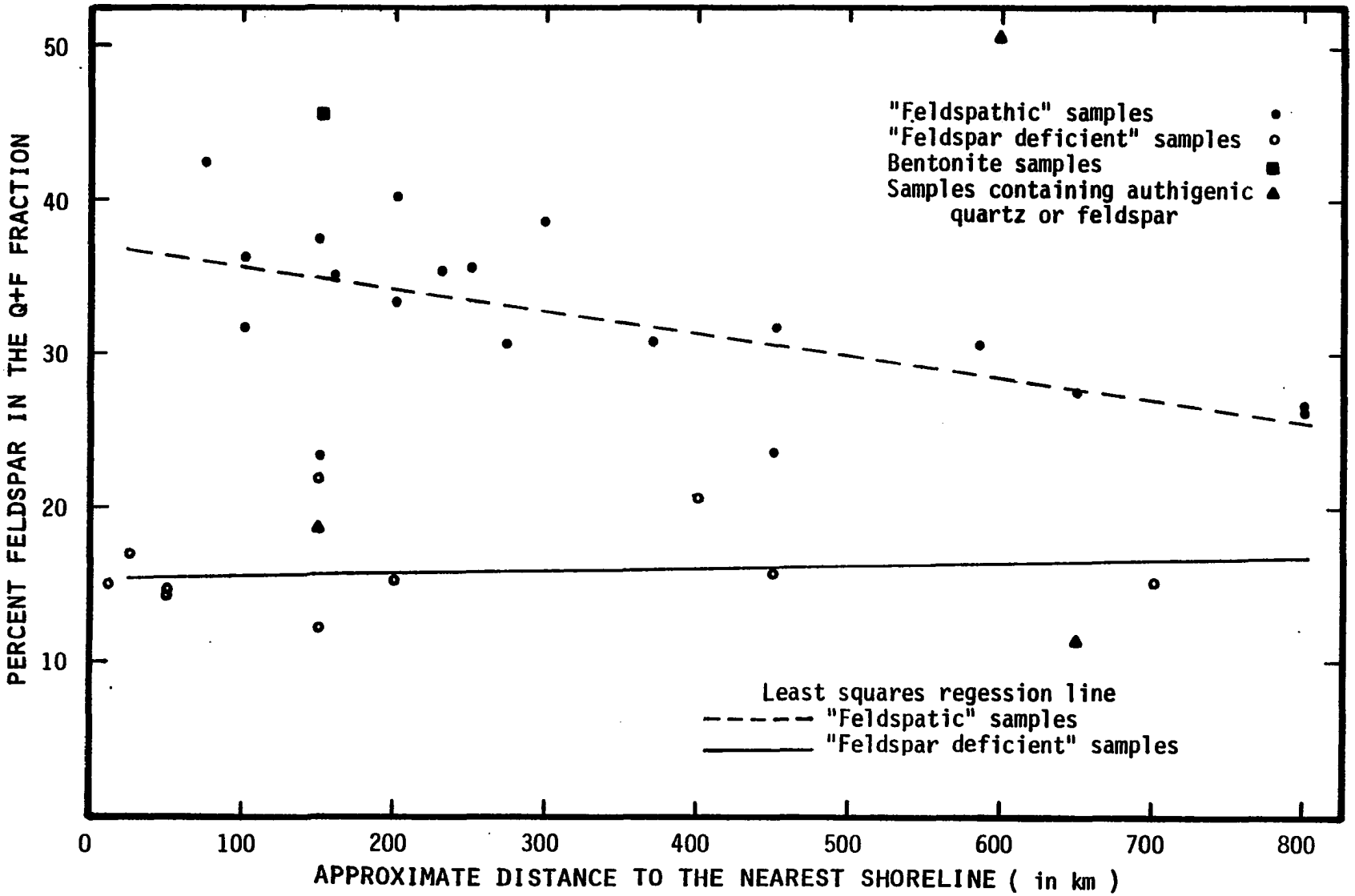

Fig. 32 Relationship between the percentage of feldspar in the Q+F (quartz and feldspar) fraction and the approximate distance to the nearest shoreline. The correlation coefficient for the "feldspatic" samples is-0.58 and the correlation coeficient for the "feldspar deficient" samples is 0.10 .

DIAGENETIC ALTERATIONS

Any discussion of the diagenetic alterations of a rock presumes that the original composition of the rock is known. Because we do not 'know' what the original compositions of these samples were, the interpretation of diagenetic alterations can be only ascertained by identifying authigenic phases or noting when the occurrence of a mineral phase is anomalous when compared to other samples. If the diagenetic alterations do not produce either identifiable authigenic phases or anomalous occurrences, the diagenetic alterations of rock can be discussed only in terms of comparison of this unit to modern sediments.

Origin of the Cristobalite

Cristobalite is known to form during the crystallization of some volcanic rocks, as a product of the weathering of volcanic rocks, as a product of hydrothermal alteration, and as an authigenic sedimentary mineral. Due to the large concentrations and wide areal distribution of Pierre samples with cristobalite present, weathering, hydrothermal and primary volcanic sources can be ruled out as the major source of this mineral. Although these sediments frequently contain many bentonite beds, the amount of bentonite present (less than 1% of the total volume of sediment) cannot account for the total amount of silica needed to produce these siliceous shales.

Conversion of Biogenic Opal to Cristobalite

Petrographic analyses of the cristobalitic samples show that at least some of the cristobalite has been formed from biologic opal. This is

demonstrated by the presence of diatom and radiolarian fossils composed of cristobalite (Fig. 33). The photomicrographs of these fossils, shown in figure 34, show varying degrees of preservation. X-ray analyses of these fossilized diatoms show that the cristobalite has the crystalline form of opal-C. Because of the fine-grained nature of these samples only rarely can the fossils be seen in thin sections. However, when the fine-grained fractions of the cristobalitic samples are removed, the coarser fractions (the fraction greater than 43 μm in size) are composed almost entirely of fossils and fossil fragments. Many of the samples containing these cristobalite fossils also contained opal-CT, which acts as a cement. The treatment to disagregate the rock (see Appendix VIII) dissolved the opal-CT and may have destroyed a significant proportion of the fossils. Therefore, their abundance in these samples may be underestimated.

Cristobalite also occurs in many grains which do not appear to be fossils. Most of these grains are polycrystalline and, except for their index of refraction, have the same appearance as the polycrystalline quartz grains (see figure 35). The most likely origin for these grains is that they formed from biogenic opal, and that during the transition from opal to cristobalite their biologic appearance has been lost.

The majority of the cristobalite present occurs not as cristobalitic fossils, but rather as a fine grained cement. The origin of this fine grained cristobalite is also thought to be the recrystallization of biogenic opal.

In Cenozoic marine sediments, cristobalite forms through the recrystallization of opaline material. The sequence for the formation of cristobalite in the Monterey Formation in California, as reported by Murata and

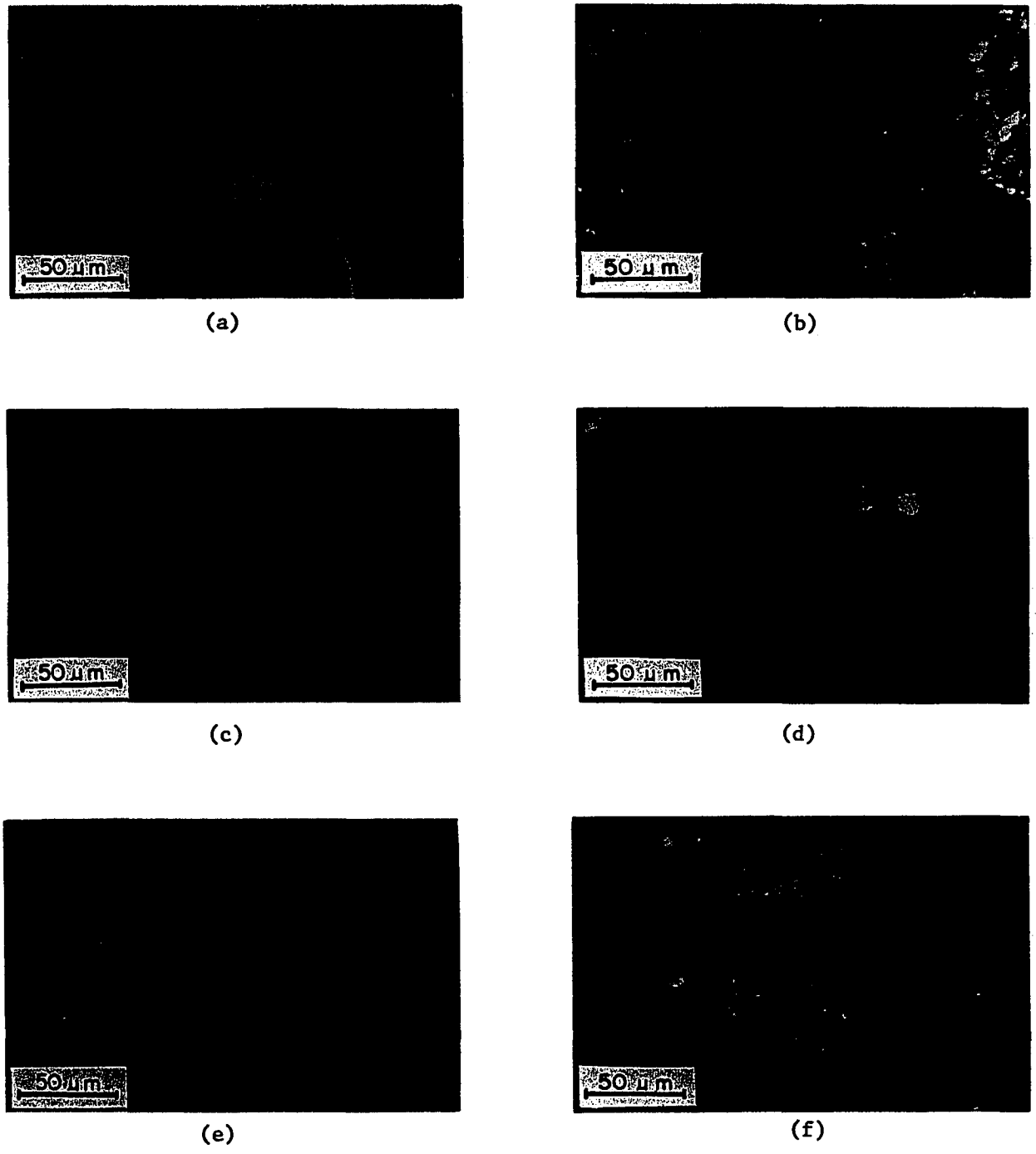

Fig. 33. Photomicrographs of cristobalite fossils. (a) Radiolarian fossil from P-186; (b) Same as (a), but with x-nicols; (c) Diatom from P-271; (d) Same as (c), but with x-nicols; (e) Radiolarian fossil from P-186; (f) Same as (e), but with x-nicols. The fossils were all identified by L. R. Wilson. The presence of cristobalite is confirmed by the low birefringence seen with x-nicols.

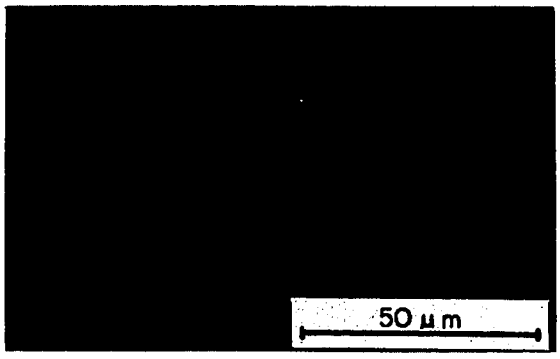

(a)

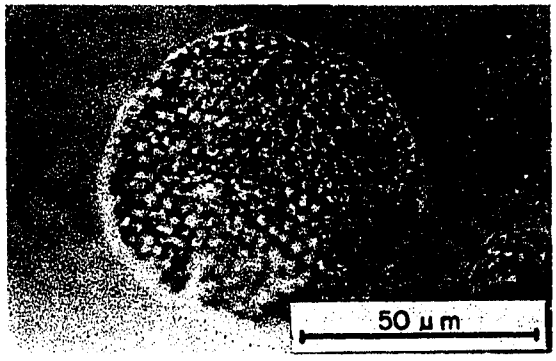

(b)

(c)

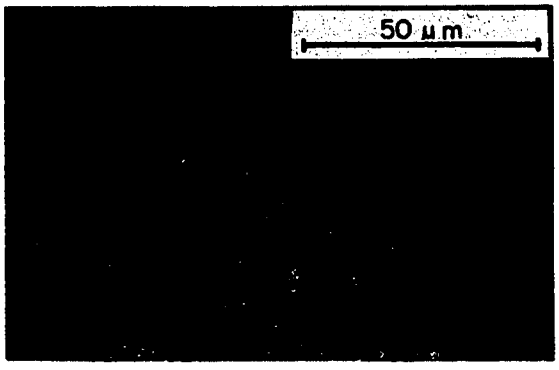

(d)

(e)

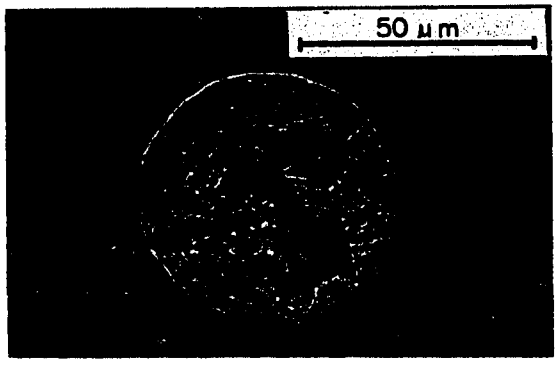

(f)

Fig. 34. Photomicrographs showing the various stages of preservation of the cristobalite diatoms. All of the photomicrographs are from sample P-270. The diatoms were identified by L. R. Wilson.

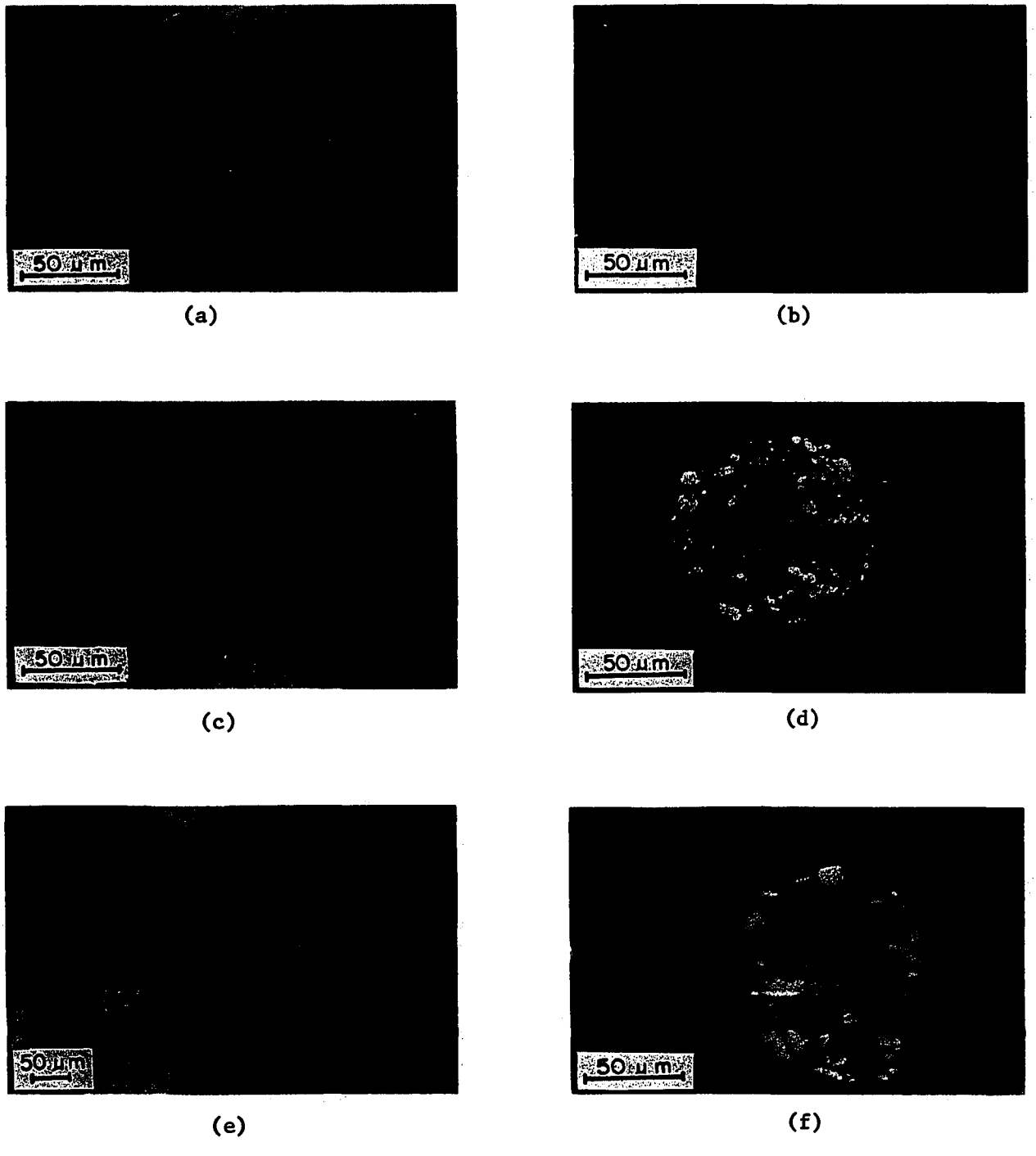

Fig. 35. Photomicrographs of cristobalite and polycrystalline quartz grains. Cristobalite grains from RB-8 (a) having the appearance of polycrystalline quartz when viewed under plain light, but under x-nicols (b) are shown to be cristobalite. Polycrystalline quartz grains from P-186 (c and d) having the same shape and general appearance as the cristobalite fossils seen in the right side of the photographs. Polycrystalline quartz grains (c and f) appear to be pseudomorphic after a foraminifera skeleton.

Larsen (1975) is: biogenic opal cristobalite diagenetic quartz. A transition from opal to cristobalite occurs at an inferred maximum burial depth of 730 meters (at a temperature of 45°C) and a transition from cristobalite to quartz occurs at about 2,030 meters (at a temperature of 105°C). Schultz (1978) estimated that the Pierre Shale, in the areas which contain much cristobalite, had a burial depth of only 300 to 600 meters. These depths of burial do not correlate to the depths at which Murata and Larsen (1975) found the conversion of biogenic opal to cristobalite in the Monterey Formation. Mizutani (1970), however, has shown that time, temperature, and pressure (depth of burial), all control the conversion of biogenic opal to cristobalite. It therefore seems likely that some combination of these three factors has caused the conversion of biogenic opal to cristobalite to occur at depths of burial less than those depths at which this conversion occurs in the Monterey Formation.

In summary, cristobalite was probably produced from the recrystallization of a biologic opal. Inorganic precipitation of opal is not thought to be likely, as the presence of living siliceous organisms has been shown to be the controlling factor in the deposition of recent opaline deposits. The silica was probably derived from volcanics in the source area then transported into the Pierre Seaway.

Origin of the Polycrystalline Quartz

From 0 to 90% of polycrystalline quartz is found in the coarser than 43 μm fraction of the Q + F fraction of the Pierre Shale samples. The percentage of polycrystalline quartz in this fraction of the shale appears to be independent of any identifiable sedimentary controls. However, the nature of the

occurrences and petrographic characteristics of the polycrystalline quartz, suggest that much of the polycrystalline quartz is authigenic and/or diagenetic.

Many polycrystalline quartz grains have shapes, crystal fabrics, and sizes similar to the cristobalite fossils and grains described earlier. Some of these grains are shown in figure 35. The polycrystalline nature of these quartz grains probably reflects pseudomorphing after the cristobalite. This inference seems likely based on the conclusions of Murata and Larsen (1975) that cristobalite recrystallizes to quartz as a function of depth of sediment burial.

Some polycrystalline quartz grains show structures similar to those seen in foraminifera (Fig. 35). The presence of pseudomorphs of quartz after foraminiferal skeletons clearly indicates that some of the carbonate in these samples has been replaced by polycrystalline quartz. In a few disaggregated samples needle-shaped crystals of calcite are found (Fig. 36b). Grains of polycrystalline quartz with similar shapes and sizes (see Fig. 36) are found in samples lacking these calcite grains. Thus, some of the polycrystalline quartz may have replaced calcite needles.

The polycrystalline quartz in some samples contains many inclusions of clay and there seems to be a complete gradation between pure polycrystalline quartz and clay (see figure 36). These occurrences suggest that the quartz originated as a clay-binding cement. The cement may have been opal or cristobalite. As mentioned before, in most of the samples containing opal-CT, the opal-CT is present as cement.

In most samples the proportion of polycrystalline quartz in the Q + F fraction of the sediment is size dependent. Figure 37 shows this relationship for three different samples. These curves show a very high percentage

(a)

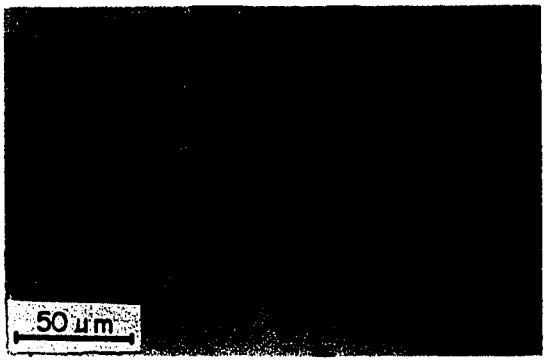

(b)

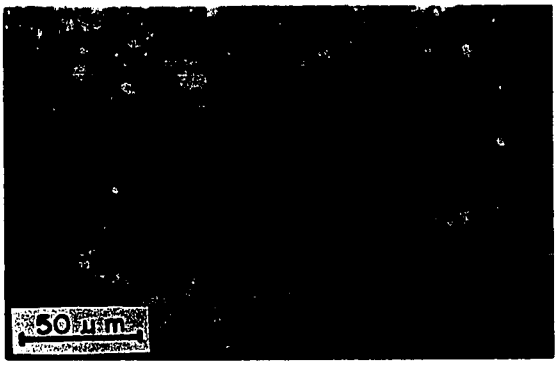

(c)

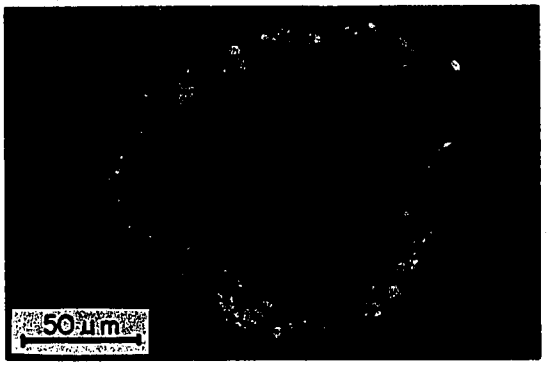

(d)

(e)

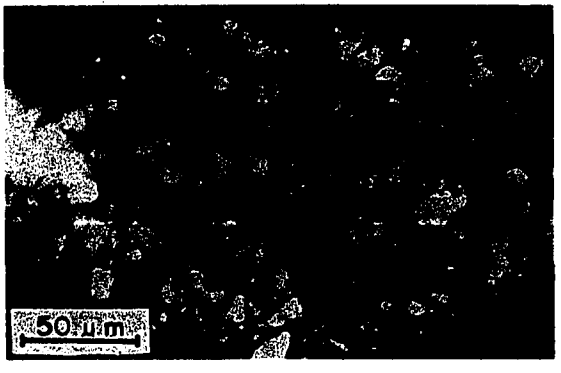

(f)

Fig. 36. Photomicrographs of polycrystalline quartz grains. The origin of the rectangular grains found in P-313 (a) are not known, but based on the occurence of the lath shaped calcite grains found in P-75 (b), one possible origin for these quartz grains is that they are pseudomorphic after other lath shaped calcite grains. Photos (c), (d), (e), and (f) show the gradation between clay and polycristolline quartz. Note the rims of polycrystalline quartz in (c), (d). and (e). The center of the grain in (f) appears brownish when viewed under plain light.

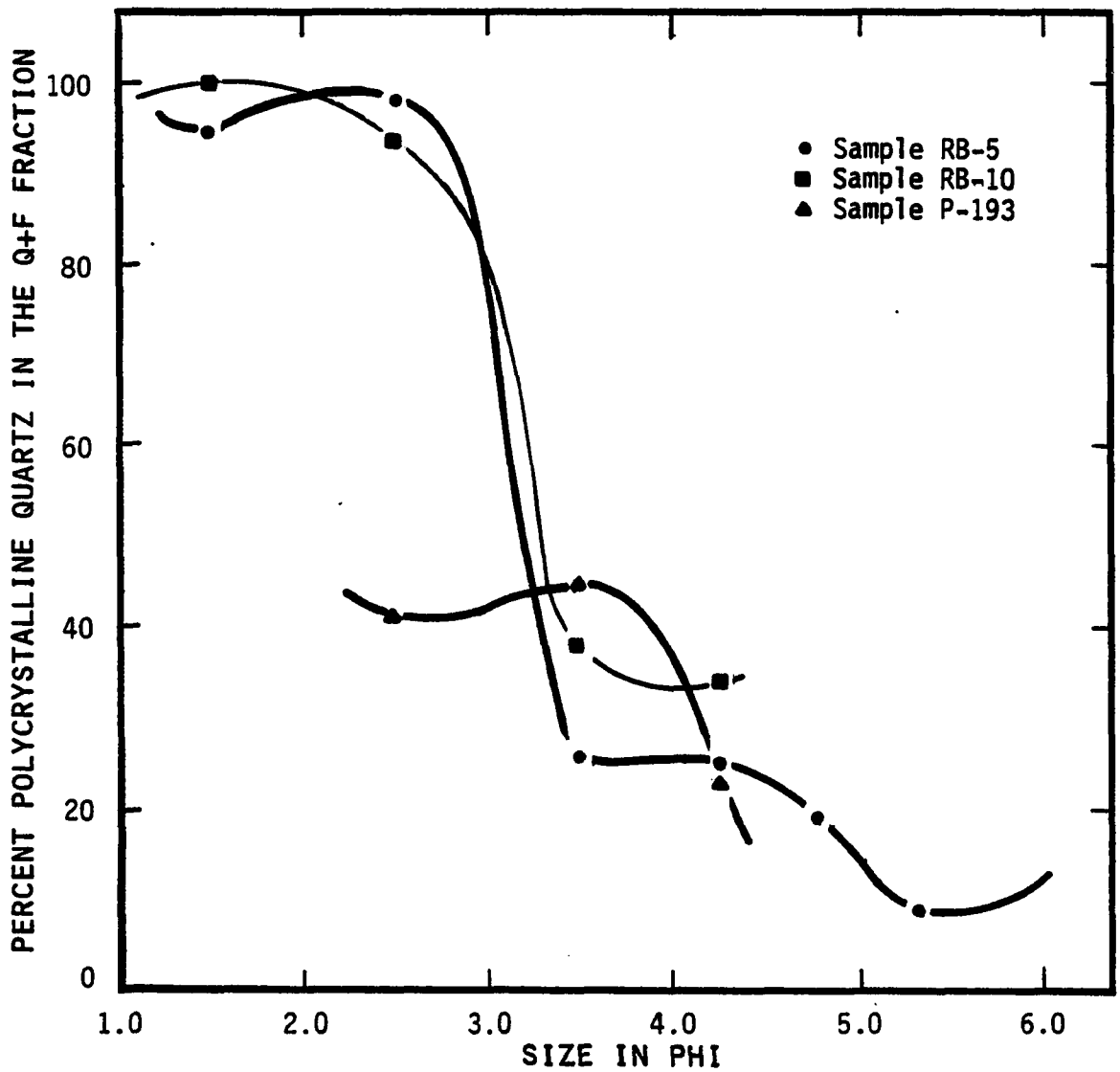

Fig.37 Relationship between the percentage of the Q+F (quartz and feldspar) fraction composed of polycrystalline quartz and the size distribution of the Q+F fraction.

of polycrystalline quartz in the coarser size fractions with the percentage of polycrystalline quartz sharply decreasing in the finer size fractions. Figure 38 shows the size distributions of the Q + F fraction and the polycrystalline quartz fraction of RB-5. The actual percentage of polycrystalline quartz in the total quartz fraction is quite small, generally less than 2%. In terms of the whole sample the percentage of polycrystalline is generally less than 1%. The non-uniform size distribution of polycrystalline relative to monocrystalline quartz indicates that the two types of quartz were derived from different sources. Had they been derived from the same source, the ratio of polycrystalline quartz to monocrystalline quartz would remain nearly constant for a given size fraction. Also, it is extremely unlikely that any of the detrital source areas for the Pierre Shale contained the ratios of polycrystalline to monocrystalline quartz grains found in the coarser size fraction. The long distances of transport and sediment mixing also preclude detrital sediment with these characteristics from reaching the site of deposition to the exclusion of other quartzose sediment. Therefore, it seems reasonable to assume that the majority of these grains are authigenic to these samples.

The polycrystalline quartz grains are probably not volcanic rock fragments (VRSs) because most of the chert remains after hydroflurosilicic acid treatment (based on 1 sample) and because Pierre bentonites, which are entirely volcanic, have very few polycrystalline grains. A comparison of the percentage of polycrystalline grains in a shale (P-351) with those of a bentonite (P-350) which was collected 2 inches above the shale indicates that the shale had 5 times more polycrystalline grains than the bentonite (5% for the bentonite, 25% for the shale). In a study of Mowry bentonites (Lower Cretaceous) Slaughter and Earley (1965) found that none of the 800

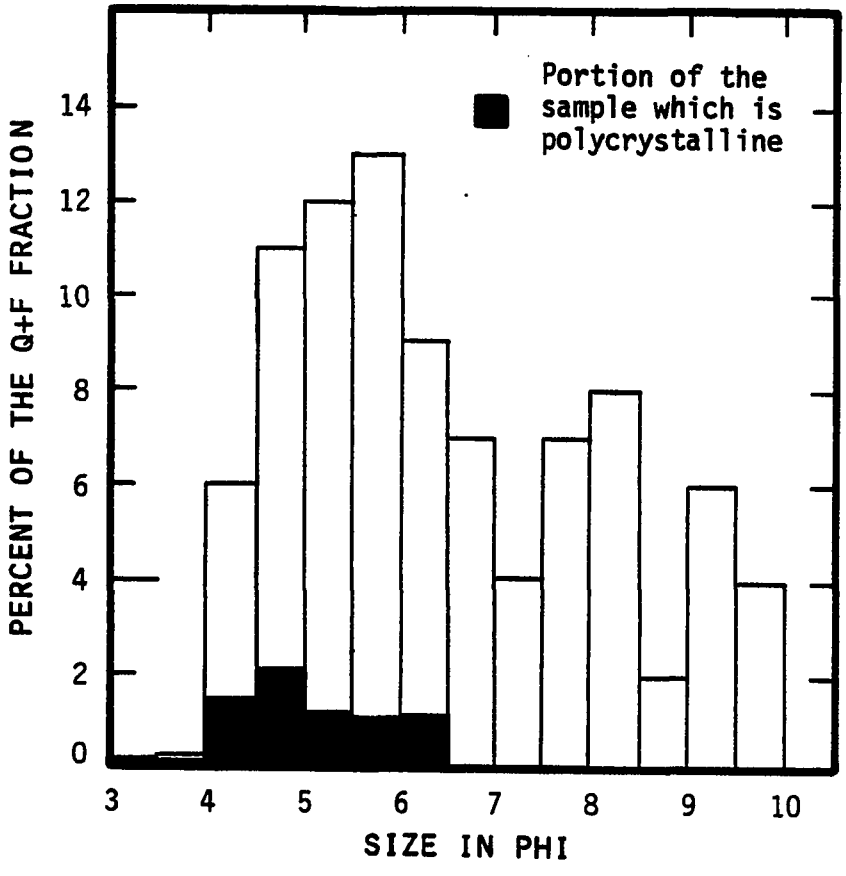

Fig. 38 Size distribution of the Q+F (quartz and feldspar) fraction of sample RB-5 showing also the size distribution of the polycrystalline quartz.

bentonites which they studies contained any volcanic glass, and only a few volcanic rock fragments were present.

Although all of the polycrystalline quartz grains found in the coarse size fraction of the Pierre Shale samples may be authigenic or diagentic, their importance in terms of the whole sample or even in terms of the quartz fraction is relatively minor. They generally make up less than .1 percent of the whole sample and less than 1% of the quartz fraction.

Conversion of Cristobalite to Quartz

The presence of cristobalite in the Pierre Shale raises the possibility of the conversion of cristobalite to quartz within the Pierre Shale. This conversion has been shown to occur at depths of 2030 m (at a temperature of 105°C) in the Monterey Shale (Murata and Larsen, 1975). This conversion of opal and cristobalite to quartz also has been shown in many of the Deep Sea Drilling Project studies.

The conversion of cristobalite to quartz in the Pierre Shale can be demonstrated by samples taken from the cores of the Bobjo wells. Some of the Bobjo well samples have all of the physical and mineralogical characteristics (except for quartz content) of the samples which have opal-cristobalite, yet they have no opal-cristobalite. The Bobjo well samples (W-O through W-8) show high quartz concentrations in the top of the section, ranging from 25 to 37%. These quartz concentrations are among the highest values found in all of the Pierre samples. Quartz concentrations are lower in all of the Pierre samples. Quartz concentrations are lower in all of the time-equivalent rocks surrounding these samples. The size distribution of the quartz in one of these samples (W-8) indicates that 25% of the quartz

in this sample is less than 0.5 μm in size. SEM studies indicate that the majority of these quartz grains are finer than 0.1 μm; in fact, the shape of the majority of the quartz grains could not be resolved using the SEM. This is significantly finer than found in other Pierre samples, and represents 3 to 5 times as much quartz as is normally found in this size fraction. The only reasonable explanation for this fine grained quartz is that it is authigenic.

This sample is located in the area where the samples are highly cristobalitic (see figure 13). Also this sample is stratigraphically located in the portion of the Pierre Shale where the cristobalitic samples normally occur. The physical similarities between this sample and the cristobalitic samples and the location of this sample, both areally and stratigraphically, indicate that the source of this quartz was the diagenetic recrystallization of biogenic opal. The other Bobjo well samples, located stratigraphically above W-8 (samples W-0 through W-7), also are presumed to have quartz which recrystallized from biogenic opal.

The maximum depth of burial for the Bobjo well samples is unknown. It is unlikely that these samples were ever exposed to temperatures or depths comparable to those in the Monterey Shale (2030 m and 105°C) where cristobalite inverts to quartz. However, kinetic data of Ernst and Calvert (1969) suggests that, for sediments as old as the Pierre, the conversion of opal-CT to quartz can occur at temperatures as low as 24°C. Therefore, it seems likely that some combination of time, temperature, and pressure (depth of burial) can be used to explain the transformation of cristobalite to quartz in the Pierre samples.

Origin of the Fine Grained Quartz

The Pierre Shale contains significantly less quartz (22%) than does the "average shale" (31%) of Shaw and Weaver (1965). There is also a significant difference between the mean size of Q + F fraction in the "average shale" of Schultz (1975) and the Pierre Shale samples. The Q + F fraction of the Pierre Shale samples average 1.8 phi (6.2 - 4.5 = 1.8) smaller than the "average shale" (one-third as large).

In the samples of the Pierre Shale an average of 9 percent of the average whole rock sample is quartz and feldspar finer than 4 microns, 12 percent is quartz and feldspars of silt size and only 1 percent of the sample is sand size quartz and feldspar. Blatt and Schultz (1976) report that the samples they studied contained 35% quartz (5% clay, 26% silt and 4% sand-sized quartz). If these size data reflect the average size distribution of quartz in the source area they indicate that recycled shales cannot be the only source of the clay size quartz in the Pierre sediment or that the clay sized quartz has been selectively removed from the "average shale."* The unusual abundance of clay sized quartz in the Pierre Shale could be explained as the result of one of the following:

1. Concentration or the selective removal of clay sized quartz from normal detrital sources, older shales and other rocks.
2. Authigenic production of a clay sized quartz.
3. Another source rock type for the clay sized quartz.
4. The mudrocks studied by Blatt and Schultz are not representative of the average shale source rock.

---

*For the "average shale" it is assumed that if there was a difference between the size distributions of the feldspar and quartz, it would not affect this relationship as the feldspars represent a minor portion of the Q + F fraction in the "average shale" and also in the Pierre Shale.

The data of Blatt and Schultz (1976) were from shale samples collected near sandstone contacts and therefore may represent a sample population of high energy mudstones. It must be pointed out, however, that in a similar study by Fleury (1971) in which the samples were not collected in this manner, the ratio of silt size quartz relative to clay size quartz was higher.

The possibility of the clay size quartz being derived from rocks other than shales is very remote as no other rock types contain any appreciable volume of clay sized quartz. Also the results of abrasion studies conducted on quartzose rock show that only minor proportions of clay size quartz are produced during abrasion.

The authigenic production of fine grained quartz has been shown for sample W-8. In this sample it appears that silica which was originally deposited as biogenic opal has crystallized to form quartz. This quartz was very fine and less than 1 μm in size. This occurrence suggests that this very fine grained authigenic quartz could be present in many of the samples, and that much of the clay sized quartz found in the Pierre Shale may be authigenic.

The size distributions of the Q + F fraction of 32 other Pierre Shale samples show that only one other sample (P-350) contains excessive amounts of quartz in the less than 1 um size fraction of the whole rock. Sample P-350 contains 7.9% quartz in the fraction compared to an average of 2.4% for the remaining samples. The sample was taken from a location which was immediately above a bentonite (sample P-351). Because of the sample's location near the bentonite and because of the presence of this fine grained

quartz, it seems likely that much of the quartz in this sample resulted from the conversion of silica (released during the devitrification of the volcanic ash located below the sample) to quartz. Much of the quartz found in the less than 1 μm fraction of the remaining samples also may be authigenic. This would not, however, be a very significant amount for the average sample as this size fraction forms only 10% of the whole Q + F fraction and only 2.4% of the whole sample.

Because authigenic quartz occurred in the less than 1 μm size fraction of one or more samples we cannot presume that all of the authigenic quartz will be found in this size fraction. Indeed much of the remaining clay size quartz may also be authigenic. However, it is significant to note that if the ratio of silt size to clay size quartz deposited in the Pierre Shale as detrital quartz was the same as that found in the "average shale," the average Pierre Shale sample would contain 7 percent authigenic quartz. That is, one-third of the quartz found in the Pierre Shale would be authigenic.

Using oxygen isotope data it is possible to calculate the maximum amount of fine grained quartz which could be authigenic quartz. This is done by assuming that the quartz fraction of the Pierre Shale is a mixture of authigenic quartz which has a $\delta^{18}O$ value of $38^{o}/oo$* and quartz from volcanic rocks which have a $\delta^{18}O$ value of $9^{o}/oo$ (volcanic quartz is used because the quartz found in volcanic rocks have the lowest $\delta^{18}O$ value of all rocks (Clayton et al., 1972). Assuming that the average oxygen isotope composition of $+20^{o}/oo$ for the 10-1 micron quartz fraction is typical of the Pierre Shale (Churchman et al., 1976), we can calculate the maximum volume of authigenic

---

*The ^{18}O value of 38 for authigenic quartz is the value suggested by Clayton et al. (1972) for quartz grown in equilibrium with sea water.

quartz in this size fraction. Calculations then show the maximum volume of authigenic quartz present is 41 percent. Sridhar et al. (1975) have interpreted the quartz oxygen isotope composition of the Pierre Shale to show that volcanic quartz is a major component of the total quartz fraction of the Pierre Shale. However, it is unreasonable to assume that the quartz in the Pierre Shale is derived only from authigenic and volcanic sources. Furthermore, the analyses of three bentonites found in the Pierre Shale as well as analyses of the Mowry Bentonites by Slaughter and Earley (1965) show that the volcanic rocks do not produce a sufficient volume of quartz in this size fraction (10-1 μm) or in the size fraction studies by Sridhar et al. (1975) to appreciably affect the oxygen isotope composition of these size fractions of the Pierre Shale. A detailed evaluation of data given by Sridhar et al. (1975) is made in Appendix X. The evaluation shows that their interpretation of their data is not valid, and that the best explanation of the data is that the quartz found in the Pierre Shale was recycled from older shales.

The $\delta^{18}O$ composition of the 1 to 10 μm fraction of shales older than the Pierre Shales and presently located in the source area of the Pierre Shale is 21°/oo (average of 23 samples from the data of Churchman et al., 1976). The average $\delta^{18}O$ value for the modern day reservoir of fine grained quartz is approximately 21°/oo, but ranges from 15 to 24 (Churchman et al. 1976). These data show that the $\delta^{18}O$ value of the quartz found in the Pierre Shale* is probably best explained in terms of the isotopic composition of the quartz available for sedimentation into the Pierre seaway rather than by the authigenic production of quartz in the Pierre Shale.

---

* $\delta^{18}O = 20^{o}/oo$

One mechanism for the concentration of clay sized quartz relative to the coarser grain size is through eolian transport. Eolian transport of sediments over very long distances has been shown to be an important factor in transporting quartz into areas of slow sedimentation (Delany et al., 1967; Aston et al. 1973; Jackson et al., 1971; Chester et al., 1972; Arrhenius, 1962). The deposition of clastic pelatic sediments has been shown to be almost entirely controlled through eolian transport of dusts (Rex and Goldberg, 1958; Delany et al., 1968).

Studies (Delany et al., 1968; Rex and Goldberg, 1958; Jackson et al., 1971; and Clayton et al., 1972) of the size distributions of wind transported quartz have shown that when transported over long distances, 25-70% of the quartz is clay size. Figure 22 shows a comparison of the size distributions of many different types of sediments. It is significant to note that the Pierre Shale samples most clearly resemble the size distribution of the sediments which were transported over long distances by eolian processes.

In summary then, it appears that, while an authigenic origin for the fine grained quartz cannot be completely ruled out, the most likely origin for the fine grained quartz is the concentration and transportation of fine grained detrital quartz into the Pierre seaway by eolian processes.

Diagenetic Alteration of the Feldspar Fraction

Little evidence has been found which suggests the feldspars in the Pierre Shale are being diagenetically altered or authigenically produced. In fact, most of the observations made so far suggest that the feldspars were derived either from older sediments or other feldspathic rocks. The only observations which may indicate that some diagenetic alteration has taken place is that almost all of the potassium feldspars have altered surfaces,

and the occurrence of what appears to be authigenic potassium feldspars in sample P-70.

The ratio of plagioclase feldspars to the potassium feldspars is 2.5:1 and is nearly constant for all of the Pierre Shale samples. The only sample which deviates significantly from this ratio is P-70. This sample contains 7.1 percent potassium feldspar which is the largest amount found in the Pierre samples, and is two to three times the amount of potassium feldspar normally found in samples from this geographic area. For this reason it is suspected that the potassium feldspar in this sample is authigenic. However, an examination, using the scanning electron microscope, of the Q + F fraction of this sample revealed no evidence of an authigenic origin.

The presence of zoning, polysynthetic twinning, lack of overgrowths, and the oligoclase composition of the feldspars in the coarser than 43 micron fraction of the Q + F fraction indicate, at least for this fraction, that the plagioclase feldspars are not authigenic.

CONCLUSIONS

This study of the mineralogy and petrology of the Pierre Shale was made to determine whether its non-clay petrology could be used to interpret its petrogenetic history. This study shows that the mineralogy and petrology are very useful in interpreting the petrogenetic history of the shale. However, the success of this approach is largely dependent upon determining the petrology and mineralogy of the whole sample as well as that of a specific mineral or mineral group. Additionally, knowledge of other non-petrologic data, such as stratigraphy, are required before complete interpretation can be made.

The results of mineralogic analysis of the solid silica fraction showed the common occurrence of cristobalite and quartz. The cristobalite occurs as both opal-C and opal-CT. The presence of cristobalite is strongly controlled by the stratigraphic location of the sample. The origin of all of the cristobalite is interpreted to be the crystallization of siliceous skeletons.

Quartz occurs as both monocrystalline and polycrystalline grains. The polycrystalline quartz is more prevalent in the coarse size fraction and is interpreted as being primarily authigenic. Quartz is the major non-clay component of the Pierre Shale, generally comprising 22% of the sample but ranging from 1 to 37.9 percent of the sample. The majority of the quartz appears to have been derived from older sedimentary rocks.

The amount of quartz found in individual samples appears to be controlled by the volcanic content of the sample and the distance between the sample location and the shoreline.

The feldspar content averages 8.5 percent of the whole sample and ranges from 2 to 15 percent. Although the feldspars represent only a minor fraction of the whole sample, they average 39 percent of the quartz and feldspar fraction of the sample. Sixty-two percent of the feldspar fraction is normative plagioclase with an average normative anorthite composition of 8.2 mole percent. Petrographic and other evidence indicate that the majority of this feldspar is derived from volcanic source rocks, the remaining feldspar being derived from recycled sediments. Only one sample showed any sign of authigenic feldspar.

Size analyses of the quartz and feldspar fraction of these samples indicated that the quartz and feldspars are significantly finer than the quartz and feldspars which have been found in other shale units. The fine grained characteristics of the quartz and feldspar are controlled by the distance and mechanism of transport, although in two cases the fine grained nature of the quartz is shown to be due to the authigenic production of the quartz.

Carbonates were found to be present in a few of the samples, but only in minor concentrations. The carbonate minerals found were generally calcite, dolomite and siderite. However, much of the carbonate occurred as mixed phases rather than pure end member phases.

The only phyllosilicate minerals which occurred in the non-clay fraction of the samples were muscovite and biotite. The occurrence of these phases appeared to be related to the volcanic source rocks.

Gypsum, jarosite, pyrite, and clinoptilolite were also found to be

present in the Pierre Shale samples. The occurrence of these minerals is interpreted to be controlled largely by post-depositional and authigenic processes and, therefore, were not used to interpret the petrogenetic history of this shale unit.

From the start of this study it was recognized that the stratigraphy of the Pierre samples could control the mineralogic and petrographic variables analyzed. Some of the most important of these variables are the distance to the nearest shoreline at the time of deposition, changes in the depositional environment with time, and changes in the mechanism of transport as a function of time. However, by handling these variables separately, the overall effect of the stratigraphic variable was reduced. For example, the distance of sediment transport was shown to be a major control in the amount and size of the quartz in the samples, but because change in the distance of transport as a function of time was fairly well known, this stratigraphic variable was used to interpret the mineralogic variation.

Because the Pierre Shale is an ancient shale unit, the likelihood of diagenetic changes is very great. In this study the only major diagenetic change in the quartz and feldspar fraction was the authigenetic production (or diagenetic conversion) of polycrystalline and monocrystalline quartz from biogenic silica. In this case the following diagenetic changes were shown.

1. opal to opal-CT
2. opal-CT to opal-C
3. opal-C and opal-CT to polycrystalline quartz
4. calcite replaced by silica to form polycrystalline quartz

While authigenic polycrystalline quartz was very common in the coarse size fractions (>43 microns) of the quartz and feldspar fraction of most of the samples, the quantity of polycrystalline quartz produced was generally insignificant. In two samples the authigenic production of very fine grained (<1 μm) quartz was recognized. In one sample (P-70) authigenic production of a potassium feldspar occurred. In general, large amounts of fine grained quartz were not produced diagenetically except in a few siliceous samples (samples containing cristobalites) which have been deeply buried (W-8) or are associated with bentonites (P-150).

Although the mineralogy of the non-clay fraction tends to vary greatly, both as a function of stratigraphic position and geographic location, only two sources of sediments are needed to explain this variation. These two sources are recycled sediments and volcanic source rocks. The mineralogy and petrology of the feldspars are indicative of a volcanic source for the majority of the feldspars. Calculations made using the feldspar data show that as much as 35 percent of the average Pierre sample may be derived from volcanic rocks. This inference is also supported by the composition of the clay fraction. The rest of the sediments comprising the Pierre Shale were derived from the recycling of older sediments. There is no evidence in the Pierre Shale samples to suggest any significant contribution from plutonic igneous or metamorphic rocks.

The results of the size analyses indicate that wind and water transport of sediment into the Pierre seaway were important, but that wind transport was dominant.

This is particularly true for samples which were deposited at distance of over 50 km from the shoreline. Analyses of the size and mineralogy of the quartz and feldspar fraction also show that the direct wind transport of volcanic sediments into the seaway was a dominant factor in the deposition of sediments.

A petrogenetic model for the deposition of sediment in the Pierre Seaway is proposed. The basic features of this model are:

1. Extremely slow rates of sediment deposition. (Rate of deposition near or below the rate found in modern pelagic environments.)
2. Two dominant source rock types. Recycled sediments (60 to 70 percent of the average sample) derived from source areas predominantly west of the seaway. The remaining sediment (30 to 40 percent of the average sample) was derived from active volcanic sources near Livingston, Montana.
3. Transport of the sediment into the seaway was predominantly by wind. The wind transported not only the fine grained quartz and clay from sedimentary source areas but enabled the volcanogenic sediments directly into the seaway. Water transport of sediments into the seaway was relatively minor at distances greater than 50 km from the shoreline.
4. After deposition into the seaway some of the volcanic sediments formed beds which are recognizable as bentonites; while much of the volcanic ash was mixed with other sediments and organic material and did not produce bentonites.

In short, the model proposed is one of pelagic sedimentation in the

Pierre Seaway coupled with a volcanic point source for as much as 40 percent of the sediments.

REFERENCES

Arrhenius, G. 1962, Pelagic sediments: In M. N. Hill (ed.) The Sea, Vol. 3, Interscience, New York, p. 655-727.

Aston, S. R., Chester, R., Johnson, L. R., and Padgham, R.C., 1973, Eolian dust from the lower atmosphere of the eastern Atlantic and Indian Oceans, China Sea and Sea of Japan: Marine Geology, v. 14, p. 15-29.

Baak, J. A., 1949, A comparative study on recent ashes of the Java volcanoes Smeru, Kelut and Merapi: Meded. Alg. Proefsta. Landbw. Bogor, Nr 83, 37 p.

Bambauer, H. U., Corlett, M., Eberhard, E., Viswanathan, K., 1967, Diagrams for the determination of plagioclases using X-ray powder methods: Schweiz. Mineralogische und Petrographische Mitteilungen, v. 47/1, p. 333-349.

Beltagy, R. C. and Padgham, R. C., 1972, The particle-size distribution of quartz in some North Atlantic deep-sea sediments: Marine Geology, v. 13, p. 297-310.

Blatt, Harvey, and Schultz, D. J., 1976, Size distribution of quartz in mudrocks: Sedimentology, v. 23, p. 857-866.

Caldwell, W. G. E., 1968, The Late Cretaceous Bearpaw Formation in the South Saskatchewan River valley: Sask. Research Counc., Geol. Div., Rept. 8, 89 p.

Chester, R., Elderfield, H., Griffin, J. J., Johnson, L. R. and Padgham, R. C., 1972, Eolian dust along the eastern margins of the Atlantic Ocean: Marine Geology, v. 13 (2), p. 91-105.

Churchman, G. J., Clayton, R. N., Sridhar, K., and Jackson, M. L., 1976 Oxygen isotopic composition of aerosol size quartz in shales: Jour. Geophysical Research, v. 81, no. 3, p. 381-386.

Clarke, F. W., 1924, Data of geochemistry: U.S. Geol. Survey Bull. 770, 841 p.

Clayton, R. N., Rex, R. W., Syers, J. K. and Jackson, M. L., 1972, Oxygen isotope abundance in quartz from Pacific pelagic sediments: J. Geophys. Res., v. 77, p. 3907-3915.

Cullity, B. D., 1956, Elements of X-ray Diffraction: Addison-Wesley Pub. Co., London, 514 p.

Dauphin, J. P., 1972, Size distribution of chemically extracted quartz used to characterize fine-grained sediments: unpublished M.S. thesis, Oregon State University, Corvallis, Oregon.

Delaney, A. C., Delaney, A. C., Parkin, D. W., Griffin, J. J., Goldberg, E. D., and Reimann, B. E. F., 1967, Airborne dust collected at Barbados: Geochim. Cosmochim. Acta. v. 31, p. 885-909.

Ericson, D. B., Ewing, Maurice, and Wollin, Goesta, 1964, The Pleistocene epoch in deep-sea sediments: Science, v. 146, no. 3645, p. 723-732.

Ernst, W. G., and Clavert, S. E., 1969, An experimental study of the recrystallization of porcelanite and its bearing on the origin of some bedded cherts: Am. Jour. Sci., v. 267-A, p. 114-133.

Fluery, M. G. R., 1971, Size distribution of quartz grains in mudrocks: unpublished M.S. thesis, University of Oklahoma, Norman, Oklahoma.

Folk, R. L., and Ward, W. C., 1957, Brazos River Bar: A Study in the significance of Grain Size Parameters: Jour. Sed. Pet., v. 27, p. 3-27.

Gill, J. R., and Cobban, W. A., 1966, The Red Bird section of the Upper Cretaceous Pierre Shale, in Wyoming, with a section on A new Echinoid from the Cretaceous Pierre Shale of eastern Wyoming, by P. M. Kier: U. S. Geol. Surevey Prof. Paper 393-A, 73 p.

_____, 1969, Paleogeographic Maps of the Western Interior: U.S.G.S. Open File Report, 6 sheets.

_____, 1973, Stratigraphy and geologic history of the Montana Group and equivalent rocks, Montana, Wyoming, and North and South Dakota: U. S. Geological Survey Professional Paper 776, 37 p.

Gilluly, James, 1963, The tectonic evolution of the western United States - 17th William Smith Lecture: Geol. Soc. London Quart. Jour., v. 119, no. 2, p. 133-174.

Goddard, Edwin D., 1965, Geologic Map of North America: U.S.G.S., Washington, D.C., 2 sheets.

Grim, R. E., 1968, Clay Mineralogy, 2d ed.: New York, McGraw-Hill, 596 p.

Hamilton, Warren, and Myers, W. B., 1974, Nature of the Boulder Batholith of Montana: Geol. Soc. Am. Bull., v.85, no. 3, p. 365-378.

Jackson, M. L., Levelt, T. W. M., Syers, J. K., Rex, R. W., Clayton, R. N., Sherman, G. D., and Uehara, G., 1971, Geomorphological relationships of tropospherically derived quartz in the soils of the Hawaiian Islands: Soil Sci. Soc. Amer. Proc., v. 35, p. 515-525.

Jeffery, P. G., 1970, Chemical Methods of Rock Analysis: International Series in Analytical Chemistry, v. 36, Pergamon Press, New York, 426 p.

Jones, J. B., Segnit, E. R., 1971, The nature of opal. I. Nomenclature and constituent phases: J. Geol. Soc. Australia, v. 18, p. 57-68.

Kay, G. M., 1955, Sediments and subsidence through time, in Poldervaart, Arie, ed., Crust of the earth-a symposium: Geol. Soc. America Spec. Paper 62, p. 665-684.

Keller, W. D. and Ting, C. P., 1950, The petrology of a specimen of the Perry Farm Shale: Jour. Sed. Pet., v. 20, no. 3, p. 123-132.

Kerns, R. L., 1967, Particle-size separation of clays: Oklahoma Geol. Notes, v. 27, p. 167-174.

Kidwell, A. L., and Hunt, J. M., 1958, Migration of oil in recent sediments of Pedernales, Venezuela, in Weeks, L. G., ed., Habitat of oil: Tulsa, Okla., Am. Assoc. Petroleum Geologists, p. 790-817.

Kiely, P. V. and Jackson. M. L., 1964, Selective dissolution of micas from potassium feldspars by sodium pyrosulfate fusion of soils and sediments: Amer. Mineralogist, v. 49, p. 1648-1659.

_____, 1965, Quartz, feldspar and mica determination for soils by sodium pyrosulfate fusion: Soil Sci. Soc. Amer. Proc. v. 29, p. 159-163.

Leith, C. K., and Mead, W. J., 1915, Metamorphic geology: New York, Henry Holt and Co., 337 p.

McGookey, D. P., Haun, J. D., Hale, L. A., Goodell, H. G., McCubbin, D. G., Weimer, R. J., and Wulf, G. R., 1972, Cretaceous System; in Geologic Atlas of the Rocky Mountain region, U.S.A., Rocky Mountain Assoc. Geologists, Denver, p. 190-228.

McLean, J. R., 1971, Stratigraphy of the Upper Cretaceous Judith River Formation in the Canadian Great Plains: Sask. Research Council, Geol. Div., Rept. 11, 96 p.

Mizutani, Shinjiro, 1970, Silica minerals in the early stage of diagenesis: Sedimentology, v. 15, no. 2, p. 419-436.

Mohr, E. C. J., and Van Baren, F. A., 1954, Tropical Soils; Interscience Pub. Inc., New York, 498 p.

Murata, K. J., and Larson, R. R., 1975, Diagenesis of Miocene siliceous shales, Temblor Range, California: U. S. Geological Survey Journal of Research, v. 3, no. 5, p. 553-566.

Radezewski, O. E., 1939, Eolian deposits in marine sediments, in recent marine sediments: Parker Trask, ed., Amer. Assoc. Petrol. Geol., Tulsa, p. 496-502.

Reeside, J. B., Jr., 1944, Maps showing thickness and general character of the Cretaceous deposits in the Western Interior of the United States: U. S. Geol. Survey Oil and Gas Inv. Prelim. Map 10.

Rex, R. W., and Golberg, E. D., 1958, Quartz contents of pelagic sediments of the Pacific Ocoean: Tellus, v. 10, p. 153-159.

Rose, H. E., 1952, Determination of the 'Extinction Coefficient' particle size relationship for spherical bodies: Journ. Applied Chemistry, v. 2, p. 80-87.

Russell, L. S., 1939, Land and sea movements in the Late Cretaceous of Western Canada: Trans. Roy. Soc. Canada. ser. 3, v. 33, sec. 4, p. 81-99.

Syers, J. K., Jackson, M. L., Berkheiser, V. E., Clayton, R. N., and Rex, R. W., 1969, Eolian sediment influence on pedogenesis during the Quaternary: Soil Sci. v. 107, p. 421-427

Schultz, D. J., 1975, Crystalline silica in mudrocks: M.S. thesis, University of Oklahoma, Norman, Oklahoma.

Schultz, L. G., 1964, Quantitative interpretation of mineralogical composition from X-ray and chemical data for the Pierre shale: U. S. Geol. Survey Prof. Paper 391-C, p. C1-C31.

_____, 1965, Mineralogy and stratigraphy of the lower part of the Pierre Shale, South Dakota and Nebraska: U. S. Geol. Survey Prof. Paper 392-B, p. B1-B19.

_____, 1978, Mixed-layered clay in the Pierre Shale and Equivalent Rocks, Northern Great Plains Region: U. S. Geol. Survey Prof. Paper 1064-A, p. A1-A28.

Shaw, D. B., and Weaver, C. E., 1965, The mineralogical composition of shales: Jour. Sed. Petrology, v. 35, p. 213-222.

Slaughter, M., Earley, J. W., 1965, Mineralogy and Geological Significance of the Mowry Bentonites, Wyoming: G. S. A. Special Paper, no. 83, 116 p.

Smith, Robert L., 1960, Ash Flows: G. S. A. Bull., v. 71, p. 795-842.

Sridhar, K., Jackson, M. L., and Clayton, R. N., 1975, Quartz oxygen isotopic stability in relation to isolation from sediments and diversity of source: Soil Sci. Soc. Amer. Proc., v. 39, p. 1209-1213.

Sridhar, K., Jackson, M. L., Clayton, R. N., Gillette, D. A., and Hawley, J. W., 1978, Oxygen Isotopic Ratios of Quartz from Wind-Erosive Soils of Southwestern United States in Relation to Aerosol Dust: Jour. Soil Sci. Soc. Am., v. 42, p. 158-162.

Tourtelot, H. A., 1962, Preliminary investigation of the geologic setting and chemical composition of the Pierre Shale, Great Plains Region: U. S. Geol. Surv. Prof. Paper, v. 390, p. 1-74.

Twenhofel, W. H., 1939, Principles of sedimentation (1st ed.): New York, McGraw-Hill Book Co., 610 p.

Weimer, R. J., 1960, Upper Cretaceous stratigraphy, Rocky Mountain area: Amer. Assoc. Petroleum Geologist Bull., v. 44, no. 1, p. 1-20.

_____, 1970, Rates of deltaic sedimentation and interbasin deformation, Upper Cretaceous of Rocky Mountain region, in Morgan, J. P., ed., Deltaic sedimentation, modern and ancient: Soc. Econ. Paleontologists and mineralogists Spec. Pub. 15, p. 270-292.

Whitehouse, U. G., Jeffrey, L. M., and Debrecht, J. D., 1960, Differential settling tendencies of clay minerals in saline waters: Clays and clay minerals (7th Nat. Conf., 1958), p. 1-79.

Williams, G. D., and Burk, C. F., Jr., 1964, Upper Cretaceous: in Geological history of western Canada, R. G. McCrossan and R. P. Glaister (Editors), Alta. Soc. Petroleum Geologists, Calgary, Alberta, p. 169-189.

Wright, T. L., 1968, X-ray and optical study of alkali feldspar II. An X-ray method of determining the composition and structural state from measurement of 20 values for three reflections: Amer. Mineral, v. 54, p. 88-104.

APPENDICES

APPENDIX I

GEOGRAPHIC AND STRATIGRAPHIC LOCATIONS AND THE GENERAL CHARACTERISTICS OF THE SAMPLES

Table 14. Geographic Location of the Samples

Sample Number	Latitude	Longitude	State or Province	County	Legal	Verbal description of location
P-1	38° 18'	103° 45'	Colorado	Crowley	Sec. 22, T20S, R57W	5 miles west of Ordway on highway 71
P-2	38° 45'	103° 43'	Colorado	Lincoln	Sec. 6, T15s, R56W	Highway 71 and Horse Creek
PA-3	38° 51'	103° 48'	Colorado	Lincoln	Sec. 12, T14S, R58W	South side of highway, taken from under a marl outcrop
PB-3	38° 51'	104° 48'	Colorado	Lincoln	Sec. 12, T14S, R58W	North side of highway, taken from under a marl outcrop
P-4	39° 04'	103° 42'	Colorado	Lincoln	Sec. 30, T11S, R56W	
P-5	39° 15'	103° 39'	Colorado	Lincoln	Sec. 17, T9S, R56W	
P-24	45° 05'	102° 23'	South Dakota	Pennington	Sec. 2, T1N, R14E	
P-51	38° 53'	101° 43'	Kansas	Wallace	NE¼, Sec. 34, T13S, R40W	
P-52	38° 55'	101° 50'	Kansas	Wallace	SW¼, Sec. 34, T12S, R41W	
P-53	38° 56'	101° 54'	Kansas	Wallace	NE¼, Sec 11, T35S, R42W	
P-66	40° 10'	101° 18'	Nebraska	Hitchcock	Sec. 16, T2N, R35W	1 mile west of Stratton
P-70	42° 44'	97° 34'	Nebraska	Knox	SW¼, Sec. 23 T33N, R2W	

Sample Number	Latitude	Longitude	State or Province	County	Legal	Verbal description of location
P-71	42° 44'	97° 40'	Nebraska	Knox	NW¼, Sec. 33, T33N, R3W	
P-75	42° 44'	97° 55'	Nebraska	Boyd	Sec. 6, T33N, R9W	1 mile past Monowi on highway 12
P-101	45° 36'	97° 48'	South Dakota	Marshall	Sec. 26, T125N, R58W	1.5 miles east of Langford on highway 25
P-102	45° 39'	97° 46'	South Dakota	Marshall	Sec. 3, T125N, R58W	3 miles south of the Spain turnoff on highway 25
P-103	45° 40'	97° 07'	South Dakota	Roberts	Sec. 25, T126N, R52W	
P-104	46° 01'	98° 42'	North Dakota	Dickey	SE¼, Sec. 10, T129N, R64W	
P-105	46° 19'	98° 40'	North Dakota	LaMovre	Sec 25, T133N, R64W	
P-139	49° 27'	98° 32'	Manitoba		Sec. 25, T6N, R8W	2 miles west of St. Lupicin
P-151	49° 12'	98° 56'	Manitoba		Sec. 16, T3N, R11W	1 mile west of Pilot Mound
P-152	49° 16'	98° 59'	Manitoba		Sec. 15, T3N, R11W	8.5 miles west of Pilot Mound on east side of river
P-153	49° 15'	99° 20'	Manitoba		Sec. 19, T3N, R14W	1 mile north of Neelin
P-154	49° 25'	99° 36'	Manitoba		Sec. 28, T5N, R16W	Located in Ninette
P-155	49° 26'	99° 38'	Manitoba		Sec.30, T5N, R16W	1 mile north of Ninette

Sample Number	Latitude	Longitude	State or Province	County	Legal	Verbal description of location
P-156	49° 26'	99° 38'	Manitoba		Sec. 30 T5N, R16W	1 mile north of Ninette, located immediately above sample P-155
P-186	50° 41'	101° 29'	Manitoba		Sec. 2, T20W, R27W	1 mile east of Millwood
P-187	50° 41'	101° 29'	Manitoba		Sec. 2, T20N, R27W	1 mile east of Millwood. Located 20 ft. higher in the section than P-186.
P-193	51° 14'	106° 53'	Sask		Sec. 3, T28N, R7W	1 mile north of Gardner Dam
P-201	50° 47'	105° 01'	Sask		Sec. 16, T21N, R22W	From Regina Beach
P-202	49° 51'	104° 36'	Sask		Sec. 36, T20W, R20W	14 miles south of Corinne
P-203	49° 50'	104° 47'	Sask		Sec. 19, T10N, R21W	1 mile west of Drummer
P-204	49° 21'	107° 05'	Sask		Sec. 30, T4N, R8W	6.5 miles south of Mankota
P-206	49° 18'	107° 45'	Sask		Sec. 1, T4N, R14W	2 miles northeast of Valmarie
P-208	49° 38'	107° 44'	Sask		Sec. 5, T8N, R13W	4 miles south of Cadillac
P-210	49° 53'	108° 29'	Sask		Sec. 8, T11N, R19W	18 miles south of Gulf Lake
P-212	50° 19'	107° 49'	Sask		Sec. 25, T15N, R14W	1 mile north of Swift Current
P-214	50° 37'	108° 15'	Sask		Sec. 23, T19N, R18W	5 miles east of Cabri

Sample Number	Latitude	Longitude	State or Province	County	Legal	Verbal description of location
P-218	51° 22'	108° 23'	Sask		Sec. 7, T28N, R17W	6 miles south of Fiske
P-220	51° 38'	108° 24'	Sask		Sec. 8, T31N, R17W	Herschal Garbage Dump located 1 mile west of Herschal
P-222	51° 37'	110° 29'	Alberta		Sec. 16, T30N, R4W	15 miles north of Oyen
P-224	52° 14'	110° 56'	Alberta		Sec. 16, T37N, R7W	11 miles north and 7 miles west of Consort
P-226	52° 19'	111° 34'	Alberta		Sec. 6, T39N, R11W	
P-228	52° 19'	111° 51'	Alberta		Sec. 3, T40N, R13W	At river south of Alliance
P-230	51° 20'	112° 30'	Alberta		Sec. 21, T27N R18W	1 mile south of East Corelee
P-232	51° 09'	112° 03'	Alberta		Sec. 18, T25N, R15W	1 mile east of Finnigan
P-234	50° 26'	112° 20'	Alberta		Sec. 15, T17N, R18W	4 miles west of Bow City
P-236	50° 10'	112° 44'	Alberta		NW¼, Sec. 18, T14N, R20W	At Travers Dam
P-237	49° 47'	112° 51'	Alberta		Sec. 6, T10N, R21W	1 mile south of Diamond
P-238	49° 47'	112° 47'	Alberta		Sec. 6, T10N, R21W	Sample taken 1 inch below P-237
P-239	49° 47'	112° 51'	Alberta		Sec. 6, T10N, R21W	Sample taken 100 ft. below P-237

Sample Number	Latitude	Longitude	State or Province	County	Legal	Verbal description of location
P-240	49° 32'	112° 51'	Alberta		Sec. 17, 7N, R22W	7 miles north of Magrath
P-242	48° 57'	112° 45'	Alberta	Glacier	Sec. 14, T37N R7W	Located at the intersection of route 414 and the Milk River
P-244	48° 41'	112° 46'	Montana	Glacier	Sec. 16, T34N, R9W	7 miles north of the intersection of highway 2 and Route 444
P-246	48° 08'	110° 03'	Montana	Chouteau	NW¼, Sec. 20 T27N, R13E	7 miles south of Big Sandy on Route 236
P-248	48° 33'	109° 43'	Montana	Hill	Sec. 5, T32N, R16W	
P-250	49° 21'	110° 18'	Alberta		Sec. 19, T5N, R2W	11 miles north of Crussdy
P-251	49° 21'	110° 18'	Alberta		Sec. 19, T5N, R2W	Located immediately below sample P-250
P-252	49° 25'	110° 17'	Alberta		Sec. 17, T6N, R2W	16 miles north of Crussdy
P-253	49° 48'	109° 46'	Sask		Sec. 18, T9N, R28W	3 miles southwest of Downey Lake
P-254	48° 34'	108° 46'	Montana	Blaine	NE¼, Sec. 8, T32N, R23E	1.5 miles north of Harlem
P-255	48° 17'	107° 57'	Montana	Phillips	Sec. 30, T29N, R28E	11 miles south of Matla on Route 191
P-261	48° 06'	105° 37'	Montana	Roose-velt	SE¼, Sec. 11, T27N, R47E	2 miles east of Wolf Point
P-270	45° 55'	100° 33'	N. Dakota	Emmons	Sec. 35, T129N, R9W	2 miles east and north of the state line

Sample Number	Latitude	Longitude	State or Province	County	Legal	Verbal Description of Location
P-273	45° 15'	100° 54'	S. Dakota	Carson	NE¼, Sec. 20, T15N, R27E	3 miles southeast of White Horse
P-279	45° 04'	100° 22'	S. Dakota	Dewey	Sec. 16, T13N, R31E	On route 212, four miles from the west bank of the Missouri River
P-292	44° 15'	104° 55'	Wyoming	Crook	NW¼, Sec. 14, T49N, R67W	3.7 miles southeast of Moorcraft on route 16
P-301	40° 04'	105° 17'	Colorado	Boulder	SE¼, Sec. 1, T1N, R71W	2 miles north of Boulder City Limits
P-302	39° 56'	105° 14'	Colorado	Boulder	SW¼, SW¼, Sec. 33, T15, R70W	Boulder County line and route 93
P-303	39° 39'	105° 09'	Colorado	Jefferson	SW¼, SW¼, Sec. 31, T45, R69W	1.4 miles east of Morrison on route 285
P-304	38° 47'	104° 47'	Colorado	El Paso	Sec. 29, T145, R66W	Three miles south of Colorado Springs on I-25 S
P-305	38° 39'	104° 42'	Colorado	El Paso	Sec. 20, T16S, R65W	2 miles south of Fountain
P-306	38° 29'	104° 37'	Colorado	El Paso	Sec. 35, T17S, R65W	El Paso County line
P-308	38° 19'	104° 37'	Colorado	Pueblo	Sec. 19, T20S, R65W	1.7 miles north of the intersection of I-25 and Route 50
P-310	38° 14'	105° 03'	Colorado	Los Anunas	Sec. 12, T21S, R69W	2.5 miles west of Wetmore on Highway 96
P-312	37° 36'	104° 44'			SE¼, Sec. 23, T28S, R66W	3 miles south of Walsenburge on I-25
P-313	37° 25'	104° 37'	Colorado	Los Anunas	Sec. 28, T30S, R64W	2 miles south of Aguilar

Sample Number	Latitude	Longitude	State or Province	County	Legal	Verbal Description of Location
P-314	37° 17'	104° 31'	Colorado	Los Anunas	Sec. 7, T32S, R63W	8 miles north of Trinidad at junction of I-25 and Hochne Road
P-316	36° 53'	104° 32'	New Mexico	Rio Arriba		Raton at junction of route 87 and I-25
P-318	36° 33'	104° 32'	New Mexico	Rio Arriba		1 mile north of Maxwell
P-320	36° 15'	104° 39'	New Mexico	Mora	Sec. 27, T215, R22E	6 miles east of Wagon Mound
P-325	40° 02'	106° 22'	Colorado	Garfield		0.5 miles west of the Colorado River on route 9, 2.5 miles from Kremmling
P-327	40° 29'	107° 02'	Colorado	Garfield		1 mile west of Milner on Route 40
P-331	40° 31'	107° 35'	Colorado	Garfield		1.1 miles west of Craig on Route 40
P-334	46° 26'	109° 47'	Montana	Wheatland		1.5 miles east of the junction of highways 191 and 12
P-343	47° 40'	108° 42'	Montana	Phillips		0.9 miles north of Missouri River
P-350	46° 49'	107° 53'	Montana	Petro-leum		12.0 miles south of Route 200 on dirt road
P-351	46° 49'	107° 53'	Montana	Petro-leum		Collected 2 inches below P-350
P-353	46° 16'	109° 15'	Montana	Golden Valley		1 mile south of Rygate on Route 300

Sample Number	Latitude	Longitude	State or Province	County	Legal	Verbal Description of Location
(Red Bird)						
RB-1	43° 16'	104° 17'	Wyoming	Niobrara	Sec. 24. T38N, R62W	95' east and 1135' south of NW section corner
RB-2	" "	" "	"	"	Sec. 23, " "	260' west and 1415 ' south of NE section corner
RB-3	" "	" "	"	"	Sec. 23, " "	650' west and 1050' south of NE section corner
RB-4	" "	" "	"	"	Sec. 23, " "	1265' west and 825' south of NE section corner
RB-5	" "	" "	"	"	Sec. 23, " "	1670' west and 545' south of NE section corner
RB-6	43° 17'	104° 17'	Wyoming	Niobrara	Sec. 23, T38N, R62W	2250' west and 520' south of NE section corner
RB-7	" "	" "	"	"	Sec. 23, " "	2720' west and 345' south of NE section corner
RB-8	" "	" "	"	"	Sec. 23, " "	3185" west and 70' south of NE section corner
RB-9	" "	" "	"	"	Sec. 14, " "	3590' west and 120' north of SW section corner
RB-10	" "	" "	"	"	Sec. 14, " "	3925' west and 310' north of SW section corner
RB-23	43° 16'	104° 18'	Wyoming	Niobrara	Sec. 13, T38N, R62W	240' east and 4555' north of SE section corner

Sample Number	Latitude	Longitude	State or Province	County	Legal	Verbal Description of Location
(Bobjo Well Samples)						
W-0	49° 21'	102° 16'	Saskatchewan		LSD 16, Sec. 4, T5N, R2W	Bobjo well core sampled from 950 to 955 feet.
W-1	" "	" "	"		" "	Bobjo well core sampled from 1050 to 1055 feet.
W-2	" "	" "	"		" "	Bobjo well core sampled from 1070 to 1075 feet.
W-3	" "	" "	"		" "	Bobjo well core sampled from 1127 to 1130 feet.
W-4	" "	" "	"		" "	Bobjo well core sampled from 1157 to 1160 feet.
W-5	" "	" "	"		" "	Bobjo well core sampled from 1167 to 1170 feet.
W-6	" "	" "	"		" "	Bobjo well core sampled from 1210 to 1212 feet.
W-7	" "	" "	"		" "	Bobjo well core sampled from 1236 to 1240 feet.
W-8	" "	" "	"		" "	Bobjo well core sampled from 1246 to 1250 feet.
W-9	" "	" "	"		" "	Bobjo well core sampled from 1440 to 1445 feet.
W-10	" "	" "	"		" "	Bobjo well core sampled from 1596 to 1600 feet.
W-11	" "	" "	"		" "	Bobjo well core sampled from 1615 to 1617 feet.

Sample Number	Latitude	Longitude	State or Province	County	Legal	Verbal Description of Location
W-12	49° 21'	102° 16'	Saskatchewan		LSD 16, Sec. 4, T5N, R2W	Bobjo well core sampled from 1629 to 1630 feet.
W-13	" "	" "	"		" "	Bobjo well core sampled from 1678 to 1679 feet.
WA-14	" "	" "	"		" "	Bobjo well core sampled from 1830 to 1831 feet.
WB-14	" "	" "	"		" "	Bobjo well core sampled from 1831 to 1833 feet.
W-15	" "	" "	"		" "	Bobjo well core sampled from 1834 to 1836 feet

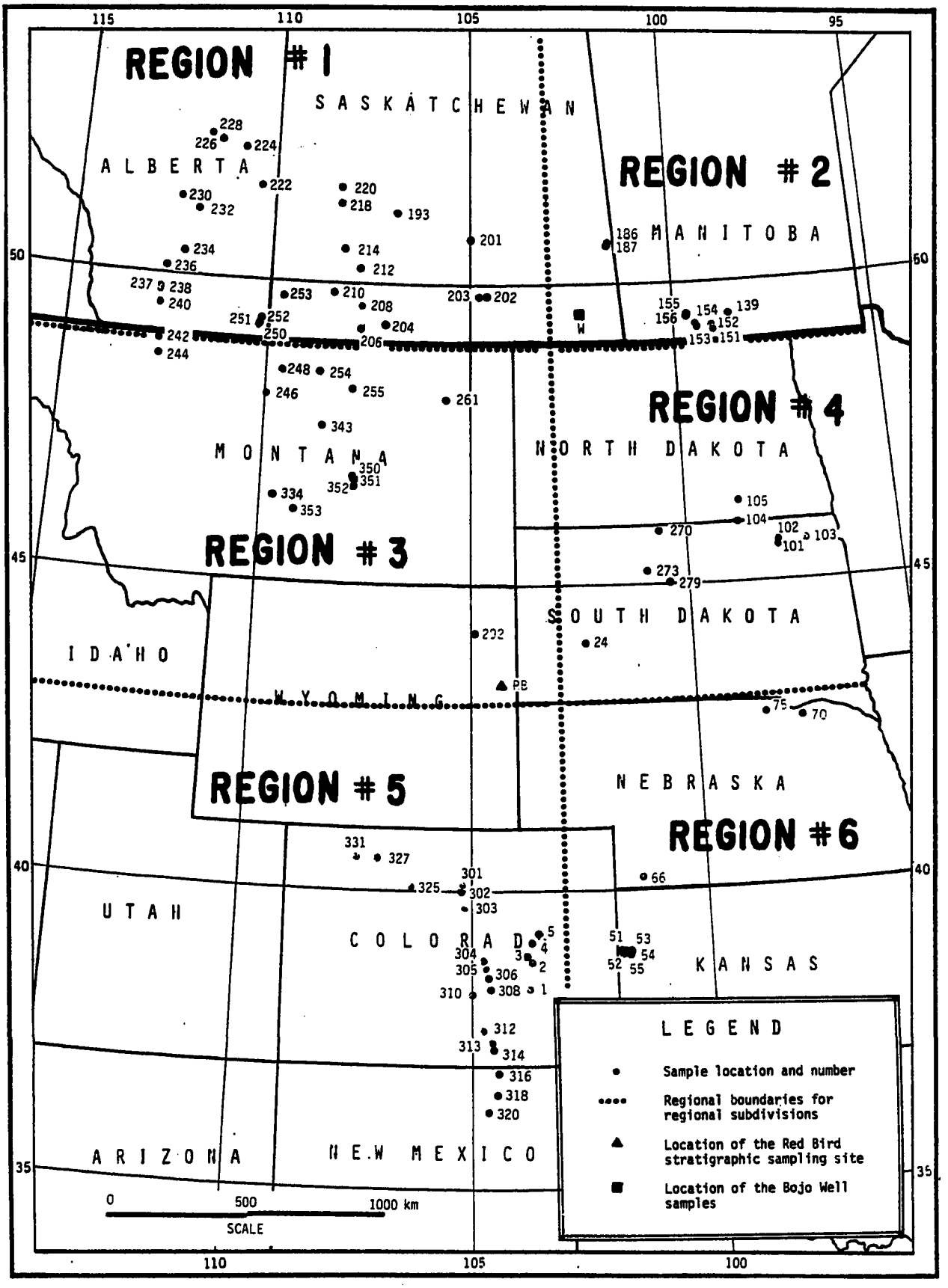

Fig. 39. Map showing the sampling locations and boundaries for the regional subdivisions of the sampled area.

Table 15. General sample characteristics and regional and stratigraphic locations.

Sample Number	* Rock Type	** Color	*** Fissility	**** Special Charac.	Region	***** Stratigraphic Level
P-1	MR	5Y8/4	P	Y	5	M
P-2	MR	5Y7/2	P	-	5	U
PA-3	MR	5Y7/2	P	-	5	U
PB-3	MR	5Y7/2	P	-	5	U
P-4	MR	N7	M	-	5	U
P-5	SMR	5Y7/2	P	-	5	U
P-24	MR	5Y4/1	VP	-	4	
P-51	MR	5Y6/1	P	-	6	L
P-52	MR	5Y8/1	B	-	6	U
P-53	MR	5Y6/1	P	-	6	M
P-66	MR	5Y8/1	M	-	6	
P-70	MR	5Y6/1	P	-	6	M
P-75	MR	N5	B	-	6	

* Rock types are abbreviated as follows: MR-mudrock; SMR-silty mudrock; MSS-muddy sandstone; B-bentonite.

** Rock colors are from the GSA Rock Color Chart.

*** The type of rock fractures are as follows: VP-very platy or very fissile; P-platy or fissile; B-blocky structure; M-massive structure; PoP-popcorn appearing structure.

**** Special characteristics are abbreviated as follows: S-siliceous; Y-yellow streaks or coatings.

***** The stratigraphic level of the sample is designated as U (upper), M (middle), and L (lower). The break between the lower and middle is defined here as being between the ammonite zones of Baculites sp. (smooth) and Baculites perpterus (early form). The break between the upper and middle Pierre is defined as being between the ammonite zones Didymoceras cheyennense and Baculites comprusus.

Sample Number	* Rock Type	** Color	*** Fissility	**** Special Charac.	Region	***** Stratigraphic Level
P-101	MR	N6	P	S	4	U
P-102	MR	N5	P	S	4	U
P-103	MR	N6	P	S	4	U
P-104	MR	N6	P	S	4	U
P-105	MR	N6	P	S	4	U
P-139	MR	N9	M	S	2	U
P-151	MR	N6	P	S	2	U
P-152	MR	N6	M	S	2	U
P-153	MR	5Y6/1	M	S	2	U
P-154	MR	N5	M	S	2	U
P-155	B	5Y8/1	PoP	-	2	U
P-156	MR	N6	P	S	2	U
P-186	MR	5Y6/1	P	-	2	U
P-187	MR	N7	P	S	2	U
P-193	MR	5Y6/1	B	-	1	U
P-201	SMR	5Y6/1	B	-	1	U
P-202	MR	5Y6/1	B	-	1	U
P-203	MR	5Y6/1	B	-	1	U
P-204	MR	N7	B	-	1	U
P206	MR	5Y6/1	B	-	1	U
P-208	SMR	5Y6/1	B	-	1	U
P-210	SMR	5Y7/2	B	-	1	U
P-212	SMR	5Y6/1	B	-	1	U
P-214	MR	5Y4/1	B	-	1	U

Sample Number	* Rock Type	** Color	*** Fissility	**** Special Charac.	Region	***** Stratigraphic Level
P-218	MSS	5Y6/2	B	-	1	U
P-220	MR	5YR4/1	VP	-	1	U
P-222	MR	5Y6/1	B	-	1	U
P-224	MR	5Y6/1	B	-	1	U
P-226	MR	5Y8/1	B	-	1	U
P-228	MR	5Y6/1	B	-	1	U
P-230	MR	5Y6/1	VP	-	1	U
P-232	MR	5Y6/1	B	-	1	U
P-234	MR	5Y4/1	P	-	1	U
P-236	MR	5Y4/1	P	-	1	U
P-237	B	5Y8/1	PoP	Black specks in rock	1	U
P-238	MR	5Y4/1	P	-	1	U
P-239	MR	5Y6/1	B	-	1	U
P-240	MR	5Y4/1	P	-	1	U
P-242	MR	5Y6/1	B	-	3	U
P-244	MR	5Y4/1	P	-	3	U
P-246	MR	5Y4/1	P	I	3	L
P-248	MR	N5	B	-	3	M
P-250	MR	5Y6/1	B	-	1	U
P-251	B	5/Y7/2	PoP	-	1	U
P-252	MR	5Y6/1	B	-	1	U
P-253	MR	5Y6/1	B	-	1	U
P-254	MR	5Y6/1	P	-	3	U
P-255	MR	5Y6/1	P	-	3	U
P-261	MR	5Y6/1	P	-	3	U

Sample Number	* Rock Type	** Color	*** Fissility	**** Special Charac.	Region	***** Stratigraphic Level
P-270	MR	N5	P	-	4	U
P-273	MR	N5	P	-	4	U
P-279	MR	N6	P	-	4	U
P-292	MR	5Y6/1	B	-	3	U
P-301	MR	N4	M	-	5	M
P-302	MR	N4	M	Y	5	U
P-303	MR	5Y7/2	B	-	5	M
P-304	MR	5Y7/2	P	-	5	U
P-305	MR	N5	P	-	5	U
P-306	MR	5Y7/2	B	-	5	U
P-308	MR	5Y3/2	P	-	5	L
P-310	MR	N4	B	-	5	L
P-312	MR	5Y7/2	B	-	5	M
P-313	MR	5Y4/1	P	-	5	M
P-314	MR	5Y4/1	P	-	5	M
P-316	MR	5Y6/1	P	-	5	M
P-318	MR	5Y4/1	M	-	5	M
P-320	MR	N4	M	-	5	L
P-325	MR	5Y6/1	P	-	5	L
P-327	MR	N3	P	-	5	M
P-331	MR	5Y6/1	P	-	5	U
P-334	MR	5Y6/1	M	-	3	L
P-343	MR	5Y4/1	M	-	3	U
P-350	MR	5Y6/1	P	-	3	U

Sample Number	* Rock Type	** Color	*** Fissility	**** Special Charac.	Region	***** Stratigraphic Level
P-351	B	5Y8/1	PoP	-	3	U
P-352	MR	5Y6/1	P	-	3	U
P-353	MR	5Y6/1	P	-	3	L
RB-1	MR	5Y6/1	B	-	3	L
RB-2	MR	5Y7/2	P	-	3	M
RB-3	MR	5Y6/1	B	-	3	M
RB-4	MR	5Y6/1	P	-	3	M
RB-5	MR	5Y7/2	P	-	3	M
RB-6	MR	5Y6/2	P	-	3	M
RB-7	MR	5Y7/2	B	-	3	U
RB-8	MR	5Y7/2	P	-	3	U
RB-9	MR	5Y7/2	B	-	3	U
RB-10	MR	5Y6/1	B	-	3	U
RB-23	MR	5Y7/2	B	-	3	U
W-0	MR	N7	B	-	2	U
W-1	MR	N5	M	-	2	U
W-2	MR	N7	M	-	2	U
W-3	MR	5Y4/1	B	-	2	U
W-4	MR	N7	M	-	2	U
W-5	MR	N7	P	-	2	U
W-6	MR	N7	B	-	2	U
W-7	MR	N7	B	-	2	U
W-8	MR	N6	M	-	2	U
W-9	MR	N7	M	-	2	M

Sample Number	* Rock Type	** Color	*** Fissility	**** Special Charac.	Region	***** Stratigraphic Level
W-10	MR	5Y4/1	P	-	2	M
W-11	MR	N7	M	-	2	M
W-12	MR	N7	M	-	2	M
W-13	MR	N7	M	-	2	M
WA-14	B	5Y8/1	PoP	-	2	M
WB-14	B	5B7/1	PoP	-	2	M
W-15	MR	N5	VP	-	2	M

APPENDIX II

SUMMARY OF BASIC DATA

Table 16. Results of quantitative analyses for moisture content, carbonate, cristobalite, sulfur-bearing phases and quartz (all percentages given in terms of the whole rock).

Sample Number	% Water Loss at 100°C	% Carbonate	% Cristobalite	Max. % Sulfur-bearing Phases	Max. % Gypsum	Max. % Jarosite	Max. % Pyrite	% Quartz
P-1	4.2	ND	ND	0.5	ND	ND	ND	36.8
P-2	5.2	ND	ND	1.2	ND	ND	ND	24.5
PA-3	5.2	2.0	ND	0.2	ND	ND	ND	27.0
PB-3	5.5	2.2	ND	0.4	ND	ND	ND	23.4
P-4	4.5	6.7	ND	2.0	2.0	ND	ND	26.9
P-5	3.9	5.3	ND	0.3	ND	ND	ND	29.6
P-24	6.4	ND	ND	2.2	2.2	ND	ND	16.2
P-51	3.7	ND	ND	2.5	ND	2.5	ND	27.9
P-52	4.6	2.2	ND	1.0	1.0	ND	ND	21.9
P-53	4.5	7.6	ND	0.1	ND	ND	ND	19.1
P-66	2.1	2.9	ND	0.1	ND	ND	ND	24.7
P-70	8.9	3.4	ND	0.4	ND	ND	ND	11.6
P-75	6.3	3.3	ND	2.2	2.2	ND	ND	13.2
P-101	7.4	ND	41.0	0.3	ND	ND	ND	6.8
P-102	8.0	ND	35.0	0.2	ND	ND	ND	5.1
P-103	7.5	ND	45.0	0.2	ND	ND	ND	7.2
P-104	6.8	ND	49.0	0.2	ND	ND	ND	5.9
P-105	5.7	ND	59.0	1.9	ND	ND	ND	5.2
P-139	4.9	ND	55.0	0.3	ND	ND	ND	10.6
P-151	5.1	ND	48.0	0.2	ND	ND	ND	11.6
P-152	2.4	ND	70.0	0.3	ND	ND	ND	5.5

ND indicates Not Detectable by either X-ray diffraction or chemical means.

Sample Number	% Water Loss at 100°C	% Carbonate	% Cristobalite	Max. % Sulfur-bearing Phases	Max. % Gypsum	Max. % Jarosite	Max. % Pyrite	% Quartz
P-153	3.8	ND	67.6	0.2	ND	ND	ND	6.2
P-154	4.4	ND	62.0	0.1	ND	ND	ND	5.0
P-155	9.6	0.0	11.0	0.2	ND	ND	ND	7.7
P-156	4.3	0.0	39.0	0.3	ND	ND	ND	14.5
P-186	7.2	ND	5.0	0.4	ND	ND	ND	17.2
P-187	4.6	ND	60.0	0.2	ND	ND	ND	5.1
P-193	4.0	1.0	ND	0.8	ND	ND	ND	22.7
P-201	4.1	0.2	ND	0.3	ND	ND	ND	26.7
P-202	4.2	ND	ND	0.3	ND	ND	ND	25.1
P-203	6.8	ND	ND	0.3	0.3	ND	ND	21.6
P-204	3.6	0.3	ND	0.3	ND	ND	ND	21.4
P-206	3.8	ND	10.0	0.1	ND	ND	ND	28.2
P-208	4.3	1.1	7.0	1.1	ND	ND	ND	22.9
P-210	3.5	1.3	ND	0.2	ND	ND	ND	25.4
P-212	3.2	1.1	ND	2.1	ND	0.7	ND	24.1
P-214	8.0	ND	ND	0.4	0.4	ND	ND	12.1
P-218	5.5	6.1	5.0	0.4	0.4	ND	ND	17.5
P-220	5.3	ND	7.4	0.6	ND	ND	ND	20.3
P-222	4.4	ND	ND	0.3	ND	ND	ND	33.2
P-224	3.9	ND	ND	0.3	ND	ND	ND	32.5
P-226	4.5	2.4	ND	2.0	2.0	ND	ND	24.7
P-228	2.4	2.6	ND	2.0	ND	ND	ND	32.2
P-230	4.8	1.0	ND	0.5	ND	ND	ND	22.2
P-232	1.9	3.7	ND	2.0	2.0	ND	ND	35.1

Sample Number	% Water Loss at 100°C	% Carbonate	% Cristobalite	Max. % Sulfur-bearing Phases	Max. % Gypsum	Max. % Jarosite	Max. % Pyrite	% Quartz
P-234	3.0	ND	ND	0.5	ND	ND	ND	30.7
P-236	3.8	ND	ND	0.8	ND	ND	ND	26.3
P-237	8.2	3.1	ND	0.6	0.6	ND	ND	0
P-238	3.6	ND	ND	0.3	ND	ND	ND	34.9
P-239	4.1	ND	ND	0.3	ND	ND	ND	34.2
P-240	4.7	ND	ND	0.1	ND	ND	ND	30.7
P-242	3.8	ND	ND	0.1	ND	ND	ND	37.9
P-244	3.9	ND	ND	0.2	ND	ND	ND	23.7
P-246	5.9	ND	ND	1.2	1.2	ND	ND	18.9
P-248	4.5	ND	ND	1.3	1.3	ND	ND	25.5
P-250	5.0	ND	ND	0.4	ND	ND	ND	23.3
P-251	9.9	ND	ND	4.8	3.6	4.8	ND	1.1
P-252	7.0	ND	ND	0.2	ND	ND	ND	17.8
P-253	5.0	ND	ND	0.4	0.4	ND	ND	25.4
P-254	4.2	ND	ND	0.4	0.4	ND	ND	28.2
P-255	5.0	5.2	ND	3.6	3.6	ND	ND	21.4
P-261	6.6	ND	ND	0.8	ND	ND	ND	22.9
P-270	6.5	ND	10.0	0.3	ND	0.3	ND	17.5
P-273	4.4	7.5	ND	0.1	0.1	ND	ND	18.7
P-279	7.6	0.0	16.0	0.3	0.3	ND	ND	11.0
P-292	5.0	1.0	ND	0.3	ND	ND	ND	24.1
P-301	1.4	5.7	ND	0.5	ND	ND	ND	33.8
P-302	2.4	9.8	ND	1.0	ND	ND	ND	28.4
P-303	3.5	3.8	ND	0.4	ND	ND	ND	24.0

Sample Number	% Water Loss at 100°C	% Carbonate	% Cristobalite	Max. % Sulfur-bearing Phases	Max. % Gypsum	Max. % Jarosite	Max. % Pyrite	% Quartz
P-304	4.4	0.6	ND	0.2	ND	ND	ND	22.0
P-305	0.8	7.7	ND	1.2	ND	ND	ND	33.4
P-306	2.2	4.3	ND	0.3	ND	ND	ND	32.7
P-308	1.2	14.0	ND	3.2	ND	ND	ND	32.5
P-310	2.0	6.9	ND	0.2	ND	ND	ND	27.8
P-312	4.6	1.1	ND	0.1	ND	ND	ND	31.3
P-313	3.1	3.9	ND	0.4	ND	ND	ND	27.6
P-314	0.4	3.5	ND	0.2	ND	ND	ND	33.6
P-316	2.0	3.3	ND	0.3	0.3	ND	ND	31.5
P-318	2.1	23.5	ND	0.6	0.6	ND	ND	22.2
P-320	1.3	42.4	ND	0.2	ND	ND	0.2	15.7
P-325	1.9	4.9	ND	0.3	ND	ND	ND	33.7
P-327	2.4	1.0	ND	0.7	ND	ND	ND	35.0
P-331	5.9	4.7	ND	0.2	ND	ND	ND	24.3
P-334	1.7	21.6	ND	0.1	0.1	ND	ND	33.7
P-343	3.8	ND	ND	1.1	ND	ND	ND	28.8
P-350	4.9	ND	ND	0.4	ND	ND	ND	35.9
P-351	8.4	13.4	ND	8.2	8.2	ND	ND	9.4
P-352	4.4	1.2	ND	0.3	ND	ND	ND	27.2
P-353	1.3	31.6	ND	0.6	ND	ND	0.6	33.3
RB-1	3.5	ND	ND	0.7	ND	ND	ND	28.2
RB-2	3.8	ND	ND	0.3	ND	ND	ND	21.7
RB-3	3.5	3.0	ND	2.0	2.0	ND	ND	19.1
RB-4	5.5	ND	ND	0.7	0.7	ND	ND	24.6

Sample Number	% Water Loss at 100°C	% Carbonate	% Cristobalite	Max. % Sulfur-bearing Phases	Max. % Gypsum	Max. % Jarosite	Max. % Pyrite	% Quartz
RB-5	4.5	1.6	ND	0.4	0.4	ND	ND	26.6
RB-6	4.2	3.3	ND	0.6	ND	ND	ND	21.7
RB-7	5.6	ND	ND	0.5	ND	ND	ND	19.0
RB-8	5.2	1.9	ND	0.7	0.7	ND	ND	24.2
RB-9	2.6	5.8	ND	0.5	ND	ND	ND	30.2
RB-10	4.2	4.0	ND	0.8	0.8	ND	ND	26.9
RB-23	2.6	3.9	ND	0.2	ND	ND	ND	31.1
W-0	3.8	ND	ND	2.5	ND	ND	2.5	27.8
W-1	3.3	0.2	ND	1.9	ND	ND	ND	33.2
W-2	4.0	ND	ND	1.7	ND	ND	ND	29.8
W-3	3.9	2.2	ND	2.0	2.0	ND	ND	28.4
W-4	4.0	1.8	ND	0.6	ND	ND	ND	28.4
W-5	4.0	1.8	ND	0.9	ND	ND	ND	27.2
W-6	4.1	1.8	ND	0.9	0.9	ND	ND	27.2
W-7	3.6	ND	ND	1.1	ND	ND	ND	36.1
W-8	2.8	ND	ND	1.2	ND	ND	ND	37.0
W-9	2.9	1.7	ND	1.7	ND	ND	ND	25.4
W-10	4.3	ND	ND	1.7	ND	ND	ND	19.3
W-11	4.0	2.4	ND	1.7	ND	ND	ND	18.7
W-12	3.9	3.1	ND	1.4	1.4	ND	ND	19.5
W-13	4.5	ND	ND	1.7	ND	ND	ND	18.6
WA-14	9.1	1.5	ND	4.5	4.5	ND	ND	0.7
WB-14	10.4	ND	ND	2.6	2.6	ND	ND	0.7
W-15	4.7	ND	ND	4.3	4.3	ND	ND	27.3

Table 17. Chemical and normative analyses for feldspar compositions and concentrations.

Sample Number	Percent of Whole Rock Fused	Chemical Composition of Fusion Residue			Norminative Feldspar Concentration (as percentage of Whole Rock)					Mole Percent Anorthite
		Weight Percent CaO	Weight Percent K_2O	Weight Percent Na_2O	Quartz	Orthoclase	Albite	Anorthite	Total Feldspar	
P-2	61.23	0.19	1.59	2.17	24.26	4.38	9.62	0.52	14.52	5.1
P-24	76.26	0.14	1.65	1.50	16.41	2.78	4.32	0.23	7.33	5.1
P-51	66.19	0.07	0.76	0.87	28.46	1.83	3.36	0.16	5.35	4.5
P-66	62.84	0.16	1.04	1.96	25.68	2.74	8.31	0.42	11.48	4.8
P-70	74.48	0.25	3.93	1.83	12.62	7.14	5.32	0.45	12.91	7.1
P-75	80.12	0.11	1.78	1.51	13.78	2.52	3.42	0.16	6.10	4.4
P-101	90.22	0.31	1.50	1.28	7.10	1.04	1.43	0.21	2.68	12.7
P-139	87.62	0.12	0.64	0.76	10.64	.56	1.08	0.10	1.74	8.6
P-186	75.70	0.23	1.01	1.57	17.80	1.75	4.36	0.39	6.50	8.3
P-187	92.84	0.38	1.32	1.29	5.25	0.67	1.05	0.19	1.91	15.2
P-193	64.31	0.42	1.02	2.22	23.03	2.58	9.03	1.04	12.66	10.4
P-203	64.27	0.45	1.03	2.45	22.02	2.62	9.97	1.13	13.71	10.1
P-252	69.74	0.58	1.10	2.47	18.15	2.37	8.52	1.22	12.11	12.5
P-261	65.06	0.43	0.99	2.06	23,23	2.46	8.21	1.04	11.71	11.2
P-270	73.19	0.31	1.40	1.73	18.27	2.66	5.30	0.58	8.54	9.9
P-273	75.89	0.02	0.81	1.29	19.15	1.39	3.54	0.04	4.97	1.0
P-279	86.09	0.19	0.93	1.37	10.63	0.92	2.17	0.18	3.28	7.7
P-313	63.60	0.15	0.34	1.75	27.90	0.87	7.24	0.39	8.50	5.0
P-318	74.55	0.03	0.05	1.02	22.34	0.09	2.97	0.05	3.11	1.6

Sample Number	Percent of Whole Rock Fused	Chemical Composition of Fusion Residue			Norminative Feldspar Concentration (as percentage of Whole Rock)					Mole Percent Anorthite
		Weight Percent CaO	Weight Percent K_2O	Weight Percent Na_2O	Quartz	Orthoclase	Albite	Anorthite	Total Feldspar	
P-325	59.91	0.06	0.33	1.11	33.90	0.94	5.07	0.18	6.19	3.4
P-327	57.75	0.03	0.45	0.72	35.83	2.87	3.48	0.08	6.42	2.2
P-331	71.30	0.05	0.49	0.96	24.46	1.00	3.13	0.10	4.23	3.2
P-334	60.22	0.03	0.69	0.83	33.98	1.94	3.77	0.08	5.80	2.2
P-343	62.72	0.17	0.68	1.40	29.10	1.80	5.95	0.44	8.18	6.9
P-350	55.42	0.30	0.62	1.08	36.23	1.95	5.48	0.92	8.35	14.4
P-351	82.45	1.90	0.73	2.39	9.54	0.91	4.78	2.31	8.00	32.6
P-353	59.40	0.06	0.91	0.89	33.70	2.63	4.12	0.16	6.90	3.6
RB-3	69.90	0.19	1.22	2.23	19.43	2.62	7.65	0.40	10.67	4.9
RB-4	63.40	0.40	0.96	1.93	25.03	2.51	8.04	1.01	11.56	11.2
RB-5	57.43	0.22	1.56	2.07	27.17	4.72	10.03	0.64	15.40	6.0
RB-8	61.98	0.56	1.23	1.98	24.60	3.33	8.60	1.47	13.41	14.6
RB-10	50.85	0.60	2.03	2.20	27.67	7.09	12.35	2.03	21.47	14.1
W-8	56.48	0.05	0.23	0.83	37.49	0.69	3.98	0.15	4.82	3.6
					$\bar{x}$ 2.43			$\bar{x}$ = 8.5	$\bar{x}$ = 8.2	

Table 18. RESULTS OF CHEMICAL ANALYSES

BY X-RAY FLUORESCENT METHODS

Sample Number	SiO_2	Al_2O_3	K_2O	SO_3^-
P-1	63.87	16.25	3.04	0.24
P-2	58.41	15.41	2.78	0.57
PA-3	58.97	15.12	2.80	0.11
PB-3	56.90	14.90	2.81	0.17
P-4	57.97	14.16	2.97	0.91
P-5	57.29	14.29	3.08	0.14
P-24	55.16	16.70	2.08	1.04
P-51	61.94	15.48	3.23	0.79
P-52	56.71	15.83	2.82	0.47
P-53	54.58	14.45	3.08	0.07
P-66	58.45	14.48	3.25	0.07
P-70	25.29	16.33	2.66	0.19
P-75	56.14	15.13	3.20	1.03
P-101	70.84	8.93	1.31	0.12
P-102	67.16	8.23	1.23	0.11
P-103	69.49	8.29	1.23	0.11
P-104	73.55	7.43	1.15	0.10
P-105	76.26	6.43	1.02	0.88
P-139	78.71	6.86	1.32	0.14
P-151	74.91	8.23	1.36	0.11
P-152	84.78	4.41	0.87	0.12
P-153	80.52	5.21	0.85	0.11
P-154	80.14	5.82	0.87	0.07
* P-155	59.23	15.80	0.87	0.11
P-156	72.59	9.58	1.49	0.13
P-186	60.07	13.85	2.28	0.21
P-187	78.67	6.10	1.15	0.08
P-193	60.97	14.80	2.51	0.39
P-201	60.39	15.67	2.38	0.13

Sample Number	SiO_2	Al_2O_3	K_2O	SO_3^-
P-202	61.74	15.16	2.36	0.13
P-203	60.58	15.73	2.59	0.13
P-204	59.42	15.77	3.40	0.12
P-206	65.81	14.13	2.31	0.04
P-208	60.58	14.61	2.27	0.50
P-210	60.00	14.58	2.55	0.11
P-212	57.48	13.78	2.12	0.97
P-214	54.00	16.34	2.36	0.18
+P-218	54.19	13.55	1.15	0.19
P-220	59.97	15.29	1.64	0.28
P-222	63.29	14.68	2.22	0.15
P-224	61.74	14.52	2.65	0.16
P-226	55.36	14.58	2.95	0.91
P-228	60.78	14.32	3.02	0.95
P-230	59.23	14.71	1.74	0.23
P-232	64.07	13.20	1.85	0.94
P-234	61.36	16.02	3.22	0.23
P-236	59.61	15.89	2.69	0.35
*P-237	50.32	17.05	0.67	0.26
P-238	63.68	13.97	2.42	0.15
P-239	64.07	13.14	1.77	0.14
P-240	61.36	16.60	2.52	0.07
P-242	63.68	13.91	2.31	0.07
P-244	57.68	15.54	2.87	0.08
P-246	56.13	15.99	2.36	0.54
P-248	60.78	15.32	2.40	0.58
P-250	59.81	15.70	2.21	0.21
*P-251	51.48	16.89	0.51	1.70
P-252	57.68	15.51	0.51	0.09

Sample Number	SiO_2	Al_2O_3	K_2O	SO_3^-
P-253	59.81	16.54	3.10	0.18
P-254	62.52	15.51	2.36	0.19
P-255	58.45	13.68	2.08	1.66
P-261	60.39	14.36	2.53	0.35
P-270	60.78	15.00	2.38	0.12
P-273	56.14	13.95	2.96	0.06
P-279	64.14	12.83	2.22	0.12
P-292	59.81	14.29	2.72	0.13
P-301	60.47	14.20	2.80	0.22
P-302	57.29	12.62	2.53	0.47
P-303	59.23	15.09	2.59	0.17
P-304	57.48	15.99	2.87	0.11
P-305	60.00	14.84	2.82	0.60
P-306	58.65	14.48	2.85	0.12
P-308	57.48	11.50	2.51	1.49
P-310	56.52	15.32	2.99	0.10
P-312	60.97	15.03	2.55	0.05
P-313	56.52	15.25	2.70	0.20
P-314	59.03	15.32	2.81	0.09
P-316	59.23	15.70	2.87	0.12
P-318	52.84	11.98	2.29	0.27
P-320	45.29	8.16	2.04	0.09
P-325	61.13	14.17	2.86	0.14
P-327	62.14	15.44	2.97	0.34
P-331	58.97	15.63	2.40	0.08
P-334	55.80	10.85	2.32	0.06
P-343	62.13	15.77	2.55	0.50
P-350	69.29	12.17	1.57	0.20
* P-351	52.06	15.19	0.64	3.82

Sample Number	SiO_2	Al_2O_3	K_2O	SO_3^-
P-352	58.07	15.06	2.63	0.13
P-353	52.64	8.29	1.98	0.26
RB-1	60.58	16.99	2.70	0.33
RB-2	55.94	16.12	2.59	0.16
RB-3	55.74	16.00	2.21	0.94
RB-4	57.68	15.50	2.34	0.33
RB-5	58.84	15.88	2.48	0.21
RB-6	57.10	15.81	2.53	0.29
RB-7	57.29	15.07	2.38	0.24
RB-8	59.03	14.45	2.86	0.31
RB-9	58.26	13.89	3.25	0.25
RB-10	59.14	13.76	2.55	0.39
RB-23	58.26	15.13	2.91	0.09
W-0	60.39	15.06	2.34	1.15
W-1	63.49	14.16	2.32	0.88
W-2	63.10	14.07	2.04	0.81
W-3	61.36	14.10	2.40	0.91
W-4	61.16	14.32	2.40	0.27
W-5	60.78	14.39	2.42	0.43
W-6	61.55	13.78	2.23	0.40
W-7	66.20	12.17	2.02	0.50
W-8	69.10	10.89	1.87	0.53
W-9	57.87	16.63	2.18	0.78
W-10	55.55	16.31	2.76	0.81
W-11	55.16	16.54	2.80	0.78
W-12	54.97	17.11	2.88	0.63
W-13	55.36	15.51	2.72	0.78
*WA-14	52.45	17.79	0.45	2.11
*WB-14	54.00	18.46	0.45	1.19

Sample Number	SiO_2	Al_2O_3	K_2O	SO_3^-
W-15	58.26	15.19	2.59	1.99

* Indicates bentonitic samples.

+ Indicates muddy sandstones.

Sample Number	SiO_2	Al_2O_3	K_2O	SO_3^-

Table 19. RESULTS OF QUALITATIVE X-RAY ANALYSES

Sample Number	CARBONATES				Cristobalite	Gypsum	Pyrite	Jarosite	Clinoptilolite	K-Spar	Plagioclase	10 Å Peak (Illite)	7 Å Peak (Kaolinite and/or Chlorite)
	Calcite	Calcite (Mixed)	Dolomite	Other									
P-1	-	?	-	-	-	-	-	-	-	1.4	2.2	2.0	1.3
P-2	-	?	-	-	-	-	-	-	-	1.2	1.8	1.4	0.4
PA-3	?	-	1.7	-	-	-	-	-	-	1.5	3.4	2.1	1.1
PB-3	-	?	2.0	-	-	-	-	-	-	1.4	2.8	1.9	0.9
P-4	-	?	?	4.0	S?	-	-	-	-	2.0	3.1	2.4	1.8
P-5	-	-	?	3.6	S?	-	-	-	-	1.6	4.0	3.6	1.5
P-24	-	-	-	-	-	1.5	-	-	-	1.4	2.5	1.1	1.7
P-51	-	0.6	0.6	-	-	-	-	?	-	1.4	1.5	1.0	1.0
P-52	0.8	-	1.3	-	-	0.8	-	-	-	1.7	1.7	2.3	1.0
P-53	3.6	-	1.0	-	-	-	-	-	-	1.0	0.8	1.6	1.1
P-66	1.1	1.1	-	-	-	-	-	-	-	2.0	3.5	3.0	0.9
P-70	-	2.1	-	-	-	-	-	-	-	1.1	1.6	1.0	0.8
P-75	-	-	?	-	-	?	-	-	-	0.6	0.8	1.7	1.3
P-101	-	-	-	-	P	-	-	-	-	1.1	0.8	-	-
P-102	-	-	-	-	P	-	-	-	-	0.7	0.7	-	-
P-103	-	-	-	-	P	-	-	-	-	0.8	0.3	-	-
P-104	-	-	-	-	P	-	-	-	-	1.0	0.7	0.4	-
P-105	-	-	-	-	P	-	-	-	-	tr	-	-	-
P-139	-	-	-	-	P	-	-	-	-	0.8	0.7	0.8	0.6
P-151	-	-	-	-	P	-	-	-	-	-	0.9	-	-
P-152	0.4	-	-	-	P	-	-	-	-	0.5	0.5	-	-

Sample Number	CARBONATES				Cristobalite	Gypsum	Pyrite	Jarosite	Clinoptilolite	K-Spar	Plagioclase	10 Å Peak (Illite)	7 Å Peak (Kaolinite and/or Chlorite)
	Calcite	Calcite (Mixed)	Dolomite	Other									
P-153	-	-	-	-	P	-	-	-	-	-	-	-	-
P-154	-	-	-	-	P	-	-	-	-	-	-	-	-
+P-155	-	-	-	-	P	-	-	-	-	0.9	1.2	-	-
P-156	-	-	-	-	P	-	-	-	-	0.5	1.1	-	0.2
P-186	-	-	-	-	P	-	-	-	-	0.9	1.1	0.3	0.4
P-187	-	-	-	-	P	-	-	-	-	0.6	-	-	-
P-193	1.1	-	-	-	-	-	-	-	-	2.0	0.5	3.0	1.7
P-201	-	?	-	-	?	-	-	-	-	1.3	2.5	1.1	1.6
P-202	0.7	-	-	-	?	-	-	-	-	2.6	3.3	0.9	-
P-203	-	-	-	-	-	?	-	-	-	2.5	4.2	1.3	1.1
P-204	-	0.9	-	-	-	-	-	-	-	2.2	3.4	1.2	0.8
P-206	-	-	-	-	P	-	-	-	-	1.0	1.7	1.6	0.9
P-208	-	0.6	-	-	?	-	-	-	1.5	3.2	3.9	1.6	1.0
P-210	-	0.9	-	-	-	-	-	-	0.8	3.0	9.5	1.3	1.2
P-212	-	1.8	-	-	-	-	-	1.3	2.0	2.2	10.0	0.9	0.4
P-214	-	-	-	-	-	1.2	-	-	-	0.8	1.0	0.5	1.3
P-218	-	1.2	?	-	P	8.4	-	-	-	11.1	10.3	1.4	0.8
P-220	-	-	-	-	P	-	-	-	-	1.4	4.1	1.1	0.6
P-222	-	-	-	-	-	-	-	-	-	0.9	2.8	1.9	0.7
P-224	-	-	-	-	-	-	-	-	0.8	1.4	3.4	2.3	0.9
P-226	0.6	-	-	-	-	2.5	-	-	-	1.0	1.6	1.5	1.4

Sample Number	CARBONATES				Cristobalite	Gypsum	Pyrite	Jarosite	Clinoptilolite	K-Spar	Plagioclase	10 Å Peak (Illite)	7 Å Peak (Kaolinite and/or Chlorite)
	Calcite	Calcite (Mixed)	Dolomite	Other									
P-228	-	-	0.6	50.6	-	-	-	-	-	2.6	4.3	2.2	1.4
P-230	-	-	0.8	-	-	-	-	-	-	1.4	5.0	0.8	0.9
P-232	-	3.0	?	R?	-	2.2	-	-	-	1.8	4.6	2.2	1.2
P-234	-	-	-	-	-	-	-	-	-	0.9	1.4	1.3	1.0
P-236	2.3	-	-	-	-	-	-	-	-	1.2	3.2	1.7	1.2
+P-237	3.8	-	-	-	?	-	-	-	-	12.8	4.4	10.1	2.6
P-238	-	-	-	-	-	-	-	-	-	1.1	1.5	1.3	1.1
P-239	-	-	-	-	-	-	-	-	-	1.8	4.1	1.6	1.2
P-240	-	?	-	-	-	-	-	-	-	0.7	1.9	1.3	1.1
P-242	-	-	-	-	-	-	-	-	-	2.2	3.2	1.7	1.2
P-244	-	-	-	-	-	-	-	-	-	1.0	3.2	2.2	1.8
P-246	-	-	-	-	-	1.7	-	-	-	1.0	1.8	1.1	1.1
P-248	-	-	?	-	?	?	-	-	-	0.9	1.3	1.0	1.1
P-250	-	-	-	-	-	-	-	-	-	2.2	3.0	1.0	0.6
+P-251	-	-	-	-	-	7.8	-	1.0	-	3.2	4.1	-	-
P-252	-	?	-	R? S?	-	-	-	-	-	2.1	4.8	1.2	-
P-253	?	-	-	-	?	?	-	-	-	1.2	2.0	1.2	-
P-254	-	-	-	-	-	?	-	-	-	1.6	3.1	1.4	0.6
P-255	-	-	1.3	5.8	-	4.9	-	-	-	1.8	4.1	1.4	0.9
P-261	?	?	-	-	-	-	-	-	-	1.4	3.8	1.0	0.6
P-270	?	?	-	S?	P	-	-	?	-	1.1	2.2	1.0	0.9

Sample Number	CARBONATES				Cristobalite	Gypsum	Pyrite	Jarosite	Clinoptilolite	K-Spar	Plagioclase	10 Å Peak (Illite)	7 Å Peak (Kaolinite and/or Chlorite)
	Calcite	Calcite (Mixed)	Dolomite	Other									
P-273	2.7	-	-	50.6	-	0.2	-	-	-	0.4	0.4	3.7	1.7
P-279	-	-	-	-	P	?	-	-	-	0.2	0.6	1.4	-
P-292	-	?	-	-	-	-	-	-	-	2.3	3.9	1.8	0.8
P-301	-	-	3.3	-	?	-	-	-	-	1.0	4.1	3.0	1.9
P-302	0.8	0.8	7.5	R? S?	-	-	-	-	-	1.5	4.4	2.7	1.6
P-303	0.6	-	2.2	S?	-	-	-	-	-	2.0	6.6	1.2	1.6
P-304	-	0.7	-	-	-	-	-	-	-	1.1	1.6	1.3	1.3
P-305	0.5	0.8	3.3	S? S?	-	-	-	-	-	1.6	4.1	2.1	2.0
P-306	-	0.6	4.0	-	4.3	-	-	-	-	1.5	4.6	2.7	1.6
P-308	1.4	3.9	1.0	S?	-	-	-	-	-	0.9	1.5	1.4	1.4
P-310	?	-	2.1	S? R?	-	-	-	-	-	1.0	1.9	2.0	1.8
P-312	-	-	1.4	-	-	-	-	-	-	?	2.7	1.8	1.7
P-313	-	-	1.6	-	-	-	-	-	-	1.0	2.0	1.3	2.6
P-314	-	-	2.2	R?	-	-	-	-	-	0.8	2.9	1.8	1.2
P-316	-	-	2.9	-	-	?	-	-	-	0.6	2.8	1.9	1.8
P-318	10.0	-	4.7	-	-	0.6	-	-	-	1.0	2.0	1.4	1.8
P-320	14.1	-	1.5	R6.0	-	-	3.0	-	-	0.5	1.1	0.8	0.7
P-325	-	0.7	3.4	-	-	-	-	-	-	1.8	0.7	2.2	1.1
P-327	-	-	0.6	-	-	-	-	-	-	0.9	0.8	3.0	2.3
P-331	-	-	1.7	-	-	-	-	-	-	1.1	1.3	2.2	1.5
P-334	3.7	-	6.8	-	-	?	-	-	-	1.5	1.8	2.1	1.5

Sample Number	CARBONATES				Cristobalite	Gypsum	Pyrite	Jarosite	Clinoptilolite	K-Spar	Plagioclase	10 Å Peak (Illite)	7 Å Peak (Kaolinite and/or Chlorite)
	Calcite	Calcite (Mixed)	Dolomite	Other									
P-343	-	-	-	-	-	-	-	-	-	1.8	2.6	1.5	0.9
P-350	-	-	-	-	-	-	-	-	-	2.0	9.5	1.0	-
+P-351	3.3	-	-	-	-	18.8	-	-	-	3.3	8.4	2.9	-
P-352	-	-	1.1	-	-	-	-	-	-	1.2	2.0	1.3	1.2
P-353	9.0	-	4.9	-	-	-	?	-	-	3.3	1.3	1.2	1.2
RB-1	-	0.7	-	-	?	-	-	-	-	1.1	1.8	1.3	1.1
RB-2	-	-	-	-	-	-	-	-	-	1.1	2.3	1.2	1.9
RB-3	-	-	-	-	-	3.0	-	-	-	1.9	3.6	1.9	2.3
RB-4	-	-	-	-	?	?	-	-	-	1.8	4.7	0.7	1.0
RB-5	-	1.0	2.5	-	1.7	?	1.2	-	-	2.2	3.8	1.6	1.3
RB-6	-	0.5	1.1	-	-	-	-	-	-	1.4	3.8	1.6	1.2
RB-7	-	-	-	-	-	-	-	-	-	1.3	2.2	1.7	0.8
RB-8	-	0.6	0.9	-	-	1.2	-	-	-	3.0	4.6	3.2	1.1
RB-9	-	0.9	4.9	-	-	-	-	-	-	2.7	5.1	3.3	1.9
RB-10	-	0.8	5.3	-	?	?	-	-	-	4.4	5.5	2.0	1.4
RB-23	-	1.0	4.7	R1.0	-	-	-	-	-	2.9	5.7	4.0	1.7
W-0	-	-	-	-	-	-	0.7	-	-	0.8	1.4	0.7	1.2
W-1	-	0.5	-	-	-	-	-	-	-	1.0	1.2	1.2	1.4
W-2	-	-	-	-	-	-	-	-	-	0.9	1.4	0.7	1.0
W-3	-	-	-	S?	-	?	-	-	-	1.0	1.1	0.7	1.2
W-4	-	-	-	S?	-	-	-	-	-	0.9	1.3	1.0	1.3

RESULTS OF QUALITATIVE X-RAY ANALYSES

Sample Number	CARBONATES				Cristobalite	Gypsum	Pyrite	Jarosite	Clinoptilolite	K-Spar	Plagioclase	10 Å Peak (Illite)	7 Å Peak (Kaolinite and/or Chlorite)
	Calcite	Calcite (Mixed)	Dolomite	Other									
W-5	-	tr	-	R?	-	-	-	-	-	1.2	1.6	0.8	1.3
W-6	-	?	-	-	-	?	-	-	-	1.0	1.2	0.9	1.0
W-7	-	-	-	-	-	-	-	-	-	1.2	0.8	0.6	1.0
W-8	0.6	-	-	-	-	-	-	-	-	0.8	0.8	-	0.8
W-9	-	0.6	0.6	-	-	-	-	-	-	1.6	2.5	1.8	1.8
W-10	-	?	-	-	-	-	-	-	-	1.3	2.5	1.2	2.2
W-11	-	-	?	-	-	-	-	-	-	0.9	1.6	1.1	1.9
W-12	-	-	-	-	-	0.7	-	-	0.7	1.2	1.7	2.5	2.5
W-13	-	?	-	-	-	-	-	-	-	1.0	2.0	1.1	2.0
+W-14a	-	-	-	-	-	1.0	-	-	-	-	-	1.8	-
+W-14b	-	-	-	-	-	0.9	-	-	-	-	-	-	-
W-15	-	-	-	-	-	0.6	-	-	-	1.0	2.0	1.6	1.4

+ Denotes bentonites.

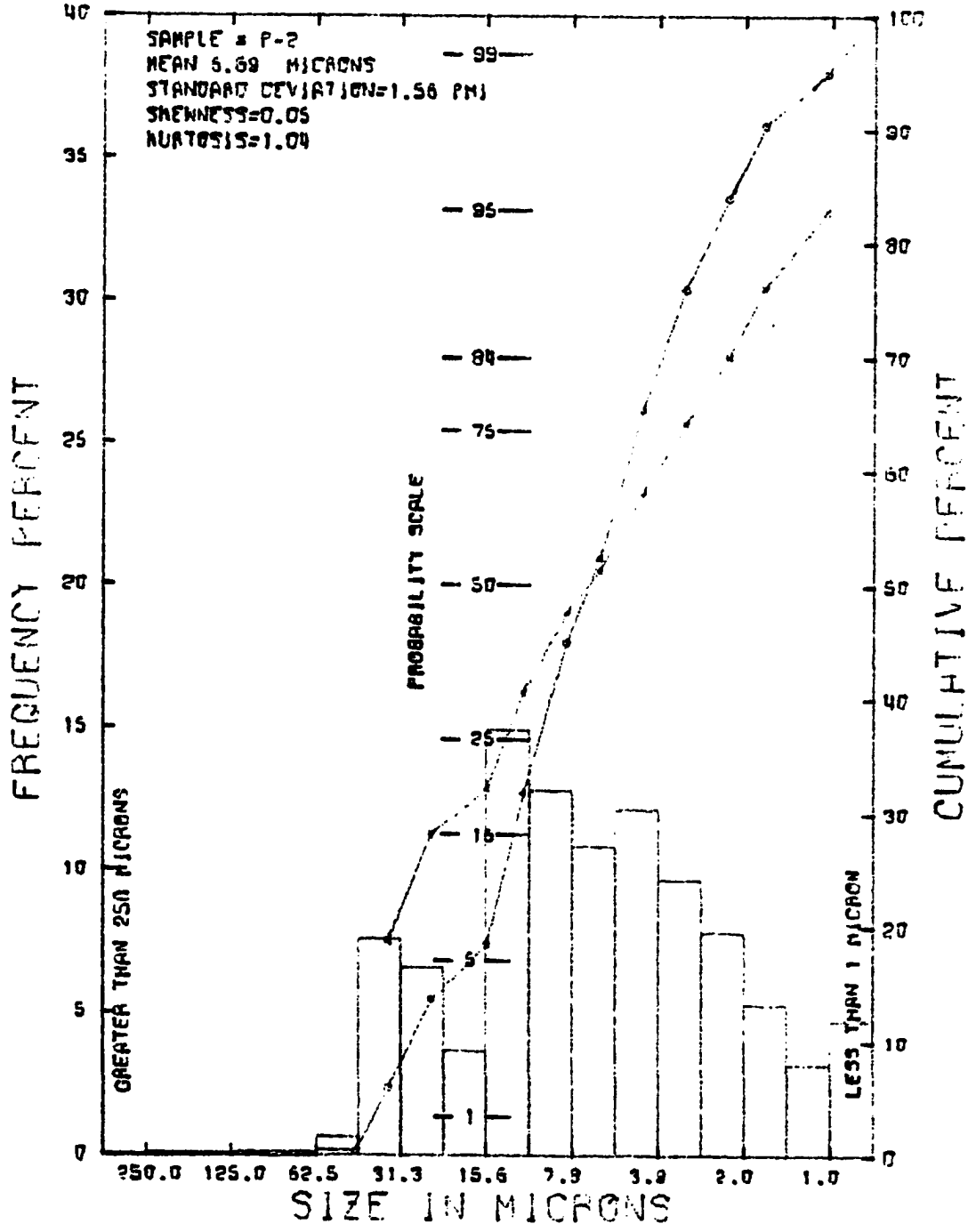
SAMPLE # P-2
MEAN 5.69 MICRONS
STANDARD DEVIATION=1.56 PHI
SKEWNESS=0.05
KURTOSIS=1.04
FREQUENCY PERCENT
CUMULATIVE PERCENT
PROBABILITY SCALE
99
95
84
75
50
25
16
5
1
GREATER THAN 250 MICRONS
LESS THAN 1 MICRON
250.0
125.0
62.5
31.3
15.6
7.8
3.9
2.0
1.0
SIZE IN MICRONS

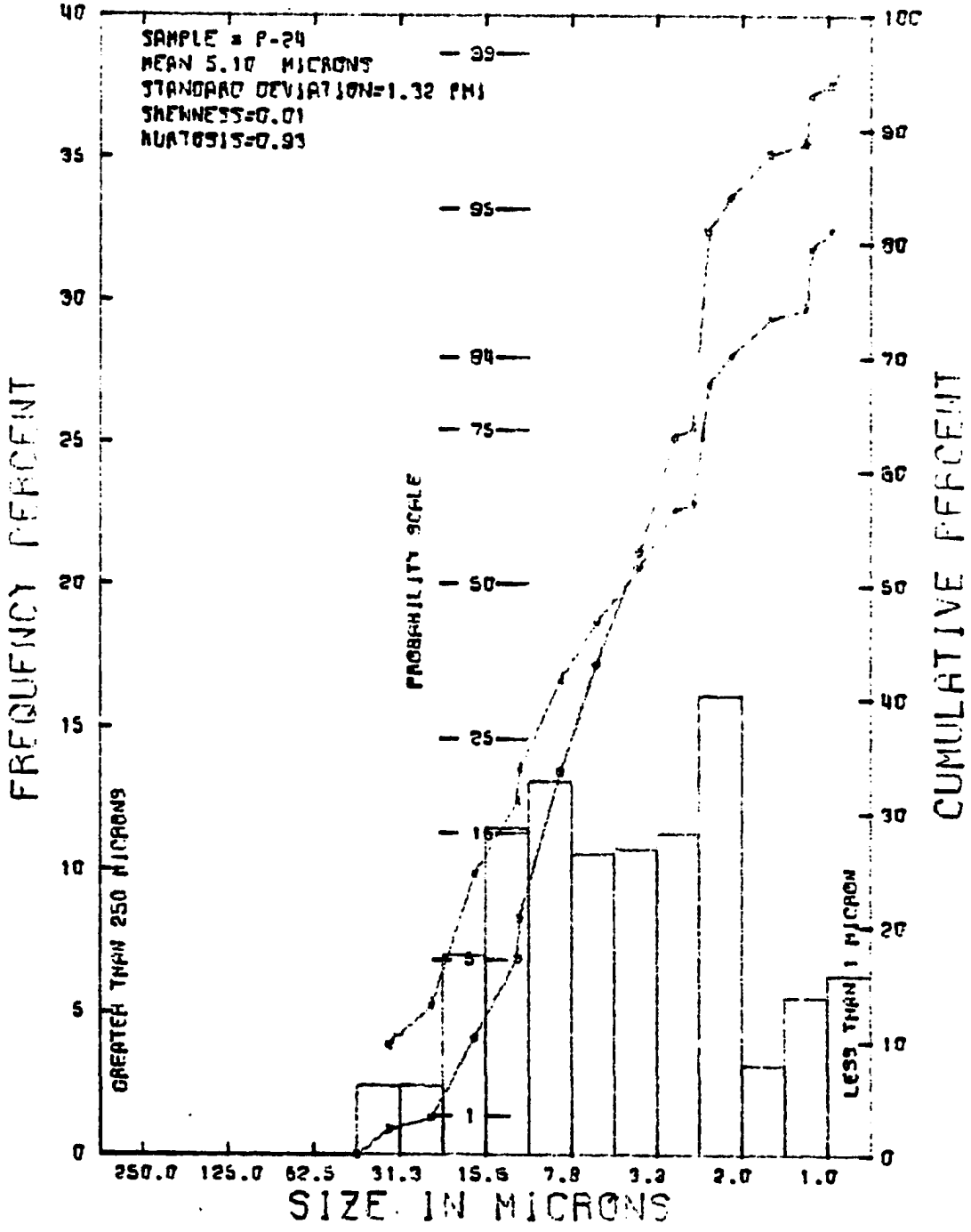
SAMPLE = P-24
MEAN 5.10 MICRONS
STANDARD DEVIATION=1.32 PHI
SKEWNESS=0.01
KURTOSIS=0.93
FREQUENCY PERCENT
CUMULATIVE PERCENT
PROBABILITY SCALE
99
95
84
75
50
25
16
5
1
GREATER THAN 250 MICRONS
LESS THAN 1 MICRON
250.0 125.0 62.5 31.3 15.6 7.8 3.9 2.0 1.0
SIZE IN MICRONS

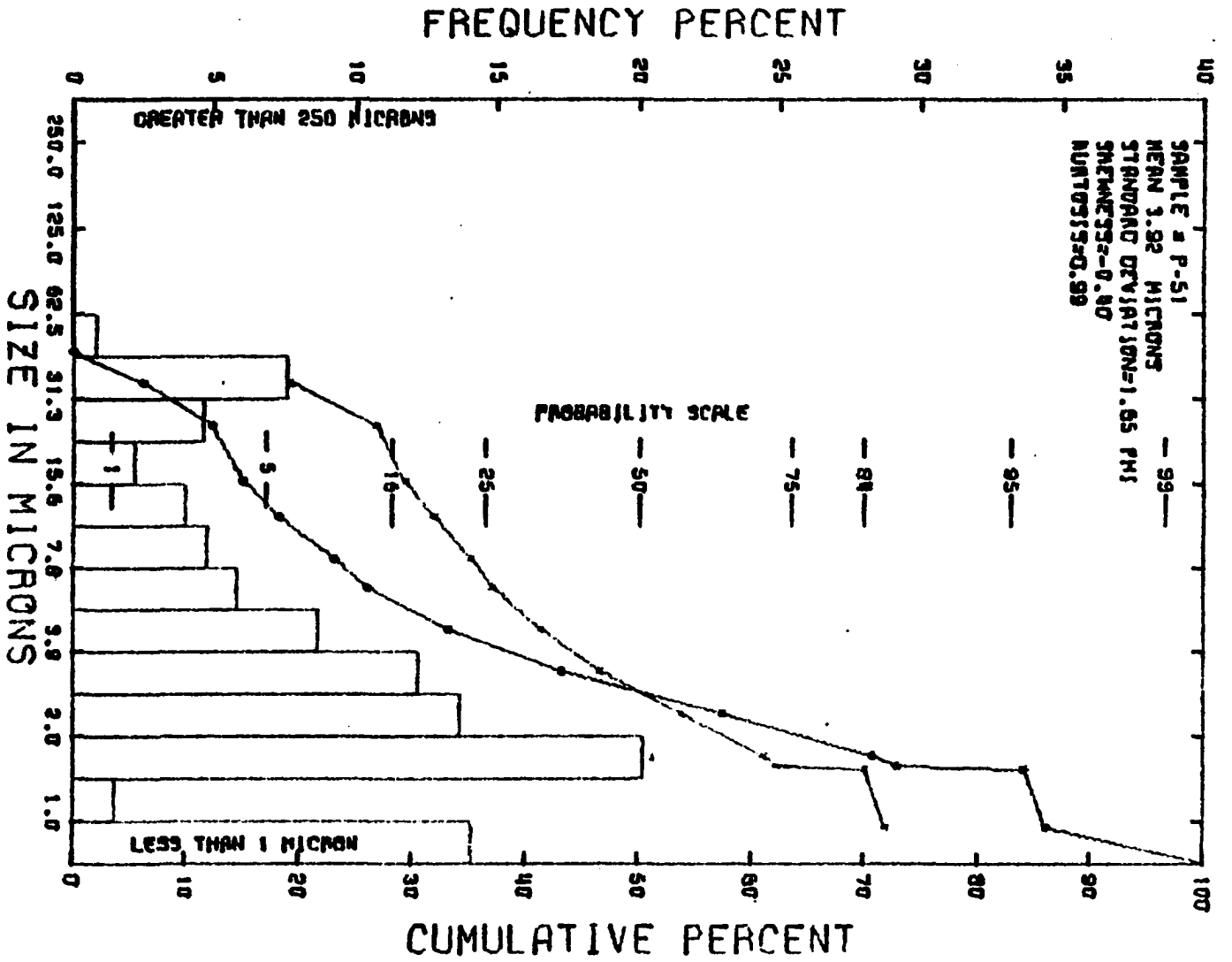
FREQUENCY PERCENT
0
5
10
15
20
25
30
35
40
GREATER THAN 250 MICRONS
SAMPLE = P-51
MEAN 3.82 MICRONS
STANDARD DEVIATION=1.65 PHI
SKEWNESS=-0.80
KURTOSIS=0.98
PROBABILITY SCALE
1
5
16
25
50
75
84
95
99
SIZE IN MICRONS
250.0
125.0
62.5
31.3
15.6
7.8
3.9
2.0
1.0
LESS THAN 1 MICRON
0
10
20
30
40
50
60
70
80
90
100
CUMULATIVE PERCENT

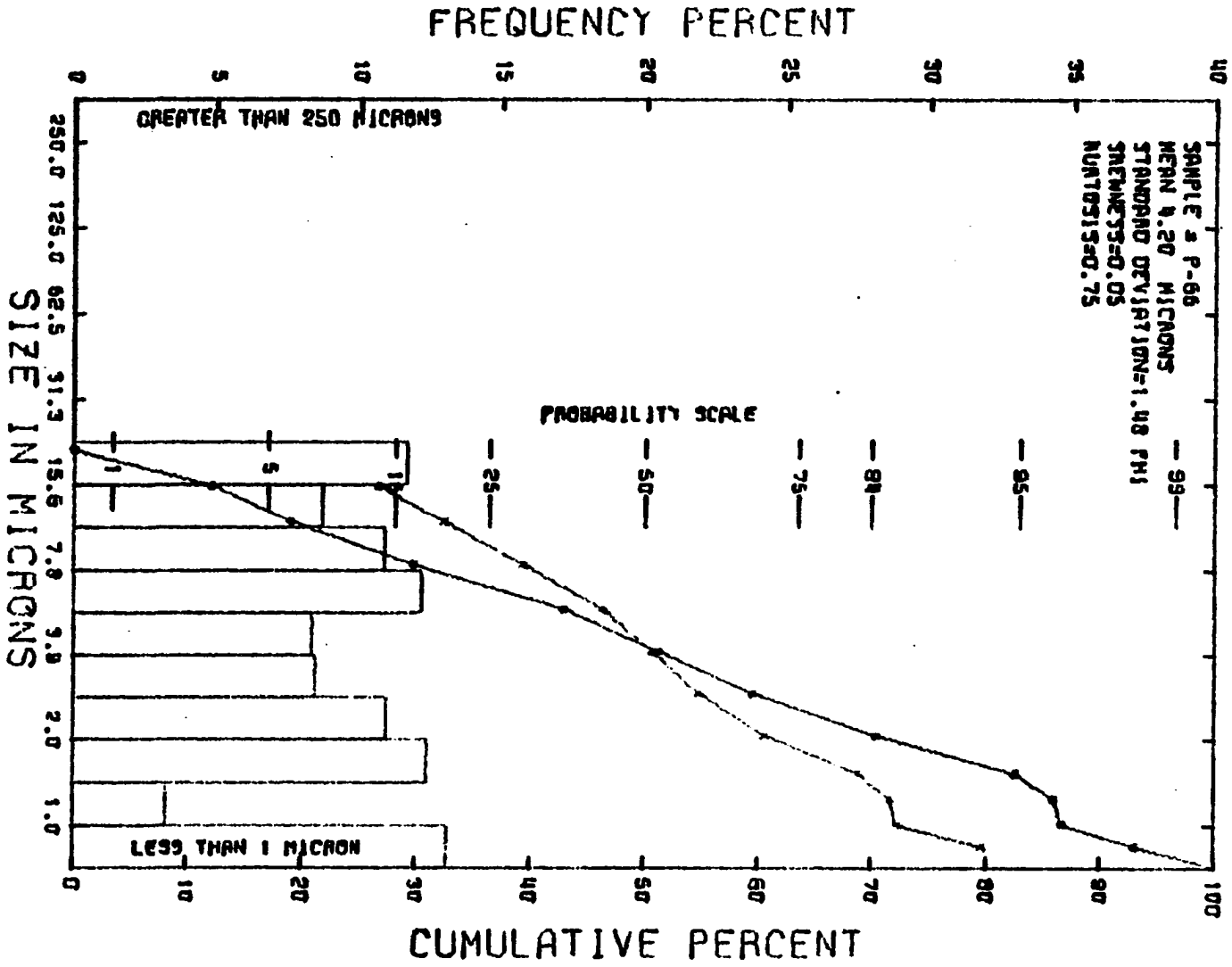
FREQUENCY PERCENT
SIZE IN MICRONS
CUMULATIVE PERCENT
GREATER THAN 250 MICRONS
LESS THAN 1 MICRON
PROBABILITY SCALE
SAMPLE # P-66
MEAN 4.20 MICRONS
STANDARD DEVIATION=1.48 PHI
SKEWNESS=0.05
KURTOSIS=0.75

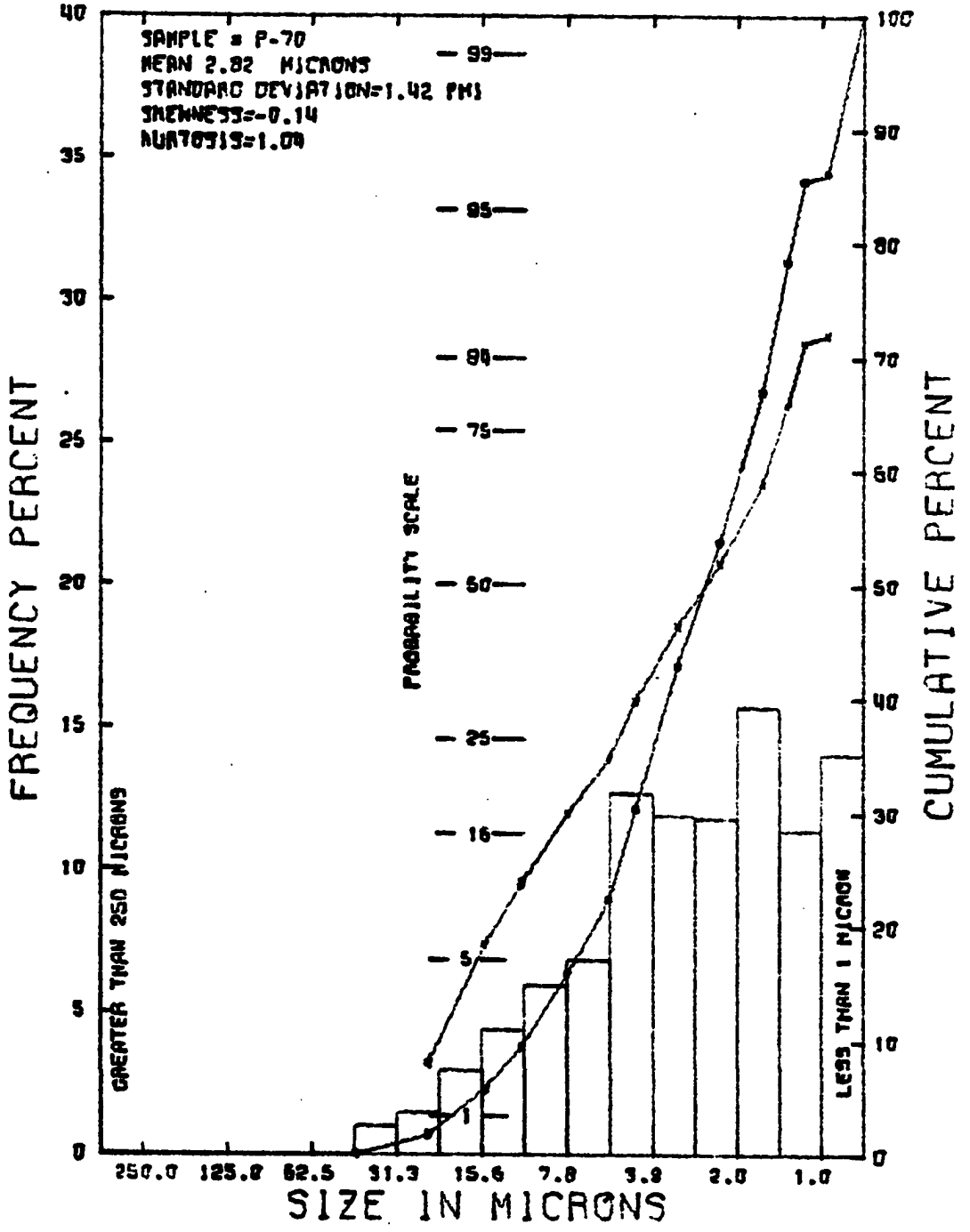
SAMPLE = P-70
MEAN 2.82 MICRONS
STANDARD DEVIATION=1.42 PHI
SKEWNESS=-0.14
KURTOSIS=1.09
FREQUENCY PERCENT
CUMULATIVE PERCENT
PROBABILITY SCALE
99
95
90
75
50
25
16
5
1
GREATER THAN 250 MICRONS
LESS THAN 1 MICRON
40
35
30
25
20
15
10
5
0
100
90
80
70
60
50
40
30
20
10
0
250.0
125.0
62.5
31.3
15.6
7.8
3.9
2.0
1.0
SIZE IN MICRONS

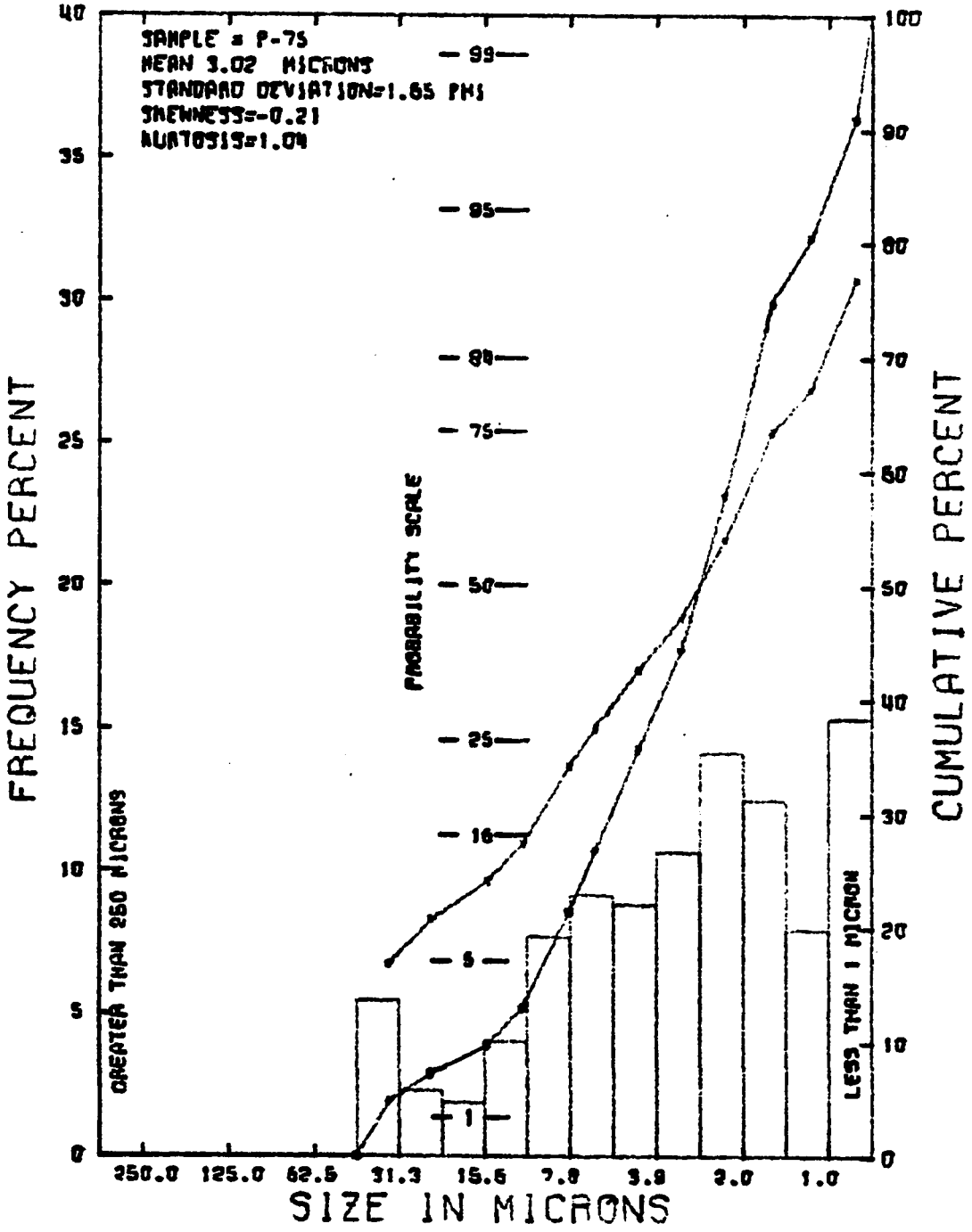
SAMPLE = P-75
MEAN 3.02 MICRONS
STANDARD DEVIATION=1.65 PHI
SKEWNESS=-0.21
KURTOSIS=1.04
PROBABILITY SCALE
99
95
90
75
50
25
16
5
1
GREATER THAN 250 MICRONS
LESS THAN 1 MICRON
FREQUENCY PERCENT
CUMULATIVE PERCENT
SIZE IN MICRONS
250.0
125.0
62.5
31.3
15.6
7.8
3.9
2.0
1.0
0
5
10
15
20
25
30
35
40
0
10
20
30
40
50
60
70
80
90
100

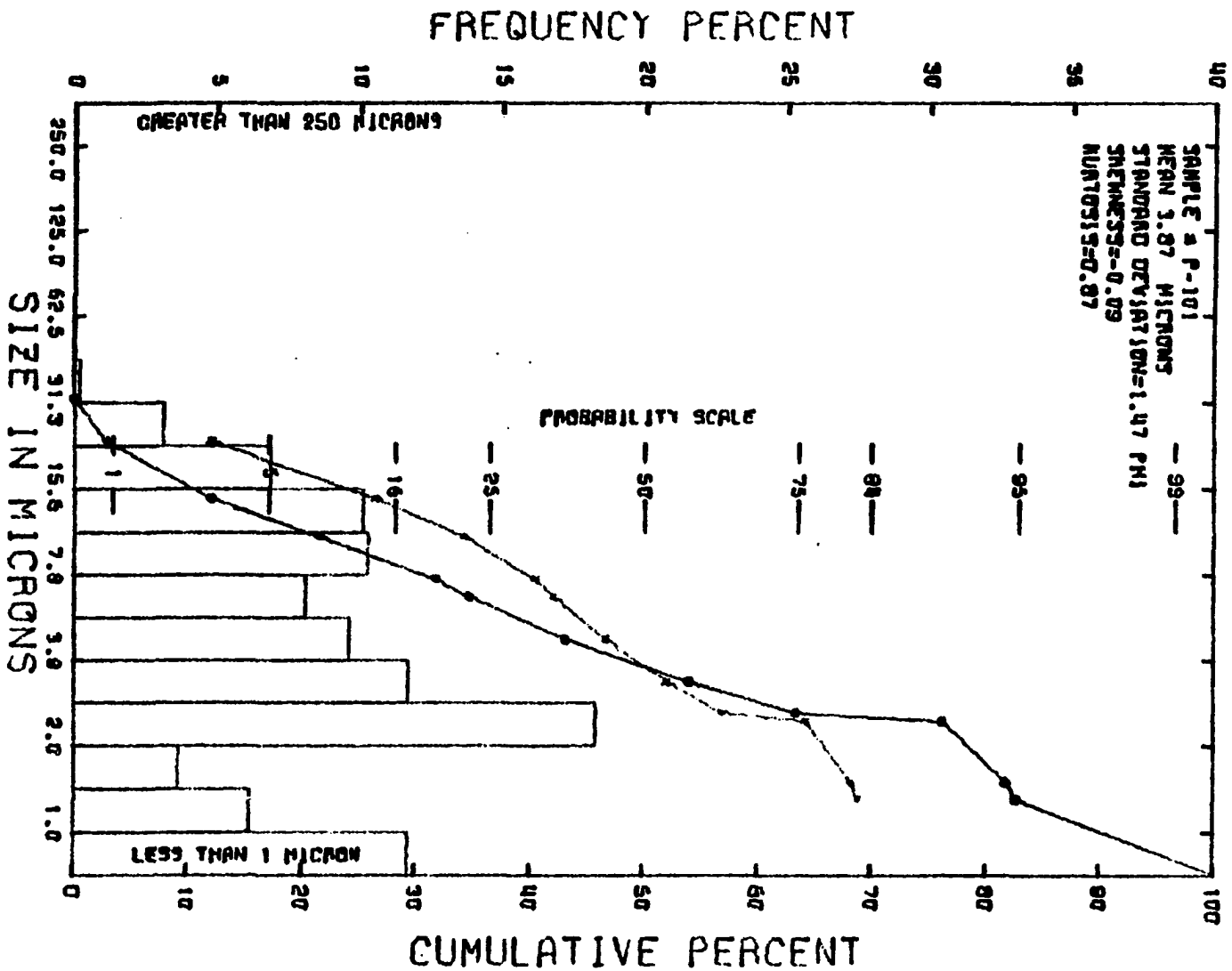
FREQUENCY PERCENT
0
5
10
15
20
25
30
35
40
GREATER THAN 250 MICRONS
SAMPLE = P-101
MEAN 3.87 MICRONS
STANDARD DEVIATION=1.47 PHI
SKEWNESS=-0.09
KURTOSIS=0.87
PROBABILITY SCALE
1
5
16
25
50
75
84
95
99
SIZE IN MICRONS
250.0
125.0
62.5
31.3
15.6
7.8
3.9
2.0
1.0
LESS THAN 1 MICRON
0
10
20
30
40
50
60
70
80
90
100
CUMULATIVE PERCENT

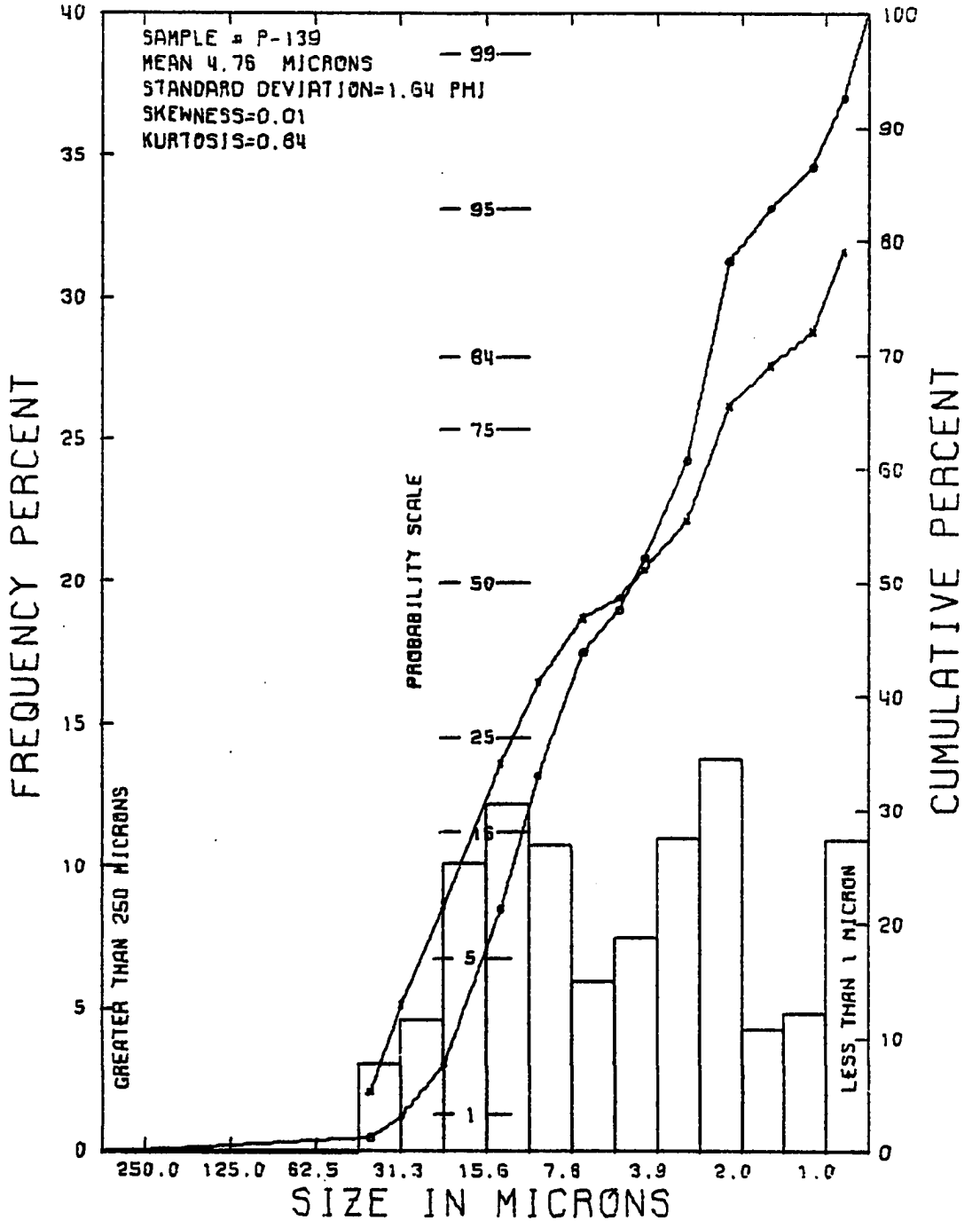
SAMPLE = P-139
MEAN 4.76 MICRONS
STANDARD DEVIATION=1.64 PHI
SKEWNESS=0.01
KURTOSIS=0.64
FREQUENCY PERCENT
CUMULATIVE PERCENT
PROBABILITY SCALE
99
95
84
75
50
25
16
5
1
GREATER THAN 250 MICRONS
LESS THAN 1 MICRON
250.0 125.0 62.5 31.3 15.6 7.8 3.9 2.0 1.0
SIZE IN MICRONS

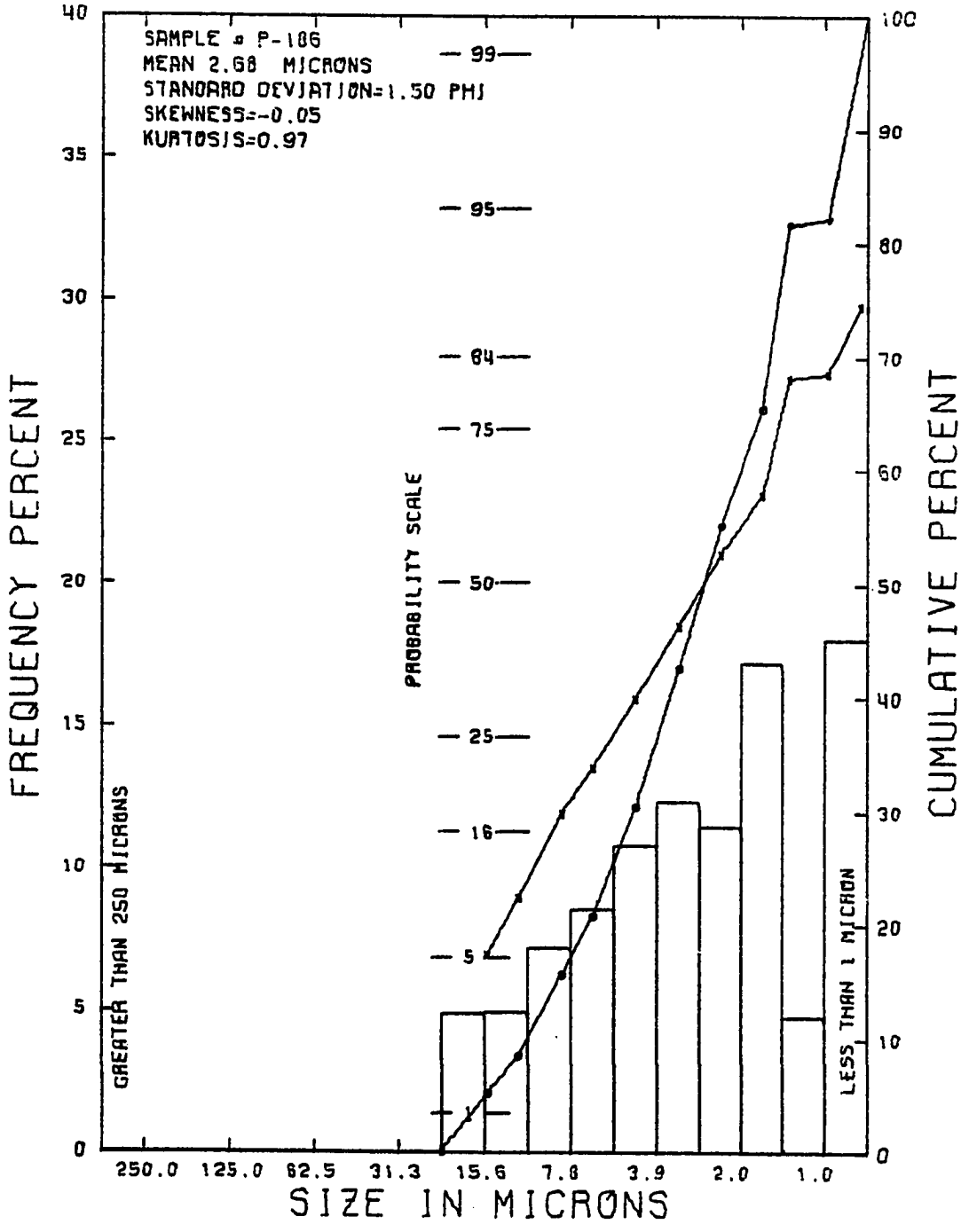
SAMPLE = P-186
MEAN 2.68 MICRONS
STANDARD DEVIATION=1.50 PHI
SKEWNESS=-0.05
KURTOSIS=0.97
FREQUENCY PERCENT
CUMULATIVE PERCENT
PROBABILITY SCALE
99
95
84
75
50
25
16
5
1
GREATER THAN 250 MICRONS
LESS THAN 1 MICRON
0
5
10
15
20
25
30
35
40
0
10
20
30
40
50
60
70
80
90
100
250.0
125.0
62.5
31.3
15.6
7.8
3.9
2.0
1.0
SIZE IN MICRONS

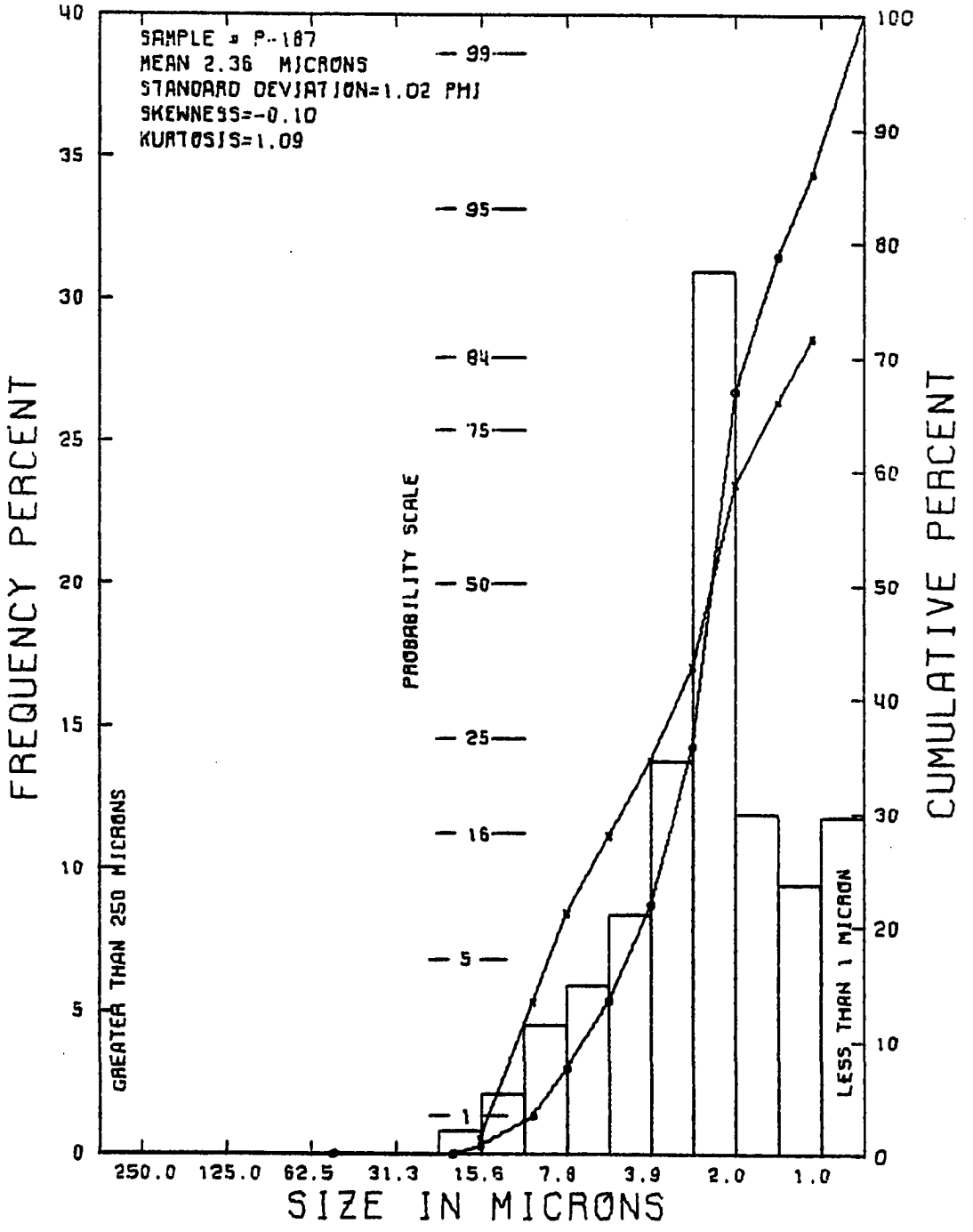
SAMPLE = P-187
MEAN 2.36 MICRONS
STANDARD DEVIATION=1.02 PHI
SKEWNESS=-0.10
KURTOSIS=1.09
FREQUENCY PERCENT
CUMULATIVE PERCENT
PROBABILITY SCALE
99
95
84
75
50
25
16
5
1
GREATER THAN 250 MICRONS
LESS THAN 1 MICRON
0
5
10
15
20
25
30
35
40
0
10
20
30
40
50
60
70
80
90
100
250.0
125.0
62.5
31.3
15.6
7.8
3.9
2.0
1.0
SIZE IN MICRONS

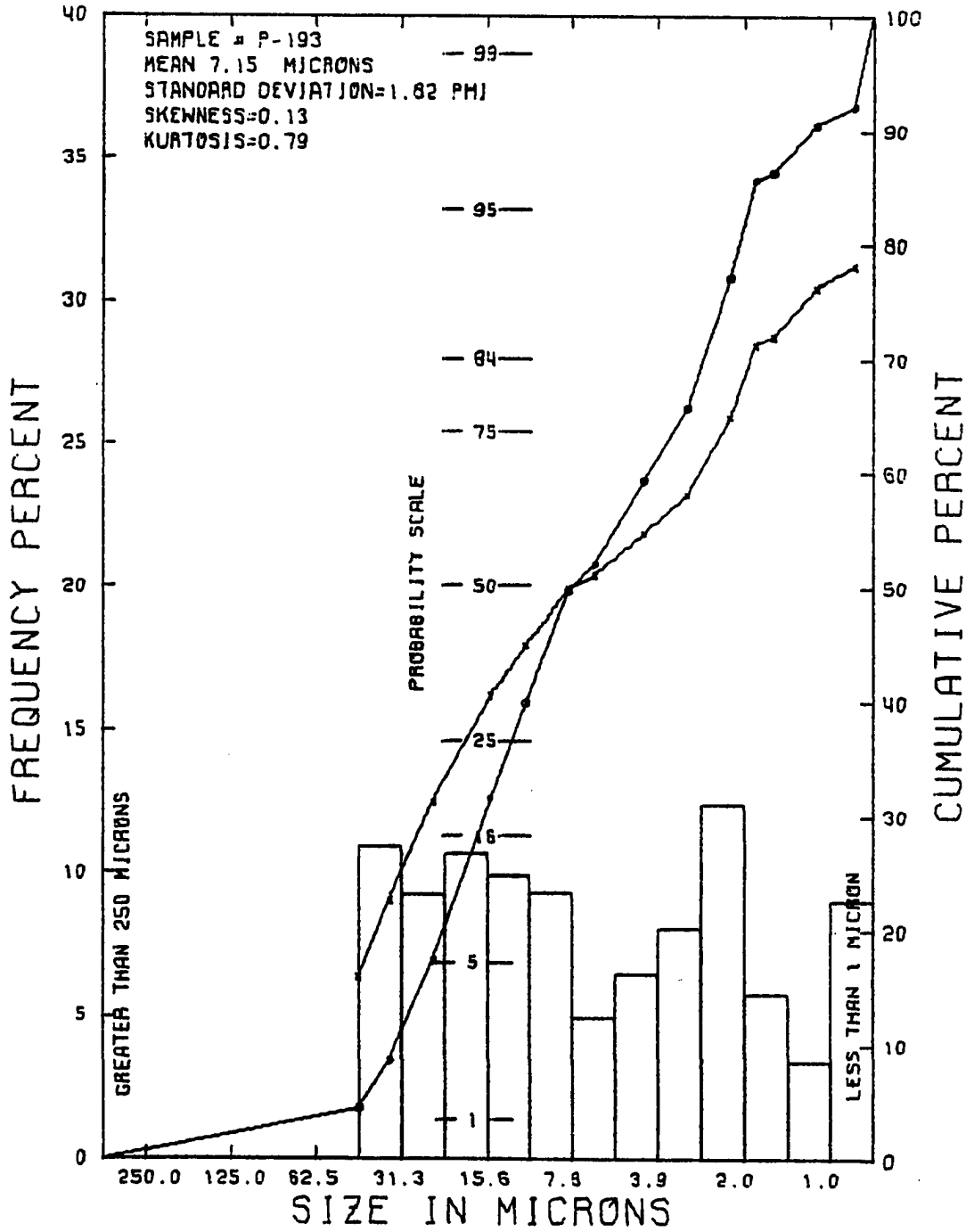
SAMPLE # P-193
MEAN 7.15 MICRONS
STANDARD DEVIATION=1.82 PHI
SKEWNESS=0.13
KURTOSIS=0.79
99
95
84
75
50
25
16
5
1
PROBABILITY SCALE
GREATER THAN 250 MICRONS
LESS THAN 1 MICRON
FREQUENCY PERCENT
CUMULATIVE PERCENT
40
35
30
25
20
15
10
5
0
100
90
80
70
60
50
40
30
20
10
0
250.0
125.0
62.5
31.3
15.6
7.8
3.9
2.0
1.0
SIZE IN MICRONS

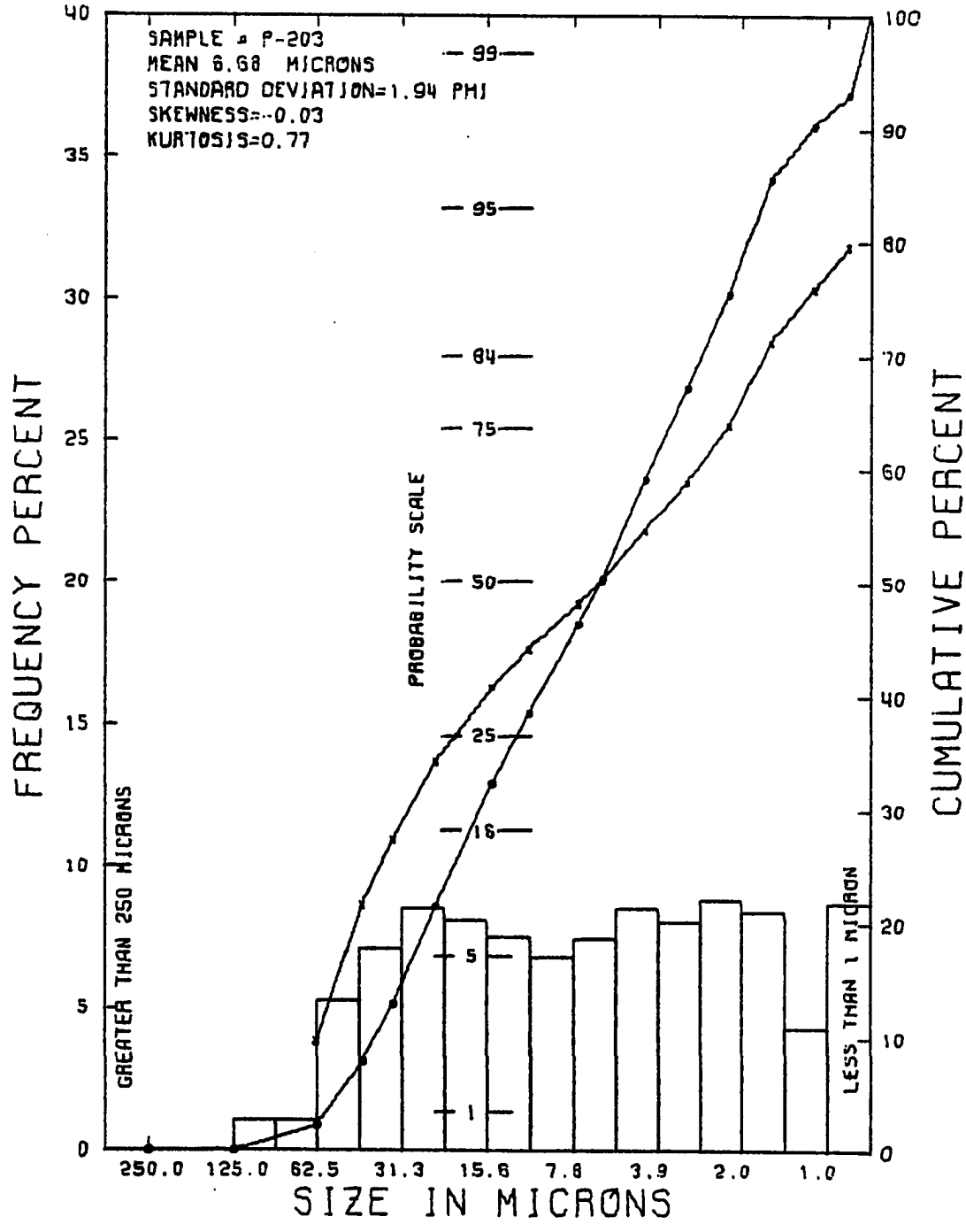
SAMPLE = P-203
MEAN 6.68 MICRONS
STANDARD DEVIATION=1.94 PHI
SKEWNESS=-0.03
KURTOSIS=0.77
99
95
84
75
50
25
16
5
1
PROBABILITY SCALE
FREQUENCY PERCENT
CUMULATIVE PERCENT
GREATER THAN 250 MICRONS
LESS THAN 1 MICRON
250.0 125.0 62.5 31.3 15.6 7.8 3.9 2.0 1.0
SIZE IN MICRONS

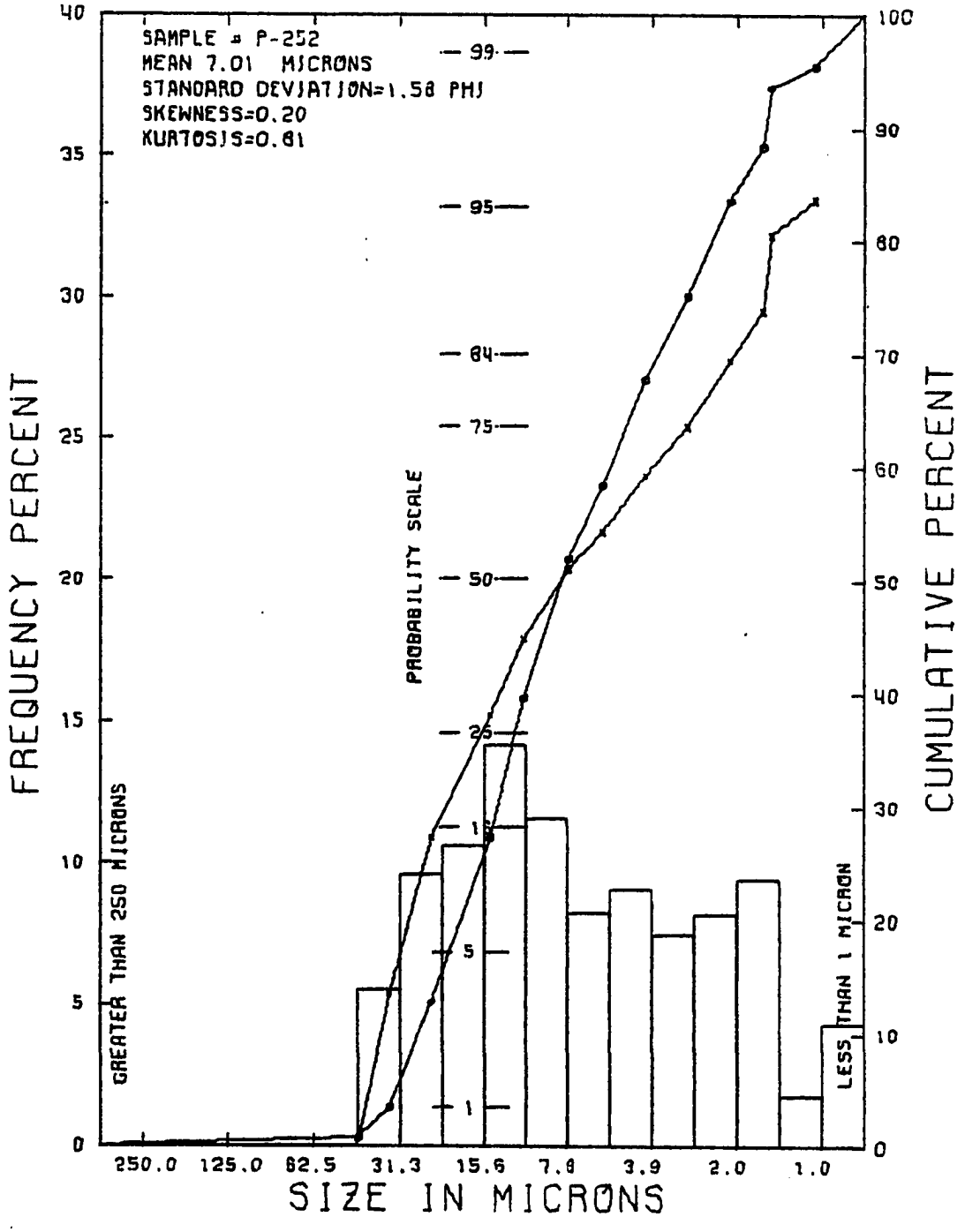
SAMPLE # P-252
MEAN 7.01 MICRONS
STANDARD DEVIATION=1.58 PHI
SKEWNESS=0.20
KURTOSIS=0.81
99
95
84
75
50
25
16
5
1
PROBABILITY SCALE
FREQUENCY PERCENT
CUMULATIVE PERCENT
GREATER THAN 250 MICRONS
LESS THAN 1 MICRON
250.0 125.0 62.5 31.3 15.6 7.8 3.9 2.0 1.0
SIZE IN MICRONS

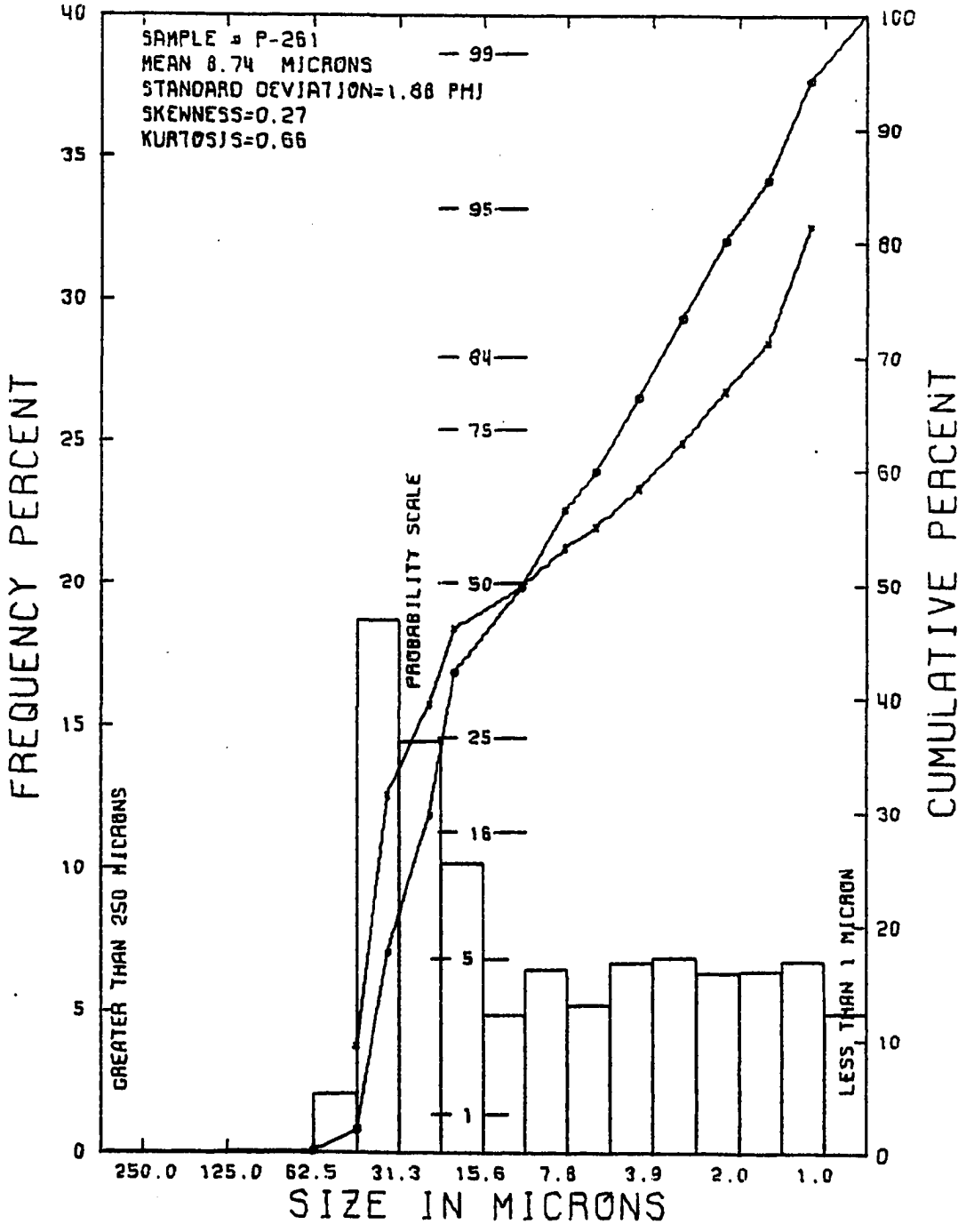
SAMPLE = P-261
MEAN 8.74 MICRONS
STANDARD DEVIATION=1.68 PHI
SKEWNESS=0.27
KURTOSIS=0.66
99
95
84
75
50
25
16
5
1
PROBABILITY SCALE
GREATER THAN 250 MICRONS
LESS THAN 1 MICRON
FREQUENCY PERCENT
CUMULATIVE PERCENT
0
5
10
15
20
25
30
35
40
0
10
20
30
40
50
60
70
80
90
100
250.0
125.0
62.5
31.3
15.6
7.8
3.9
2.0
1.0
SIZE IN MICRONS

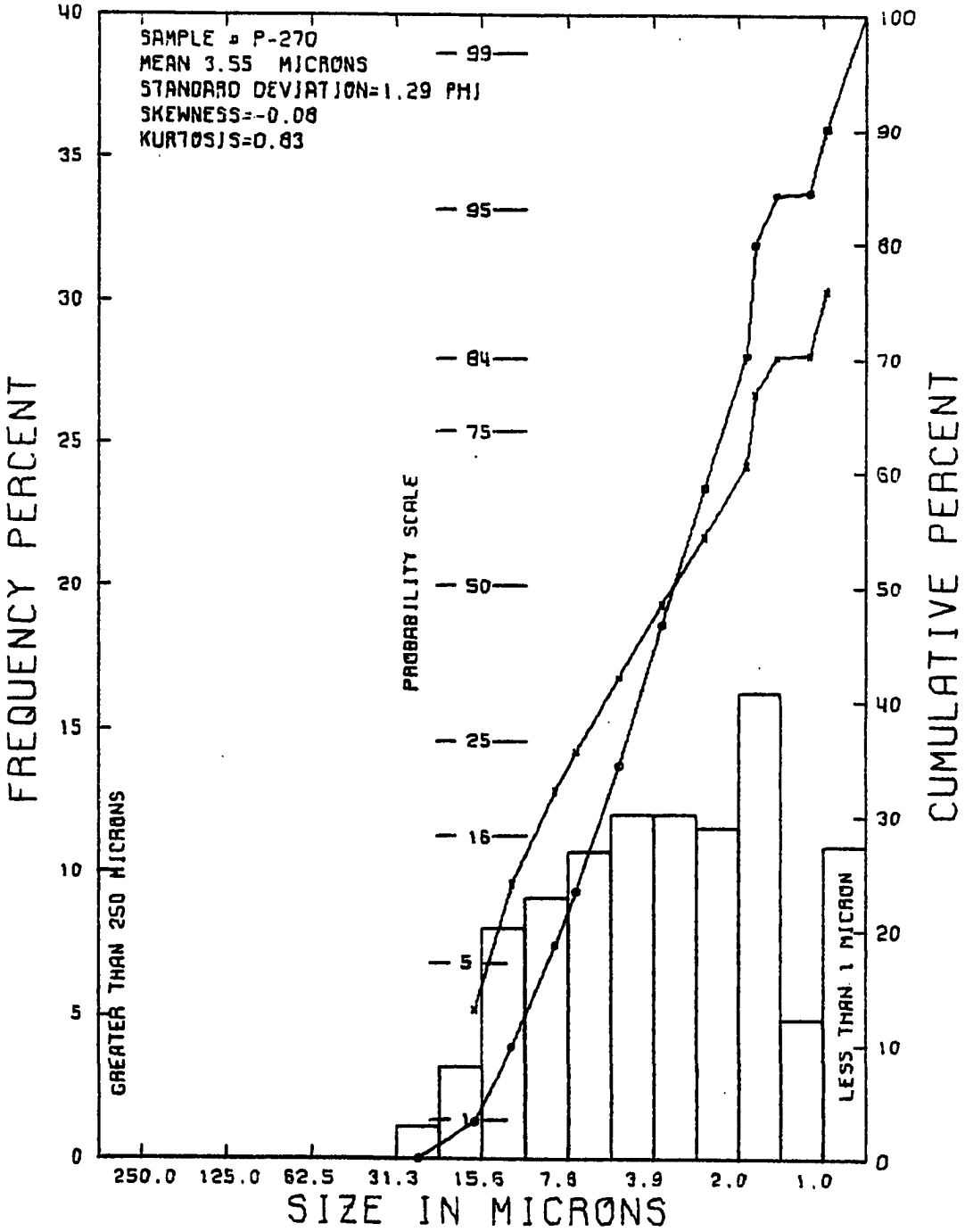
SAMPLE = P-270
MEAN 3.55 MICRONS
STANDARD DEVIATION=1.29 PHI
SKEWNESS=-0.08
KURTOSIS=0.83
FREQUENCY PERCENT
CUMULATIVE PERCENT
PROBABILITY SCALE
99
95
84
75
50
25
16
5
1
GREATER THAN 250 MICRONS
LESS THAN 1 MICRON
0
5
10
15
20
25
30
35
40
0
10
20
30
40
50
60
70
80
90
100
250.0
125.0
62.5
31.3
15.6
7.8
3.9
2.0
1.0
SIZE IN MICRONS

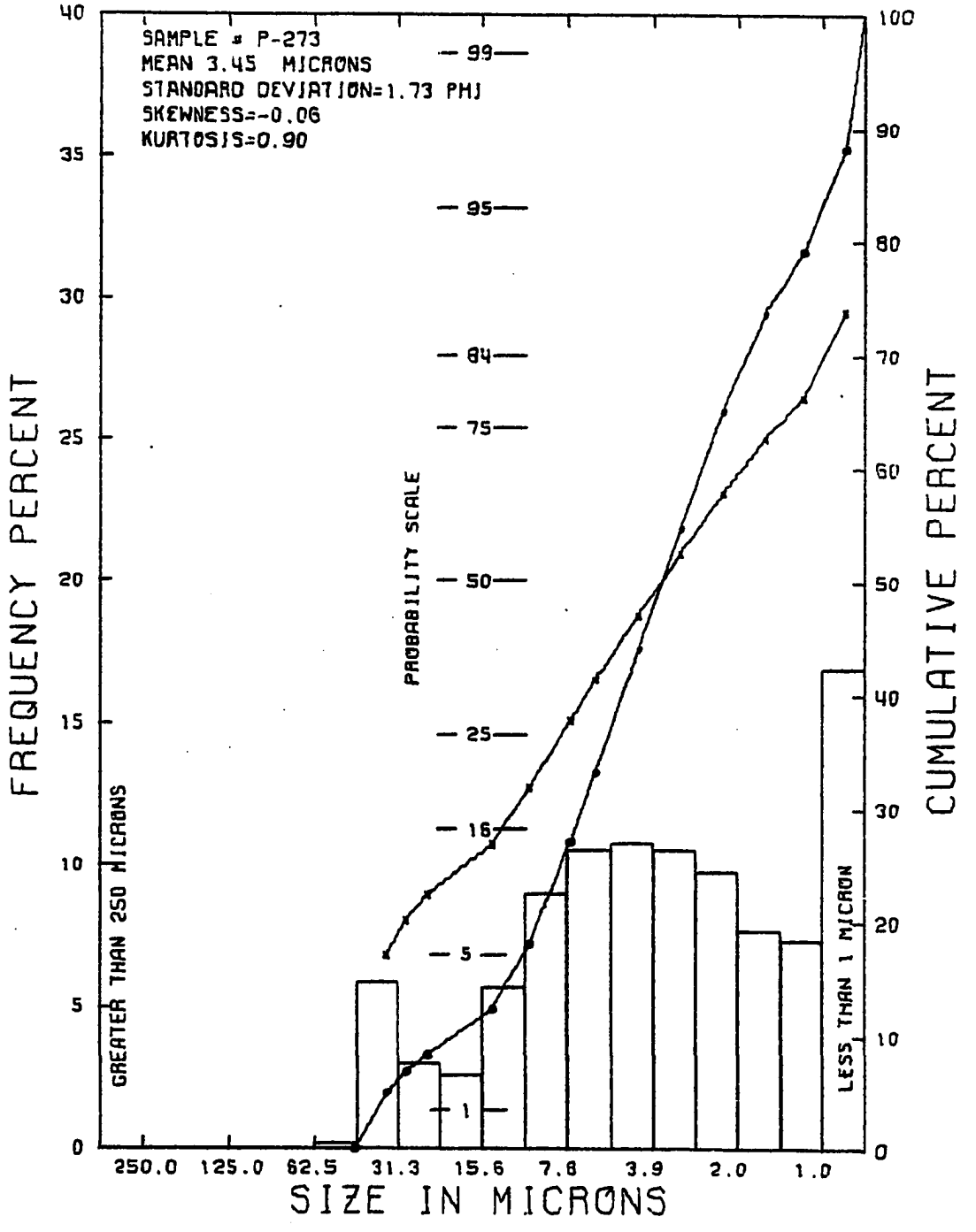
SAMPLE # P-273
MEAN 3.45 MICRONS
STANDARD DEVIATION=1.73 PHI
SKEWNESS=-0.06
KURTOSIS=0.90
99
95
84
75
50
25
16
5
1
PROBABILITY SCALE
FREQUENCY PERCENT
CUMULATIVE PERCENT
GREATER THAN 250 MICRONS
LESS THAN 1 MICRON
250.0 125.0 62.5 31.3 15.6 7.8 3.9 2.0 1.0
SIZE IN MICRONS

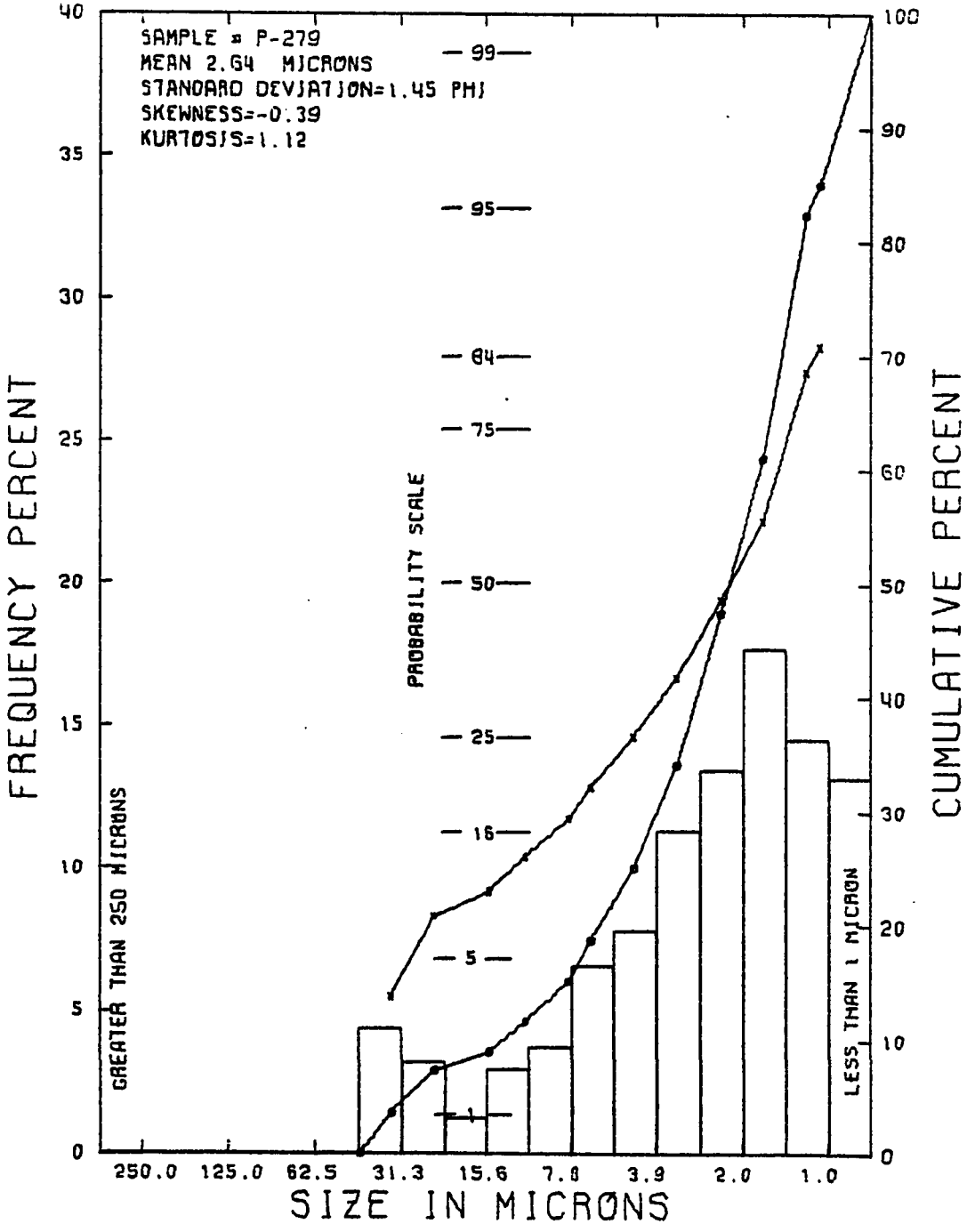
SAMPLE = P-279
MEAN 2.64 MICRONS
STANDARD DEVIATION=1.45 PHI
SKEWNESS=-0.39
KURTOSIS=1.12
FREQUENCY PERCENT
CUMULATIVE PERCENT
PROBABILITY SCALE
99
95
84
75
50
25
16
5
1
GREATER THAN 250 MICRONS
LESS THAN 1 MICRON
250.0 125.0 62.5 31.3 15.6 7.8 3.9 2.0 1.0
SIZE IN MICRONS

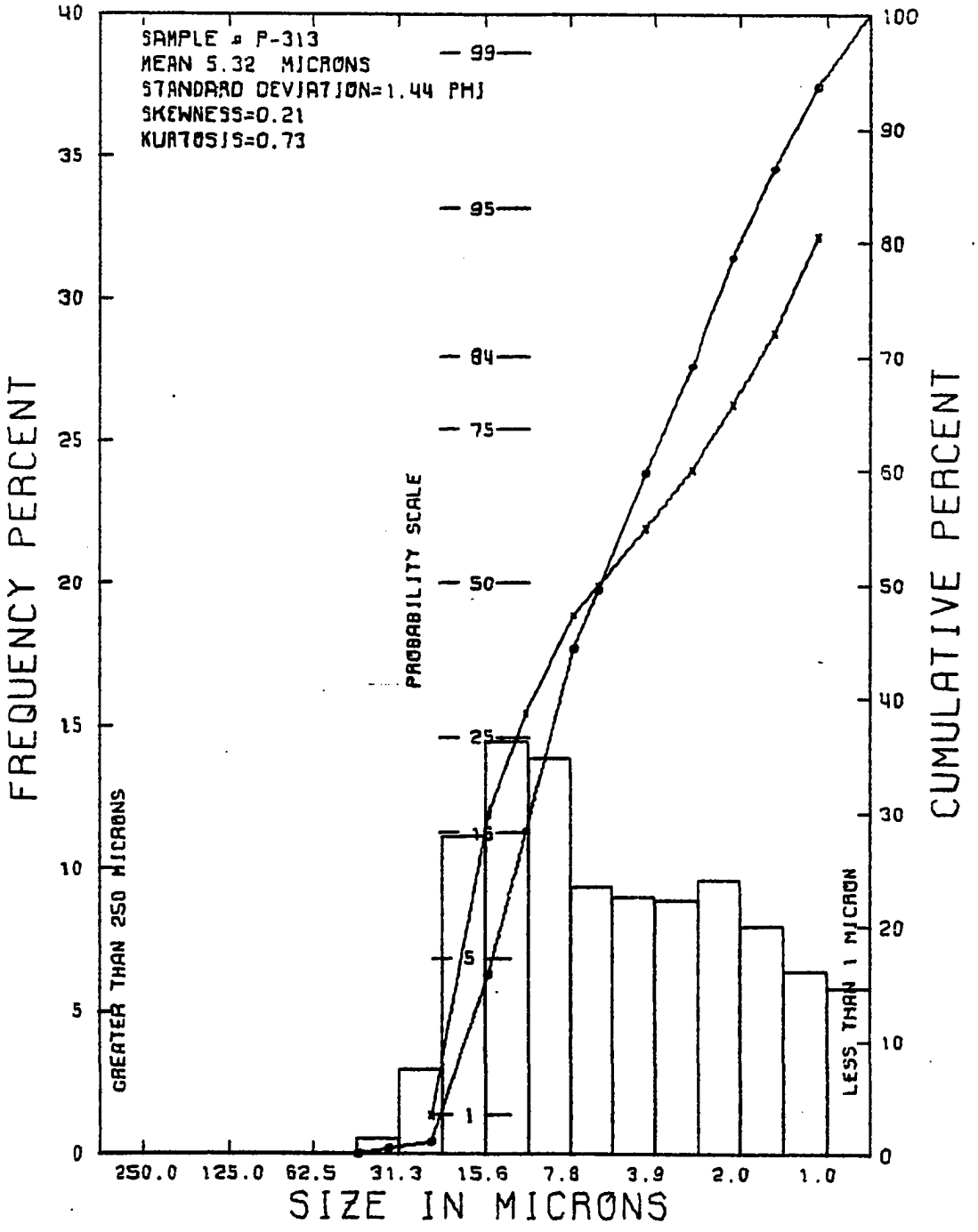
SAMPLE # P-313
MEAN 5.32 MICRONS
STANDARD DEVIATION=1.44 PHI
SKEWNESS=0.21
KURTOSIS=0.73
FREQUENCY PERCENT
CUMULATIVE PERCENT
PROBABILITY SCALE
99
95
84
75
50
25
16
5
1
GREATER THAN 250 MICRONS
LESS THAN 1 MICRON
250.0 125.0 62.5 31.3 15.6 7.8 3.9 2.0 1.0
SIZE IN MICRONS

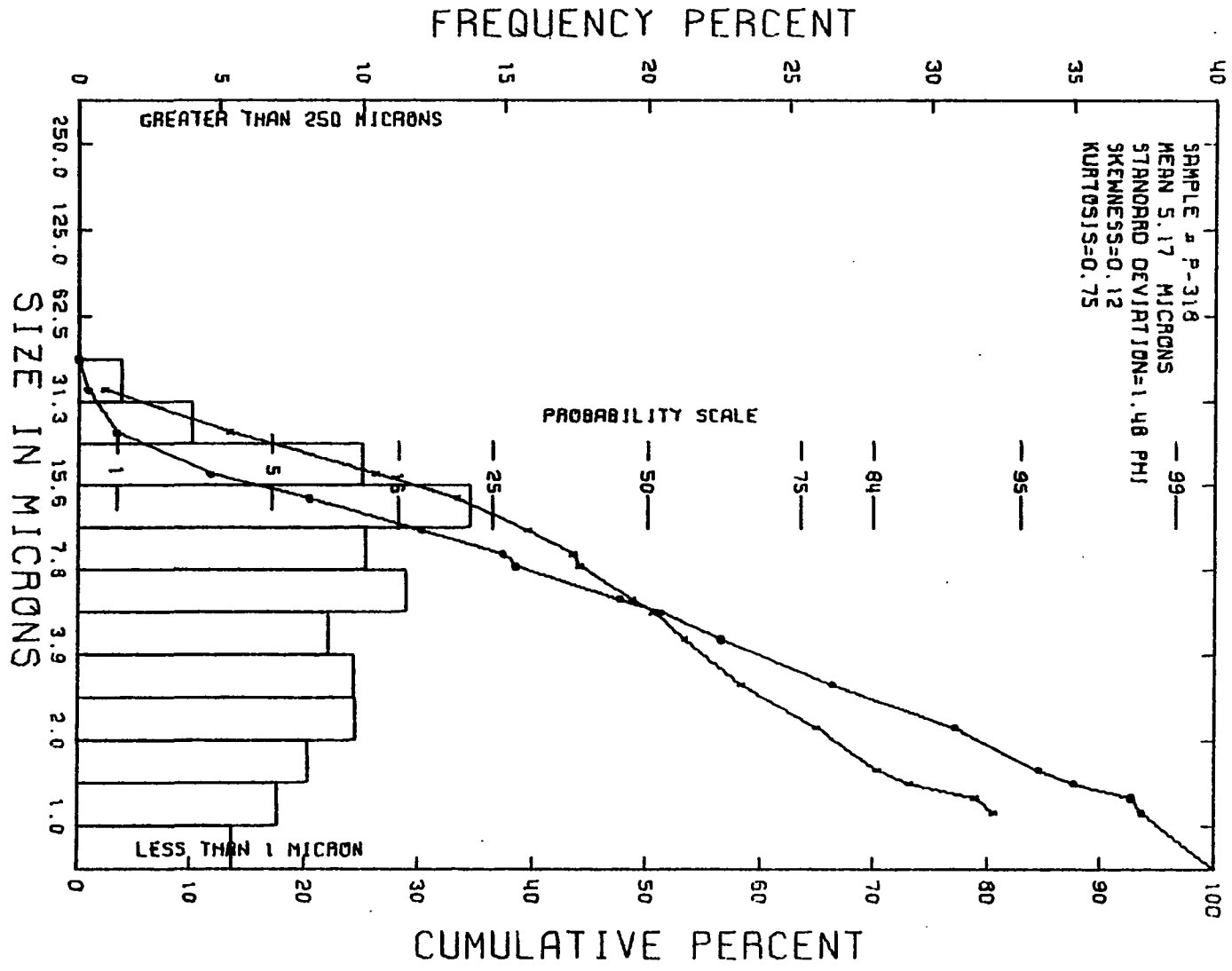
FREQUENCY PERCENT
0
5
10
15
20
25
30
35
40
GREATER THAN 250 MICRONS
SAMPLE = P-318
MEAN 5.17 MICRONS
STANDARD DEVIATION=1.48 PHI
SKEWNESS=0.12
KURTOSIS=0.75
99
95
84
75
50
25
16
5
1
PROBABILITY SCALE
SIZE IN MICRONS
250.0
125.0
62.5
31.3
15.6
7.8
3.9
2.0
1.0
LESS THAN 1 MICRON
0
10
20
30
40
50
60
70
80
90
100
CUMULATIVE PERCENT

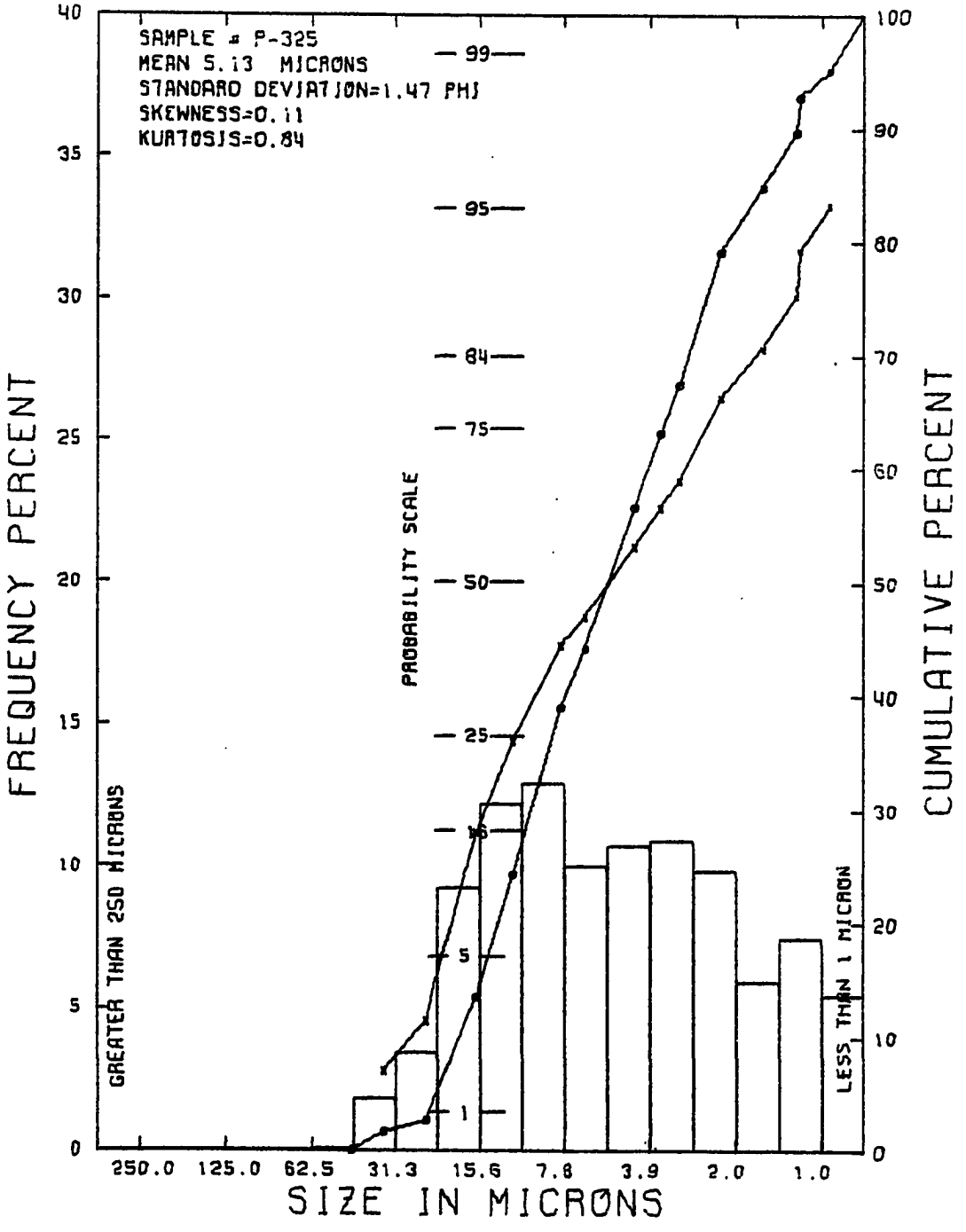
SAMPLE # P-325
MEAN 5.13 MICRONS
STANDARD DEVIATION=1.47 PHI
SKEWNESS=0.11
KURTOSIS=0.84
FREQUENCY PERCENT
CUMULATIVE PERCENT
PROBABILITY SCALE
99
95
84
75
50
25
16
5
1
GREATER THAN 250 MICRONS
LESS THAN 1 MICRON
250.0 125.0 62.5 31.3 15.6 7.8 3.9 2.0 1.0
SIZE IN MICRONS

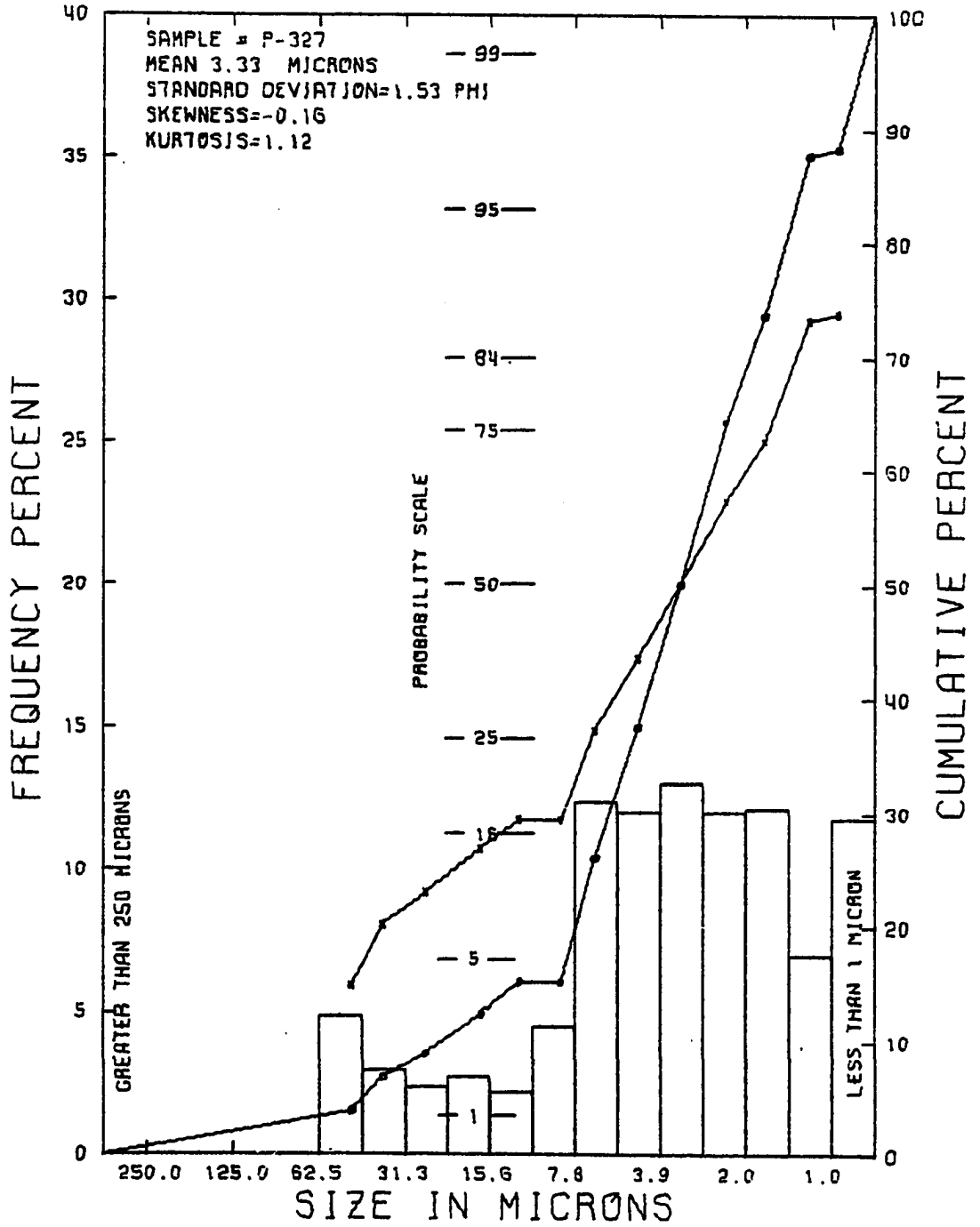
SAMPLE = P-327
MEAN 3.33 MICRONS
STANDARD DEVIATION=1.53 PHI
SKEWNESS=-0.16
KURTOSIS=1.12
99
95
84
75
50
25
16
5
1
PROBABILITY SCALE
GREATER THAN 250 MICRONS
LESS THAN 1 MICRON
FREQUENCY PERCENT
CUMULATIVE PERCENT
0
5
10
15
20
25
30
35
40
0
10
20
30
40
50
60
70
80
90
100
250.0
125.0
62.5
31.3
15.6
7.8
3.9
2.0
1.0
SIZE IN MICRONS

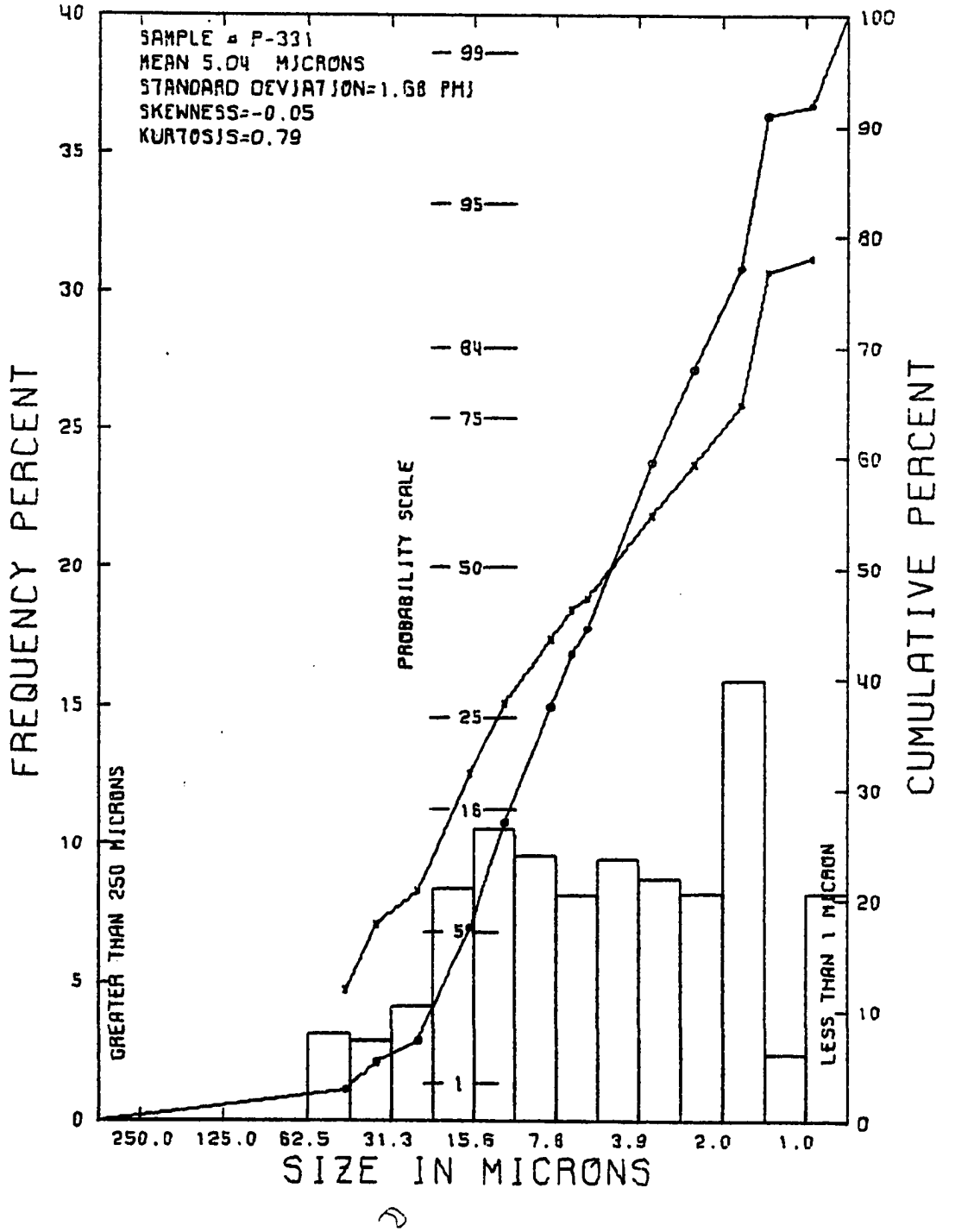
SAMPLE = P-331
MEAN 5.04 MICRONS
STANDARD DEVIATION=1.68 PHI
SKEWNESS=-0.05
KURTOSIS=0.79
FREQUENCY PERCENT
CUMULATIVE PERCENT
PROBABILITY SCALE
99
95
84
75
50
25
16
5
1
GREATER THAN 250 MICRONS
LESS THAN 1 MICRON
250.0 125.0 62.5 31.3 15.6 7.8 3.9 2.0 1.0
SIZE IN MICRONS

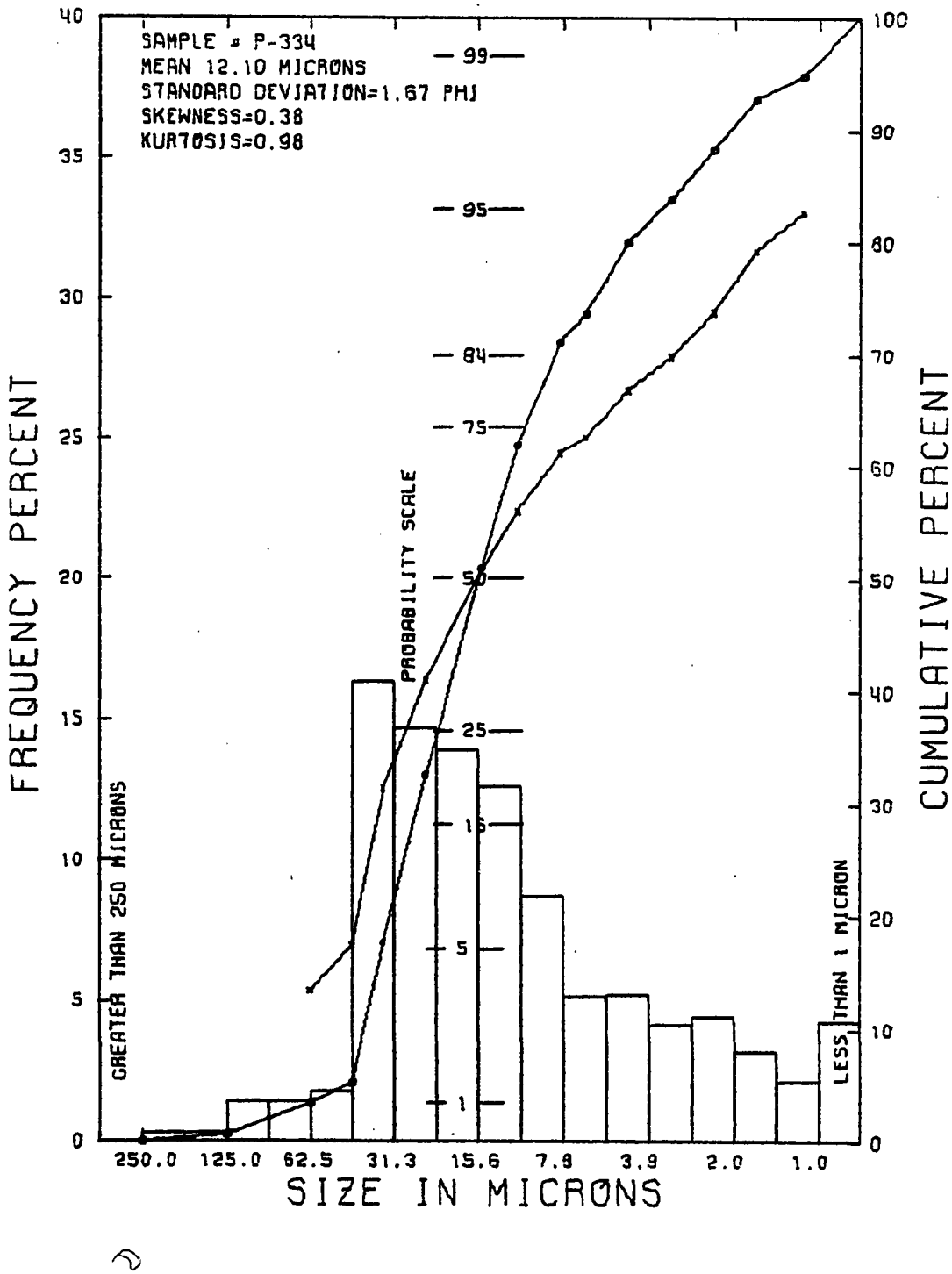
SAMPLE # P-334
MEAN 12.10 MICRONS
STANDARD DEVIATION=1.67 PHI
SKEWNESS=0.38
KURTOSIS=0.98
FREQUENCY PERCENT
CUMULATIVE PERCENT
PROBABILITY SCALE
99
95
84
75
50
25
16
5
1
GREATER THAN 250 MICRONS
LESS THAN 1 MICRON
250.0 125.0 62.5 31.3 15.6 7.8 3.9 2.0 1.0
SIZE IN MICRONS

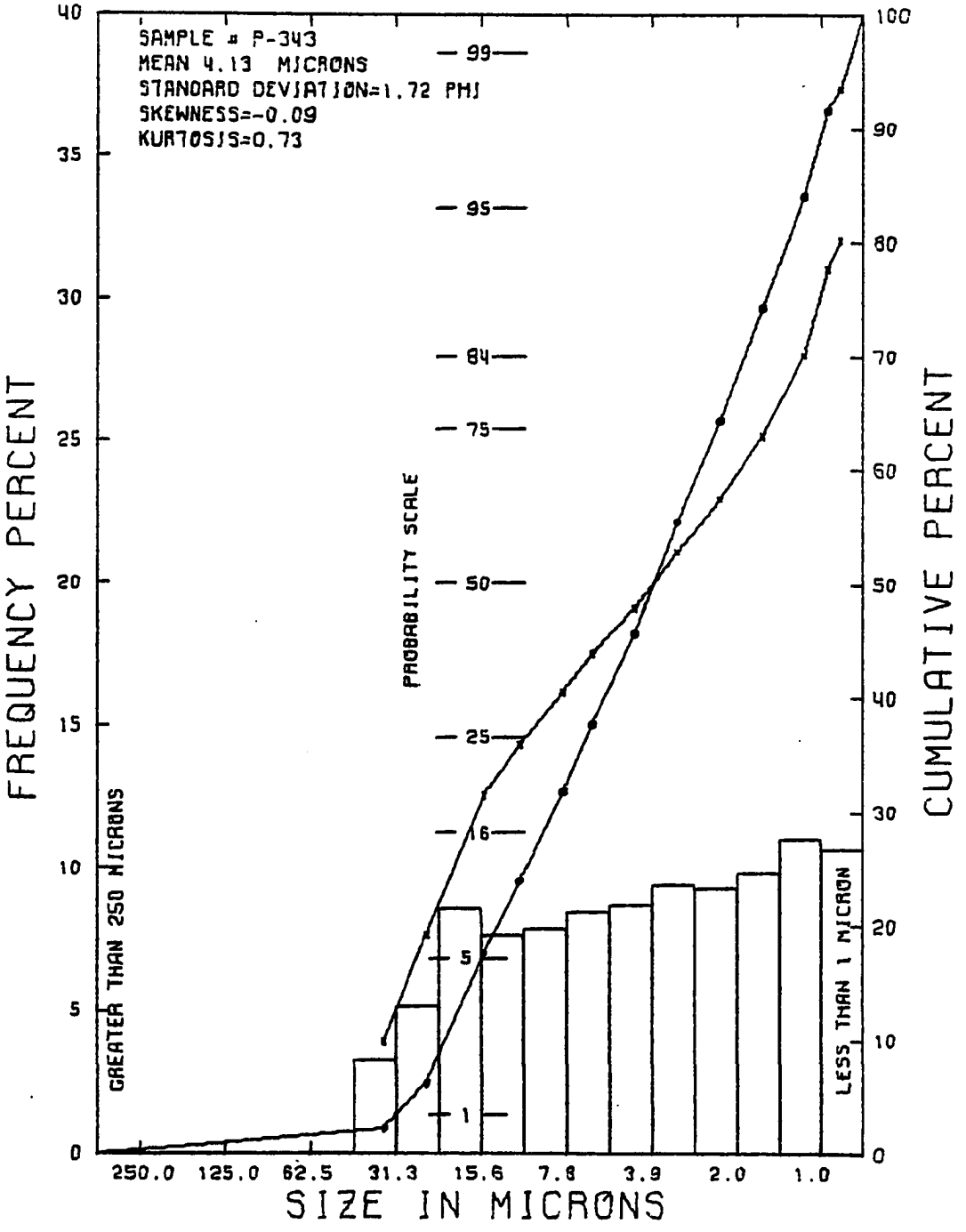
SAMPLE # P-343
MEAN 4.13 MICRONS
STANDARD DEVIATION=1.72 PHI
SKEWNESS=-0.09
KURTOSIS=0.73
99
95
84
75
50
25
16
5
1
PROBABILITY SCALE
FREQUENCY PERCENT
CUMULATIVE PERCENT
GREATER THAN 250 MICRONS
LESS THAN 1 MICRON
250.0 125.0 62.5 31.3 15.6 7.8 3.9 2.0 1.0
SIZE IN MICRONS

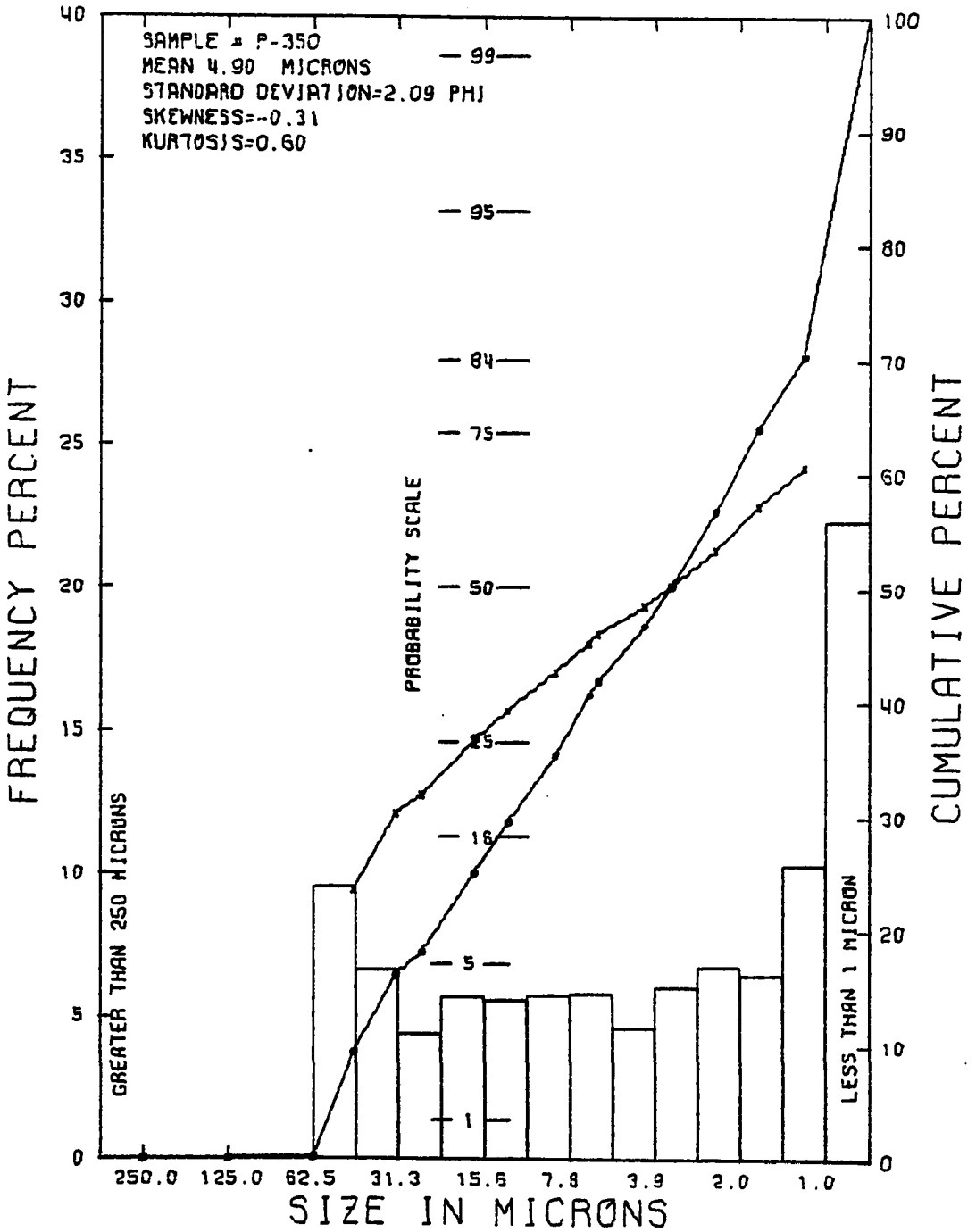
SAMPLE = P-350
MEAN 4.90 MICRONS
STANDARD DEVIATION=2.09 PHI
SKEWNESS=-0.31
KURTOSIS=0.60
FREQUENCY PERCENT
CUMULATIVE PERCENT
PROBABILITY SCALE
99
95
84
75
50
25
16
5
1
GREATER THAN 250 MICRONS
LESS THAN 1 MICRON
0
5
10
15
20
25
30
35
40
0
10
20
30
40
50
60
70
80
90
100
250.0
125.0
62.5
31.3
15.6
7.8
3.9
2.0
1.0
SIZE IN MICRONS

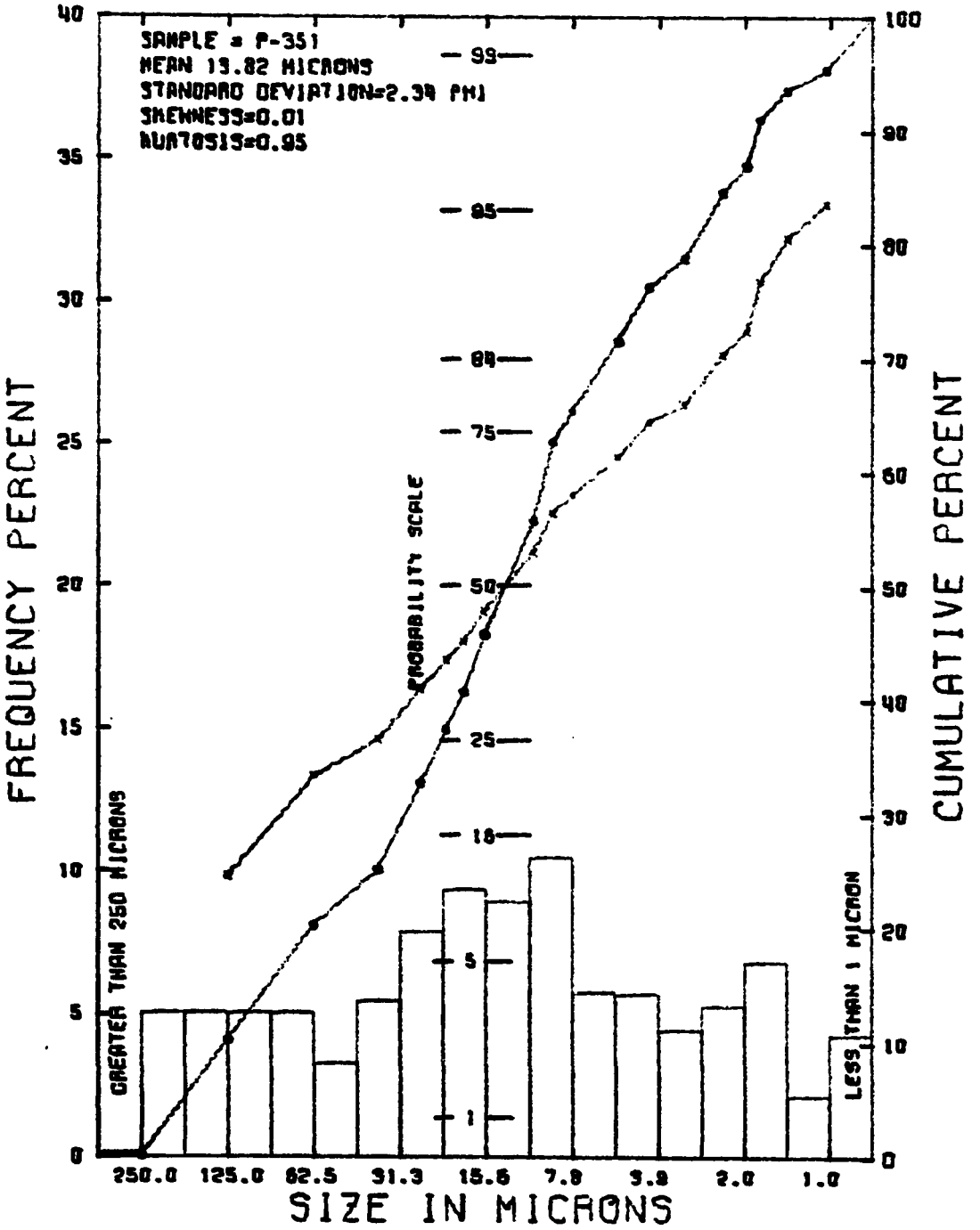
SAMPLE = P-351
MEAN 13.82 MICRONS
STANDARD DEVIATION=2.38 PHI
SKEWNESS=0.01
KURTOSIS=0.95
FREQUENCY PERCENT
CUMULATIVE PERCENT
PROBABILITY SCALE
99
95
90
75
50
25
10
5
1
GREATER THAN 250 MICRONS
LESS THAN 1 MICRON
250.0
125.0
62.5
31.3
15.6
7.8
3.9
2.0
1.0
SIZE IN MICRONS

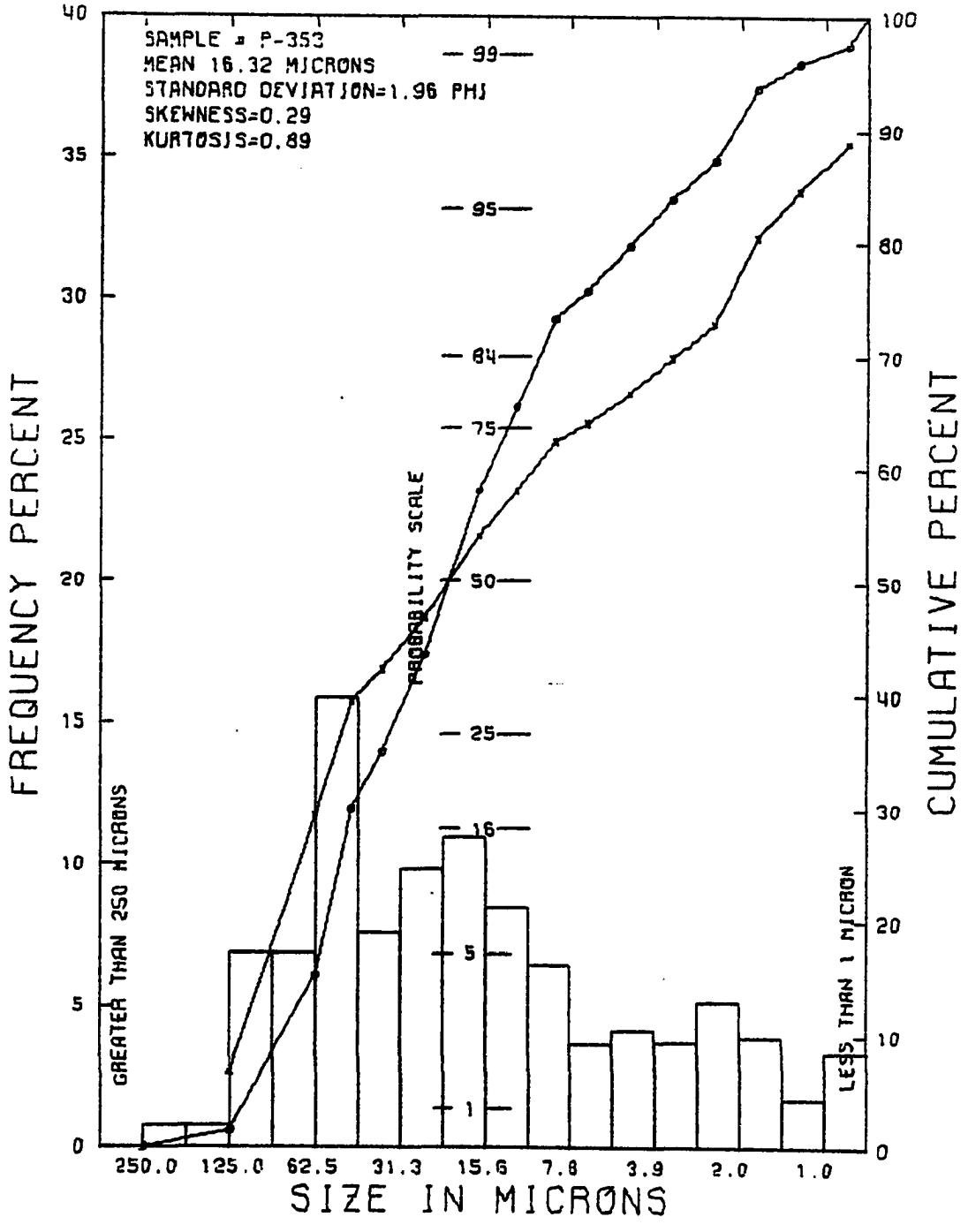
SAMPLE = P-353
MEAN 16.32 MICRONS
STANDARD DEVIATION=1.96 PHI
SKEWNESS=0.29
KURTOSIS=0.89
FREQUENCY PERCENT
CUMULATIVE PERCENT
PROBABILITY SCALE
99
95
84
75
50
25
16
5
1
GREATER THAN 250 MICRONS
LESS THAN 1 MICRON
250.0
125.0
62.5
31.3
15.6
7.8
3.9
2.0
1.0
SIZE IN MICRONS

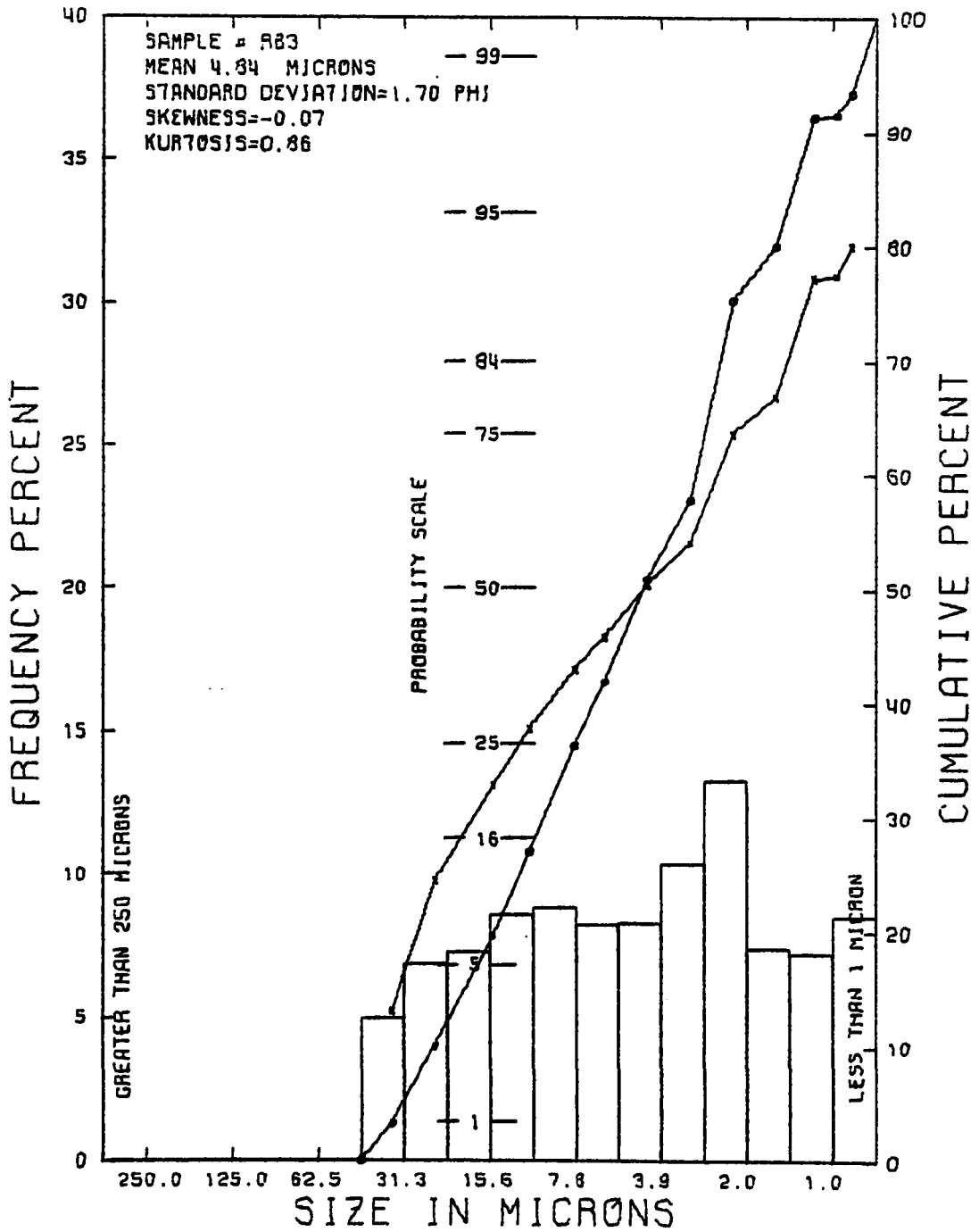
SAMPLE = A83
MEAN 4.84 MICRONS
STANDARD DEVIATION=1.70 PHI
SKEWNESS=-0.07
KURTOSIS=0.86
FREQUENCY PERCENT
CUMULATIVE PERCENT
PROBABILITY SCALE
99
95
84
75
50
25
16
5
1
GREATER THAN 250 MICRONS
LESS THAN 1 MICRON
250.0 125.0 62.5 31.3 15.6 7.8 3.9 2.0 1.0
SIZE IN MICRONS

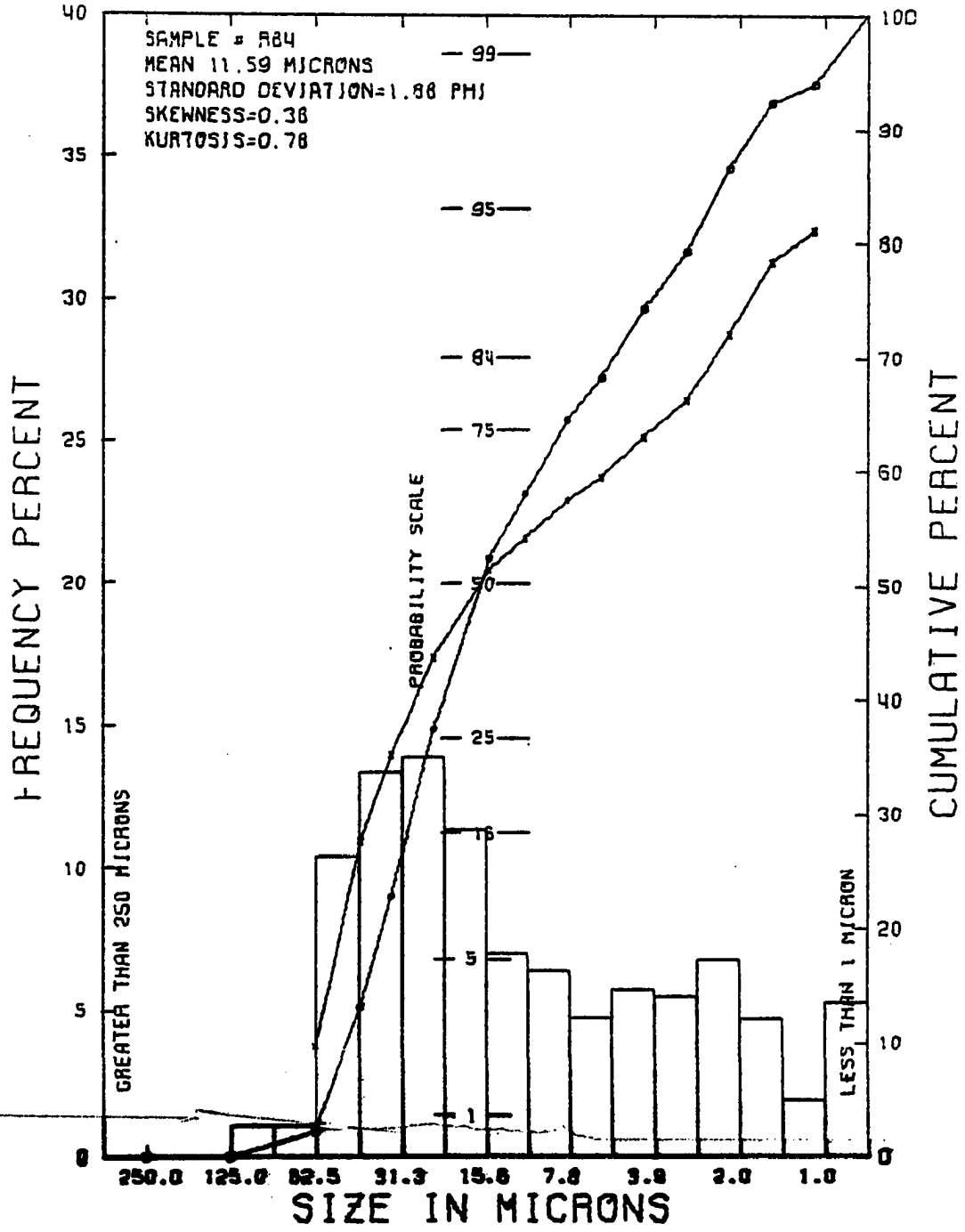
SAMPLE # R84
MEAN 11.59 MICRONS
STANDARD DEVIATION=1.86 PHI
SKEWNESS=0.36
KURTOSIS=0.78
FREQUENCY PERCENT
CUMULATIVE PERCENT
PROBABILITY SCALE
99
95
84
75
50
25
16
5
1
GREATER THAN 250 MICRONS
LESS THAN 1 MICRON
250.0 125.0 62.5 31.3 15.6 7.8 3.9 2.0 1.0
SIZE IN MICRONS

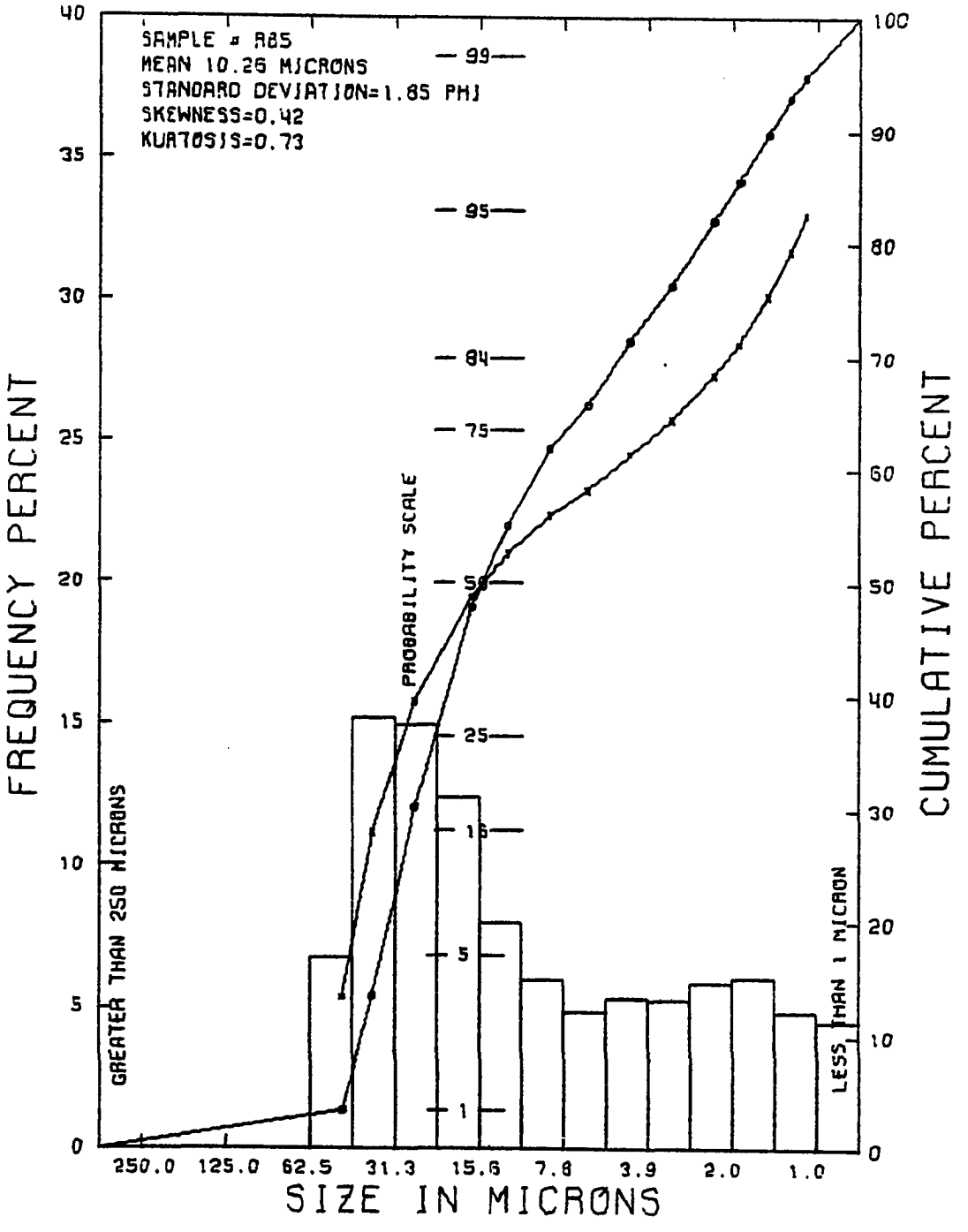
SAMPLE # R85
MEAN 10.26 MICRONS
STANDARD DEVIATION=1.85 PHI
SKEWNESS=0.42
KURTOSIS=0.73
FREQUENCY PERCENT
CUMULATIVE PERCENT
PROBABILITY SCALE
99
95
84
75
50
25
16
5
1
GREATER THAN 250 MICRONS
LESS THAN 1 MICRON
250.0 125.0 62.5 31.3 15.6 7.8 3.9 2.0 1.0
SIZE IN MICRONS

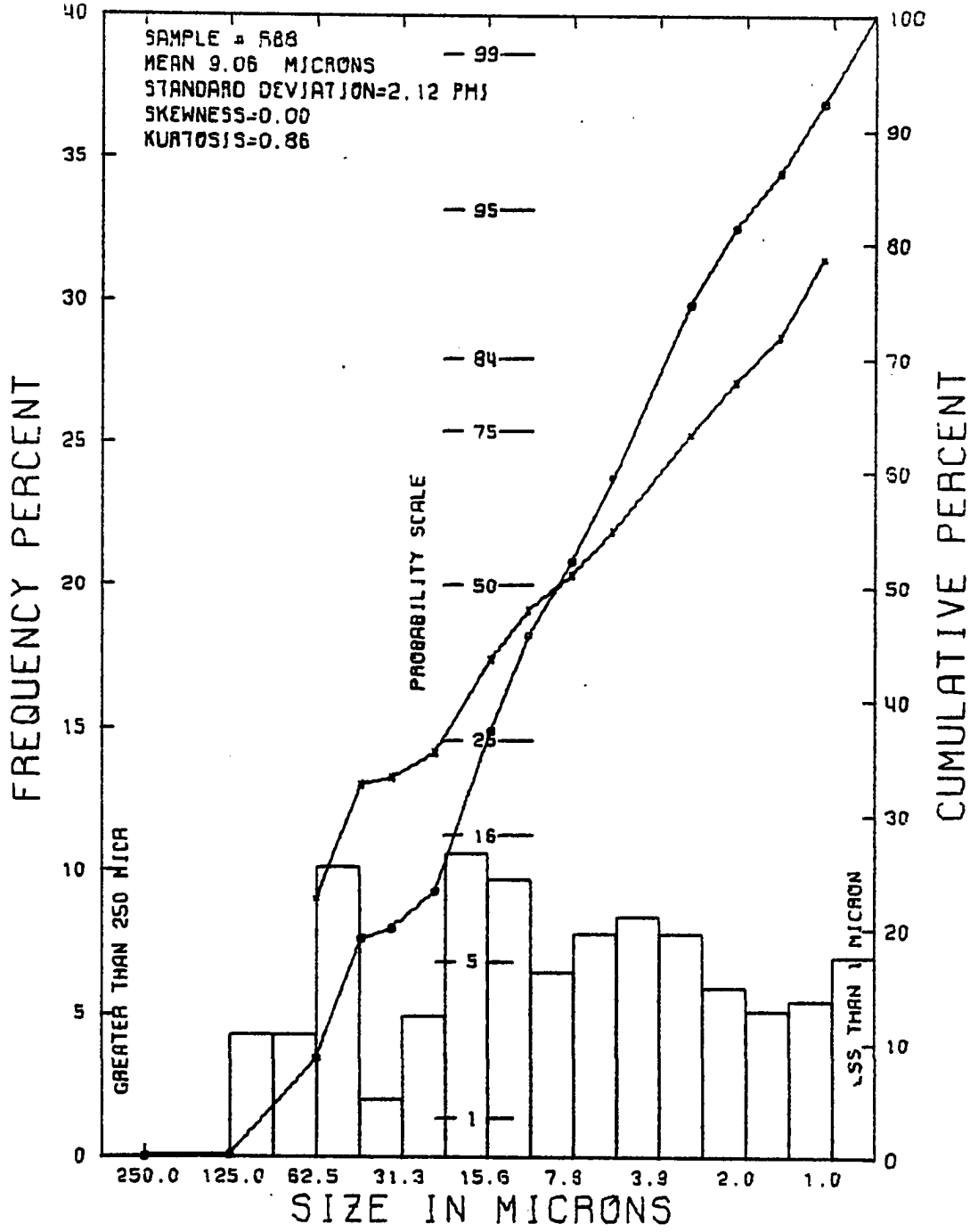
SAMPLE = 588
MEAN 9.06 MICRONS
STANDARD DEVIATION=2.12 PHI
SKEWNESS=0.00
KURTOSIS=0.86
99
95
84
75
50
25
16
5
1
PROBABILITY SCALE
FREQUENCY PERCENT
CUMULATIVE PERCENT
GREATER THAN 250 MICRON
LESS THAN 1 MICRON
250.0 125.0 62.5 31.3 15.6 7.8 3.9 2.0 1.0
SIZE IN MICRONS

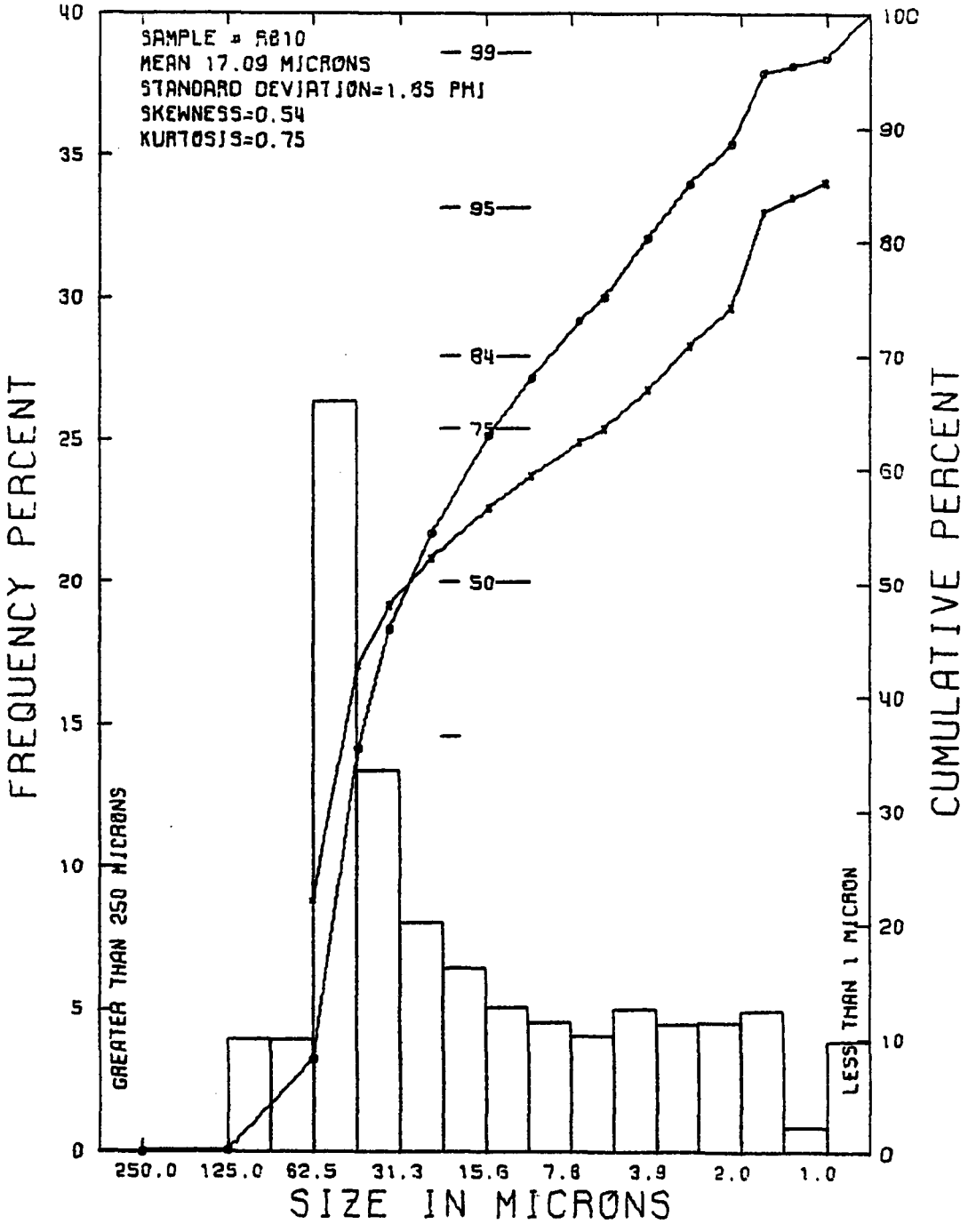
SAMPLE # R810
MEAN 17.09 MICRONS
STANDARD DEVIATION=1.85 PHI
SKEWNESS=0.54
KURTOSIS=0.75
99
95
84
75
50
FREQUENCY PERCENT
CUMULATIVE PERCENT
GREATER THAN 250 MICRONS
LESS THAN 1 MICRON
250.0 125.0 62.5 31.3 15.6 7.8 3.9 2.0 1.0
SIZE IN MICRONS

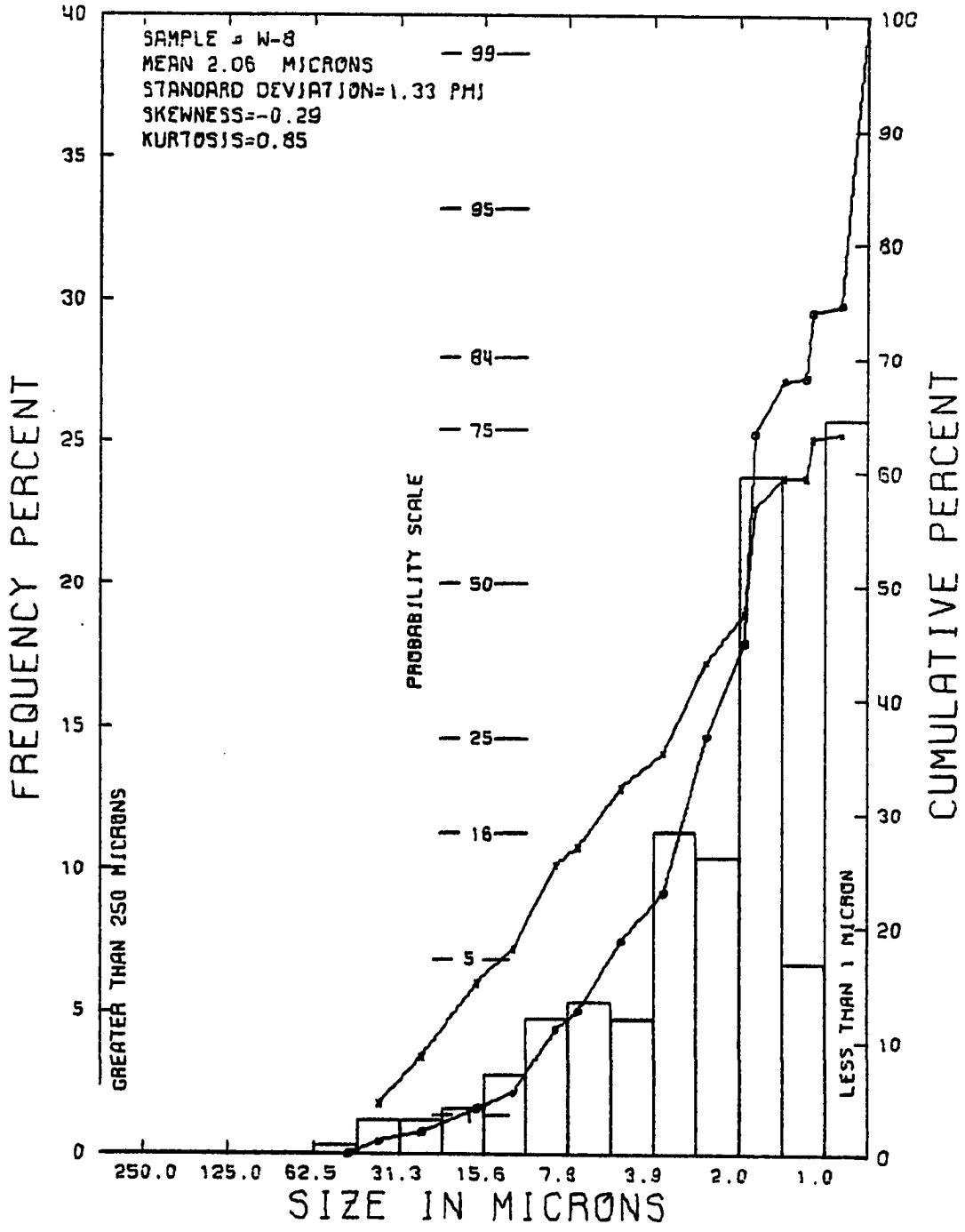
SAMPLE = W-8
MEAN 2.06 MICRONS
STANDARD DEVIATION=1.33 PHI
SKEWNESS=-0.29
KURTOSIS=0.85
FREQUENCY PERCENT
CUMULATIVE PERCENT
PROBABILITY SCALE
99
95
84
75
50
25
16
5
GREATER THAN 250 MICRONS
LESS THAN 1 MICRON
0
5
10
15
20
25
30
35
40
0
10
20
30
40
50
60
70
80
90
100
250.0
125.0
62.5
31.3
15.6
7.8
3.9
2.0
1.0
SIZE IN MICRONS

APPENDIX III

METHODS USED TO DETERMINE THE STRATIGRAPHIC POSITION AND PALEOGEOGRAPHIC LOCATION OF THE SAMPLES

The stratigraphic position of each sample was determined using geologic reports and maps of the area from which the sample was taken. The stratigraphic information available varied from the very detailed stratigraphic information given for Red Bird, Wyoming (Gill and Cobban, 1966), in which each ammonite zone is differentiated, to State Geologic Maps which specified only that the sample was Pierre Shale. Most commonly, however, the stratigraphic position could be isolated as being from a specific member of the Pierre Shale. For many samples, particularly samples from the Dakotas and Manitoba, Canada, the stratigraphic position could be determined using their lithology. For example, the Odonah Shale is an equivalent of the Uppermost Pierre Shale and is locally differentiated from other shales in the area by its siliceous characteristics.

As the type of stratigraphic information available varied greatly and because the time interval represented by different stratigraphic units was dependent on the location of the sample, the stratigraphic information was related to a common datum. The common datum used were the ammonite zones proposed by Gill and Cobban (1966). Ammonite zones were used as a common datum as they are nearly isochronous and allow the Pierre Shale to be divided into many narrowly ranging time increments. In their studies Gill and Cobban (1973)

have recognized 31 ammonite range zones, and estimate that each of these range zones represent approximately one-half million years. They have also related these range zones to other stratigraphic subdivisions.

Table 20 shows the stratigraphic location of each sample and the distance to the nearest shorline. These distances to the nearest shoreline were determined using the paleogeographic maps of Gill and Cobban (1969, and 1973).

Table 20. Stratigraphic Location of Samples *

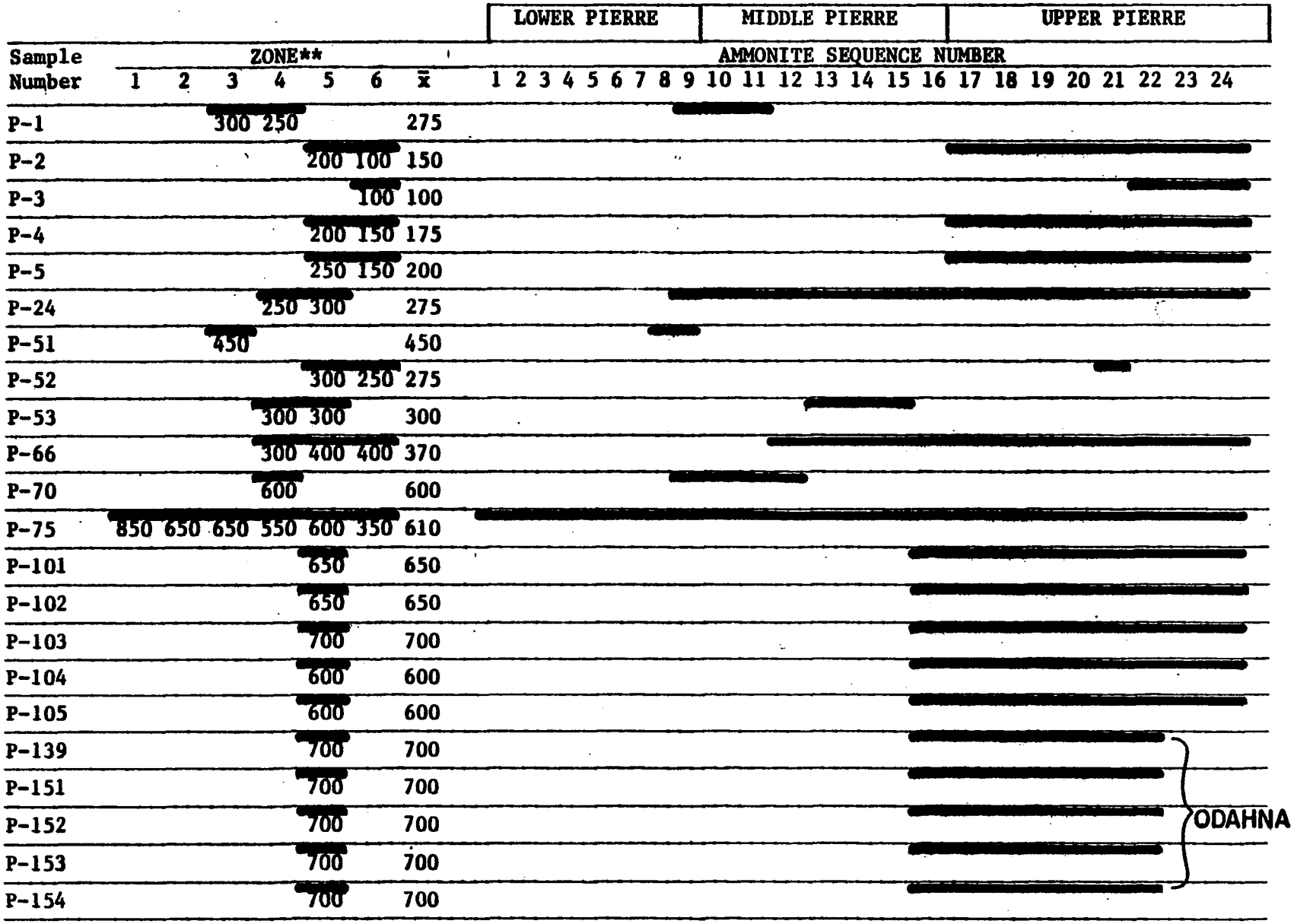

* Note; Numbers appearing below the bars represent distances to the nearest shoreline.

** The numbers used here to represent the ammonite zones in which the strand lines were mapped by Gill and Cobban (1969), see figure 5 (page 10).

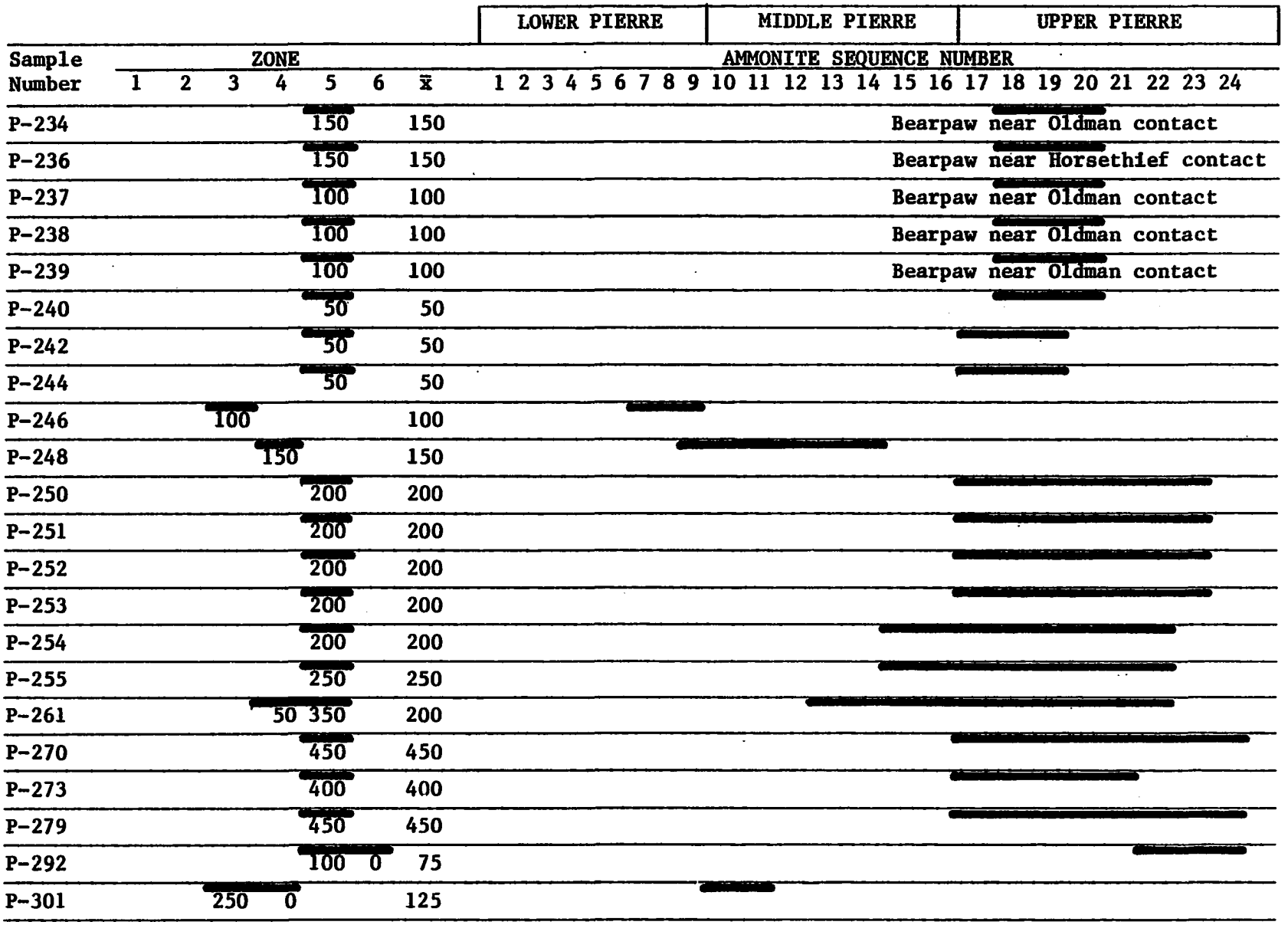
LOWER PIERRE
MIDDLE PIERRE
UPPER PIERRE
Sample Number
ZONE
AMMONITE SEQUENCE NUMBER
1 2 3 4 5 6 x̄
1 2 3 4 5 6 7 8 9 10 11 12 13 14 15 16 17 18 19 20 21 22 23 24
P-234 150 150 Bearpaw near Oldman contact
P-236 150 150 Bearpaw near Horsethief contact
P-237 100 100 Bearpaw near Oldman contact
P-238 100 100 Bearpaw near Oldman contact
P-239 100 100 Bearpaw near Oldman contact
P-240 50 50
P-242 50 50
P-244 50 50
P-246 100 100
P-248 150 150
P-250 200 200
P-251 200 200
P-252 200 200
P-253 200 200
P-254 200 200
P-255 250 250
P-261 50 350 200
P-270 450 450
P-273 400 400
P-279 450 450
P-292 100 0 75
P-301 250 0 125

	LOWER PIERRE			MIDDLE PIERRE									UPPER PIERRE												
Sample Number	ZONE							AMMONITE SEQUENCE NUMBER																	
	1	2	3	4	5	6	$\bar{x}$	1	2	3	4	5	6	7	8	9	10	11	12	13	14	15	16	17	18	19	20	21	22	23	24
P-155					700		700																								ODAHNA
P-156					700		700																								
P-186					800		800																								
P-187					800		800																								
P-193					250		250																								
P-201					550		550																	Bearpaw							
P-202					300		300																	Bearpaw near Eastend contact							
P-203					300		300																	Bearpaw near Eastend contact							
P-204					100		100																	Bearpaw near Eastend contact							
P-206					300		300																	Bearpaw							
P-208					250		250																	Bearpaw near Eastend contact							
P-210					150		150																	Bearpaw near Eastend contact							
P-212					350		350																	Bearpaw							
P-214				50			50																	Judith River							
P-218					50		50																	Bearpaw (Interbedded with sand)							
P-220					50		50																	Bearpaw (Interbedded with sand)							
P-222					50		50																	Bearpaw near Oldman contact							
P-224					75		75																	Bearpaw near Belly River contact							
P-226					50		50																	Bearpaw (Interbedded with sand)							
P-228					50		50																	Bearpaw near Horsethief contact							
P-230					200		200																	Bearpaw near Horsethief contact							
P-232					200		200																	Bearpaw near Horsethief contact							

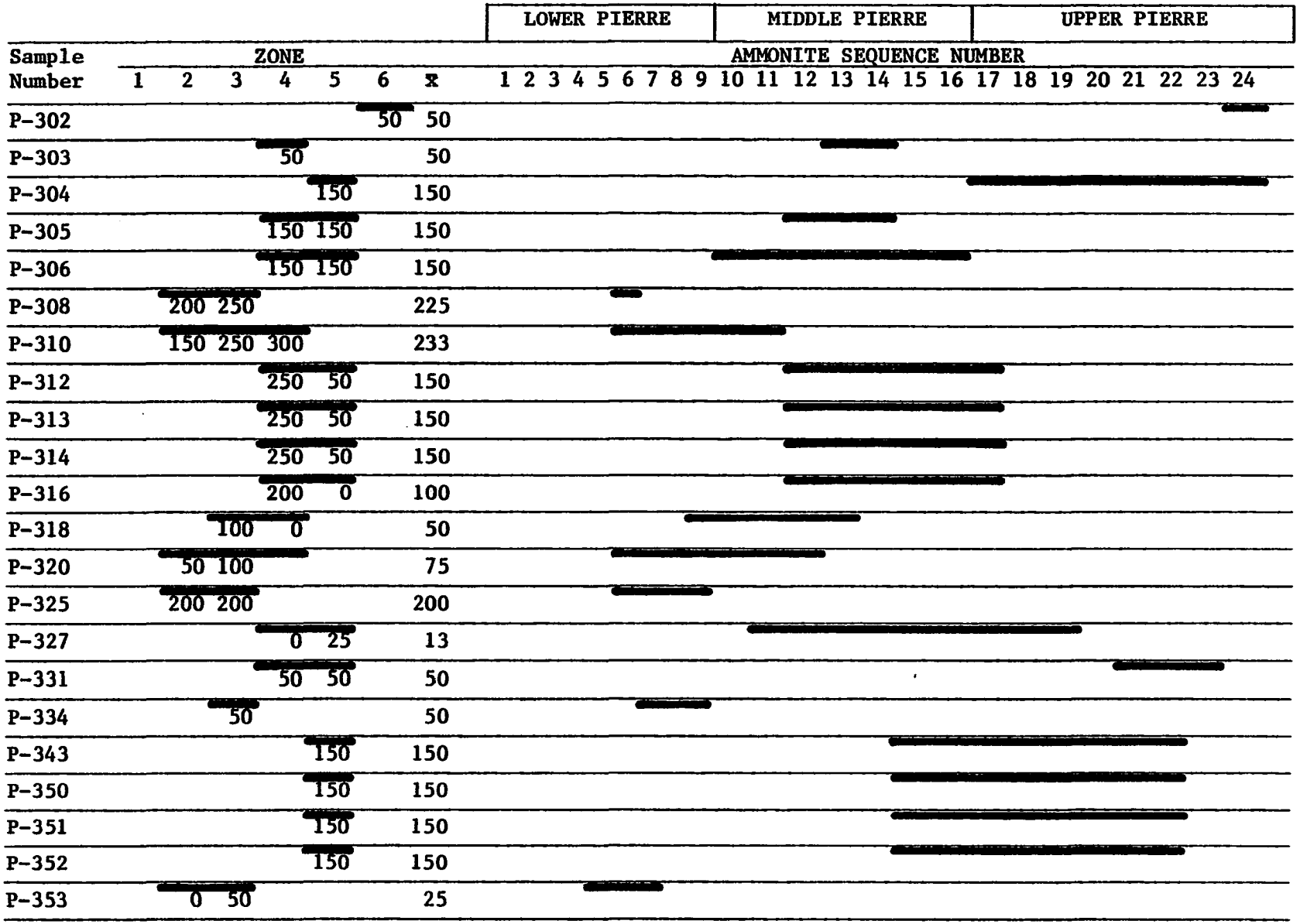
LOWER PIERRE
MIDDLE PIERRE
UPPER PIERRE
Sample Number
ZONE
AMMONITE SEQUENCE NUMBER
1 2 3 4 5 6 x̄
1 2 3 4 5 6 7 8 9 10 11 12 13 14 15 16 17 18 19 20 21 22 23 24
P-302 50 50
P-303 50 50
P-304 150 150
P-305 150 150 150
P-306 150 150 150
P-308 200 250 225
P-310 150 250 300 233
P-312 250 50 150
P-313 250 50 150
P-314 250 50 150
P-316 200 0 100
P-318 100 0 50
P-320 50 100 75
P-325 200 200 200
P-327 0 25 13
P-331 50 50 50
P-334 50 50
P-343 150 150
P-350 150 150
P-351 150 150
P-352 150 150
P-353 0 50 25

								LOWER PIERRE											MIDDLE PIERRE											UPPER PIERRE								
Sample	ZONE							AMMONITE SEQUENCE NUMBER																														
Number	1	2	3	4	5	6	Σ	1	2	3	4	5	6	7	8	9	10	11	12	13	14	15	16	17	18	19	20	21	22	23	24					
RB-1							240								250		230																			
RB-2							230										230																			
RB-3							230										230																			
RB-4							100										100																			
RB-5							100											100																		
RB-6							170													170																
RB-7							210																				210									
RB-8							160																					160								
RB-9							115																						130	100						
RB-10							75																									100	50			
RB-23							100											100																		
W-0					650		650																													
W-1					650		650																													
W-2					650		650																													
W-3					650		650																													
W-4					650		650																													
W-5					650		650																													
W-6					650		650																													
W-7					650		650																													
W-8					650		650																													
W-9				300			300																													

								LOWER PIERRE									MIDDLE PIERRE									UPPER PIERRE							
Sample	ZONE							AWMONITE SEQUENCE NUMBER																									
Number	1	2	3	4	5	6	$\bar{x}$	1	2	3	4	5	6	7	8	9	10	11	12	13	14	15	16	17	18	19	20	21	22	23	24
W-10			700	300			500																								
W-11			700	300			500																								
W-12			700	300			500																								
W-13			700	300			500																								
W-14(a)		450	700				575																								
W-14(b)		450	700				575																								
W-15		450	700				575																								

APPENDIX IV

QUALITATIVE AND QUANITATIVE X-RAY DIFFRACTION ANALYSIS TECHNIQUES

Three different procedures and types of X-ray diffraction analyses have been used in this study. The different procedures were used to obtain the following data: 1) qualitative analysis of quartz, cristobalite, and clay minerals, and 2) quantitative analysis of quartz and cristobalite. For all of the above described analyses a Seimans Diffractometer was used with the following machine settings: 1) Cu Kα radiation, 2) 35 kilovolts, and 3) 18 milliamperes.

Qualitative Analysis

Qualitative analyses were done by making diffractograms for each sample using constant machine settings. These machine settings were: divergence slit of 1.2°, receiving slit of .2°, chart speed of 1 cm/min scale factor of 4×10^4 CPM, statistical error of 2%, and goniometer speed of 1°2θ/min. In order to obtain uniform and reproducible diffraction intensities the samples were all mounted using the same technique. The technique used was to grind approximately 2 grams of sample to 80 mesh and then make spectrographic pellets of the sample. These pellets were then loaded into a specially designed sample holder and the

diffractogram produced.

After obtaining the diffractogram, the heights of the major diffracting peak for each of the minerals was measured. The peaks used and the position of the peaks for each mineral are given in table 21. The heights of these peaks were then given a relative rating. The rating scheme used is as follows:

0 no detectable peak

? questionable peak (unsure if it is a peak or background)

- peak significantly smaller than the average peak height

x average peak height

+ peak significantly larger than the average peak height

The results of this procedure are given in Appendix I.

Quantitative Analysis

The precision of quantitative X-ray analyses are affected by variables such as machine fluctuations, sample preparation, sample mounting, and method of measuring peak intensity. In this study the method of mounting the sample and method of measuring peak intensity introduced the most error.

To reduce the variations caused by the method of sample preparation and mounting, the samples were ground to 80 mesh, pressed into a spectographic pellet, and mounted in a rotating sample holder. The spectrographic pellets eliminated the problem of variations in the thickness of the sample exposed to the X-ray diffraction beam as the thickness of the pellet (approximately 3 mm) represents an infinite thickness to the X-ray beam. Rotating the pellet while the sample was

Table 21. Location of the x-ray diffraction peaks used for the qualitative mineral analyses.

Minerals	Peak position in degrees 2θ (CuKα radiation)
Quartz	26.6
Disordered Cristobalite	21.8
Plagioclase	28.0
K-feldspar	27.5
Calcite, pure	29.4
Calcite, mixed *	29.6-30.0
Dolomite, pure	31.0
Siderite, mixed *	31.7-31.9
Rhodochrosite, mixed *	30.8-31.5
Gypsum	11.6
Jarosite	29.1
Alunite	30.0
Pyrite	33.1
Clinoptilolite	10.0
Kaolinite and Chlorite	12.5

* The term mixed is used to denote carbonate phases which are not pure end member minerals, for example, calcite ($CaCO_3$) which contains extensive substitution of Mg^{+2} for Ca^{+2}.

analyzed exposed much more sample to the X-ray beam, and eliminated variation due to sample holder orientation, thus eliminating much of the effect of sample variations normally found in an X-ray mount.

To measure the intensity of the diffracted beam, a diffractogram was made of the peak. The peak height and width at half the peak height were measured. The product of these measurements gives a measure of the peak intensity. Using these methods and the following machine settings the desired precision was obtained:

1) divergence slit 1.2°
2) receiving slit .4°
3) chart speed 4 cm/min
4) counts per minute 2×10^5 and 4×10^5
5) statistical error 1%
6) goniometer speed 1° 2θ/min

For the quartz analyses the precision was evaluated by analyzing ten splits from each of three different samples. The precision of the cristobalite was evaluated using ten splits of one sample. The results of these analyses are shown in table 22. From these analyses it can be expected that at the 95% confidence level replications of the measurement of peak intensities will be within 10% of the measured mean value.

The accuracy of quantitative X-ray analysis is dependent on the accuracy of the standards as well as the precision of the analyses. To achieve maximum accuracy the composition of the matrix and grain size of the mineral being analyzed should be the same in both the sample and the standards. For these reasons samples of the Pierre Shale were used as the standards, or as the matrix of the standards, compositional

Table 22. Evaluation of the precession of the X-ray technique used in this study.

	Weight Percent Quartz		
Split #	Sample #1	Sample #2	Sample #3
1	6.3	28.1	32.7
2	6.4	28.1	37.2
3	6.5	27.2	36.4
4	6.5	27.2	36.2
5	6.4	27.0	35.0
6	6.5	28.8	35.4
7	6.4	26.8	36.7
8	6.8	27.1	36.3
9	5.8	27.1	35.7
10	6.6	27.8	36.6
Mean	6.4	27.5	35.8
Standard Deviation	.26	.64	1.27
Standard Error	.08	.20	.40
*Relative Error	8.0%	4.6%	5.6%

*Relative error is given in terms of weight percent of the amount present, and is calculated at two standard deviations.

variations could still cause errors in the analyses. Changes in the chemical composition of the matrix will cause a change in the mass absorption coefficient of the matrix (μ/ρ). Any change in (μ/ρ) will cause a change in the intensity of the diffracted X-rays.

For powder diffraction methods the expression from Cullity (1956)

$$I = \left(\frac{Io\ e^4}{m^2\ c^4}\right)\left(\frac{\lambda^3\ A}{32\pi r}\right)\frac{1}{v^2}\left[|f|^2\ p\left(\frac{1+\cos^2 2\theta}{\sin^2\theta\cos\theta}\right)\right]\left(\frac{c^{-2m}}{2(\mu/\rho)^p}\right)$$

where:

I = integrated intensity per unit length of diffraction line

Io = Intensity of incident beam

e,m = charge and mass of the electron

c = velocity of light

2 = wavelength of incident radiation

A = wave amplitude

v = volume of unit cell

f = structure factor

p = multiplicity factor

θ = Bragg angle

c^{-2m} = temperature factor

(μ/ρ) = mass absorption coefficient

relates the intensity of a diffracted line to the intensity of the incident beam in a pure phase. When considering selected line of a pure phase (α) this expression may be simplified to the following expression

$$I = \frac{K_1}{(\mu/\rho)}$$

where K is a constant.

In considering the pure phase (α) in a mixture (m) the right side of the equation must be multiplied by the concentration of phase in the mixture. Also the mass absorption coefficient of the mixture $(\mu/\rho)_m$ must be used rather than that of the pure phase. These changes result in the following expression:

$$I = \frac{K_1 C}{(\mu/\rho)_m} \quad \text{or} \quad C = \frac{I \ (\mu/\rho)_m}{K_1}$$

where C is the concentration (in weight percent) of phase

These expressions show that any change in $(\mu/\rho)_m$ will be directly reflected in the concentration. That is, a 10% change in $(\mu/\rho)_m$ will give a 10% change in the concentration.

By assuming that the chemical compositions of the Pierre samples given in Tourtelot (1962) are representative of Pierre Shale, the expected variations in the mass absorption coefficients of the matrix can be determined. The mass absorption coefficients calculated using the data from Tourtelot are given in table 23. Also given in table 23 is the relative percent error

$$\text{relative \% error} = \frac{((\mu/\rho) \text{ average matrix} - (\mu/\rho) \text{ sample matrix})}{(\mu/\rho) \text{ average matrix}} \times 100$$

which would be introduced into the measurement of the X-ray intensities if the mass absorption coefficient were assumed to be constant for all samples.

These results show that the expected error caused by variations in the composition of the sample matrix is always less than 10% except when the samples contain more than 5% carbonate. Because high concentrations of carbonate minerals cause significant errors, samples

Table 23. Mass Absorption Coefficients of Samples of the Pierre Shale calculated from the data of Tourtelot (1962).

Sample Number	Mass absorption coefficient (μ/ρ)	% Relative Error Calculated Using Mean (μ/ρ) for All samples*	% Relative Error Calculated Using Mean (μ/ρ) for Samples containing <5% carbonate**	% Carbonate
C871	48.7	.1	1.2	
C872	48.1	-.5	.6	
C873	47.8	-.8	.3	
C874	47.0	-1.6	-.5	
C875	47.7	-.9	.2	
C870	46.8	-1.8	-.7	
C876	47.5	-1.1	0.0	
C877	48.7	-.1	+1.2	
C886	48.2	-.4	.7	5%
C887	46.5	-2.1	1.0	
C881	47.3	-1.3	-.2	
C882	48.1	-.5	.6	
C883	48.4	-.2	.9	
C884	48.0	-.6	.5	
C885	47.9	-.7	.4	
C878	45.8	-2.8	-1.7	
C879	64.3	15.7	-	38%
C880	46.7	-1.9	-.8	
C888	46.6	-2.2	-.9	
C889	56.9	8.3	-	37%
C890	47.6	-1.0	.1	4%
C891	44.9	-3.9	2.6	

* (μ/ρ) = mean (μ/ρ) of all samples

** (μ/ρ) = mean (μ/ρ) of all samples except those containing more than 5% carbonates.

containing over 10% carbonates were not analyzed using this procedure. If the effect of the matrix is not considered, the error caused by variations in the (μ/ρ) of the matrix is less than 10 relative percent except in samples containing more than 5% carbonate minerals.

Quartz Standards. The standards used for working curve for the determination of quartz concentrations were samples of Pierre Shale in which the quartz concentrations had been determined using the methods given in Appendix VII. The accuracy of these quartz analyses is discussed in Appendix VIII and the error caused by the standards is shown to be less than 10% of the amount present. The calibration curve for these analyses is shown in Figure 40.

The results of these analyses are given in Appendix II.

Cristobalite Standards. The cristobalite standards used for these analyses were Pierre Shale samples in which the concentration of cristobalite could be determined accurately using a chemical and mineralogic mass balance. This mass balance is described by the following equation :

$$C_{\text{cristobalite}} = C_{\substack{\text{total} \\ SiO_2}} - C_{\text{quartz}} - R \times C_{Al_2O_3}$$

where

C is the concentration of subscripted phases

and

R is the average ratio of SiO_2 to Al_2O_3 for all phases containing SiO_2 or Al_2O_3 except quartz and cristobalite.

The only important phases containing SiO_2 and/or Al_2O_3 found in Pierre

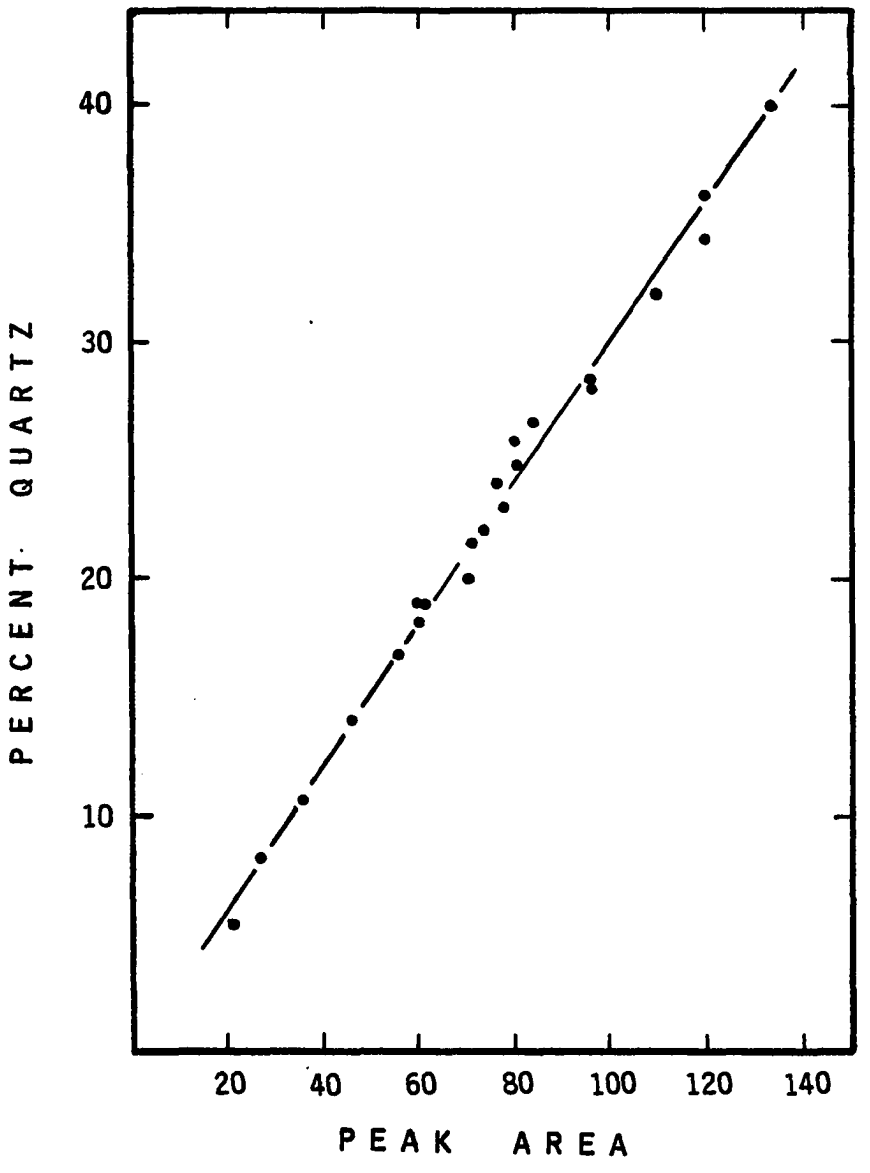

Fig. 40 Standard curve used in the quantitative x-ray diffraction analyses for the determination of quartz concentrations

Shale samples besides quartz and cristobalite are the clays and feldspars. Since the value of C quartz was known, the value of R was determined for each of the Pierre Shale samples which did not contain cristobalite using the following expression:

$$R = \frac{C_{SiO_2\,total} - C_{SiO_2\,quartz}}{C_{Al_2O_3}}$$

These values were then averaged to obtain an average value of R. The average value of R is 2.3 with a standard deviation of 0.23 and a range from 1.66 to 3.63.

Since all of the concentrations used in these equations are accurate to within ±5% of the amount present, the error in the cristobalite concentrations must be less than ±5% of the largest component unless the value used for R is not accurate to within ±5% of the real value for R. Since the individual values of R varied by almost a factor of two, the error caused by using an average value for R may be quite substantial. The error caused by R also vary dependent on C Al_2O_3. Due to this error caused by R this method can only be used for samples containing low concentrations of Al_2O_3. Figure 41 is a graph of concentration of cristobalite calculated using this method versus the intensity of the cristobalite x-ray peak at 21.8 degrees for 14 samples containing cristobalite. This graph shows how the error increases with decreasing cristobalite concentrations. To avoid this error sample P-187 was chosen to be used as a standard. Calculations of this concentration of cristobalite in this sample show it to be 59.6 ±3%. This sample was mixed with other Pierre samples to obtain the standard curve shown in figure 41. Another standard curve shown in figure 42 was used to determine cristobalite concentrations of less than 14%.

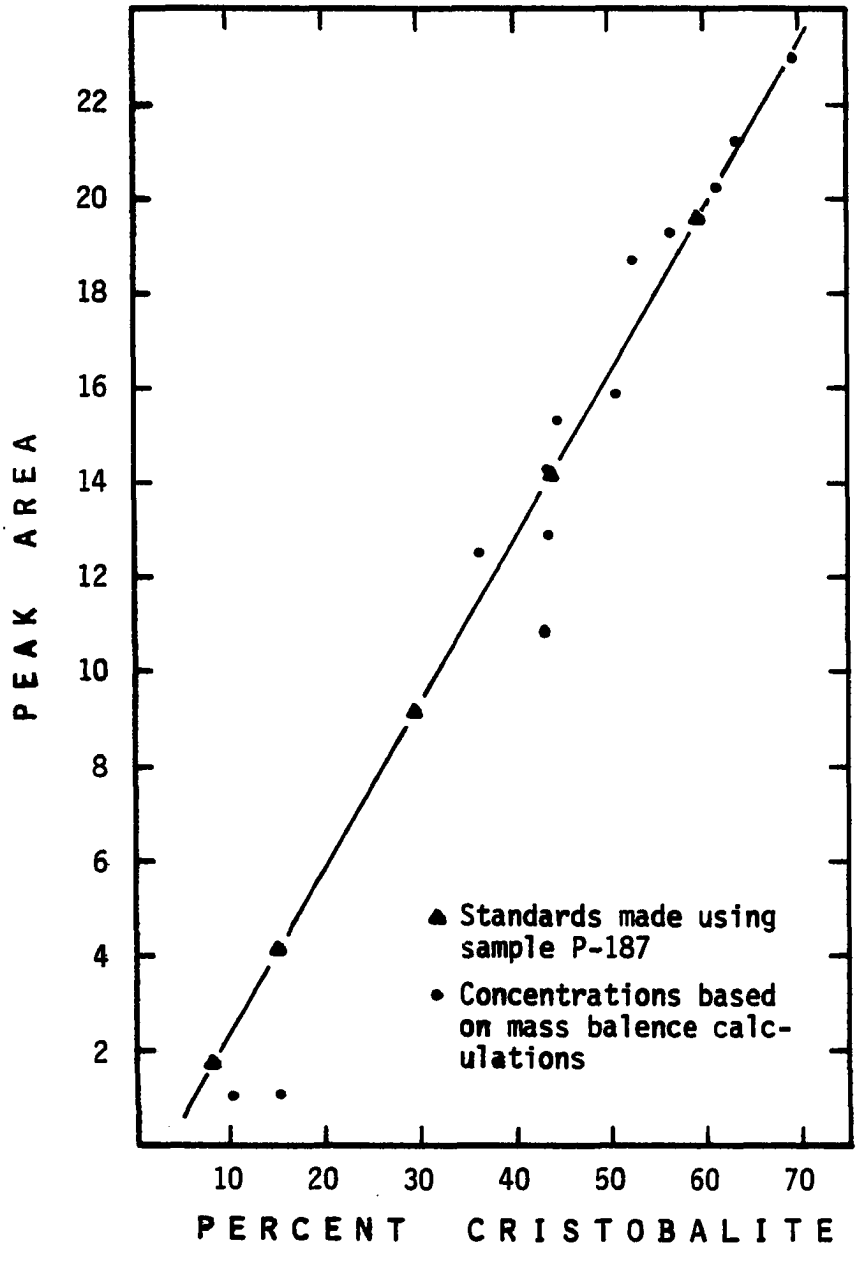

Fig.41 standard curve used in the quantitative x-ray diffraction analyses for the determination of cristobalite concentrations between 15 and 70 percent.

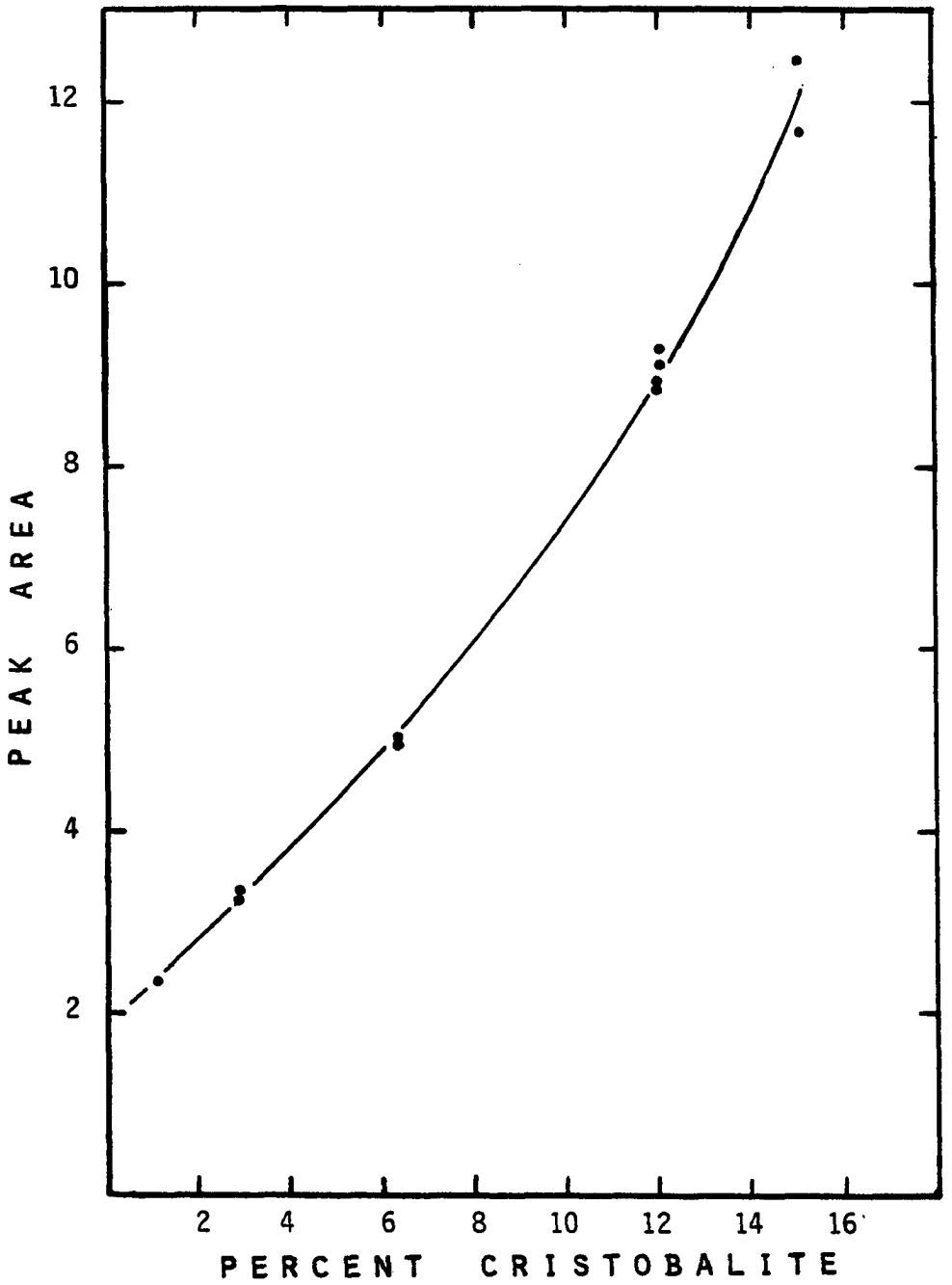

Fig. 42 Standard curve used in the quantitative x-ray diffraction analyses for the determination of cristobalite concentrations between 0 and 15 percent.

Because the concentration of cristobalite in the standards is known to within ±10 percent of the amount present and the x-ray precision is greater than ±10 percent of the amount present at the 95% confidence level, the results of the cristobalite determinations are assumed to have the same accuracy.

APPENDIX V

QUANTITATIVE X-RAY FLUORESCENCE ANALYSES TECHNIQUES

X-ray fluorescence techniques were used to analyze for the oxides of silicon, aluminum, potassium, and sulfur. These analyses were done using a Siemans SRS spectometer, with a solid state digital counter designed for this unit.

The samples used for X-ray fluorescence analyses were ground to 80 mesh, a 2 gram split of the ground sample was pressed into a spectrographic pellet using 30 tons pressure on a 1¼" die. No binder was used as the clay present in the sample was very cohesive and made a dense smooth pellet. Analyses of duplicate samples prepared using this method were reproducible to 2% of the amount present. (The reproducibility determinations were done using 10 different splits of three different samples and analyzing for potassium.) The samples were analyzed using the machine setting shown in table 24. The samples were rotated while they were being analyzed. One-minute counting periods were used when determining the X-ray intensity at both the peak location and background location. The counting rate was always less than 100,000 counts per minute, well within the linear

Table 24. Machine Setting

INSTRUMENT CONTROL	INSTRUMENT SETTING FOR ANALYSIS OF			
	SiO_2	Al_2O_3	K_2O	SO_3
X-ray tube type	Chromium	Chromium	Chromium	
X-ray tube voltage (KV)	30	30	30	30
X-ray tube amperage (MA)	60	60	65	60
Sample holder type	Al	Coal	Al	Al
Sample holder size	23°	23°	23°	23°
Collimator slit size	.40°	.40°	.40°	.40°
Gas flow counter	Yes	Yes	Yes	Yes
Gas type	P-10	P-10	P-10	P-10
Rate of gas flow	5 ft 3/hr.	5 ft 3/hr.	5 ft 3/hr.	6 ft 3/hr.
Counter window type	6 μ Myler	6 μ Myler	6 μ Myler	6 μ Myler
Vacuum strength	<150 u	<150 u	<150 u	<150 u
Counter voltage	2250	2250	2250	2150
Base line voltage	5	5	8	6.2
Window voltage	23	30	4.5	15
Attenuation	10	10	10	10
Analyzing crystal type	PET	KAP	LiF	PET
Location of peak measurements	108.9300	144.7500	136.9000	75.5800
Location of background measurements	135.0000	135.0000	133.0000	80.0000

range of the counting circuits used.

The standards used for these analyses were Pierre Shale samples which had been analyzed previously by Dave Foster, Oklahoma Geological Survey chemist, using wet chemical methods. Foster estimates his accuracy to be $\pm$1.0 percent of the amount present. Because Pierre Shale samples were used as standards, and due to the chemical similarities of these samples (see Appendix II) the matrix errors present in these analyses are considered to be insignificant. The standard curves used for these analyses are shown in figures 43 , 44 , 45 , and 46 .

To insure the reproducibility of the analyses, high and low standards were run after every ten samples. If the high and low standards differed by more than 1% of the previous values, all samples run between these sets of standards were rerun. The overall accuracy of these analyses is considered to be $\pm$2.5% of the amount present.

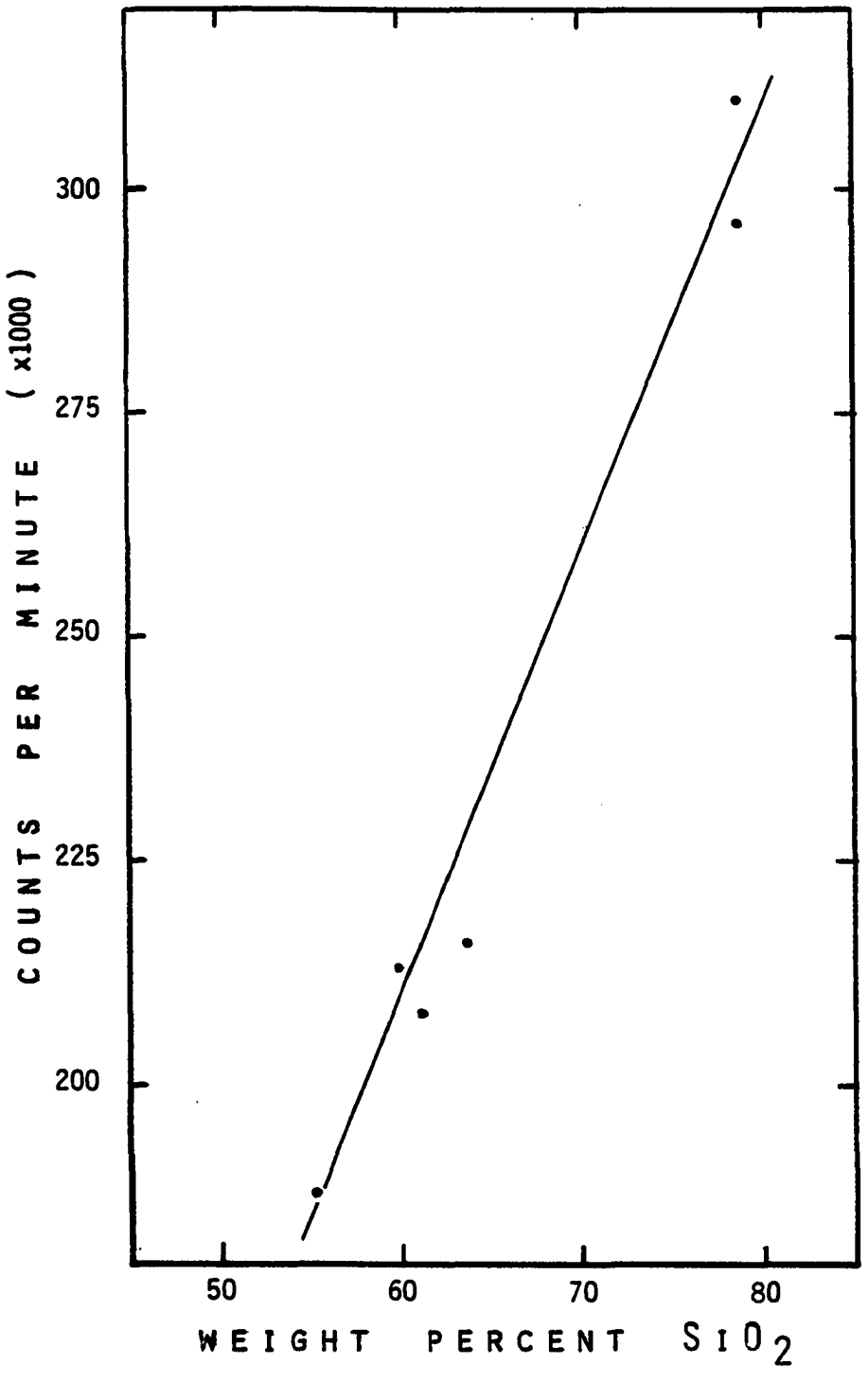

Fig. 43 standard curve used in the quantitative x-ray fluorescence analyses for the determination of the whole rock SiO_2 concentrations.

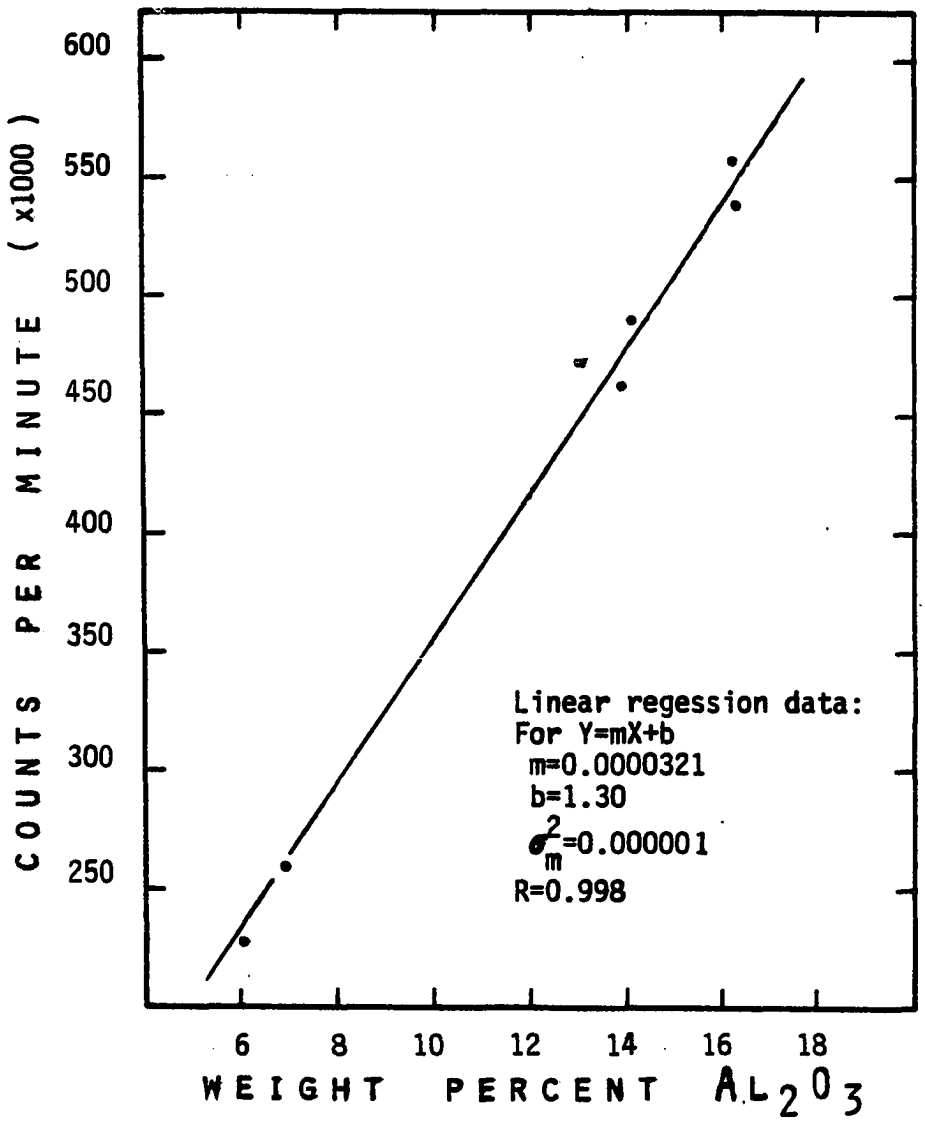

Fig. 44 Standard curve used in the quantitative x-ray fluorescence analyses for the determination of the whole rock Al_2O_3 concentrations.

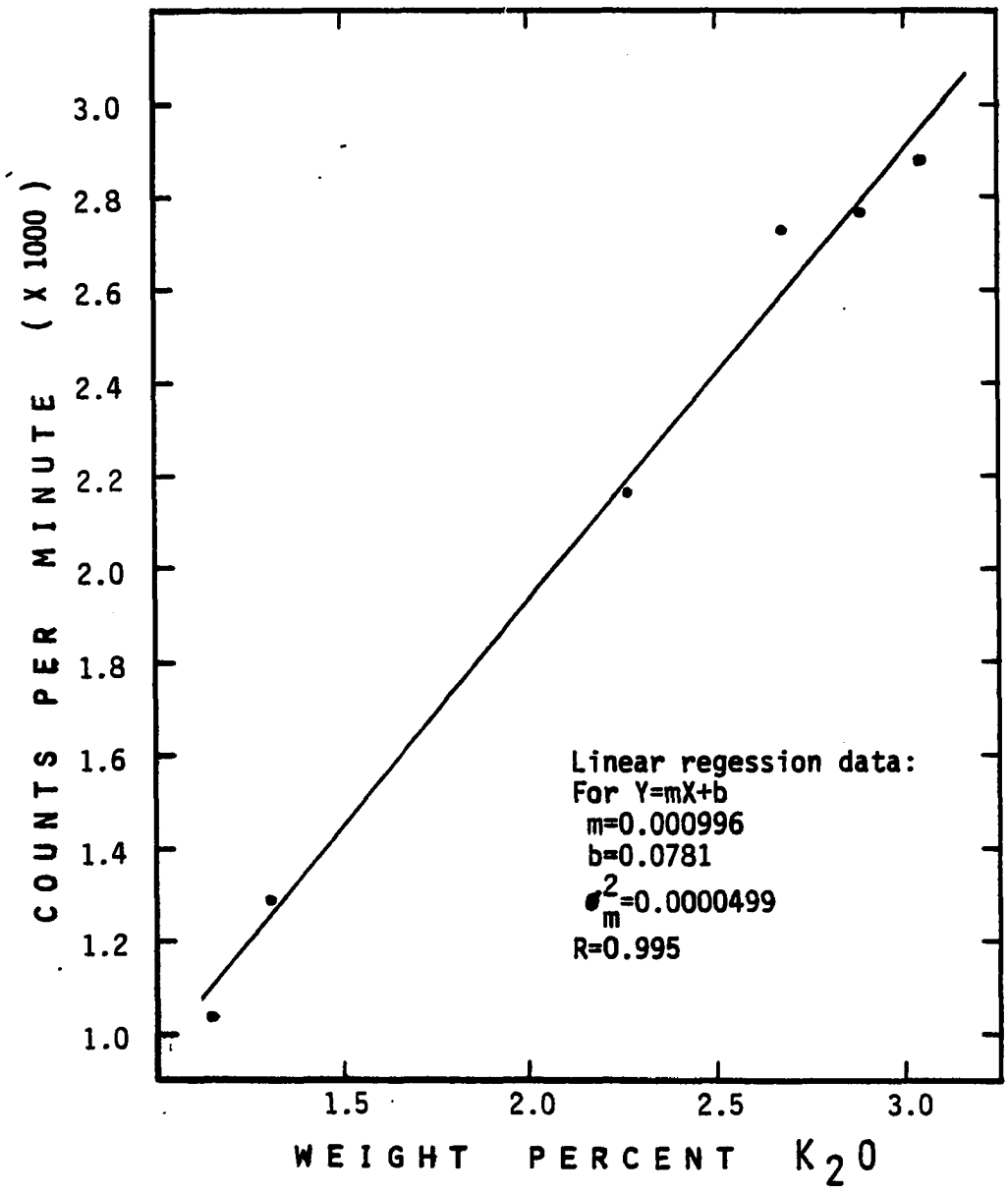

Fig.45 Standard curve used in the quantitative x-ray fluorescence analyses for the determination of the whole rock K_2O concentrations.

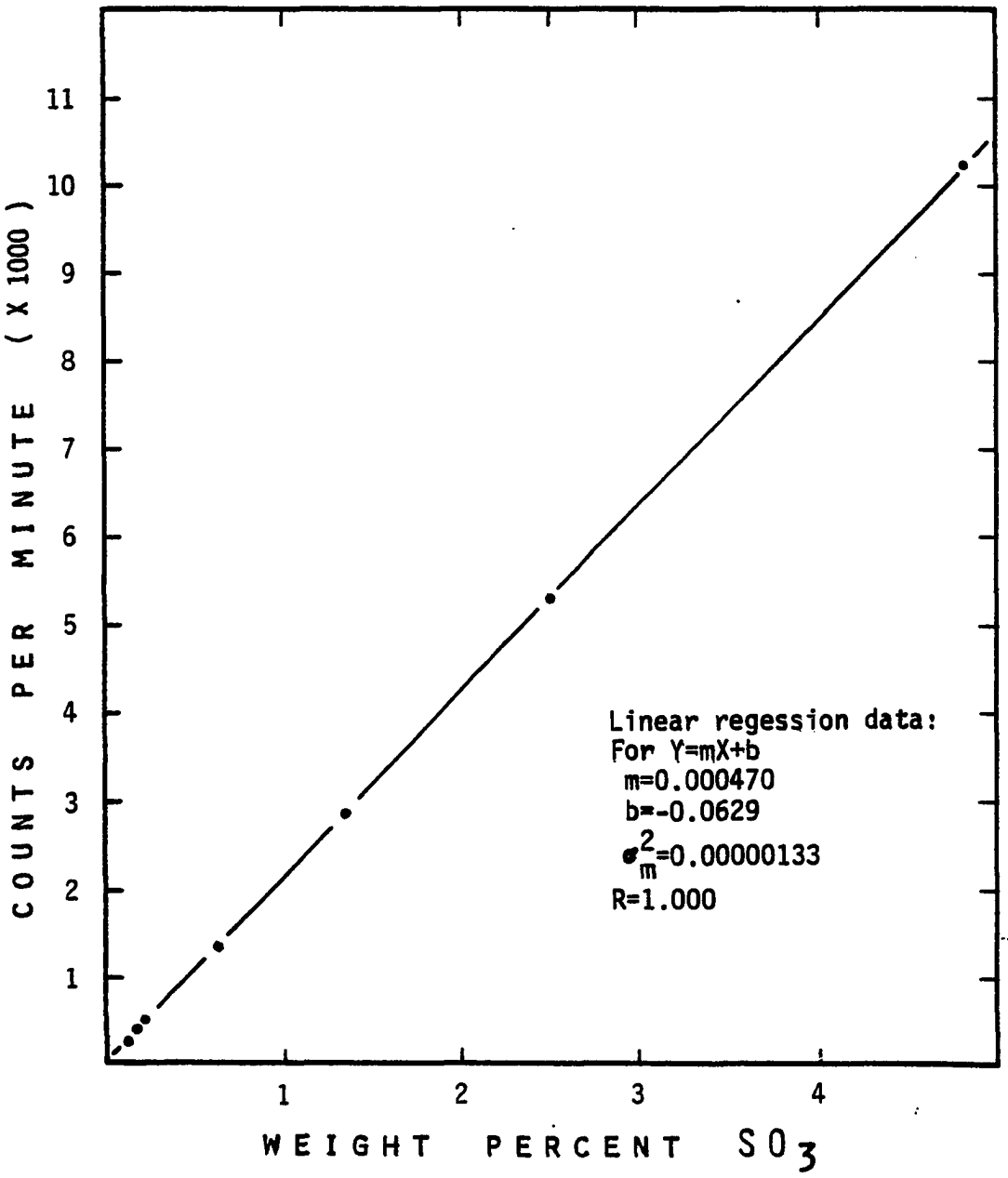

Fig. 46 Standard curve used in the quantitative x-ray fluorescence analyses for the determination of whole rock SO_3 concentrations.

APPENDIX VI

CARBONATE AND WATER LOSS

ANALYSIS TECHNIQUES

The amounts of the carbonate minerals present in the samples were determined by a technique based on the determination of the percentage of the sample soluble in 1.0N HCl. Because some components of the samples other than carbonates are soluble in 1.0N HCl, the average concentration of these components as determined by using these procedures on Pierre Shale samples containing no carbonates. This value was then subtracted from the total amount of soluble components.

Procedure: The following is a brief outline of the procedure used to determine the fraction soluble in 1.0N HCl.

I. Dry 50 ml pointed centrifuge tube overnight at 110°C and then weigh accurately to .001 grams.

II. Weigh approximately 1 gram of sample into the 50 ml centrifuge tube.

III. Place sample and pointed centrifuge tube into oven and dry at 110°C overnight.

IV. Weigh sample accurately to .001 grams.

V. Slowly add 40 ml of 1.0N HCl to the centrifuge tube and mix the acid and sample.

VI. Mix every 15 minutes until sample no longer releases gas when mixed.

VII. Centrifuge sample for 30 minutes at 2,000 RPM, and then decant the supernatant.

VIII. Fill centrifuge tube with distilled water, mix, centrifuge, and decant as in step VII.

IX. Repeat step VIII.

X. Dry centrifuge tube and sample overnight at 110°C and then weigh sample accurately to .001 grams.

Non-carbonates Soluble in 1.0N HCl: Most of the samples contain some carbonate which may or may not be detectible by X-ray techniques, therefore none of the samples could be assumed to be carbonate free. As a result, the amount of non-carbonate material soluble in HCl could not be determined directly on carbonate free samples. In order to circumvent this problem, a more accurate method of carbonate determination (Jeffery, 1970) was employed. The technique used to obtain accurate carbonate concentration was based on the determination of the concentration of carbonate CO_2 gas by a gravimetric method described by Jeffery (1970). These values were then multiplied by the conversion factor of the appropriate type of carbonate. The types and relative amounts of carbonates present were determined from the X-ray diffraction data given in Table 25. The acid soluble non-carbonate component (the difference between the fraction soluble in HCl and the carbonate fraction) was determined for each of nine samples. (The method of Jeffery (1970) was not used for all samples as it is very time consuming.)

Table 25. Types and relative amounts of carbonates present determined from x-ray diffraction data.

	X-ray dolomite peak height	X-ray calcite peak height	% CO_3	% Dolomite	% Calcite	% Carbonate	% Weight Loss in 1N HCl	Difference
RB-9	13.8	2.4	2.58	5.1	.4	5.5	7.9	2.4
P-51	.9	1.7	.1	.1	.1	.2	2.0	2.0
P-230	1.3	-	.52	1.1	-	1.1	3.0	1.9
P-302	18.7	2.0	4.52	8.5	1.0	9.5	12.6	3.1
P-310	6.1	1.4	3.37	5.7	1.5	7.2	10.2	3.0
P-313	4.0	-	1.69	3.5	-	3.5	5.9	2.4
P-318	8.6	16.7	10.7	7.5	16.1	23.6	26.2	2.6
P-320	3.6	55.6	19.5	2.5	41.5	44.0	45.4	1.4
P-353	12.5	21.6	14.6	11.3	20.9	32.2	34.1	1.9

$\bar{x}$ = 2.3

q = .55

The mean value of the acid-soluble non-carbonate fraction of these samples is 2.3% with a standard deviation of .55.

The value of 2.3% was assumed to be the amount of non-carbonate soluble in all of the samples and was subtracted from the total amount soluble in 1.0N HCl. The residual was then considered to be the carbonate fraction. Because of the relatively high value of the standard deviation (.55%) for the acid soluble non-carbonate components, samples having carbonate values of less than 1% are reported only as having less than 1% carbonate.

Comparison of the X-ray data to these carbonate determinations have shown that, if no carbonate is shown on the bulk X-ray diffractograms (see Appendix II), the amount of carbonate present is less than 1%. Therefore, all samples which show no carbonate diffraction peaks are assumed to have less than 1% carbonate minerals.

Examination of duplicate samples have shown that the reproducibility of the amount of soluble material is always less than $\pm$.5%; therefore the error in these analyses is considered to be the error present in the determination of the amount of non-carbonate material soluble in 1.0N HCl (.55%).

APPENDIX VII

SELECTIVE MINERAL DISSOLUTION

(BISULFATE FUSIONS) TECHNIQUES

Kiely and Jackson (1964) demonstrated a method for the determination of quartz and feldspar concentrations, in soils and in some rock samples, using sodium pyrosulfate fusions. In a subsequent paper, Kiely and Jackson (1965) demonstrated that this technique could also be used to determine the concentration and normative composition of the feldspar fraction of soils.[1]

While this technique is applicable for some of the Pierre Shale samples, the technique could not be used for the majority of the Pierre Shale samples for the following reasons:

1. The amount of sample fused (0.2 grams) was too small for samples of the Pierre Shale to produce sufficient material for the chemical analyses required.
2. The excessive centrifugation time which is required for complete recovery of the fine grained quartz and feldspar found in the Pierre Shale was deemed prohibitive.
3. Their technique does not remove all the unstable phases.

For these reasons it was found necessary to modify their technique.

[1] The basis for this technique is the selective dissolution of the clay relative to the quartz and feldspars contained in the samples. Following the removal of the clays the quartz and feldspar are chemically analyzed to determine the normative feldspar composition and content.

Procedure

The determination of the quartz and feldspars was done using a combination of two procedures; a fusion in sodium bisulfate to concentrate the quartz and feldspars, followed by chemical analysis of the quartz and feldspar fraction of the sample. The following is an outline of the procedures used:

I. Concentration of the quartz and feldspars.

A. Grind the sample to pass through 177 micron sieve.

B. Accurately weigh approximately 2 grams of sample in a platinum crucible.

C. Add 20 grams of sodium bisulfate to the crucible.

D. Add a few drops of water to the crucible and mix the contents of the crucible. (Add just enough water to wet sample.)

E. Cover the crucible and place it 9 cm from the top of a Meker burner.

F. Light the burner and heat the crucible slowly until all frothing stops. While heating the crucible in this step, the sides and top of the crucible should also be heated to prevent the sample from bubbling out of the crucible.

G. Fuse the sample for 15 minutes by using the maximum heat of the Meker burner. The bottom of the crucible should be located about 9 cm above the top of the Meker burner.

H. Transfer the crucible and contents to a 600 ml beaker containing 300 ml of 1.0N HCl.

I. Heat the beaker on a hot plate and remove the crucible and cover as soon as the fused cake dissolves sufficiently. (Wash the crucible and cover using a wash bottle containing 1.0N HCl.)

J. Continue heating until the fusion cake is completely dissolved.

K. Filter using a Buchner funnel and Whatman #40 filter paper.

L. Rinse the filtrate using 1.ON HCl followed by distilled water.

M. Transfer filtrate and filter paper into 400 ml of .5N NaOH.

N. Heat to boiling and then boil for 20 minutes.

O. Transfer filtrate and filter paper into the Buchner funnel and filter using another sheet of Whatman #40 filter paper.

P. Wash once with 1.ON NaOH, once with distilled water, then wash three times with alternate washings of 1 N HCl and distilled water. Following these washings, wash three additional times with distilled water.

Q. Ignite filter paper in a pre-weighed crucible. After cooling weigh the crucible containing the quartz and feldspar.

II. Chemical analyses of quartz plus feldspar concentrate.

A. Weigh .1 grams of sample into a pre-weighed porcelain crucible. Sample weight must be accurate to .0005 grams.

B. Add .6 grams of lithium metaborate to the porcelain crucible.

C. Mix lithium metaborate and sample in the porcelain crucible.

D. Clean a graphite crucible by fusing approximately .6 grams of lithium metaborate in the crucible at 1000°C for ten minutes. After the crucible has cooled remove and discard the borate bead formed during the fusion.

E. Carefully transfer the sample and lithium metaborate into the clean graphite crucible.

F. Fuse sample and lithium metaborate at 1000°C for 15 minutes. (Allow the oven to reach 1000°C before starting to time the

fusion.)

G. Cool the crucible and then transfer the fusion bead into a 600 ml Nalgene beaker containing 100 ml of 4% nitric acid.

H. Place the beaker on a magnetic stirrer and continue stirring until the fusion bead is completely dissolved.

I. Filter, using #1 Whatman filter paper, into a 250 ml volumetric flask.

J. Wash beaker and filter paper three times using .4% nitric acid.

K. Wash filter paper three times using distilled water.

L. Bring total volume of solution to 250 ml using distilled water.

M. Analyze solutions for Na, K, and Ca using standard atomic absorption techniques. Standards were made from stock solutions of known concentrations of Na, K, and Ca and a lithium metaborate solution (for matrix correction). Calcium analyses were made using dilutions containing 1% Lanthanum Oxide.

Discussion of Bisulfate Technique

The major differences between this technique and the technique of Kiely and Jackson (1964) are summarized below:

1. The addition of water to the sample before the fusion.
2. The initial sample weight of 2.0 grams rather than 0.2 grams.
3. The volume and concentration of the HCl. (300 ml rather than 60 ml and 1.0 rather than 3.0 normal HCl.)
4. The volume of NaOH (400 ml rather than 60 ml).
5. The length of time that the sample was boiled in the 1.0N NaOH. (20 minutes rather than 3 minutes.)

6. Filter paper was used rather than centrifugation.

A larger starting sample weight was found to be a necessity because the amount of quartz and feldspar reclaimed after the fusion was in most cases too small when .2 grams was used. The chemical analysis technique we use requires .1 grams and therefore, unless the mudrock contained 50% quartz plus feldspar, a starting weight of .2 grams was too small. We also wanted to be able to use the results of a single fusion to do petrographic and size distribution analysis. Because the average mudrock contains approximately 35% quartz plus feldspar (Shaw and Weaver, 1965) it was felt that two grams would be an adequate and convenient amount of sample to work with. Without the addition of water the smaller size fractions of the samples could be seen floating on the top of the molten bisulfate during the fusion. One normal HCl was found adequate to dissolve the fusion cake. The larger volumes of HCl and NaOH were used to keep the concentrations of the dissolved species well below their saturation points. The length of time that the sample was boiled in .5N NaOH was increased to 20 minutes to dissolve cristobalite and completely dissolve the silicate wreckage produced when fusing muscovite. Filtration was used rather than centrifugation because it increases the efficiency of reclaiming the quartz and feldspars in the finer grain sizes and is much more rapid (see later discussion).

Because of these changes in the technique, the effect of this treatment on the phyllosilicates, feldspar and quartz was reevaluated.

Effects of the Bisulfate Fusion on Clay Components of the Shales

The accuracy of this technique is largely dependent upon its effectiveness in removing all components of the samples except the quartz and feldspars. Many components of the samples are readily dissolved or destroyed by high temperatures (organic matter), concentrated acid (carbonate, iron oxides, chlorites, pyrites, and sulfates), or concentrated basic conditions (cristobalite) employed during various stages of this technique. The only components likely to be found in significant amounts in these samples which are not destroyed solely by the extreme conditions are phyllosilicate minerals.

To show the effectiveness of the fusion in destroying the phyllosilicates various phyllosilicates were fused using the technique previously described. The results are shown in tables 26 and 27. As can be seen from these tables, the fusion did not completely destroy these samples. Except for the muscovite coarser than 74μm it was found that the materials remaining after the fusion were impurities. X-ray and optical examination of the material remaining indicated that all of this material was quartz and feldspar. There was no indication that any of the remaining material was a phyllosilicate. Fusion of muscovite grains larger than 74μm indicated that with increasing grain size less muscovite was destroyed. In the size fractions less than 177 microns the amount of muscovite wreckage remaining after the fusion was less than five percent of the residue, the remaining 95 percent

Table 26. Effect of the fusion on the phyllosilicates (excluding montmorillonite).

Mineral	Size in μm	Starting Weight	% Remaining	Composition of Residue
Muscovite #1	250-177	1.0 grams	6.8	Muscovite wreckage + Quartz
	177-125	1.0 grams	6.2	Muscovite wreckage + Quartz
	177-125	1.0 grams	2.5	Muscovite wreckage + Quartz
	125-74	1.0 grams	1.8	Muscovite wreckage + Quartz
Muscovite #2	250-210	1.0 grams	12	Muscovite wreckage + Quartz
	149-125	1.0 grams	4.4	Muscovite wreckage + Quartz
	74-62	1.0 grams	1.5	Quartz
			1.7	Quartz
			.9	Quartz
Muscovite #3	74-62	1.1 grams	1.2	Quartz
	74-62	2.1 grams	1.3	Quartz
	74-62	2.6 grams	1.0	Quartz
Biotite	74-62	.9 grams	.9	Quartz
Kaolinite API #9	<177	1.2 grams	4.0	Quartz
Beavers Bend Illite	<177	1.0 grams	16.2	Quartz
Beavers Bend Illite (<1 μm)	<177	2.0 grams	.4	Quartz
Morris Illite	<177	1.0 grams	17.7	Quartz

Table 27. Effect of the fusion on montmorillonite.

Mineral*	Starting Weight	% Remaining	Composition of Residue
API #26	1.2	13.4	Feldspar Quartz
API #26	1.2	12.8	Feldspar Quartz
API #26	1.0	13.7	Feldspar Quartz
W-14-B	.5	2.8	Quartz Feldspar
W-14-B	1.0	2.1	Quartz Feldspar
W-14-B	2.0	2.7	Quartz Feldspar
W-14-B	3.0	2.1	Quartz Feldspar
Baroid (Wyo. Bentonite)	1.0	.3	Quartz Feldspar
API #23	2.0	6.0	Feldspar Quartz

* All samples were ground to less than 177 μm (80 mesh)

being composed of quartz and traces of feldspar (percentages are based on petrographic visual estimates from grain mounts).

Size of the material fused is an important factor in the effectiveness of the fusions. Therefore, to insure complete destruction the mudrocks were carefully disaggregated until only quartz and feldspar remained on a 177 micron sieve. This quartz and feldspar was then added to the rest of the sample which had passed through the sieve. Careful disaggregation was necessary because we were also studying the size distribution of quartz and feldspar and some mudrocks contain quartz and feldspar coarser than 177 microns. If the size distribution will not be determined, the sample can be ground until all material passes through the 177 micron sieve. The 177 micron size was chosen for the following reasons:

1. Illites, kaolinites and montmorillonites finer than 177 microns are completely destroyed by the fusion (see tables 3 and 4).
2. Only very small amounts (much less than 1% of the initial amount) of muscovite wreckage remain after fusing muscovite finer than 177 microns. Muscovite is rare in mudrocks and therefore the error introduced here is certainly of no importance.
3. This is a convenient size to work with because it is relatively coarse and reduces the amount of disaggregation or grinding prior to fusing.

Effects of the Bisulfate Fusion on Quartz and Feldspars

The effect of the fusion on pure quartz samples as a function of size is shown in table 3 of text. When the 2-1 micron fraction containing only quartz is filtered significant amounts of material can be seen to pass through the filter. Therefore, most of the quartz losses during fusions are thought to be largely mechanical rather than chemical. When processing natural samples this mechanical loss is reduced due to the following effects.

1. The fine fractions are held in the fused clay wreckage while being filtered after the acid treatment.
2. The presence of larger grains in natural samples tends to block the larger holes in the filter.
3. During the NaOH treatment quartz and feldspar grains flocculate, therefore increasing their effective size. These floccules will not pass through the filter paper.

Chemical analyses of the 2-1 mμ quartz before and after the fusion show no significant changes; thus indicating that the numerous washings are effective in removing any absorbed cations.

To determine the effect of the fusion on the amount and composition of feldspars, five different types of feldspars were size fractionated and then each size fraction was fused and chemically analyzed according to the methods outlined previously. The types of feldspars used were microcline (74% K_2O, 26% Na_2O), albite (Ab 91%, An 9%), oligoclase (Ab 22%, An 78%), andesine (Ab 52%, An 48%), and bytownite (Ab 26%, An 74%). The microcline, albite, and oligoclase contained

minor amounts of quartz (generally less than 5%) which could not be removed. The andesine contained a heavy mineral which was removed with heavy liquids.

The results of the feldspar fusions are given in tables 28 and table 2 of text. These results show that the effect of the fusion on the feldspars is very dependent on the size and composition of the feldspars. Also, all of the feldspars gained sodium during the fusion. This is particularly evident for the potassium feldspars. The correction factors given in table 28 are the factors which are needed to correct for the effects of the fusion. If there were no effect, the conversion factor would be equal to 1.0. The correction factors were calculated as follows:

$$Ce = \left(\frac{e_b}{e_a F}\right) \cdot 100$$

where

Ce = correction factor for element e

e_b = element concentration before fusion

e_a = element concentration after fusion

F = percent feldspar remaining after fusion

and

$$Y = \frac{Na_a - Na_b}{K_b}$$

where

Y = correction factor for sodium uptake during fusion of potassium feldspar

Na_b = sodium concentration before fusion

Na_a = sodium concentration after fusion

K_b = potassium concentration before fusion

Table 28. Correction factors for various feldspars.

Mineral	Size Range in Microns	% loss or gain of element due to the fusion			Conversion Factors			
		Ca	K	Na	Ca	K	Na	Y
Orthoclase	61-43	-	1.3	5.0	-	1.04	.98	.010
	43-30	-	1.3	6.2	-	1.04	.99	.013
	30-20	-	-4.6	12.1	-	1.10	.94	.026
	20-10	-	-14.2	6.9	-	1.22	.98	.015
	10- 4	-	-5.2	15.4	-	1.11	.91	.034
	4- 1	-	-25.0	42.1	-	1.62	.86	.096
Albite	61-43	8.4	-	5.0	.97	-	1.01	-
	43-30	5.0	-	6.3	1.01	-	6.00	-
	30-20	16.52	-	7.6	.95	-	.98	-
	20-10	3.9	-	8.0	1.00	-	.96	-
	10- 4	7.2	-	6.3	1.05	-	1.06	-
	4- 1	7.8	-	9.6	1.12	-	1.10	-
Oligoclase	61-43	4.1	-	4.6	1.00	-	.99	-
	43-30	.2	-	3.7	1.06	-	1.02	-
	30-20	4.4	-	2.5	1.01	-	1.03	-
	20-10	1.9	-	4.1	1.10	-	1.07	-
	10- 4	4.3	-	3.9	1.04	-	1.05	-
	4- 1	6.2	-	0.7	1.13	-	1.08	-
Andesine	61-43	-.9	-	-.3	1.14	-	1.14	-
	43-30	3.3	-	6.6	1.13	-	1.09	-
	30-20	5.6	-	7.0	1.13	-	1.10	-
	20-10	3.7	-	7.3	1.25	-	1.21	-
	10- 4	10.9	-	13.4	1.21	-	1.18	-
	4- 1	15.2	-	20.9	1.31	-	1.25	-
Bytownite	61-43	-9.8	-	-12.0	1.45	-	1.48	-
	43-30	-8.6	-	4.1	1.64	-	1.44	-
	30-20	-4.5	-	4.8	1.66	-	1.52	-
	20- 4	-72.3	-	132.3	16.13	-	1.92	-
	4-.2	-66.9	-	70.1	16.24	-	3.16	-

The correction factors can be applied to correct the feldspars for the effect of the fusion by using the following formuli:

For potassium feldspars

$$K_a = K \cdot C_K$$

For plagioclase feldspars

$$Ca_a = Ca \cdot C_{Ca}$$

$$Na_a = (Na - (Y \cdot K_a)) \cdot C_{Na}$$

where

K_a, Ca_a, and Na_a are the concentration of K, Ca, and Na which have been adjusted for the effects of the fusions.

K, Ca, and Na are the concentrations of K, Ca, and Na found in the fused residue.

C_K, C_{Ca} and C_{Na} are the correction factors for their respective elements.

Y is the correction factor needed to adjust the sodium values for the sodium uptake in the potassium feldspars.

In table 29 the results from Kiely and Jackson's (1965) techniques are given for comparison to those shown in table 28. Comparison of the data in these tables shows little difference in the correction factors. Because these data and the data previously discussed are so similar to the data of Kiely and Jackson (1964) (1965), further testing of the technique for its effect on other minerals was not deemed necessary and are assumed to be similar to those of Kiely and Jackson. The only exception to this is cristobalite which is completely destroyed using our technique.

Table 29. Summary of the effect of the fusion on feldspars as found by Kiely and Jackson (1965).

Mineral	Size Range in Microns	% Retained in Fusion	% loss or gain of element due to the fusion			Conversion Factors			
			Ca	K	Na	Ca	K	Na	Y
Microcline	2000-5000	97.5	-	0.0	0.0	-	1.03	1.03	0.00
(87% Kspar,	500- 50	96.5	-	0.0	0.0	-	1.04	1.04	0.00
13% Na-	50- 20	96.0	-	0.0	13.3	-	1.04	.92	0.02
plagio-	20- 5	93.6	-	2.9	23.5	-	1.10	.86	0.04
clase)	5- 2	84.4	-	3.9	70.0	-	1.23	.69	0.14
	2- 0.2	64.0	-	9.6	105.0	-	1.72	.76	0.25
Oligoclase	500- 50	95.2	0.0	-1.4	0.0	1.05	1.06	1.05	
(Ab 81%,	50- 20	94.5	0.0	-1.4	0.0	1.06	1.07	1.06	
An 19%)	20- 5	92.7	0.0	-5.3	0.0	1.08	1.12	1.08	
	5- 2	86.2	0.0	17.6	0.0	1.16	1.40	1.16	
	2- 0.2	68.3	0.0	-45.0	0.0	1.46	2.65	1.46	
Labradorite	500- 200	93.7	-10.6	-17.5	9.3	1.19	1.29	.976	
(Ab 48%,	200- 50	93.6	-11.7	-19.3	9.3	1.21	1.32	.977	
An 52%)	50- 20	90.9	-12.6	-27.8	8.0	1.26	1.52	1.02	
	20- 5	77.4	-22.0	-30.5	5.9	1.65	1.86	1.22	
	5- 2	41.9	-32.6	-37.3	5.1	3.54	3.81	2.27	
	2- 0.2	16.4	-	-51.0	14.2	-	12.4	5.34	
Bytownite	500- 50	81.3	-10.7	16.6	-17.8	1.37	1.05	1.50	
(Ab 25%,	50- 20	55.9	-16.5	9.1	-22.3	2.14	1.64	2.30	
An 75%)	20- 5	33.8	-28.2	30.0	-25.0	4.12	2.12	3.94	
	5- 2	2.1	-	-	-	-	-	-	
	2- 0.2	1.0	-	-	-	-	-	-	

Reproducibility of Quartz and Feldspar Determinations

To determine the reproducibility of this technique duplicates of four samples were rerun three times each through the whole procedure. A fifth sample was rerun four times through the whole procedure and two additional samples were fused once but analyzed with the atomic absorption unit 5 separate times. In one sample (RB-8) chemical analyses were run three times on the fused material from one fusion. The results of these analyses are given in table 30. As can be seen from table 14 the quartz values determined by this technique are generally reproducible to within 5% of the amount present at one standard deviation.

The variations in feldspar are largely controlled by the amount of feldspars present and the size of the quartz plus feldspar fraction. For example the mean grain size of RB-8 and RB-5 is nearly twice as large as for P-279 and P-318. The Ca and K concentrations found in samples P-279 and P-318 are just barely above their detection levels for the method of chemical analysis used.

The reproducibility of the total feldspar concentrations at one standard deviation is considered to be within 20% of the amount present when the feldspars represent less than 20% of the quartz plus feldspar fraction and 10% when they represent more than 20% of quartz plus feldspar fraction.

Application of Correction Factors

In order to correct for the effects of the fusion on the feldspars the size and composition should be known. The composition of the

Table 30. Summary of reproducibility determinations.

Q = Quartz, O = Orthoclase, Ab = Albite, An = Anorthite, and TF = Total Feldspar.

Sample Number		% remaining after fusion	Q	O	Ab	An	TF	Mean Size Q+TF
RB5*	1	41.6	63.8	11.1	23.6	1.5	36.2	10.26μm
	2	41.4	65.1	10.9	22.6	1.5	34.8	
	3	40.9	66.4	10.2	22.0	1.5	33.7	
$\bar{x}$		41.3	65.1	10.7	22.7	1.5	34.9	
σ		0.4	1.3	0.5	0.8	0.0	1.3	
$\sigma_{\bar{x}}$***		0.9	2.0	4.4	3.6	0.0	3.6	
RB8	1a**	37.4	60.3	9.0	26.6	4.1	39.7	9.06μm
	1b**	-	60.6	8.9	26.1	4.4	39.4	
	1c**	-	59.7	9.0	27.1	4.2	40.3	
	2*	38.2	64.7	8.8	22.6	3.9	35.3	
	3*	37.1	60.6	8.7	26.9	3.8	39.4	
$\bar{x}$		37.5	61.2	8.9	25.9	4.1	38.8	
σ		0.6	2.0	0.1	1.9	0.2	2.0	
$\sigma_{\bar{x}}$		1.5	3.3	1.5	7.2	5.8	5.2	
P279*	1	15.0	73.1	9.2	16.7	1.1	26.9	2.64μm
	2	12.7	82.5	4.8	12.0	0.7	17.5	
	3	13.5	76.4	6.6	15.6	1.3	23.6	
$\bar{x}$		13.7	77.3	6.9	14.8	1.0	22.7	
σ		1.2	4.8	2.2	2.5	0.3	4.8	
$\sigma_{\bar{x}}$		8.8	6.2	32.0	16.6	30.6	21.1	
P318*	1	25.3	87.8	0.3	11.7	0.2	12.2	5.17μm
	2	27.4	87.3	0.9	11.5	0.3	12.7	
	3	26.3	84.7	0.6	14.4	0.3	15.3	
$\bar{x}$		26.3	86.6	0.6	12.5	0.3	13.4	
σ		1.1	1.7	0.3	1.6	0.06	1.7	
$\sigma_{\bar{x}}$		4.0	1.9	50.0	13.0	19.2	12.7	
3-a*		-	80.1	8.7	10.3	0.9	19.9	90.3μm
b		-	79.9	8.7	11.1	0.2	20.1	
c		-	81.5	8.2	9.9	0.4	18.5	
d		-	81.9	8.2	9.6	0.4	18.1	
e		-	81.6	8.6	9.4	0.4	18.4	
f		-	81.7	8.5	9.3	0.5	18.3	
$\bar{x}$		-	81.1	8.5	9.9	0.4	18.9	
σ		-	0.9	0.2	0.7	0.3	0.9	
$\sigma_{\bar{x}}$		-	1.1	2.6	7.0	80.4	4.6	

Sample Number	% remaining after fusion	Q	O	Ab	An	TF	Mean Size Q+TF
4-1**	40.7	71.8	9.8	17.3	1.0	28.2	21.8μm
2	42.7	73.2	10.6	15.4	0.7	26.8	
3	41.6	75.2	9.7	14.6	0.5	24.9	
4	43.4	71.9	9.1	15.3	0.7	25.1	
$\bar{x}$	42.1	73.0	9.8	15.7	0.7	26.3	
σ	1.2	1.6	0.6	1.2	0.2	1.6	
$\sigma_{\bar{x}}$	2.8	2.2	6.3	7.4	29.4	5.9	
5-a *	-	79.5	8.3	11.1	1.1	20.5	82.4μm
b	-	79.4	8.7	11.9	0.03	20.6	
c	-	81.1	8.3	10.3	0.3	18.9	
d	-	82.6	8.2	8.9	0.3	17.4	
e	-	81.6	8.1	10.0	0.3	18.4	
f	-	81.9	8.1	9.7	0.4	18.1	
$\bar{x}$	-	81.0	8.3	10.3	0.4	19.0	
σ	-	1.3	0.6	1.1	0.3	1.3	
$\sigma_{\bar{x}}$	-	1.6	6.8	10.2	82.0	6.9	

* Different fusions and different atomic absorption analyses. Percentages are of the quartz plus feldspar fraction.

** Single fusions, separate atomic absorption analyses. Percentages are of the quartz plus feldspar fraction.

*** $\sigma_{\bar{x}} = (\frac{\sigma}{\bar{x}}) \times 100$

NOTE: Samples 3,4,and 5 are samples analyzed by R. G. Charles.

feldspars can be estimated from the results of the chemical analysis. However, it is not practical to size the samples into the size fractions used in table 28. Therefore, the mean size of the quartz plus feldspar fraction for each sample was used as the guide in selecting the correction factors. For the samples analyzed in this study petrographic observations indicated that the plagioclases were all either albite or oligoclase, therefore for the Ca and Na corrections, the average of the correction factors for these two plagioclases was used. A computer program was written to convert the raw atomic absorption data into percentages of quartz and normative feldspars. This program also makes the corrections discussed above. Quartz values are determined by the difference between the starting weight of quartz plus feldspar concentrate chemically analyzed and the calculated normative feldspar weights.

Effect of the Fusion on the Size Distribution of the Quartz Plus Feldspar Fraction

The fusion technique affects the size distribution of the quartz plus feldspar fraction of the sample. The question of how much the grain size distribution is affected is difficult to determine. This is because fusions of artificial mixtures do not filter in the same manner as natural samples (see earlier discussion of the effect of the fusion on quartz), and also because it is very difficult to match the size distribution and composition of artificial mixtures to those of the natural samples being analyzed.

Despite these problems an attempt was made to determine the effect

of the fusion on the grain size distribution of a quartz powder. Three size distributions were run on the powder. Then three artificial muds were formed by combining 65% Beaver's Bend illite with 35% of this quartz powder. The illite was all less than 1 μm to prevent the addition of quartz impurities. These three muds were fused as described above and then their size distributions were determined using the settling tube. Quartz recovery for these fusions ranged from 100.89% to 100.28%. The recovery values of greater than 100% are due to quartz within the illite. A fusion of just the illite showed it to contain .38% quartz. As shown in table 31 the fusion has no significant effect on the size distribution.

Table 31. Comparison of size distribution statistics for standard quartz before and after bisulfate fusion with Beaver's Bend illite.

Non-Fused Samples	Mean	Standard Deviation	Skewness	Kurtosis
1	6.37	1.36	.2408	.9031
2	6.35	1.26	.2336	.9428
3	6.19	1.34	.2370	.7989
mean =	6.30	1.32	.2371	.8816
Fused Samples				
1	6.32	1.32	.2540	.9576
2	6.30	1.44	.2641	1.2345
3	6.31	1.35	.2650	.9462
mean =	6.31	1.37	.2610	1.0461

Summary of tests comparing these data to test for the effects of the fusion on the size distribution of a sample.

Size Statistic	t	P	Conclusion
Mean	.172	.15	No significant difference, therefore the fusion does not influence the mean.
Standard Deviation	1.056	.70	No significant difference.
Kurtosis	1.589	.80	No significant difference.
Skewness	5.215	.99	A significant difference statistically. The fusion causes the size distribution to become more finely skewed. However, the magnitude of the change (.024) is of questionable geologic significance.

APPENDIX VIII

METHOD OF SIZE ANALYSIS OF THE QUARTZ AND FELDSPAR FRACTION

Size analysis of the quartz and feldspar fraction of the samples was made using different methods to obtain data for both coarse and fine grain sizes.

The grain size of the coarse fraction (greater than 43 μ) was determined using the following procedure:

I. Grind approximately 50 grams of sample using a rotary grinder. Weigh. (The jaws of the rotary grinder are set 1 mm apart to prevent the grinding of particles finer than 1 mm.)

II. Mix with distilled water and disaggregate for 5 minutes using a Bronson ultrasonic disaggregator.

III. Wet sieve to remove all grains less than 43 μ.

IV. Repeat steps II and III until the sample is completely disaggregated. If the sample does not disaggregate, boil it for 15 minutes in .5 N NaOH and 5 minutes in 1.0 N HCl and repeat steps II and III.

V. Remove remaining clay minerals and phyllosilicates using the methods given in Appendix

VI. Wet sieve to remove any grains less than 43 u.

VII. Dry and weigh.

VIII. Sieve using 3 inch standard sieve with the following meshes: 35, 60, 120, and 230.

IX. Weigh each sieve fraction.

The results of this procedure give the data necessary to calculate the percentage of the whole rock that is quartz and feldspar in each of the size fractions.

The fine grain sizes were determined using the following procedure:

I. Grind two grams of sample to 80 mesh and weigh.

II. Fuse the sample to remove all minerals except quartz and feldspar using the methods given in Appendix VII.

III. Weigh the sample.

IV. Determine the size distribution of the fine grain sizes using the settling tube method explained in Appendix IX.

The data collected using the settling tube were then combined with data collected from the material coarser than 43 μ and the size distribution of the sediment was calculated using a computer program. The computer program calculates the size distribution of the less than 43 μ fraction, and then adds the coarser size fractions and calculates the size distribution of the whole sample. The grain size statistics were calculated using the graphic method used by Folk and Ward (1957).

APPENDIX IX

THEORY AND OPERATION OF THE PHOTO-ELECTRIC SETTLING TUBE

The photo-electric settling tube apparatus works on the principal of gravitational settling. A light meter is used to determine the amount of sediment which has settled as a function of time. A photo-electric settling tube apparatus was used for this study for two reasons: 1) Size determinations can be made on less than .1 gram of sediment; 2) It is inexpensive to build and operate.

Theory of the Photo-Electric Settling Tube Apparatus

The determination of sediment concentration as a function of time is based upon changes in the photo-extinction of light as a result of changing sediment concentration. As light is passed through a water-sediment mixture, the light is absorbed and reflected by the sediment. This absorption is a function of both concentration and particle size. The relationship between absorption, concentration and particle size is given in the following expression (Rose, 1952).

$$\log_e \frac{I_0}{I_2} - \log_e \frac{I_0}{I} = \frac{}{4}\ Cl\ \frac{d_2}{d_1}\ K_{e_x}\ n \cdot d_x^2 \quad \text{...equation 1}$$

where C is the concentration of the sediment in the suspension in g./c.c., l the length of the light path through the suspension, n the number of particles of size d_x per g. of powder, K_{e_x} the extinction coefficient for a particle of size d_x, d_1, d_2 the lower and upper limits respectively of particle size of the sample in the beam, I_0 the incident light intensity and I_2 and I_1 the intensity of the emergent beam when material of size from zero to diameter d_2 and d_1 respectively is in the beam.

Maximum accuracy is achieved when the particles of sediment are spherical or have the same cross sectional area. For the quartz-feldspar sediments analyzed in this study this is a reasonable assumption.

The extinction coefficient (Ke) is the ratio of light obscured by a particle to the light which would be obscured if the square law of geometrical optics held for the particles under consideration. Deviations from the square law of geometrical optics increase as the wavelength of the light being used approaches the size of the particle obscuring the light (Rose, 1952). Therefore deviations from the square law of geometrical optics increase with decreasing grain size and the extinction coefficient changes as a function of grain size and the optics of the settling tube apparatus.

Apparatus Design

The settling tube is a graduated cylinder located in a rectangular-shaped water bath. The settling tube and water bath are located in an optical system. All of these components are located in a lightproof

plywood box. A schematic of the two settling tubes used in this study is shown in figure 47.

The optical system consists of a light source, two convex lenses, a series of slits and a photo-cell. The light source is a 6 volt light bulb powered by a constant potential power source. The first lens is used to produce a parallel light beam. The second lens focuses the light beam on the surface of the photo-cell. Four slits are used to collimate the light beam. Two slits were located in front and two behind the optical center of the settling tube, the location and size of these slits are as follows: (positive direction is towards the light source) tube #1 +41.5 cm, +9.2 cm, -9.2 cm, and -18.5 cm; tube #2 +9.2 cm, +41.9 cm, -9.2 cm, -41.9 cm. The slit for tube #1 located nearest to the light source was 1.1 mm by 3.2 cm; the remaining slits were .64 mm by 3.2 cm. Slit dimensions for tube #2 are all 4.0 cm by .64 mm.

The photo-cell is a cadmium sulfide cell. The cell is also powered by the constant potential power supply. The resistance from the photo-cell is converted to a voltage by a Wheatstone bridge, this voltage is recorded on a Siemans recording potentiometer.

Testing and Calibration of the Apparatus

Before using the settling tubes for determining size distributions, they were tested and calibrated. I tested and calibrated tube #1, while R. G. Charles calibrated tube #2. The following tests were made to insure that the optical system was functioning properly:

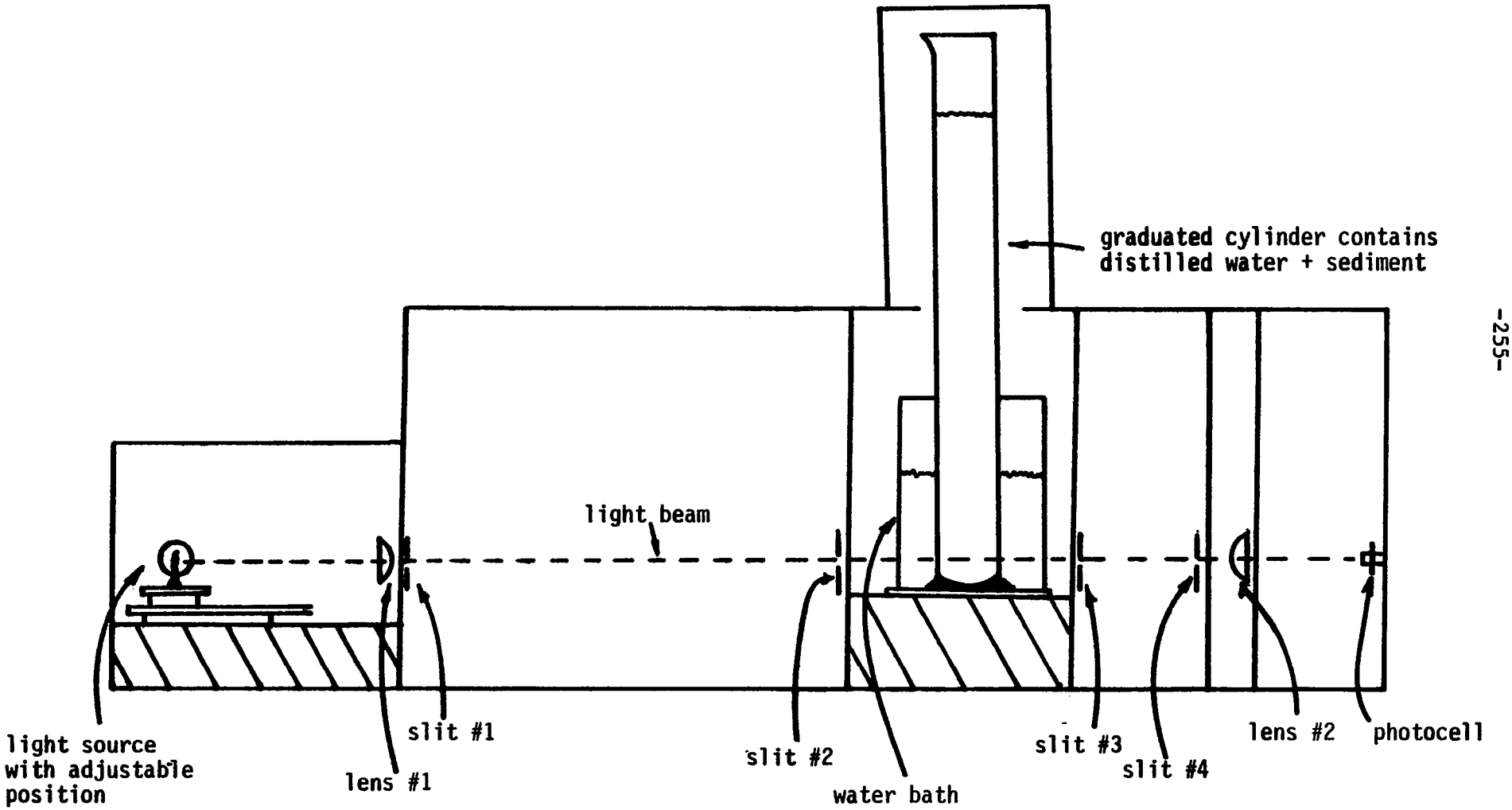

Fig. 47. illustration of the basic design of the settling tubes used in this study.

1. Constant light intensity (Io).
2. Minimum fatigue of the photo-cell.
3. A linear relationship exists between concentration and absorption ($\ln \frac{I_o}{I_1}$).

The tests showed that the variation of the initial intensity (Io) remained within $\pm$2.5% of the original setting for lengths of time up to 48 hours. Since intensity is related to concentration as a logarithmic function, this variation does not appreciably affect the accuracy of the size distributions.

The photo-cell shows some fatigue when the light source is first turned on, but the amount of fatigue decreases with time. For this reason th- light source is left on continuously so that fatigue of the photo-cell does not cause any appreciable error.

Tests also showed that the relationship between concentration and absorption is linear for at least three orders of magnitude ($\ln \frac{Io}{I}$ between 0 and 3).

In order to correctly evaluate the size distribution of a sediment using this apparatus, the extinction coefficients for the optical system of the apparatus must be determined. In order to determine the extinction coefficients a series of narrowly sized sediments were needed. These sediments were obtained by crushing vein quartz and then sizing the quartz. Particle-size separations were made using the method of Kerns (1967) which is based on the differential settling velocities of grains in water as a function of size. The size fractions used are given in table 32. The size distributions of each of these fractions

Table 32. Results of the determination of Ke_x for tube #1 by successive approximations. All size data are given in microns

PARTICLE SIZE RANGE	APPROXIMATION NUMBER						
	1		2		3		4
	Mean Size	Ke_x	Mean Size	Ke_x	Mean Size	Ke_x	Mean Size
62-43	43.7	2.14	43.9	2.17	44.0	2.17	44.0
43.0-31.0	33.4	2.26	33.7	2.28	33.6	2.28	33.6
31.0-16.0	20.8	2.31	20.3	2.32	20.3	2.33	20.3
16.0- 8.0	11.2	2.38	10.7	2.43	11.4	2.41	11.4
8.0- 4.0	6.48	2.74	6.62	2.80	6.62	2.80	6.62
4.0- 2.0	2.89	2.95	2.86	2.94	2.88	2.96	2.88
2.0- 1.0	1.55	2.63	1.44	2.57	1.47	2.45	1.47
1.5- .5	1.36	2.13	.98	1.51	1.03	1.51	1.01
1.0- .5	.95	.96	.63	.64	.69	.69	.62
<.5	.50	.38	.40	.38	.40	.38	.40

Table 33. Determination of Ke_x for tube #2 using the same sediments as in tube #1. Calibration by Charles.

PARTICLE SIZE RANGE (microns)	Mean Size (microns)	Ke_x
62-43	44.0	1.90
43.0-31.0	33.6	2.02
31.0-16.0	20.3	2.28
16.0- 8.0	11.4	2.30
8.0- 4.0	6.62	2.88
4.0- 2.0	2.88	2.91
2.0- 1.0	1.47	2.29
1.5- .5	1.01	1.51
1.0- .5	.62	.62
<.5	.40	.35

were then determined using the settling tube apparatus. The size distributions were calculated using equation 1 with Ke_x equal to unity. For these narrowly sized sediments using a value of unity for Ke_x will not greatly affect the size distributions because the Ke_x varies only slightly over the range of particle sizes found in these sediments. After determining the mean size of the sediment, suspensions of known concentration were made and the absorption of light in these suspensions was determined using the settling tube apparatus. The extinction coefficient for these different grain sizes was determined by solving equation 1 for Ke_x. Because the mean sizes used to calculate Ke_x were obtained using equation 1 and Ke_x equal to 1.0, these size distributions were inaccurate. Therefore, the size distributions were recalculated and then the new values were used to recalculate Ke_x. This method of repeated approximation was done until there was no significant difference between two iterations. Table 32 indicates the results of this procedure. In calibrating tube number 2 the iteration procedure was not necessary because the mean size of each standard quartz powder was known from the calibration of tube number 1. Table 33 lists the calibration constants for tube 2.

Operational Procedures

The following is an outline of the sequence of steps used when obtaining data from the settling tube.

I. Adjust Power Supply*

A. Fill the settling tube with 100 ml of distilled water.

* Power supply must be on for 24 hours before adjustments can be made.

B. Adjust the constant potential power supply to obtain a reading of 2.0 volts from the photo-cell. (Two volts was selected for convenience only, other voltages can be used.)

II. Preparation of Sample

A. Place .1 to .2 grams of fused sediment in a 250 ml beaker with 100 ml of distilled water.

B. Ultrasonically disperse sediment-water mixture for 5 minutes using the Bronson Sonifier. (Use the highest energy settings of the Sonifier.)

C. Cool sediment-water mixture to near room temperature.

III. Operation of the Settling Tube Apparatus

A. Record room temperature.

B. Record voltage from the photo-cell (this is the initial voltage and should be 2.0 V).

C. Pour the sediment-water mixture into the settling tube. Wash any sediment remaining in the beaker into the settling tube using a wash bottle filled with distilled water.

D. Fill the settling tube to 1000 ml with distilled water.

E. Using the plastic stirring rod, mix the sediment-water mixture for 90 seconds.*

F. Raise the plastic stirring rod and read the voltage from the settling tube. If the voltage is between .1 and

* The plastic stirring rod is turned by a drill. The drill speed is controlled by a rheostat set at 40 V.

.005, continue; if not, start over using either more sediment (voltage greater than .1 V) or less sediment (voltage less than .1 V).

G. Remix and record the voltage from the photo-cell using the recording potentiometer for the next 1.5 hours. The following potentiometer chart speeds are used: first 10 minutes 1 cm/minute, then .1 cm/minute.

H. Remix the sediment-water mixture. After the mixture has been mixed for 90 seconds siphon the water-sediment mixture down to approximately 350 ml.

I. Record the voltage using the recording potentiometer for the next 24 to 30 hours. The following chart speeds are used: first 2 hours .1 cm/min., then 1 cm/hr.

J. Remove settling tube and read the sediment-water volume.

K. Read the voltage records for the voltage at the following times and volumes of the water-sediment mixture. Other times may also be read.

Time	Fall Distance	Volume of Water-Sediment Mixture	Approximate Size
3 min.	3.5 cm	1000 ml	4.5Ø
5 "	"	"	5.0
10 "	"	"	5.5
25 "	"	"	6.0
45 "	"	"	6.5
90 "	"	"	7.0
45 "	10 cm	350 ml	7.5
90 "	"	"	8.0
3 hrs.	"	"	8.5
6 "	"	"	9.0
12 "	"	"	9.5
24 "	"	"	10.0
>24 "	"	"	

Some samples which are coarse grained require a slightly different procedure. For these samples a large amount of material (greater than the amount available from one fusion) is needed to produce the proper starting opacity in 1000 mls of distilled water. Consequently, some changes in the procedure described above were made, these are:

1. 600 mls was used as the initial volume of sediment-water mixture.
2. The chart speeds were 2 cm/minute for the first hour, then 2 cm/hour for the remaining 53 hours.
3. No changes in the sediment-water mixture volume are made.
4. Since the fall distances are different, the voltages are read from the chart paper at different time, these are:

Time	Fall Distance	Volume of Water-Sediment Mixture	Approximate Size
1.5 min.	20 cm	600 ml	4.5ø
3 "			5.0
6 "			5.5
13 "			6.0
25.5 "			6.5
51 "			7.0
1.5 hrs.			7.5
3.5 "			8.0
6.5 "			8.5
13 "			9.0
26.5 "			9.5
54 "			10.0

The data from the settling tube was then processed using a computer program to solve equation #1 and determine the size distribution of the sediment.

Accuracy of the Photo-Extinction Settling Tube

The accuracy of the settling tube was tested by comparing the size distribution obtained using the settling tube and the size distribution obtained by pipette analysis using the methods of Folk (1968). There is no significant difference between the two methods, nor between the two tubes.

APPENDIX X

A RE-EVALUATION OF THE USE OF OXYGEN ISOTOPE DATA TO INTERPRET THE PETROGENETIC HISTORY OF THE PIERRE SHALE

Recently there have been many studies using the oxygen isotope composition of mudrock to interpret the petrogenetic histories of both modern and ancient mudrock units. Of particular interest to this study are the studies by Sridhar et al. (1975) and Churchman et al. (1976). In these studies the results of the oxygen isotope analyses were used to interpret the provenance of the Pierre Shale. These studies interpreted the increasing ratio of $\delta^{18}O$ towards the center of the Pierre Seaway to show that a significant portion of the quartz in the Pierre Seaway was derived from volcanic quartz.

The purpose of this appendix is to show that the oxygen isotope data can be explained better as being derived from the existing (at the time) reservoir of quartz and that no significant authigenic and/or volcanic quartz source is needed to explain the quartz oxygen isotopes found in the Pierre Shale.

Churchman et al. (1976) based their conclusions on the results shown in Figure 48. This figure shows that there is a definite trend of increasing $\delta^{18}O$ with increasing distances away from the western shoreline (increasing distance from the shoreline is from left to right in Figure 48).

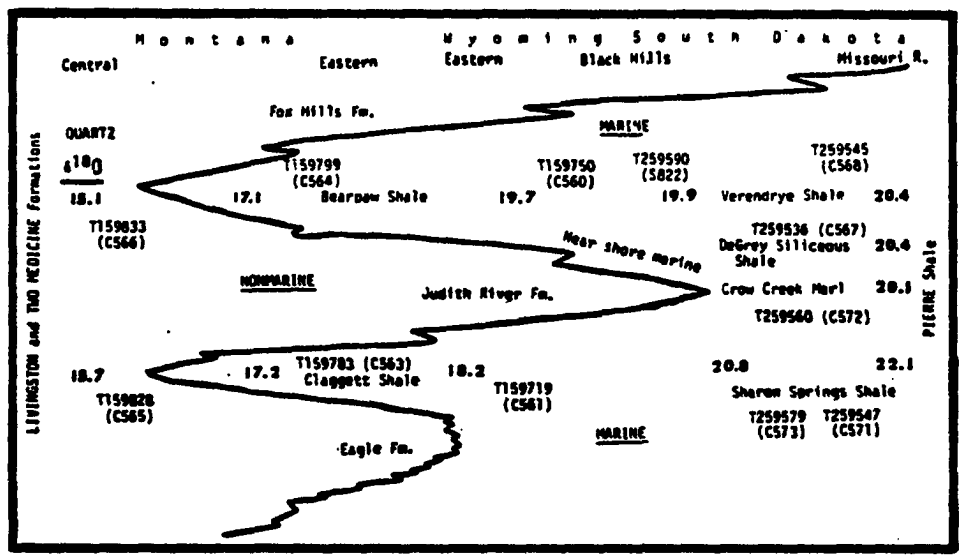

Fig. 48 Oxygen isotopic ratios of total quartz in relation to stratigraphy for the Pierre Shale and equivalent rocks. The stratigraphic relationships are after figure 2 of Tourtelot (1962). Modified from Churchman et al. (1976, figure 2).

This trend was interpreted by Churchman et al. (1976) as follows:

> The oxygen isotope ratios of quartz from the Pierre shale system increase with an increase in the distance from the western shoreline of the Cretaceous sea (Figure 49). The higher $\delta^{18}O$ values of quartz in shales from the central basin (further from the western shore) are attributable to a higher proportion of quartz derived from low-temperature sources such as chert formed from biogenic silica directly or in Paleozoic sediments eroded in from the east. The lower $\delta^{18}O$ values of quartz from the western shore samples reflect a higher proportion of quartz formed at high temperature, evidently derived by Cretaceous outwash from volcanic rocks of mountains to the west.

While the trend of increasing $\delta^{18}O$ with distance from shoreline does appear to be real; the provenance of the quartz is not the only variable likely to change. Perhaps the most likely variable to change is the size distribution of the quartz found in these sediments.

Many of the studies of oxygen isotopes of fine grained sediments (Clayton et al., 1972; Syers et al., 1969; Jackson et al., 1971; Churchman et al., 1976; Sridhar et al., 1975, 1978) have shown that the $\delta^{18}O$ compositions of the quartz are size dependent. To determine whether or not the size distribution of the quartz may have affected the results of Churchman et al. (1976), shown in Figure 48, the quartz size data given by Churchman et al. (1976) was compared to the $\delta^{18}O$ values obtained for these samples. The results of this comparison are shown in Figure 49. This figure shows that there is a remarkably good correlation between the size distribution of the whole quartz fraction (using the percentage of the quartz fraction greater than 10 microns as a measure of the size distribution of the whole quartz fraction) and the $\delta^{18}O$ composition of the 1-10 micron quartz fraction. While Churchman et al. (1976) acknowledged that there was some difference in

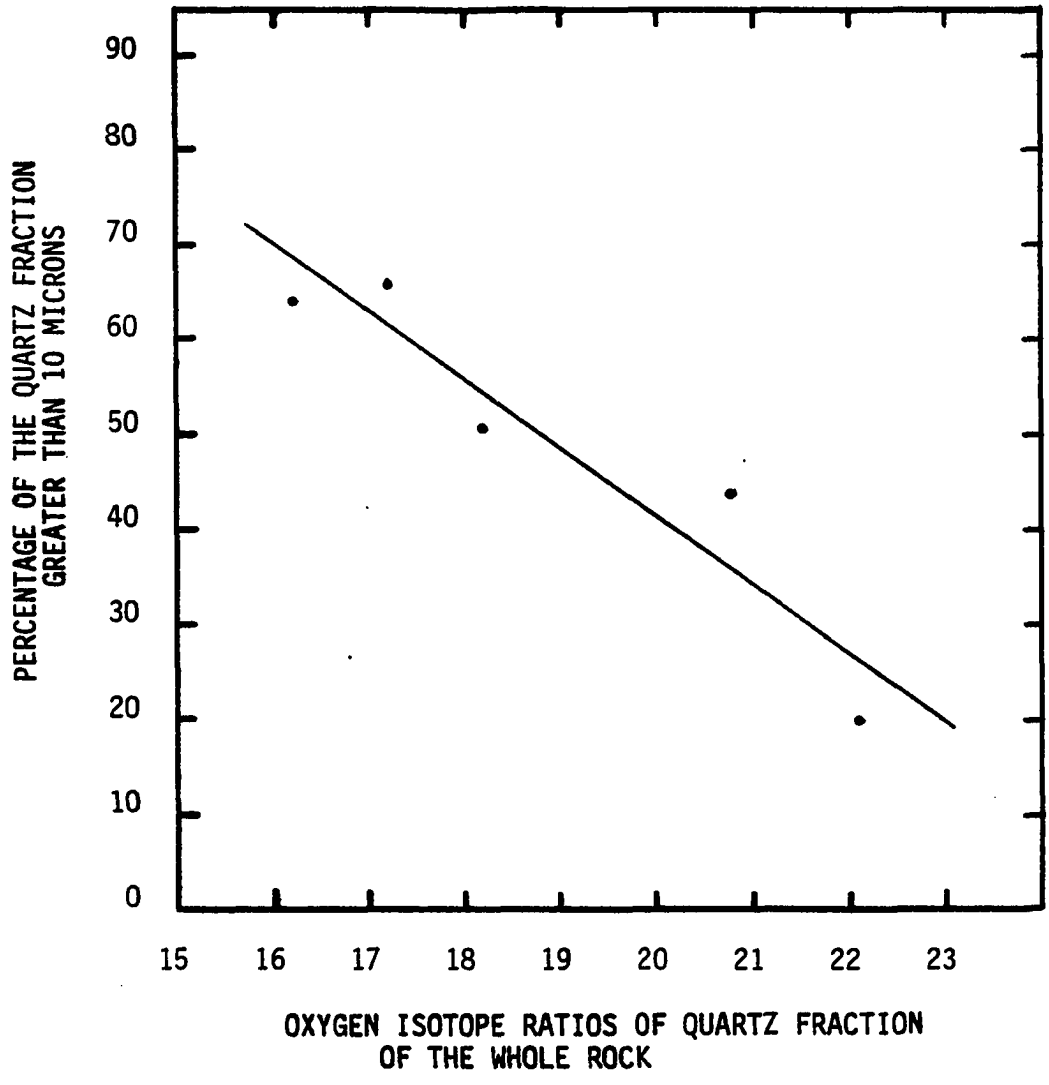

Fig. 49 A comparison of oxygen isotope ratios of the quartz fraction of the whole rock to fraction of five Pierre Shale samples to the percentage of the quartz found in this sample which is greater than 10 microns. Data from Churchman et al, 1976.

the size distribution of the quartz, he dismissed its relative importance to the $\delta^{18}O$ values with the following statement:

> The cumulative curves for quartz size distributions within a 1- to 10-μm range of two pelagic sediments (Clayton et al., 1972) and 11 high-elevation Hawaiian soils (Jackson et al., 1971) reveal considerable variation in particle size, yet the $\delta^{18}O$ values differ only by 0.3°/oo, which indicates a similar provenance of the quartz in these materials. However, while cumulative curves of the two Pierre shales are similar (divergence of only 10% at 4μm, their $\delta^{18}O$ values diverge 2.3°/oo; this difference relates to their different provenances (distance from the western shore.

In an earlier paper Sridhar et al. (1975) analyzed the 1-3.5, 3.5-7, and 7-10 micron fractions of two of the samples used by Churchman et al. (1975). These analyses showed that the quartz from the "near-shore" sample had significantly lower $\delta^{18}O$ than did the "central basin" sample. The $\delta^{18}O$ values obtained as a function of size are shown in Figure 50. As shown in this figure, the two sample trends are remarkably parallel although the intercepts are separated by a $\delta^{18}O$ value of 2.9. This difference in the $\delta^{18}O$ values for these two samples was then interpreted by Sridhar et al. (1975) as being due to a difference in the provenance of the quartz contained in the samples.

The difference in the isotopic composition of these two samples can, however, be interpreted as a function of their original quartz size distribution. The original quartz size distribution of these two samples was very different. The "near-shore" sample had a mean size much greater than 10 microns (66% of the quartz was greater than 10 microns) while the mean size of the "central basin" sample was between 1 and 10 microns (19% of the quartz was greater than 10 microns). This difference in the size distribution would cause the mean size of their size fractions to be skewed towards either the coarser or finer ends of the size fraction. For example, it is not impossible that the mean size of their 1 to 3.5 micron fractions

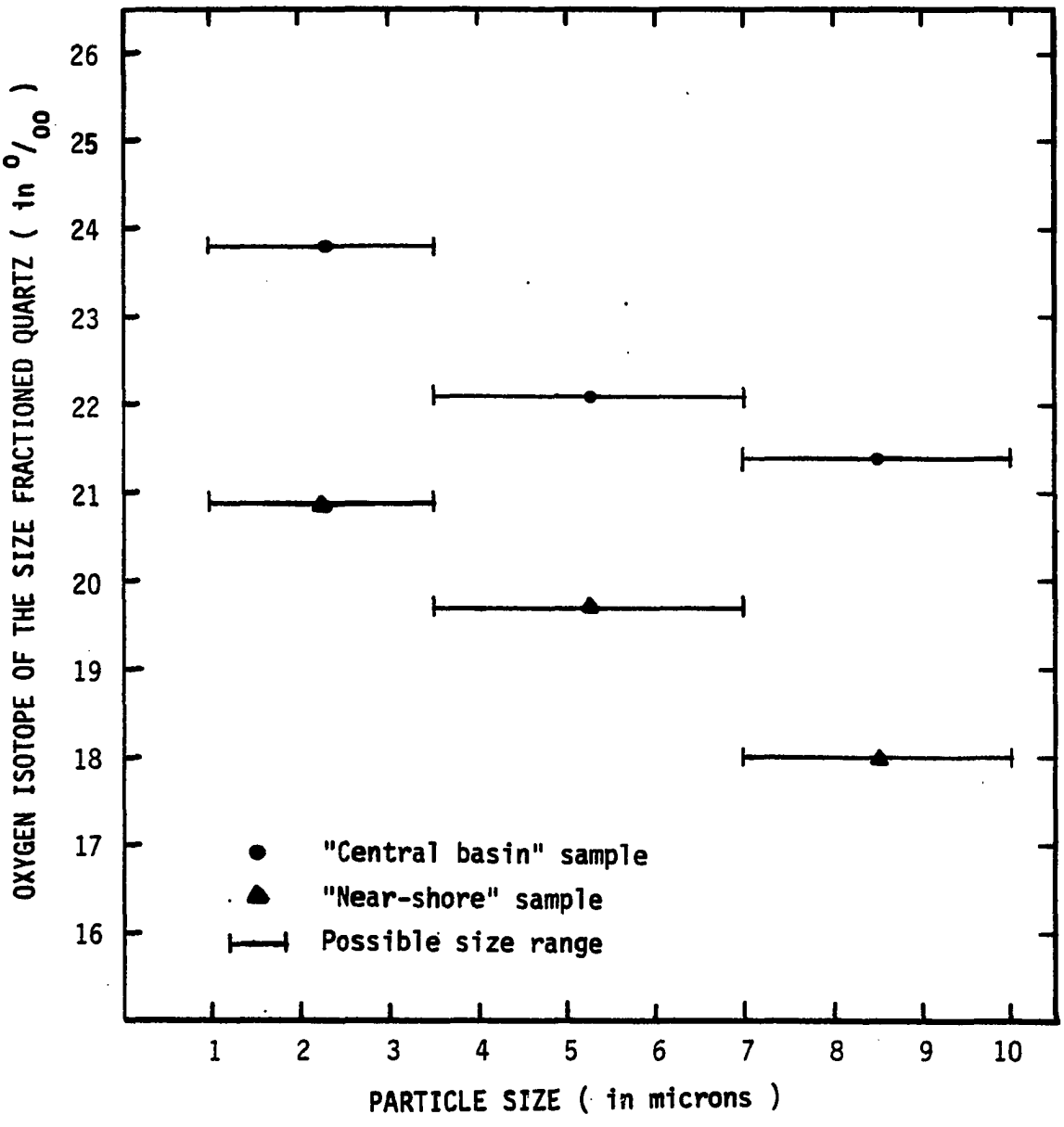

Fig. 50 Oxygen isotope ratios for size fractions of the quartz fraction of two Pierre Shale samples. Data is from Sridhar et al, 1975.

was 1.5 for the "central basin" sample and 3 for the "near-shore" sample. Sridhar et al. (1975) also noted that the "central basin" quartz concentrate contained many aggregates which they termed "chert clusters." These "chert clusters" are very likely aggregates of much finer quartz grains which were created during the isolation of the quartz from the shale.

Furthermore, the methods used to size fractionate these samples were inadequate. In working with montmorillonitic clays for size separations, it is imperative that the viscosity of clay-quartz suspension be controlled and monitored. If the viscosity is not controlled, extremely large errors in the particle size separates can and should be expected due to the difference in the particle fall velocities, which are a function of the viscosity of the suspension. No mention is made in the techniques section of the paper of any use of mechanical methods used to disperse the sample without which, based on my experiences with the Pierre shale, complete dispersal of the sample is not possible. Also in the technique given in the paper, during size separation only one decantation of the suspension was made. This will also cause the size analysis of the sample to be biased as only about half of the material finer than the indicated size will be removed.

Considering this defect in their techniques, I can see no compelling reason to believe that the results of Sridhar et al. (1975) are not the result of the variation in the oxygen isotope composition of quartz as a function of size.

The interpretation of Churchman et al. (1976) may also be challenged on the basis of the quartz content found in volcanic ashes. The work of Slaughter and Earley (1965) have shown that,at least in the Mowry Bentonites,

there is little, if any, quartz in the 10 to 1 micron size fraction. If we assume that the interpretation of Church et al. (1976) is correct, 13% of the quartz in the 10 to 1 μm fraction must be volcanic quartz. Since 15% of the average Pierre sample is quartz sized, between 1 and 10 μm, the volcanic ash would have to furnish two grams of quartz in this size fraction for every 100 grams of sample.

Assuming that the quartz content of the Mowry Bentonites can be used to estimate the average quartz content of volcanic ashes, the data of Slaughter and Earley may be used to estimate the volume of ash required to produce two grams of volcanic ash. Since X-ray data shows that most of the bentonites contain no quartz and only occasionally trace amounts of quartz, we can safely assume that the average bentonites contains a maximum of 1% quartz in the clay fraction. Slaughter and Earley (1965) also show that the silt fraction is generally only 10% of the whole sample and that only about 10% of this fraction is quartz; therefore the average bentonite will contain only 1% quartz in the silt fraction. Hence we may assume that the average bentonite contains less than 2% quartz (1% 10-4 μm + 1% 4-1 μm) in the 10 to 1 micron size fraction. Therefore in order to furnish 2 grams of volcanic quartz to 100 grams of a "near-shore" Pierre shale sample we must produce an equal volume of bentonite or rather the sample must be a bentonite.

In summary, it appears that the oxygen isotope data presented by Churchman et al. (1976) and Sridhar et al. (1975) is better explained in terms of grain size variations than in terms of provenance.